LBL-28709
UC-413
CONF-900295

Lawrence Berkeley Laboratory
UNIVERSITY OF CALIFORNIA

WORKSHOP ON NUCLEAR DYNAMICS VI

17-24 February 1990
Jackson Hole, Wyoming

Editor: Jørgen Randrup

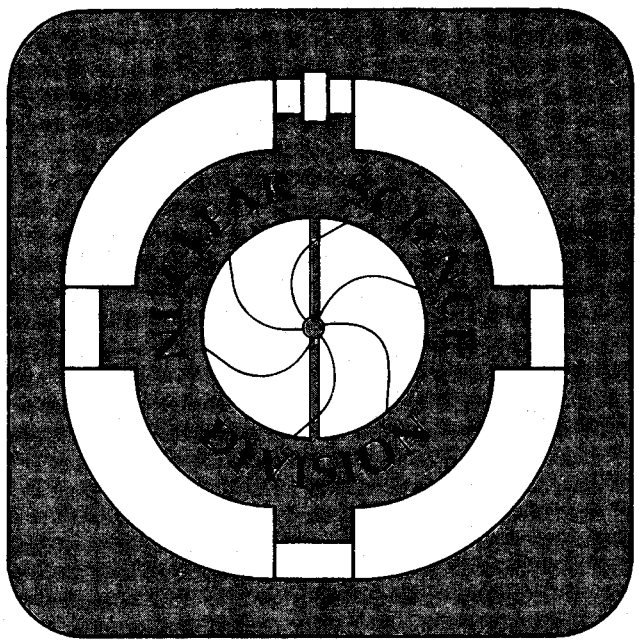

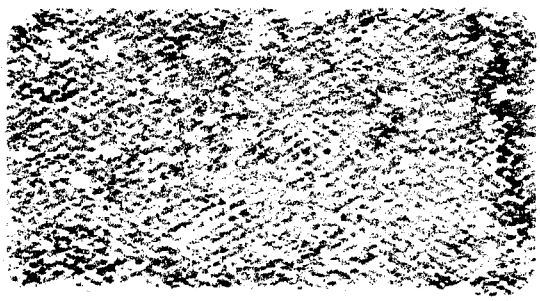

LBL-28709
cop. 1

Prepared for the U.S. Department of Energy under Contract Number DE-AC03-76SF00098.

DISCLAIMER

This document was prepared as an account of work sponsored by the United States Government. While this document is believed to contain correct information, neither the United States Government nor any agency thereof, nor the Regents of the University of California, nor any of their employees, makes any warranty, express or implied, or assumes any legal responsibility for the accuracy, completeness, or usefulness of any information, apparatus, product, or process disclosed, or represents that its use would not infringe privately owned rights. Reference herein to any specific commercial product, process, or service by its trade name, trademark, manufacturer, or otherwise, does not necessarily constitute or imply its endorsement, recommendation, or favoring by the United States Government or any agency thereof, or the Regents of the University of California. The views and opinions of authors expressed herein do not necessarily state or reflect those of the United States Government or any agency thereof or the Regents of the University of California.

LBL-28709

WORKSHOP ON NUCLEAR DYNAMICS VI

17-24 February 1990
Jackson Hole, Wyoming

ORGANIZERS:

Gary D. Westfall (Workshop Chairman)
Joseph I. Kapusta (Program Chairman)
Daniel A. Cebra (Workshop Secretary)

STEERING COMMITTEE:

Birger Bo Back *John R. Huizenga*
Joseph I. Kapusta *J. Rayford Nix* *Jørgen Randrup*
Victor E. Viola *Gary D. Westfall*

EDITOR OF THE PROCEEDINGS:

Jørgen Randrup
Nuclear Science Division, Lawrence Berkeley Laboratory
University of California, Berkeley, California 94720

Supported by the Director, Office of Energy Research, Office of High Energy and Nuclear Physics, Division of High Energy Physics, of the U.S. Department of Energy under Contract No. DE-AC03-76SF00098.

Preface

This meeting is the sixth in a series of Workshops on Nuclear Dynamics that began in 1980 at Granlibakken in California. The goal of these Workshops is to bring together researchers with a wide variety of backgrounds in nucleus-nucleus collisions, each representing a frontier of knowledge in the dynamics of nuclear matter. These frontiers range from the compressibility of ground-state nuclei to the hydrodynamics of ultrarelativistic collisions. By bringing these seemingly distant subjects together at a Workshop on Nuclear Dynamics, the participants have been able to gain insights from those working on problems in different energy ranges than their own.

This document forms the proceeding for the Workshop which consisted of fortyfour presentations organized into ten sessions. The atmosphere of the meeting was enhanced by housing the participants, the scientific sessions, and the Workshop dinners in the same building. This arrangement allowed a large amount of informal interaction in addition to the formal talks.

During the Workshop, the Steering Committee held its regular business meeting. As usual, there was some rotation of the membership and the new Steering Committee will consist of *Birger Bo Back, Wolfgang Bauer, John R. Huizenga, J. Rayford Nix, Joseph I. Kapusta*, and *Jørgen Randrup*. It was decided to hold the next meeting during the last week of January, 1991 in Key West, Florida; the Workshop Chairman will be Joe Kapusta. In two years time, February 1992, this meeting will again be held at Jackson Hole, Wyoming, and Wolfgang Bauer will be the Workshop Chairman.

I wish to thank all the participants for helping to make this meeting a success. Special thanks are due to Dan Cebra for serving as the Workshop Secretary.

Gary D. Westfall
Chairman of the Sixth Winter Workshop on Nuclear Dynamics

Winter Workshop on Nuclear Dynamics

I. Granlibakken, California: 17-21 March 1980
W.D. Myers, J. Randrup, G.D. Westfall

II. Granlibakken, California: 22-26 April 1982
W.D. Myers, J.J. Griffin, J.R. Huizenga, J.R. Nix, F. Plasil, V.E. Viola

III. Copper Mountain, Colarado: 5-9 March 1984
W.D. Myers, C.K. Gelbke, J.J. Griffin, J.R. Huizenga, J.R. Nix, F. Plasil, V.E. Viola

IV. Copper Mountain, Colarado: 24-28 February 1986
J.J. Griffin, J.R. Huizenga, J.R. Nix, F. Plasil, J. Randrup, V.E. Viola

V. Sun Valley, Idaho: 22-26 February 1988
J.R. Huizenga, J.I. Kapusta, J.R. Nix, J. Randrup, V.E. Viola, G.D. Westfall

VI. Jackson Hole, Wyoming: 17-24 February 1990
B.B. Back, J.R. Huizenga, J.I. Kapusta, J.R. Nix, J. Randrup, V.E. Viola, G.D. Westfall

VII. Key West, Florida: January 1991 (planned)
B.B. Back, W. Bauer, J.R. Huizenga, J.I. Kapusta, J.R. Nix, J. Randrup

VIII. Jackson Hole, Wyoming: February 1990 (planned)
B.B. Back, W. Bauer, J.R. Huizenga, J.I. Kapusta, J.R. Nix, J. Randrup

1990 WINTER WORKSHOP ON NUCLEAR DYNAMICS

Session 1	Chair: *N.K. Glendenning* (Sunday, February 18)	
W.D. Myers	The Surface Energy and the Compressibility	1
D. Keane	Experimental Constraints on Binary Collision Cross Sections in the Nuclear Medium	5
B.B. Back	Fission at Sub-Barrier Energies	9
P.J. Ellis	Super-RPA Ground State Correlations	13
Session 2	Chair: *C. Alonso* (Sunday, February 18)	
Y. Blumenfeld	Multi-Fragment Decay of Hot Nuclei at Intermediate Energy	17
D.A. Cebra	Sequential Emission and Multifragmentaion at Intermediate Energy	21
J.A. López	Sequential Binary Decay and Multifragmentation in Light Particle Breakup	25
J. Gallego	Towards a Theoretical Analysis for Ne+Ne at 45 MeV/N	29
S. Ayik	A One-Body Transport Model of Fluctuation Processes in Nuclear Collisions	33
Session 3	Chair: *G. Welke* (Monday, February 19)	
G.D. Westfall	Energy and Mass Dependence of Collective Flow in Intermediate-Energy Nucleus-Nucleus Collisions	37
M.C. Lemaire	Studies of Nuclear Flow	40
J.R. Wilson	Hydrodynamic Modeling of Heavy-Ion Collisions	47
C. Gale	Transverse Momentum in High-Energy Heavy-Ion Collisions and the Nuclear Equation of State	51
W. Bauer	Critical Pion Opacity	55

Session 4 Chair: *W. Bauer* (Monday, February 19)

J.J. Griffin Quantitative Phenomenology for the e^+e^- Puzzle, and Predicted Sharp Annihilative Positrons from U+Ta Collisions 59

S. Das Gupta The Second-Order Variation in Thomas-Fermi Theory 63

S.I. Chase Pion Production in Au+Au at 1.15 GeV/N from the Bevalac Streamer Chamber 67

W.A. Friedman Energy and Entropy Considerations in Nuclear Multifragmentation 71

Session 5 Chair: *L.P. Csernai* (Tuesday, February 20)

F. Plasil Nuclear Collisions at 200 GeV/N from WA80 Experiment at CERN 75

J.W. Harris Collision Dynamics and Particle Production in Relativistic Nucleus-Nucleus Collisions at CERN 79

P.V. Ruuskanen Are We Closer to Pion Condensate or Quark-Gluon Plasma? 85

M. Prakash Rapidity Spectra of Secondary Particles from Nuclear Collisions at Ultrarelativistic Energies? 90

N.K. Glendenning Fast Pulsar, Strange Stars 94

Session 6 Chair: *G.D. Westfall* (Tuesday, February 20)

Z. Fraenkel Fission Reactions with Intermediate-Energy Heavy Ions 99

R. Legrain Characteristics of Intermediate-Mass Fragment Emission from Ne+Ag and Ne+Au at 60 MeV/N 103

S.J. Yennello Search for Multifragmentation near Threshold in the ^{3}He + ^{nat}Ag System 107

P.L. Gonthier Sources of Light Particles in Peripheral Collisions 111

Session 7 Chair: *W. Benenson* (Wednesday, February 21)

S. Voloshin Intermittency in High-Energy Collisions 115

J.R. Nix Microscopic Field Theoretical Approach to Ultrarelativistic Nucleus-Nucleus Collisions 119

L.P. Csernai Collective Flow at Ultrarelativistic Energies 123

Session 8	Chair: *K. Kwiatkowski* (Thursday, February 22)	
J.E. Clayton	High-Energy Gamma Ray Production in Heavy-Ion Collisions	127
H.S. Matis	Production of e^+e^- pairs at the Bevalac	131
J.I. Kapusta	Dilepton Production Theory	135
E. Braaten	The Production of Soft Dileptons from a Hot Quark-Gluon Plasma	139
Session 9	Chair: *J.W. Harris* (Thursday, February 22)	
R. Vogt	Mean Field Pion Interactions in a Hydrodynamic Model	143
A.Z. Mekjian	Fragmentation Phenomena	147
J. Randrup	Dynamical Effects in Nuclear Multifragmentation	151
A.J. Mignerey	The Search for Multifragmentation	155
D.E. Fields	Excitation Functions for Complex Fragments Emitted in ^{14}N-Induced Reactions at E/A=20-100 MeV	159
Session 10	Chair: *J.R. Nix* (Friday, February 23)	
H.S. Köhler	Equation of State from Heavy-Ion Collisions and Many-Body Theory	163
G.F. Burgio	Relaxation Times and Particle Production in Medium-Energy Heavy-Ion Collisions	167
E.A. Remler	Off-Shell Effects in Multi-Particle Scattering	171
P. Danielewicz	Multiparticle Interactions in High-Energy Collisions with Nuclei	175
G. Fai	Meson-Quark Coupling in the Chromo-Dielectric	179
Addendum		
C. Alonso	On Relativistic Hydrodynamics	183

THE SURFACE ENERGY AND THE COMPRESSIBILITY †

W.D. Myers
Nuclear Science Division
Lawrence Berkeley Laboratory
1 Cyclotron Road
Berkeley, California 94720

The surface energy and the compressibility are closely related since, after all, the surface energy arises in part from the fact that there is a loss of binding associated with reduced density, and the compressibility coefficient K_∞ is the quantity that governs this effect for small density deviations. In fact, we find in our work [1)] (which is the continuation of a series of Thomas-Fermi calculations using the Seyler-Blanchard interaction)[2)] that the value of K_∞ is determined by the combined requirement that the surface diffuseness correspond to the one measured in electron scattering and the surface energy is the one that corresponds to a fit of the model to nuclear masses. The effect on the surface energy of varying the diffuseness b or the compressibility K_∞ can be seen in fig. 1.

Even though K_∞ has been determined, the effective value of the compressibility K_{eff} for a finite nucleus can be quite a bit smaller because the resistance of the nucleus to changes in scale consists not only of a bulk effect but depends also on surface, curvature and higher order effects. In fig. 2 the calculated values for the binding energy per particle E/A and the effective stiffness K_{eff} for a wide range of $N = Z$ nuclei (without Coulomb energy) are compared. In both cases the values are plotted versus $A^{-1/3}$ so that a curve through the points will intersect the ordinate at the nuclear matter value of the quantity in question. The slope of the line gives the dependence on surface area and the other terms are associated with higher order effects. It is interesting to note that in both parts of this figure the higher order terms in the power series expansion tend to cancel. What this means for the quantity E/A is that a simple Liquid Drop Model consisting only of a volume and surface term can be expected to work very well. For the quantity K_{eff} it means that there is probably little point in trying to go beyond a simple two term description of the effective stiffness in terms of volume and surface effects.

†This work was supported by the Director, Office of Energy Research, Office of High Energy and Nuclear Physics, Nuclear Physics Division of the US Department of Energy under Contract DE - AC03 - 76SF00098.

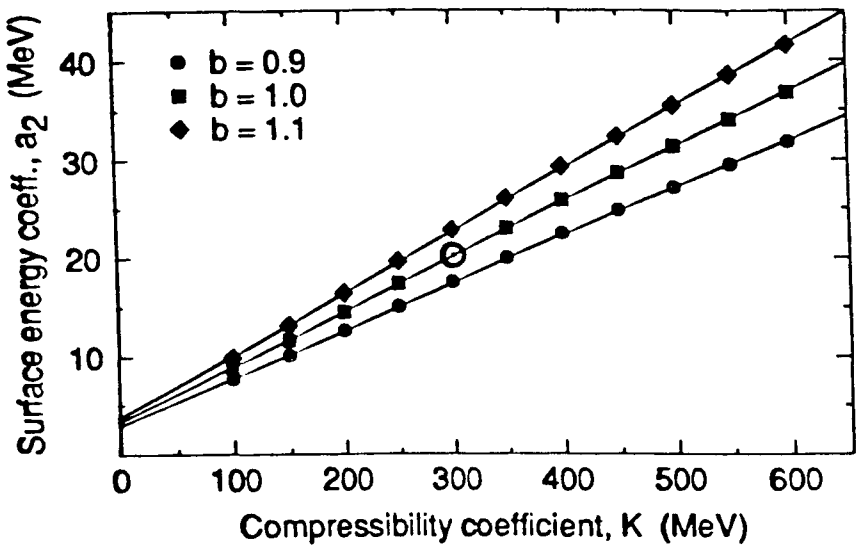

Fig. 1 The value of the surface energy coefficient a_2 is plotted against K_∞ for three different values of the nuclear diffuseness b. The point corresponding to our choice of parameters is in the circle in the center of the figure.

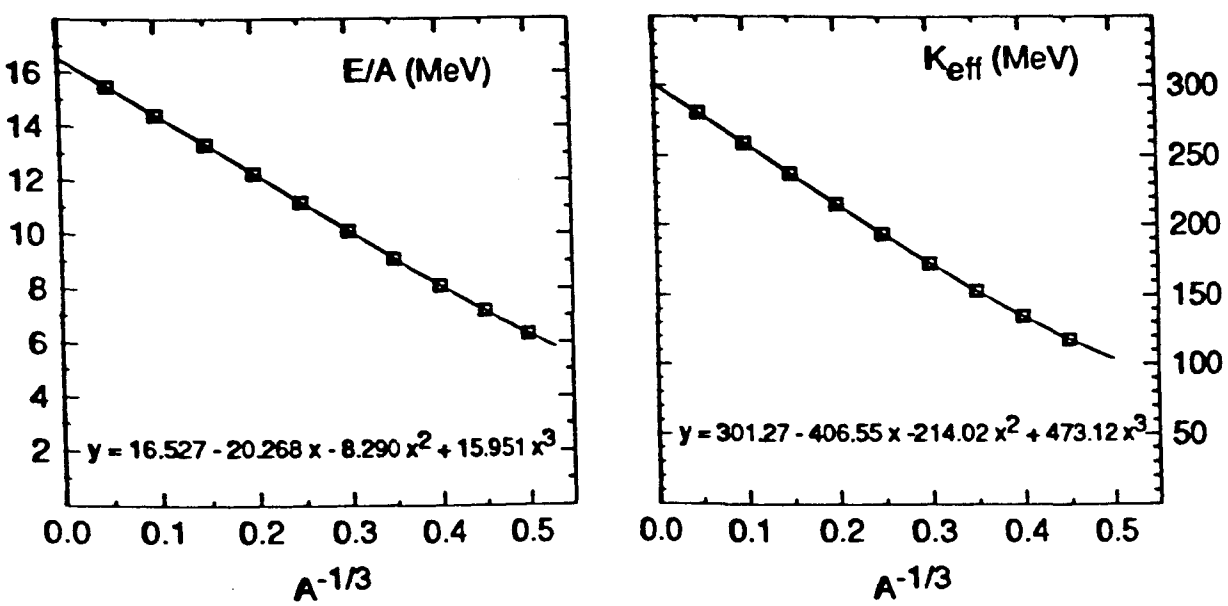

Fig. 2 A plot of the calculated energy per particle E/A versus $A^{-1/3}$ for finite $N = Z$ nuclei (without Coulomb energy) is compared with a similar plot for the quantity K_{eff}.

The effective compressibility depends not only on the size of the nucleus but also on its composition. In fig. 3 the calculated value of K_{eff} for a number of nuclei has been plotted versus the mass number A for three different cases. The open triangles correspond to values similar to those in fig. 2 with $N = Z$ and no Coulomb energy. The circles correspond to the K_{eff} values that would result if the composition of each nucleus was changed to the neutron-proton ratio holding at β-stability. The square symbols correspond to also including the effect of the Coulomb energy. The effect of the neutron excess and the Coulomb repulsion can be clearly seen.

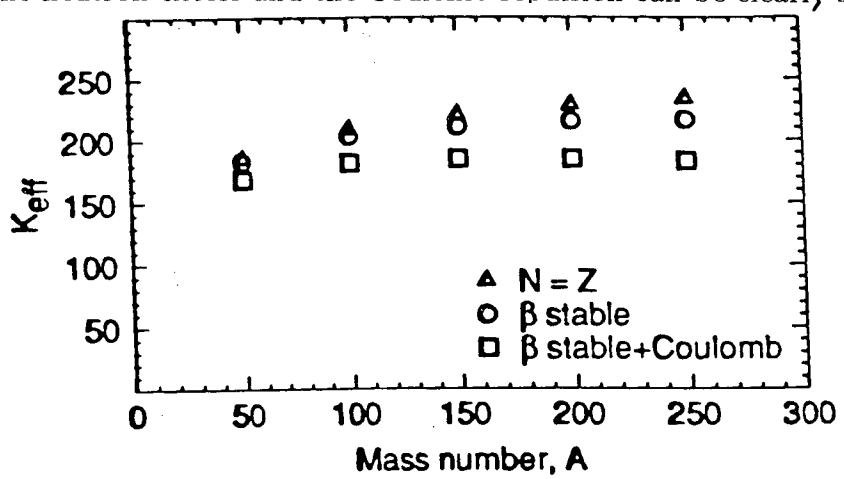

Fig. 3 The effective value of the compressibility K_{eff} for a number of nuclei is plotted versus their mass number$A$. The triangles correspond to $N = Z$ and have the same values as in fig. 2. The circles show the reduction that occurs when the N, Z ratio is changed to correspond to β stability. The effect of adding the Coulomb repulsion is indicated by the square symbols.

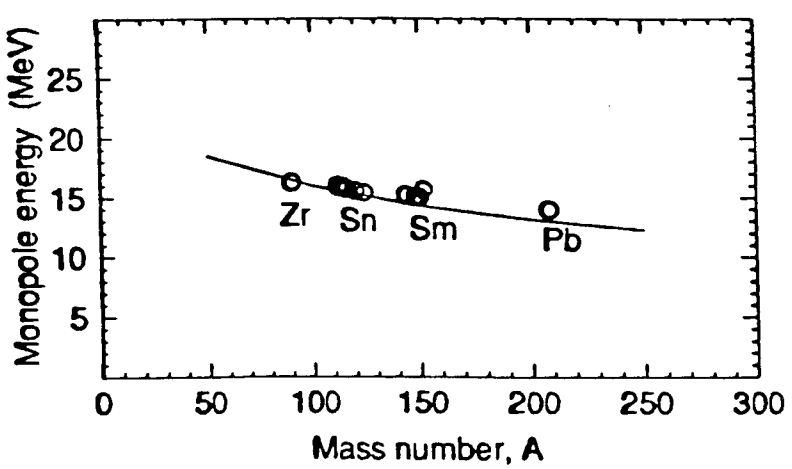

Fig. 4 The solid line corresponds to our estimate of the energy of the Giant Monopole Resonance using the hydrodynamical expression above. The circles correspond to measured values[3)] whose errors are claimed to be smaller than the size of the symbols.

In addition, in fig. 4 we show our prediction for the energy of the Giant Monopole Resonance based on these values of K_{eff} and the simple hydrodynamical expression $E_{GMR} = \hbar\frac{\pi}{\sqrt{15}}\sqrt{K_{eff}/B}$, where $B = m\langle r^2\rangle$, $\langle r^2\rangle = \frac{3}{5}R^2 + 3b^2$, $R = 1.13\,A^{1/3}\,\mathrm{fm}$ and $b = 1\,\mathrm{fm}$.[4] This expression was derived from eq. (6A-50) in ref.[5], which is $\omega = \pi u_c/R_o$, where $u_c = \sqrt{\frac{K}{9m}}$. To arrive at our expression, which includes a diffuseness correction, we replaced R_o by $\sqrt{\frac{5}{3}\langle r^2\rangle}$.

The author wishes to acknowledge discussions with W.J. Swiatecki who was responsible for a number of the ideas presented here. He also wants to acknowledge the important contribution made by P. Möller.

References

1) This paper is a shortened and slightly modified version of the paper "Aspects of Incompressibility" that will appear in *The Proceedings of the Gross Properties of Nuclei and Nuclear Excitations International Workshop XVIII*, Hirschegg, Austria,15-20 January 1990.

2) Seyler, R.G. and Blanchard, C.H., Phys. Rev. **124**, 227 (1961); **131**, 355 (1963).

Myers, W.D. and Swiatecki, W.J., Ann. of Phys. **55**, 395 (1969).

von Groote, H., Proc. 3rd Int. Conf. on nuclei far from stability, ed. R. Klapisch, CERN 76-13 p. 595 (1976).

Küpper, W.A., Wegmann, G. and Hilf, E.R., Ann. of Phys. **88**, 454 (1974); Küpper, W.A., Ph.D. Thesis, Univ. Munich (1978).

Myers, W.D., Swiatecki, W.J. and Wang, C.S., Nucl. Phys. **A436**, 185 (1985).

3) Sharma, M.M., Proc. NATO Adv. Study Institute on Nuclear Equation of State, Peñiscola, Spain, May 22 - June 2 (1989).

4) Myers, W.D. and Schmidt, K.-H., Nucl. Phys. **A410**, 61 (1983).

5) A. Bohr and B.R. Mottelson, "Nuclear Structure" Vol. 2, W.A. Benjamin, Inc., 1975.

Experimental Constraints on Binary Collision Cross Sections in the Nuclear Medium

Jinghua Jiang, John Cogar and Declan Keane
Department of Physics, Kent State University, Kent, Ohio 44242

Christoph Hartnack and Horst Stöcker
Institut für Theoretische Physik, Goethe-Universität, D-6000 Frankfurt am Main, Germany

Although a significant fraction of the relativistic heavy ion research effort over the past ten years has been directed towards understanding the nuclear equation of state (EOS) in the hadron gas phase, a consensus has yet to be reached on the more limited question of whether the evidence favors the so-called "stiff" or "soft" EOS. A number of difficulties — both theoretical and experimental — have contributed to this situation; this paper focuses on one of these difficulties, *i.e.*, on the topic of determining the cross section for nucleon-nucleon collisions in the nuclear medium, σ_{NN}^{eff}.

A crucial feature of microscopic transport theories like the Boltzmann-Uehling-Uhlenbeck[1] (BUU) and Vlasov-Uehling-Uhlenbeck[2] (VUU) models, and the more recent Quantum Molecular Dynamic[3,4] (QMD) approach, is the assumption that the nucleus-nucleus collision process can be described in part by a classical sequence of 2-body collisions according to σ_{NN}^{UU} — the experimental scattering cross sections for free particles corrected for Pauli blocking of occupied final states, as per the Uehling-Uhlenbeck equation.Calculations by ter Haar and Malfliet[5] have since indicated that an additional in-medium correction is needed: $\alpha = \sigma_{NN}^{eff}/\sigma_{NN}^{UU} \approx 0.7$ rather than 1, while Cugnon *et al.*[6] have argued that α might be strongly dependent on momentum, density and temperature. Clearly, there is a need to directly resolve these theoretical uncertainties with the help of experimental data, and in order to test the assumption that a constant value of α can be used, the widest possible range of experimental conditions should be studied.

The transport models incorporate the effect of the EOS through a mean field interaction that influences the trajectories of particles between the hard binary scatterings. Collective flow observables such as $p^x(y)$, the mean component of transverse momentum per nucleon in the event reaction plane as a function of rapidity,[7] are found to be sensitive to both the EOS and σ_{NN}^{eff}.[8,9,4] These findings cover various projectile and target masses, bombarding energies and impact parameters, and can be summarized by noting that a decrease in σ_{NN}^{eff} in BUU/VUU or QMD simulations by a factor of $\sim \frac{1}{\sqrt{2}}$ typically changes the predicted flow by an amount equivalent to changing the EOS from stiff to soft; likewise, a $\sim \sqrt{2}$ increase in σ_{NN}^{eff} is equivalent to changing the EOS from soft to stiff. Thus, a minimal requirement for distinguishing between these two standard parametrizations of the EOS is that the total uncertainty in σ_{NN}^{eff} should be less than a few tens of percent.

The models indicate that observables averaged over all reaction planes, such as momentum or rapidity spectra, are independent of the EOS while retaining some sensitivity to σ_{NN}^{eff}.[10,4] Measurements of both flow and reaction-plane-averaged parameters thus offer the possibility of simultaneously constraining the EOS *and* σ_{NN}^{eff}.

A previously reported[10] rapidity spectrum for high multiplicity 1.2 A GeV Ar + BaI_2 events in the Bevalac streamer chamber favors VUU predictions with $\alpha \approx 1$. Experimental rapidity spectra are strongly dependent on multiplicity, and predicted spectra are likewise very sensitive to impact parameter; consequently, particular attention was devoted to simulating the experimental

multiplicity selection as realistically as possible. Nevertheless, systematic uncertainties associated with the multiplicity simulation remain, and provide a motivation for further comparisons using inclusive data.

Aichelin *et al.*[11] have recently compared predictions of several microscopic transport models to inclusive p-like momentum spectra at $\theta_{lab} = 20°$, $40°$ and $60°$ for 0.8 A GeV La + La, as measured at the Bevalac B30 spectrometer by Hayashi *et al.*[12] The term *p-like* signifies that the contribution from protons in all fragments (up to ^{4}He) is included, and so the comparison should be negligibly affected by the fact that final state clustering is difficult to predict and is not implemented in most models. Aichelin *et al.* found good agreement among four independent transport models,[1,2,3,13] but reported that the codes overpredicted the invariant cross sections $\sigma_I = (E/p^2)\ d^2\sigma/dp\ d\Omega$ at 20° by a factor of 1.5 to 2 for $p_{lab} > 1$ GeV/c (see Figure 1). This discrepancy has been interpreted as a possible failure of the models to adequately incorporate all the effects of the nuclear medium. However, the present work demonstrates that an interpretation in terms of $\alpha \approx 1$ is favored, and the discrepancy can be explained by the fact that the models were not filtered to simulate the experimental conditions.

In the experiment of Hayashi *et al.*, the kinetic energy of the partially-stripped beam ions in the Bevatron was 800 A MeV. We estimate an energy loss of 20 to 30 A MeV up to the mean interaction point in the target; moreover, projectile-target symmetry requires that contours of σ_I plotted in the plane of rapidity and transverse momentum be symmetric about mid-rapidity, and an assumed bombarding energy of about 0.77 A GeV at the target improves the overall symmetry. The kinematic region $\theta_{lab} = 20°$, $p_{lab} > 1$ GeV/c corresponds to rapidities near that of the projectile, and in this region, $\sigma_I(p_{lab})$ is strongly dependent on the beam energy. Figure 1 demonstrates that lowering the VUU beam energy from 0.80 A GeV to 0.77 A GeV reduces the discrepancy in $\sigma_I(p_{lab})$ between VUU and experiment at $\theta_{lab} = 20°$.

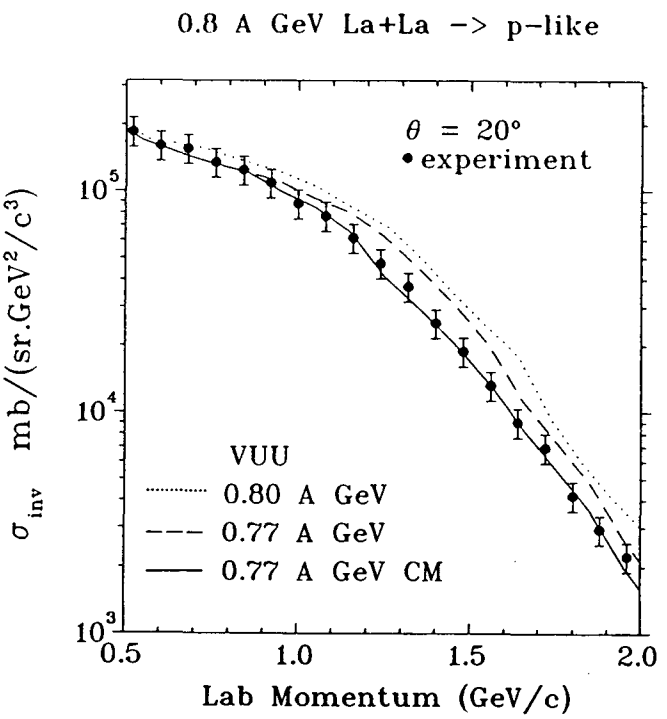

FIG. 1: Inclusive proton-like cross section at $\theta_{lab} = 20°$, in 0.8 A GeV La + La collisions. The experimental data of Hayashi *et al.* are compared with the Vlasov-Uehling-Uhlenbeck transport model.

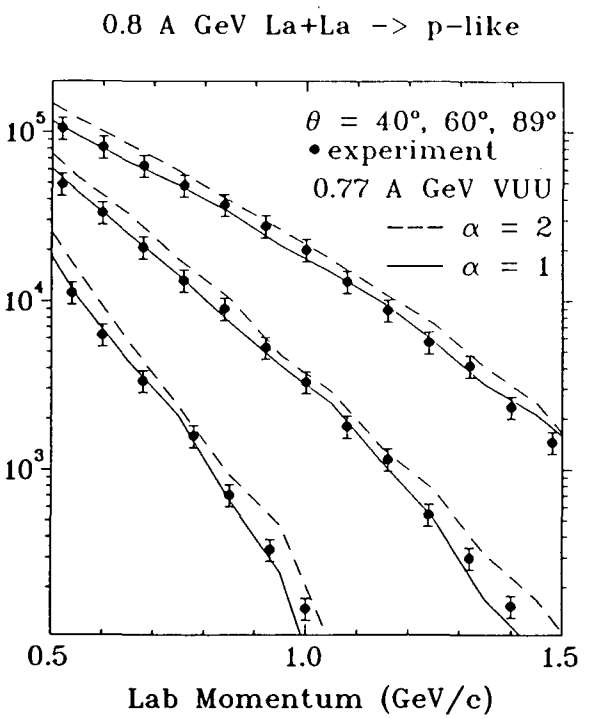

FIG. 2: As Fig. 1, except at three angles covering mid-rapidity to target rapidity. The two curves show the sensitivity to a doubling of the in-medium binary collision cross sections in VUU.

There are also distortions associated with evaluating $\sigma_I = (E/p^2)\, d^2\sigma/dp\, d\Omega$ in bins of finite Δp and $\Delta\Omega$, which can be seen as systematic shifts in σ_I calculated in different Lorentz frames. Except where noted otherwise, all σ_I predictions in this paper were evaluated in the lab frame using the same Δp and $\Delta\theta$ as the experiment. The solid line in Figure 1 shows σ_I as calculated in the center-of-mass frame, using the same Δp and $\Delta\theta$ as in the lab frame. The c.m. calculation satisfies the requirement for symmetry about mid-rapidity, whereas the lab frame calculation does not.

Overall, there is little evidence for a discrepancy at 20° that can be attributed to a fundamental shortcoming in the VUU model. We emphasize that both the beam energy loss and the σ_I distortion in the lab frame are of diminishing importance at the larger polar angles, and are within statistical uncertainties for the kinematic region spanning mid-rapidity back to the target rapidity. Accordingly, it is most appropriate to use this region for detailed comparisons between transport models and experiment.

Figure 2 shows the data of Hayashi *et al.* at three angles spanning rapidities $y_{lab} = 0$ through $\sim \frac{2}{3} y_{beam}$. The error bars give the total systematic uncertainty; statistical errors are not included, but are negligible when averaged over many points. The VUU predictions corrresponding to $\alpha = 1$ are in excellent overall agreement with experiment, and $\alpha = 1$ is favored over $\alpha = 2$. However, it is clear that the sensitivity to α and the systematic uncertainties in the data are such that the previously-discussed goal of constraining α to within a few tens of percent is out of reach in this case.

Figure 3 shows data for Ar + KCl at 0.8 A GeV, also measured at the Bevalac B30 spectrometer by Nagamiya *et al.*[14] The VUU calculations are again in excellent agreement with experiment and still favor $\alpha \sim 1$, albeit at a rather low level of sensitivity. The effects of beam energy loss are negligible in the case of a $Z = 18$ projectile.

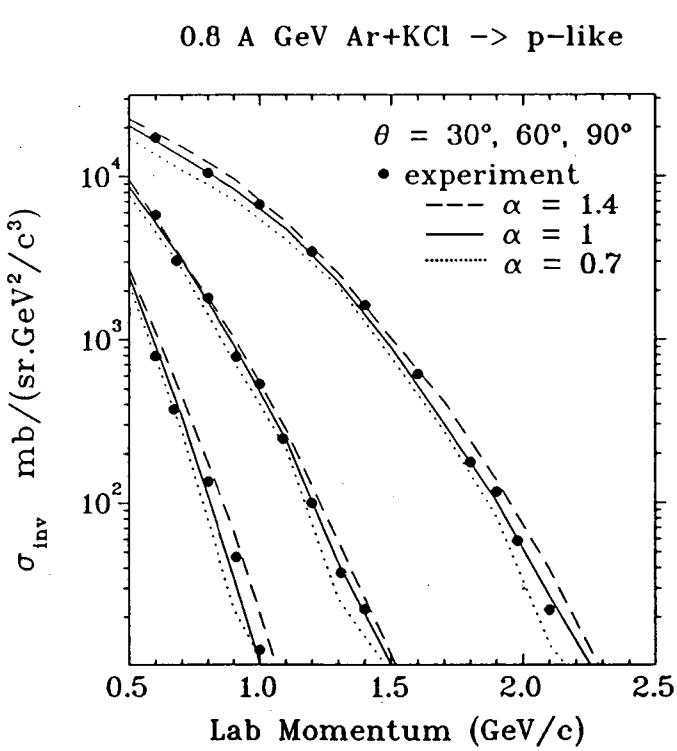

FIG. 3: Inclusive proton-like cross sections for a lighter mass-symmetric system, Ar + KCl.

The fact that the above comparisons for La + La and Ar + KCl both favor $\alpha \sim 1$, in conjunction with a similar finding for the high multiplicity Ar + BaI_2 streamer chamber data of ref 10, sets limits to the possible dependence of α on details of the medium. To illustrate this point, we have calculated the density in a volume surrounding each nucleon-nucleon collision point (not counting the two colliding nucleons), and averaged over all NN collisions in all events. This quantity reflects the average density of the nuclear medium, and would be zero for collisions between free nucleons. The results for the three systems of interest are shown in Table I. It can be seen that the average in-medium density may increase as much as $\sim$ 30% between inclusive Ar + KCl and moderately central Ar + BaI_2 events. Further comparisons of momentum spectra are in progress in an effort to infer values of α over a wider range of conditions.

TABLE I: Mean density $< \rho/\rho_0 >$ in a spherical volume of radius 2 fm centered on each NN collision, based on a VUU simulation.

	E_{beam} (A GeV)	hard	soft
Ar + KCl (all b)	0.8	0.95	1.13
La + La (all b)	0.8	1.08	1.18
Ar + BaI_2 ($b < 6$ fm)	1.2	1.25	1.38

In summary, we conclude that the VUU model can reproduce momentum/rapidity spectra — both inclusive and high-multiplicity selected — within current experimental uncertainties. These uncertainties are generally too large to constrain the cross section for binary collisions in the nuclear medium, σ_{NN}^{eff}, at the level of precision needed in order that transport models might be used with confidence to infer properties of the nuclear equation of state. If σ_{NN}^{eff} depends on in-medium effects that are neglected in the current transport models, the available evidence suggests that the additional correction factor is within the range $\frac{1}{2}$ to 2, and cannot be strongly dependent on details of the medium, such as density. Finally, our findings reinforce the need for new, more precise measurements of cross sections for the various fragment species for a wide range of projectile/target masses and bombarding energies, preferably in conjunction with information about the event reaction plane and multiplicity.

This work has been supported in part by the U.S. Department of Energy under Grant DE-FG02-89ER40531. We acknowledge computing facilities provided by the Ohio Supercomputer Center.

1. G. Bertsch, S. DasGupta, and H. Kruse, Phys. Rev. C **29**, 673 (1984); J. Aichelin and G. Bertsch, Phys. Rev. C **31**, 1730 (1985).
2. H. Kruse, B.V. Jacak, and H. Stöcker, Phys. Rev. Lett. **54**, 289 (1985); J.J. Molitoris and H. Stöcker, Phys. Rev. C **32**, 346 (1985); J.J. Molitoris, H. Stöcker, and B.L. Winer, Phys. Rev. C **36**, 220 (1987).
3. J. Aichelin and H. Stöcker, Phys. Lett. B**176**, 14 (1986); J. Aichelin, A. Rosenhauer, G. Peilert, H. Stöcker, and W. Greiner, Phys. Rev. Lett. **58**, 1926 (1987); G. Peilert, A. Rosenhauer, H. Stöcker, W. Greiner, and J. Aichelin, Mod. Phys. Lett. **A3**, 459 (1988); J. Aichelin, G. Peilert, A. Bohnet, A. Rosenhauer, H. Stöcker, and W. Greiner, Phys. Rev. C **37**, 2451 (1988).
4. G. Peilert, H. Stöcker, W. Greiner, A. Rosenhauer, A. Bohnet, and J. Aichelin, Phys. Rev. C **39**, 1402 (1989).
5. B. ter Haar and R. Malfliet, Phys. Lett. **172B**, 10 (1986); Phys. Rep. **149**, 207 (1987).
6. J. Cugnon, A. Lejeune, and P. Grangé, Phys. Rev. C **35**, 861 (1987).
7. P. Danielewicz and G. Odyniec, Phys. Lett. **157B**, 146 (1985).
8. M. Gyulassy, K.A. Frankel, and H. Stöcker, Phys. Lett. **110B**, 185 (1982).
9. G.F. Bertsch, W.G. Lynch, and M.B. Tsang, Phys. Lett. **189B**, 384 (1987).
10. D. Keane, S.Y. Chu, S.Y. Fung, Y.M. Liu, L.J. Qiao, G. VanDalen, M. Vient, S. Wang, J.J. Molitoris, and H. Stöcker, Phys. Rev. C **37**, 1447 (1988).
11. J. Aichelin, J. Cugnon, Z. Fraenkel, K. Frankel, C. Gale, M. Gyulassy, D. Keane, C.M. Ko, J. Randrup, A. Rosenhauer, H. Stöcker, G. Welke, and L.Q. Wu, Phys. Rev. Lett. **62**, 1461 (1989).
12. S. Hayashi, Y. Miake, T. Nagae, S. Nagamiya, H. Hamagaki, O. Hashimoto, Y. Shida, I. Tanihata, K. Kimura, O. Yamakawa, T. Kobayashi, and X.X. Bai, Phys. Rev. C **38**, 1229 (1988).
13. C.M. Ko, Q. Li, and R. Wang, Phys. Rev. Lett. **59**, 1084 (1987); C.M. Ko and Q. Li, Phys. Rev. C **37**, 2270 (1988); Q. Li, J.Q. Wu, and C.M. Ko, Phys. Rev. C **39**, 849 (1989).
14. S. Nagamiya, M.-C. Lemaire, E. Moeller, S. Schnetzer, G. Shapiro, H. Steiner, and I. Tanihata, Phys. Rev. C **24**, 971 (1981).

Fission at Sub-barrier Energies

B. B. Back, R. R. Betts, P.Fernandez,
B. G. Glagola, T. Happ, and D. Henderson
Argonne National Laboratory, Argonne, IL 60439, USA

H. Ikezoe
J.A.E.R.I, Ibaraki-ken, Japan

Ph. Benet
Purdue University, West Lafayette, IN 47906, USA

ABSTRACT: Fission fragment angular distributions have been measured for the reaction $^{16}O+^{232}Th$ at beam energies of 78.2, 82.2, 86.6, and 100.6 MeV. In this experiment, it was possible to determine the relative contributions of fragments from both the fission decay of the ^{248}Cf compound nuclei, formed in complete fusion reactions between the target and the projectile, and the sequential fission decay of nuclei in the Th region, populated in inelastic scattering and/or transfer reactions on the Th target. This separation was made possible by using flight-time measurements. It was found that fragments from fission of ^{248}Cf showed a somewhat smaller angular anisotropy as compared with earlier measurements in which the sequential fission component was not excluded. The anisotropies found in the present experiment are, however, even with this correction, somewhat larger than expected on the basis of theoretical models.

I. INTRODUCTION

The distribution of partial waves leading to complete fusion between heavy ions has been the subject of intense studies in recent years. Theoretically, this subject is strongly related to the understanding of the many observations of enhanced sub-barrier fusion cross sections. Several effects responsible for this enhancement have been identified, such as deformation [1], zero-point shape vibrations [2], and coupled-channel effects [3,4]. It now appears that the bulk of sub-barrier fusion data can be explained quite well within this theoretical framework, when certain allowances are made for parameter optimization. It has been pointed out [5] that under certain assumptions there is a direct correspondence between the fusion cross section at sub-barrier energies and the partial-wave distribution of the fusion system. One would therefore expect that the partial-wave distribution should be rather accurately described by a model calculation which adequately reproduces the sub-barrier part of the fusion excitation function. Several experimental measurements [6,7] indicate, however, that there is a stronger population of higher partial waves over that expected on the basis of model calculations which succesfully reproduce the sub-barrier fusion cross section. The most spectacular discrepancy of this type has recently been reported in the results of experiments, where the mean square spin in sub-barrier fusion reactions was derived from measurements of fission angular distributions[8,9]. Neither of these experiments attempted, however, to discriminate against possible contributions from sequential fission, leaving the question of the effects of this process on the observed anisotropies unanswered. In the present experiment, we have succeeded in separating the two contributions and find that the component arising from compound fission alone shows a somewhat smaller angular anisotropy, correspondiong to a reduced mean-square spin of the fissioning system. These anisotropies are, however, still larger than expected theoretically. Thus, despite the recent substantial improvements in the understanding of sub-barrier fusion processes, there still seems to be room for further work in this area.

II. EXPERIMENT

The experiments were carried out with ^{16}O beams of energies 78.2, 82.2, 86.6, and 100.6 MeV from the ATLAS superconducting linac at Argonne. Singles fission fragments were registered in an array of ten 400 mm^2 Si- detectors in the angular

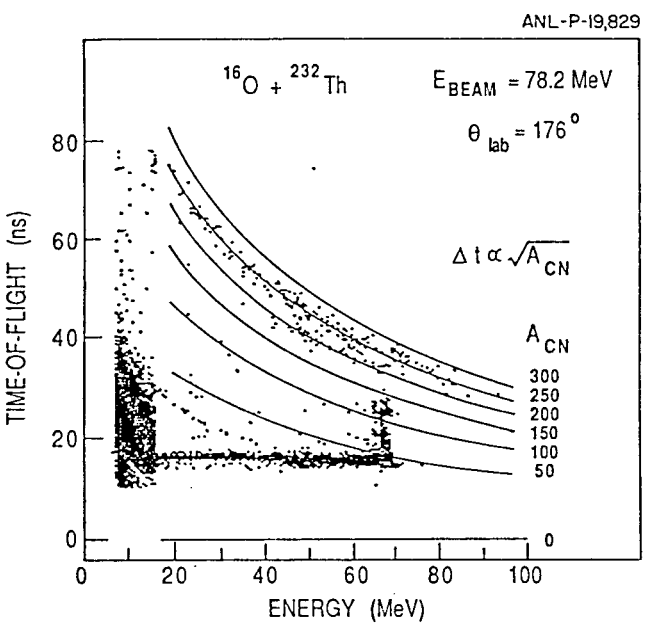

Figure 1: Time-of-flight *vs.* energy spectrum

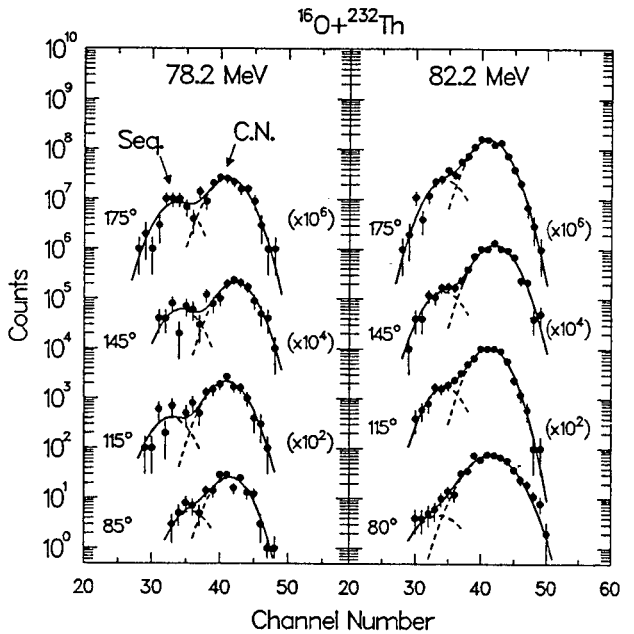

Figure 2: Pseudo-mass spectra

range from 85° to 175°. The flight time of the fragments over the 40 cm distance from the target to the detector was measured by utilizing the time structure ($\Delta t \approx 300ps$) of the beam. A typical spectrum of the time-of-flight vs. energy is shown in Fig. 1. We have drawn a curve labeled $A = 250$ through the main component of fission fragments assuming that this component arise chiefly from the fission of ^{248}Cf nuclei formed in complete fusion reactions. The other curves in the figure are derived from this, assuming that the time-of-flight of fragments from other sources (e.g. sequential fission) scales with $\Delta t \propto \sqrt{A_{CN}}$, A_{CN} being the mass of the fissioning system. In addition, we observe a second component approximately centered around the curve labeled $A_{CN} = 200$. This component is associated with the group of light fragments emitted in fission of Th-like nuclei at low excitation energy. Such fragment have masses centered around $A_f = 100$ and may therefore very well be expected to fall on the curve for fission of a nucleus with mass $A_{CN} \sim 200$. In the mass asymmetric fission decay of Th nuclei, the heavy fragments are centered at $A_f \sim 130$, and they are therefore expected to overlap strongly with the fragments in the heavy end of the symmetric mass distribution for ^{248}Cf fission. The fact that the fission decay of the target-like nuclei at low excitation energy is strongly asymmetric therefore enables us to isolate this component.

III. SEQUENTIAL FISSION

In the further analysis, the data have been projected along the curves indicated in Fig. 1 and binned by a factor of six to obtain one-dimensional pseudo-mass spectra. Such spectra are shown in Fig. 2. The solid curves represents the best fits to the distributions using two gaussians. The individual gaussian peaks are indicated by the dashed curves. Both the automatic fitting procedure and a visual inspection of the pseudo-mass spectra clearly indicate that they are composed of two components, namely a component centered at channel $\sim$ 34, which contains light fragments from the sequential fission of the target-like nuclei, and a component centered at channel $\sim$ 42, which contains both compound fission fragments

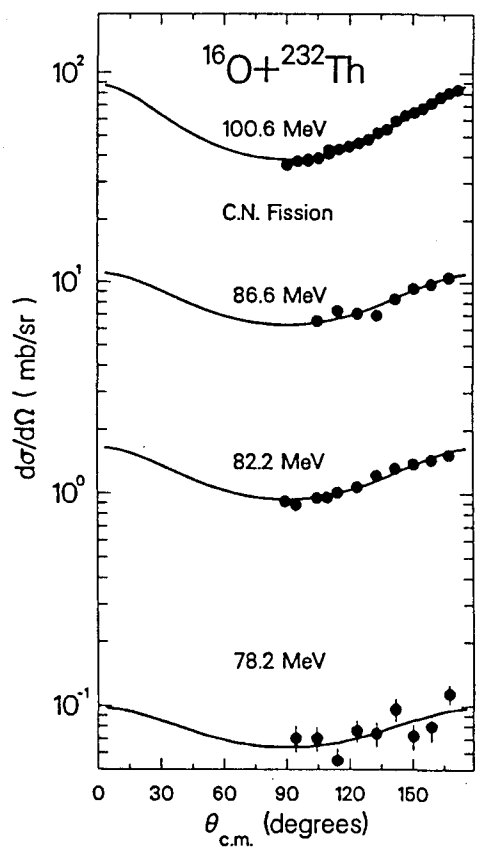

Figure 3: Fission fragment angular distributions

and the heavy fragment group from fission of the target-like nuclei.

IV. DATA ANALYSIS

The angular distributions for compound nucleus fission derived from decomposition of the pseudo-mass spectra are shown in Fig. 3 as solid points. The solid curves represent optimal fits to the data using the standard expression based on the saddle point model for fission angular distributions [10], namely

$$W(\theta) \propto \sum_{I=0}^{\infty}(2I+1)T_I \sum_{K=-I}^{I} \rho_I(K) \mid d^I_{0K}(\theta) \mid,$$

where I is the nuclear spin, T_I is the transmission coefficient for fusion of the partial wave $\ell = I$, K is the axial component of the spin, and $d^I_{0K}(\theta)$ is a d-function. The distribution of K-values is gaussian with a variance of K_0^2, which, in the saddle point model, is given by the nuclear temperature T and the moments of inertia of the nucleus at the saddle point. In practice, $W(\theta)$ is essentially determined by the ratio $K_0^2/\langle I^2\rangle$, which allows for the determination of the mean square spin $\langle I^2\rangle$ from the angular distribution of fission fragments, if the variance, K_0^2, is known from other measurements or theory.

In the present work, we have taken the partial wave distributions for fusion from a fit to the presently available experimental fusion-fission cross sections [10,8,9]- assuming that the evaporation residue cross section is negligible - using a fusion model based on the proximity potential and which includes the effects of target deformation, zero-point vibrations, and barrier penetration. The fits are obtained by varying the value of K_0^2, the variance of the distribution of spin projections onto the nuclear symmetry axis. The angular anisotropies, $W(180^o)/W(90^0)$ for the present work (•) are compared with previous measurements (◇ Back *et al.* [10], ○ Vandenbosch *et al.* [8] , and □ Zhang *et al.* [9]) in Fig. 4. Despite the large error bars of the present data, which originate partly from the limited statistics and partly from the decomposition of the data, we see that the anisotropy in the $E_{cm} = 73 - 80$ MeV region is somewhat reduced when the sequential fission component is subtracted. The solid curve in Fig. 4 is based on saddle point shapes given by the rotating liquid drop model [11] and the partial wave distribution from the model calculations, which reproduce the fusion-fission excitation function. From a study of the α + ^{244}Cm reactions, which also forms the ^{248}Cf compound system with spins in the same range as the presently studied reaction, it is known that the fission decay of ^{248}Cf is well described by the saddle point model of fission. The observed - albeit somewhat reduced - discrepancy between theory and experiment is therefore ascribed to an incomplete description of the partial wave distribution in sub-barrier heavy ion fusion reactions.

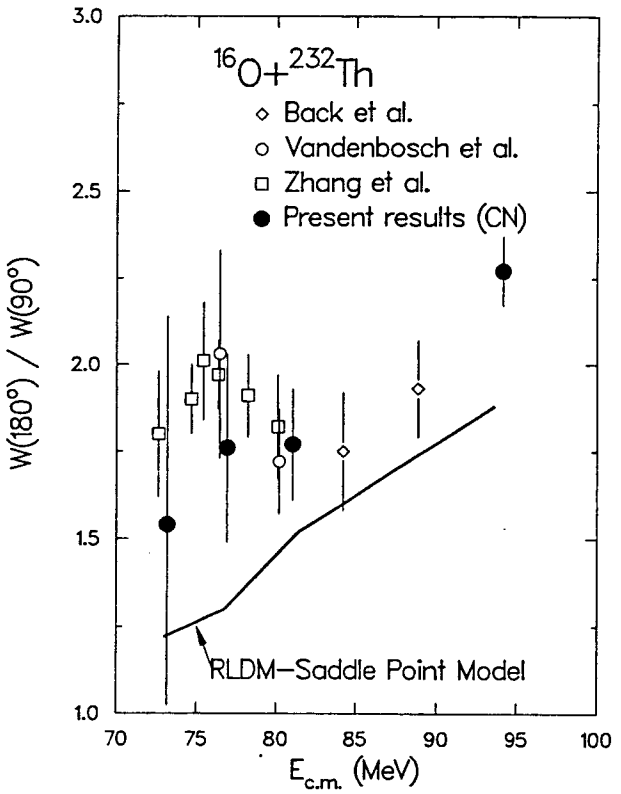

Figure 4: Anisotropies of fission fragments shown as a function of excitation energy of the fissioning system

V. CONCLUSION

Provided that the variance, K_0^2, of the total spin projection onto the nuclear symmetry axis is known from other sources (light ion induced experiments and/or theory), measurements of fission angular distributions provide accurate information on the mean square spin of the fission system. One difficulty in utilizing this technique at sub-barrier energies stems from the fact that a substantial fraction of the fragments originate from fission decay of target-like nuclei, which have been excited in quasi-elastic reactions. This component increases in relative strength with decreasing beam energy. In the present work we have shown that it is possible to determine the relative contribution of fission fragments from sequential and compound fission by measuring the flight time as well as the energy of singles fission fragments as a function of scattering angle. Isolating the component from compound fission decay, we find that the earlier discrepancy between experimental and theoretical angular anisotropies is reduced, although not quite enough to show agreement with theory. We therefore conclude that the mean square spin of the fused system is larger than predicted by the model calcuations which reproduce the sub-barrier excitation function. It therefore appears that further theoretical work is needed in order to obtain a better understanding of the fusion process for heavy ions at sub-barrier energies.

This work was performed under the auspices of the U.S. Department of Energy under Contract No. W-31-109-ENG-38.

References

[1] C.-Y.Wong, Phys. Lett. **31**, 766 (1973)
[2] H.Esbensen, Nucl. Phys,**A352**, 147 (1981)
[3] C.H.Dasso *et al.*,Nucl. Phys. **A405**, 381 (1983)
[4] C.H.Dasso *et al.*, Phys. Lett. **B183**, 141 (1987)
[5] C.H.Dasso *et al.*, Phys. Rev. Lett. **57**, 1498 (1986)
[6] S.Gil *et al.*,Phys. Rev. **C31**, 1752 (1985)
[7] M.L.Halbert *et al.*,Phys. Rev. **C40**, 2558 (1989)
[8] R.Vandenbosch *et al.*,Phys. Rev. Lett. **56**, 1234, (1986)
[9] H.Zhang *et al.*, Preprint (1989)
[10] B.B.Back *et al.*,Phys. Rev. **C32**, 195 (1985)
[11] S.Cohen *et al.*,Ann. Phys. (NY) **82**, 557 (1974)

Super-RPA Ground State Correlations

P.J. Ellis
School of Physics and Astronomy, University of Minnesota
Minneapolis, MN 55455, USA

H.A. Mavromatis
Physics Dept., King Fahd University of Petroleum and Minerals
Dhahran 31261, Saudi Arabia

H. Müther
Institut für Theoretische Physik, Universität Tübingen
Tübingen, West Germany

The random phase approximation (RPA) has been widely used in nuclear physics. Two different forms have been employed:– one sums the particle-hole correlations which we refer to as the ph RPA and the other sums particle-particle and hole-hole correlations, *i.e.*, pairing-type correlations and we refer to this as the pp RPA (for recent work, see Ref. [1,2]) and references therein). Kuo and coworkers[2]) have shown that the pp RPA has the important effect of decreasing the saturation density of nuclear matter towards the experimental value.

The energy diagrams which are summed by the RPA technique are illustrated in fig. 1, where we have used Hugenholtz notation so that the heavy dot indicates an antisymmetrized two-body interaction. The two diagram series are completely distinct except for the second order diagram which is common to both. This is rather like doing a shell model calculation, but only including the pp or the ph interactions, which few would advocate. Our purpose therefore is to investigate an approach in which the pp and ph interactions are summed simultaneously, thus allowing "cross-ring" diagrams which have both types of interaction. We also wish to allow all ph interactions within a propagating 2p2h state, thus including "exchange" diagrams additional to the standard ph RPA. The lowest order diagrams of these two types are shown in fig. 2.

In order to sum this set of diagrams, we use standard pertubation theory for a non-degenerate system, see *e.g.* Ref. [3]). Writing the approximate true wavefunction as

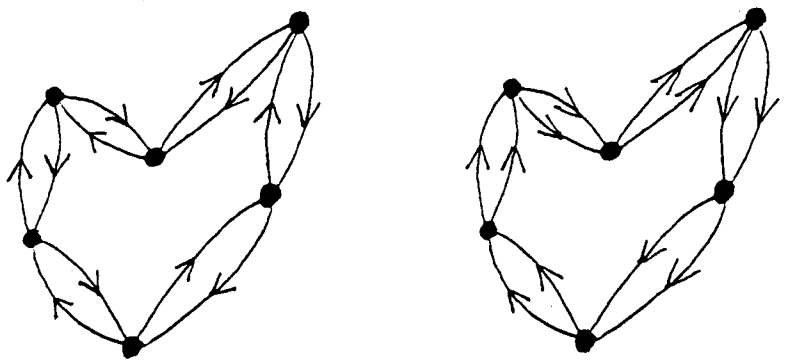

Figure 1: Energy diagrams for the standard ph and pp RPA.

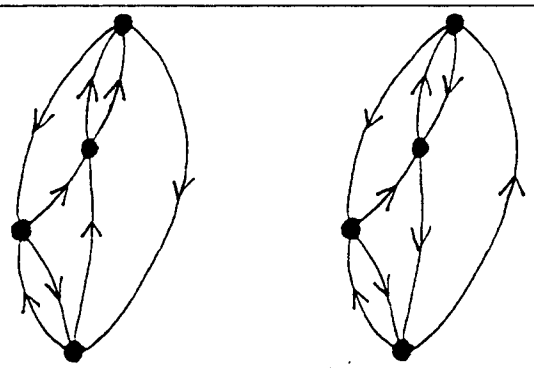

Figure 2: Examples of "cross-ring" and "exchange" diagrams.

$$|\psi\rangle = \exp\Big[\sum_{ab\alpha\beta} c_{ab\alpha\beta} a_a^\dagger a_b^\dagger a_\beta a_\alpha\Big]|\phi_0\rangle \,, \tag{1}$$

where $|\phi_0\rangle$ is the unperturbed wavefunction, we then set up a multiple-scattering series for the coefficients c. Using, for simplicity, an uncoupled basis and labelling particles (holes) by latin (greek) letters, we obtain

$$\begin{aligned} c_{ab\alpha\beta} = \frac{1}{\epsilon_{ab\alpha\beta}}\Big\{ & \tfrac{1}{4}B_{ab\alpha\beta} + \tfrac{1}{2}\mathcal{A}_{abcd}c_{cd\alpha\beta} + \tfrac{1}{2}c_{ab\gamma\delta}\mathcal{A}_{\gamma\delta\alpha\beta} \\ & -A_{a\gamma c\alpha}\left(c_{cb\gamma\beta} - c_{cb\beta\gamma} - c_{bc\gamma\beta} + c_{bc\beta\gamma}\right) + c_{ab\gamma\delta}B_{\gamma\delta ef}c_{ef\alpha\beta} \\ & + \left(c_{ac\alpha\gamma} - c_{ac\gamma\alpha} - c_{ca\alpha\gamma} + c_{ca\gamma\alpha}\right) \\ & \times\tfrac{1}{2}B_{\gamma\delta cd}\left(c_{bd\beta\delta} - c_{bd\delta\beta} - c_{db\beta\delta} + c_{db\delta\beta}\right)\Big\} \,, \end{aligned} \tag{2}$$

where repeated indices within the braces are to be summed and the energy denominator ϵ gives the energy of the holes minus that of the particles. Here

the first term produces the 2p2h state and then the second and third terms allow pairs of particles and holes, respectively, to scatter. The fourth term gives the ph scattering for the four possible ph pairs. The fifth and sixth terms include the backward-going vertices, the former for 2h scattering to 2p and the latter for ph scattering to ph.

Various approximations can be obtained by restricting the terms on the right hand side of eq. (2). Including only terms 1,2 and 4 yields the pp RPA, see Ref. [4]). Including terms 1,3 and 5 yields a new antisymmetrized form of the ph RPA— the standard ph RPA is obtained by restricting the terms with a single interchange of indices to lowest order *e.g.*, $c_{cb\beta\gamma} = B_{cb\beta\gamma}/4\epsilon_{cb\beta\gamma}$. Then setting $c_{ab\alpha\beta} + c_{ba\beta\alpha} = c'_{ab\alpha\beta} - B_{ab\alpha\beta}/4\epsilon_{ab\alpha\beta}$, the equation for c' is schematically

$$c' = \frac{1}{\epsilon}\{B - Ac' - c'A + c'Bc'\} \ . \tag{3}$$

These equations are of standard form[5]) and display the lowest order correction required when antisymmetrized matrix elements are used. Finally including terms 1,2 and 3 is equivalent to carrying out a shell model diagonalization in the 2p2h space and coupling it to a single B-vertex[1]).

From the coefficients c the correlation energy can easily be obtained

$$\Delta E = \sum_{ab\alpha\beta} B_{\alpha\beta ab} c_{ab\alpha\beta} \ . \tag{4}$$

Although we shall not give them here, equations can also be given for the norm of the wavefunction and the single particle occupation probabilities. We solve eq. (2) by iteration in an angular momentum coupled basis and then deduce the correlation energy from eq. (4).

For the moment we have only a rather limited set of results. We shall discuss $2\hbar\omega$ excitations from the 0p to 1s0d shell in ^{16}O in a harmonic oscillator basis. We shall give results obtained with the interaction $0.5V_{\text{Sussex}}$, which we have used basically for checking our code against results for the correlation energy obtained with independent methods[1]. The Sussex interaction[6] is probably not very realistic and we have arbitrarily reduced its strength to avoid imaginary ph RPA eigenvalues. We shall also give results obtained with G-matrix elements calculated from the Reid soft-core potential[7]). Here we use a doubly-partitioned space to avoid double counting of the ladder diagrams and adopt average starting energies (see Ref. [1]) for details).

In the table, the first row gives the second order results and the other rows give the results from third order onwards in various approximations. The label TDA refers to the case where the diagram contains only two B-vertices, whereas in RPA any number is allowed. For the reduced Sussex interaction it is not surprising that there is little difference between TDA and RPA. The pp correlations are larger than the ph ones and the latter are further reduced when the exchange diagrams are included. This reduction is offset by including the cross-ring diagrams in the complete result (from eqs. (2) and (4)) which is very close to the sum of the standard pp and ph RPA results in this case.

		$0.5V_{\text{Sussex}}$	V_{Reid}
2nd order		−2.78	−10.73
TDA	pp	−0.53	−0.79
	ph	−0.37	−1.23
	ph+exchange	−0.20	−0.75
	complete	−0.87	−1.69
RPA	pp	−0.56	−0.98
	ph	−0.47	−1.99
	ph+exchange	−0.26	−1.16
	complete	−1.03	−2.51

Turning to the Reid potential, the RPA shows significant enhancement over the TDA. The ph result here is larger than the pp case, but it becomes comparable when the exchange diagrams are incorporated. The inclusion of the cross-ring diagrams in the complete result enhances the correlation energy. Thus the diagrams from third order onwards increase the second order result by roughly 25%. Naively adding the pp and ph results is not a good approximation here, since it overestimates the correlation energy by about 20%. Thus there is a rather delicate interplay between the various correlations and this is likely to be sensitive to the interaction employed.

Ultimately we hope to consider excitations through the 2s1d0g shell in ^{16}O, and a more restricted range in ^{40}Ca, employing both the Reid and the Bonn potentials and Hartree-Fock as well as oscillator bases. As well as the correlation energy, it will be important to study the occupation probabilities and the ground state density.

References

[1] H.A. Mavromatis, H. Müther, T. Taigel and T.T.S. Kuo, Nucl. Phys. **A470** (1987) 185

[2] H.Q. Song, S.D. Yang and T.T.S. Kuo, Nucl. Phys. **A462** (1987) 491; M.F. Jiang, T.T.S. Kuo and H. Müther, Phys. Rev. **C40** (1989) 1833

[3] B.H. Brandow, Rev. Mod. Phys. **39** (1967) 771

[4] P.J. Ellis, Nucl. Phys. **A467** (1987) 173

[5] P.J. Ellis, Nucl. Phys. **A155** (1970) 625

[6] J.P. Elliott, A.D. Jackson, H.A. Mavromatis, E.A. Sanderson and B. Singh, Nucl. Phys. **A121** (1968) 241

[7] R.V. Reid, Ann. Phys. (NY) **50** (1968) 411

MULTIFRAGMENT DECAY OF HOT NUCLEI AT INTERMEDIATE ENERGY

Y. Blumenfeld[a], N. Colonna, D.N. Delis, K. Hanold, J.C. Meng[b], G.F. Peaslee, G.J.Wozniak, and L.G. Moretto

Nuclear Science Division, Lawrence Berkeley Laboratory, Berkeley,Ca 94720

B. Libby

Department of Chemistry, University of Maryland, College Park, Md 20742

G. Guarino

Instituto Nazionale di Fisica Nucleare (INFN), Sezione di Bari, Bari 70126, Italy

N. Santoruvo and I. Iori

Universita di Milano, Milano 20133, Italy

Abstract

Multifragment events from 35 and 40 MeV/N ^{139}La + ^{12}C, ^{27}Al, ^{40}Ca and ^{51}V reactions can be assigned to sources characterized by their energy and mass through the incomplete fusion model kinematics. Excitation functions for the various multifragment channels appear to be nearly independent of the system and bombarding energy.

Intermediate energy heavy ion reactions have focused experimental[1,2] and theoretical[3,4] attention on multifragmentation and its possible association with the formation and decay of very hot nuclei[5]. A proper description of multifragment decay of hot nuclei requires the characterization of the source in terms of its size (mass, charge) and excitation energy, as well as of its branching ratios for the binary, ternary, etc. decay channels. Excitation functions for the various channels may provide the interpretative key to understanding whether the underlying decay mechanism is statistical or otherwise. Such functions have been predicted by several theoretical models, such as sequential compound nucleus decay[6] or prompt multifragment decay[3,4].

In order to study multifragment events ^{139}La beams from the Lawrence Berkeley Laboratory Bevalac were used to bombard ^{12}C, ^{27}Al, ^{40}Ca, and ^{51}V targets at an incident energy of 35 MeV/N, and ^{40}Ca and ^{51}V at 40 MeV/N. In such reverse kinematics reactions, the fragments have high kinetic energies and are emitted within a narrow cone around the beam direction. Thus, a satisfactory detection efficiency (~40% for 1 fragment) was obtained by using two close-packed square arrays of 9 Si(0.3 mm)-Si(5 mm)-plastic position sensitive telescopes placed on either side of the beam. The ΔE-E measurements yielded unit charge resolution up to Z = 57 for most telescopes. The energy calibrations were performed by running several low intensity beams with different atomic numbers directly into all the detectors and the error on these calibrations is less than 2%. The velocities of the fragments were inferred from their kinetic energy and charge, using the mass parametrization of ref. 7.

In the incomplete fusion regime a strong correlation is expected between the velocity of the hot nucleus and its mass and excitation energy. Such a correlation was recently established for the 18 MeV/N La + Ni reaction[8]. By relating the center-of-mass velocity of binary events to the mass and excitation energy of the product nucleus, it was possible to study at one bombarding energy the decay properties of hot nuclei over an excitation energy range

---

[a] On leave from Institut de Physique Nucleaire, Orsay, France

[b] On leave from Institute of Atomic Energy, Beijing, China

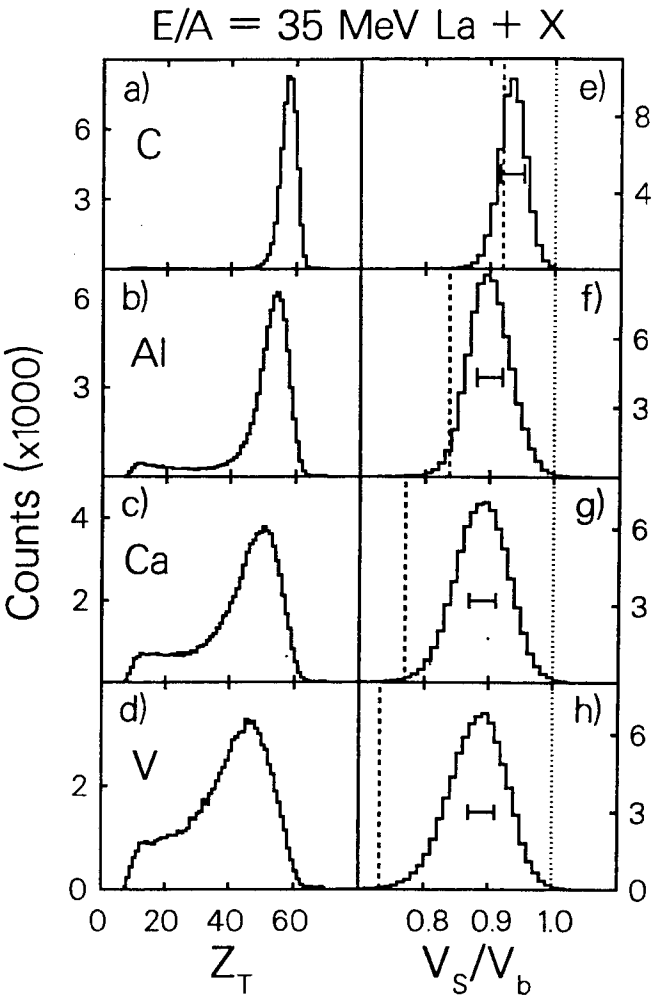

Fig. 1 : a-d) Distributions of the sum of the measured charges for 2-fold events for the 35MeV/N ^{139}La + ^{12}C, ^{27}Al, ^{40}Ca, and ^{51}V reactions. e-h) Distributions of source velocities expressed as a ratio of the source to beam velocity for the same reactions. The dotted line indicates the beam velocity and the dashed lines the source velocities expected for complete fusion. The horizontal bars indicate the expected broadening of the source velocity distribution due to light particle evaporation for the mean excitation energy.

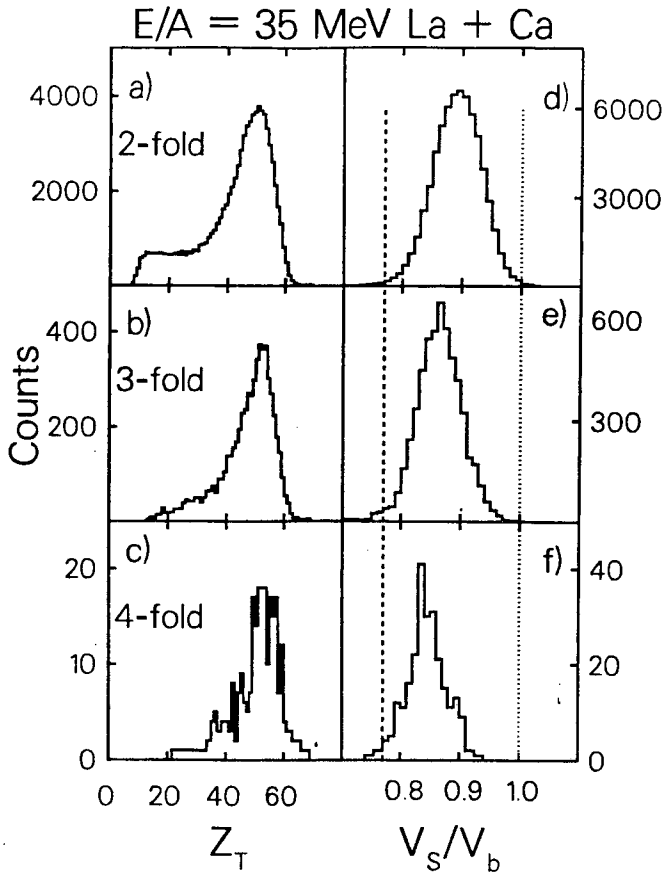

Fig. 2 : Same as fig. 1 for 2-, 3-, and 4-fold events from the ^{139}La + ^{40}Ca reaction at E_{lab} = 35MeV/N.

extending up to 4 MeV/N. In this talk we wish to show that, in a similar manner, ternary and quaternary can be associated with specific sources formed through incomplete fusion processes.

A prerequisite to such an analysis is to detect for each event a large part of the initial charge. Figure 1 (a-d) presents the distributions of the sum of the measured charges for 2-fold events at E_{lab} = 35 MeV/N. (An n-fold event is defined as an event where n fragments of charge Z>3 were detected.) For the ^{12}C target a narrow peak is observed. This peak broadens for heavier targets,reflecting the wider range of excitation energies resulting from the larger range of mass transfers, which gives rise to increasing amounts of light particle evaporation. With increasing target mass, the tailing to low Z values increases. This tail is due to 3- or 4-body events where only two bodies were detected, and shows the increasing importance of multibody reactions for the heavier targets. The same distributions for 3- and 4-fold events (figs. 2b,c for ^{139}La + ^{40}Ca) exhibit a peak at approximately the same total charge as the 2-fold events, but with a reduced low Z continuum, showing that a high percentage of these multi-fold events are essentially complete.

The following analysis is restricted to events where the total measured charge is at least 30, in order to insure a reasonable representation of the kinematical skeleton of the reaction. If the fragments originate from the decay of a single source, then its velocity is determined by
$V_S = \Sigma_i m_i V_i / \Sigma_i m_i$. In the incomplete fusion picture[5], the excitation energy E^* is approximately related to the parallel source velocity V_S by $E^* = E_b(1-V_S/V_b)$, where E_b is the bombarding energy and V_b the beam velocity.

Source velocity distributions for the ^{12}C, ^{27}Al, ^{40}Ca, and ^{51}V targets are presented in fig.1 (e-h) for the 35 MeV/N bombarding energy. The peak of the distribution shifts downwards with increasing target mass showing that, on average,more mass is picked up from the heavier targets. The peak also broadens considerably when going from the ^{12}C to ^{51}V target. Part of this width is due to the actual range of source velocities, arising presumably from different impact parameters, and part to the perturbation introduced by light particle evaporation prior and subsequent to heavy fragment emission. This "noise" has been estimated with the statistical decay code GEMINI[7], filtered by the appropriate detector geometry, and is represented by the horizontal bars on fig.1 (e-h). In the case of ^{12}C the width can be explained almost entirely by light particle evaporation, showing that, due to the interplay between the incomplete fusion mechanism and the complex fragment decay probability, a very limited range of excitation energies contributes to complex fragment emission. However, this is no longer the case for the heavier targets, where a large range of excitation energies is indeed observed.

When the events are separated according to the fragment multiplicity (see fig.2 (d-f)), the requirement of a larger multiplicity of complex fragments selects out events with lower source velocities, i.e. higher excitation energies. For the ^{40}Ca target at E_{lab} = 35 MeV/N, the estimated most probable excitation energies are 530, 660, and 750 MeV for 2-, 3-, and 4-fold events, respectively. The same trend is observed for all targets. A similar result was recently observed in the $^{20}Ne+ {}^{197}Au$ reaction at 60 MeV/N, but only for 2- and 3- body final states[9].

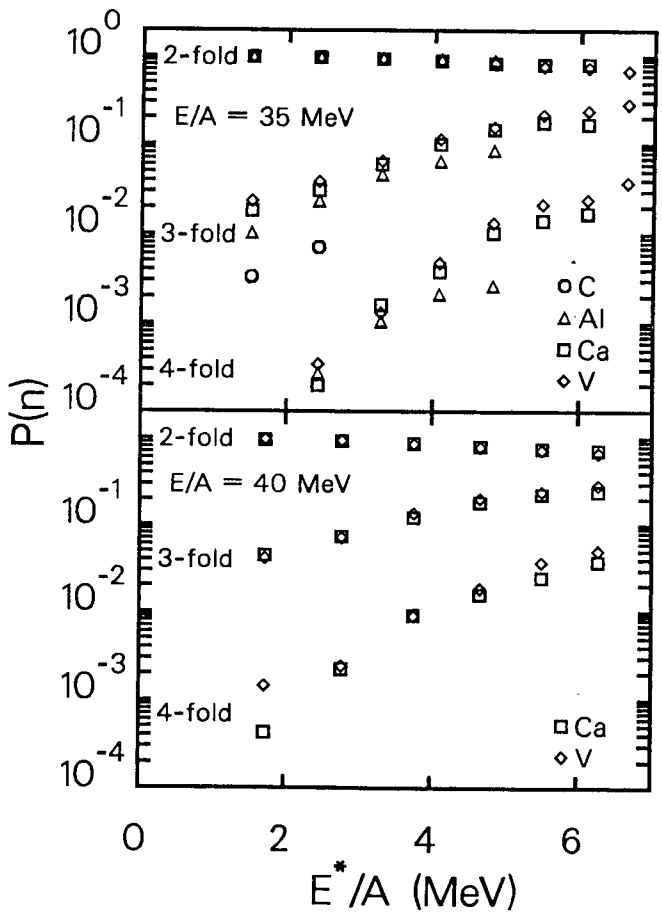

Fig.3. : Proportion of 2-, 3-, and 4-fold events as a function of excitation energy per nucleon for the targets studied at E_{lab} = 35 MeV/N (top) and 40 MeV/N (bottom). The estimated masses of the hot nuclei vary from 145 at 2 MeV/N to 175 at 6 MeV/N

To investigate the behavior of nuclei as their excitation energy increases,excitation functions for the multi-fold events have been constructed from the results obtained for the various source velocities. The cross section for multibody events at a given excitation energy depends on the probability of producing nuclei with this excitation energy via the incomplete fusion process. In order to remove this dependence, we have plotted the proportion of n-fold events with respect to the total number of coincidence events:
$P(n) = N(n)/(N(2)+N(3)+N(4)+ ....)$, where N(n) is the number of n-fold events. These excitation functions (fig.3) have not been corrected for the detection efficiency. Such a correction requires knowledge of the precise kinematical nature of the events, such as mass distributions and relative velocities of the fragments and will not be attempted here. Nevertheless, several remarkable features can be noted.

First, the probabilities for 3- and 4-fold events increase substantially with the excitation energy of the source up to the highest energies observed (~1000 MeV or 6 MeV/N). Such behavior would be expected from any statistical model and is an *a posteriori* verification of the relation between source velocity and excitation energy over the entire source velocity range studied. This energy dependence also confirms that the width of the velocity distribution originates mostly in the incomplete fusion process, and is only partly due to sequential light particle decay.

Second, the relative proportions of multi-fold events for the three heaviest targets and the two bombarding

energies are very similar, suggesting that the sources produced in these reactions depend mainly on how much mass is picked up by the projectile from the target and relatively little on the actual nature of the target. This is precisely what constitutes the essence of the incomplete fusion model! A closer look at fig.3 shows a slight decrease of the multi-fold probability for lighter targets, as wellas for the lower bombarding energy for a given target. The transition state model of statistical decay[6] predicts a strong decrease of the complex fragment decay probability with decreasing angular momentum[10]. Thus an additional source of the differences could be that the hot nuclei are formed in the various reactions with slightly different angular momenta.

Finally, the proportion of multi-fold events increases smoothly with excitation energy up to approximately 6MeV/N. The statistical multifragmentation calculations of Bondorf et al.[3] predict a sudden rise in the multibody probability at ~3 MeV/N for a nucleus of mass 100. Gross et al.[4] predict a similar transition towards nuclear cracking at an excitation energy of ~5 MeV/N for a ^{131}Xe nucleus. Experimentally we see no evidence for such phase transitions, and the data suggest that the decay of the hot nuclei under study (A~160) is governed by the same mechanism up to an excitation energy approaching the total binding energy of these nuclei.

In this talk we have demonstrated a technique which permits the characterization of hot nuclei and of their decay over a wide range of excitation energies using a single bombarding energy. The source velocity technique was extended to multibody events and employed in conjunctionwith the incomplete fusion model to estimate the excitation energy on an event-by-event basis. This, in turn, has allowed us to present excitation functions for multifragment events. These excitation functions are largely independent of target-projectile combination and of bombarding energy, lending support to the incomplete fusion picture and to the idea of an intermediate system whose decay properties depend only on its excitation energy and angular momentum. Up to an excitation energy of 1000 MeV (~6 MeV/N) no evidence for a phase transition towards nuclear cracking was found.

This work was supported by the Director, Office of Energy Research, Office of High Energy and Nuclear Physics, Division of Nuclear Physics, of the U.S. Department of Energy under Contract No. DE-AC03-76SF00098.

References

1) Y.D.Kim et al., Phys. Rev. Lett. **63**, 494 (1989)
2) R.Trockel et al., Phys. Rev. **C39**, 729 (1989)
3) J.Bondorf, R.Donangelo, I.N.Mishustin, and H.Schulz, Nucl. Phys. **A444**, 460 (1985)
4) D.H.E. Gross, Yu-ming Zheng and H. Massman, Phys. Lett. **B200**, 397 (1987)
5) D. Guerreau in *Int'l. School on Nuclear Physics : Nuclear matter and Heavy Ion Collisions*, Les Houches, France Feb. 1989, Preprint Ganil P89-07
6) L.G. Moretto, Nucl. Phys. **A247**, 211 (1975)
7) R.J.Charity et al., Nucl. Phys. **A483**, 371 (1988)
8) N.Colonna et al., Phys. Rev. Lett. **62**, 1833 (1989)
9) R.Bougault et al., Phys. Lett. **B232**, 291 (1989)
10) R.J.Charity et al., Nucl. Phys. **A476**, 516 (1988)

Sequential Emission and Multi-Fragmentation at Intermediate Energy

D.A. Cebra, S. Howden, J. Karn, A. Nadasen[a], C.A. Ogilvie[b], A. Vander Molen, G.D. Westfall, W.K. Wilson, J.S. Winfield

National Superconducting Cyclotron Laboratory and
Department of Physics and Astronomy
Michigan State University, East Lansing, MI 48824-1321, USA

E. Norbeck

Department of Physics
University of Iowa, Iowa City, IA 52242 USA

Multi-fragmentation is a reaction process that has been proposed to occur on short time-scales and is expected to become the dominant form of nuclear disassembly for excitation energies above 4 MeV/nucleon[1,2]. The main feature that distinguishes this process from other disassembly mechanisms is the copious production of intermediate mass fragments (IMFs). As the excitation energy of the nuclear system is increased, the magnitude of the internal pressure and density fluctuations increases rapidly. These fluctuations tear the nucleus apart when the energy contained within them exceeds the binding energy of the system. Information about the growth rate of the fluctuations will provide insights on the equation of state of nuclear matter. The most direct measurement is a determination of the threshold for the onset of multi-fragmentation.

Simple observation of exit channels containing multiple IMFs has been demonstrated not to be sufficient to conclusively identify a multi-fragmentation process[3]. Several recent studies have probed the question of the time-scale of the disassembly process using observables that are sensitive to of the disassembly process[4,5,6,7]. These studies span a range of excitation energies from 1 MeV/nucleon up to 6 MeV/nucleon. All the studies have been able to reproduce the studied observables with models that assume a form of sequential decay leading to a multi-particle final state. Thus no conclusive evidence of the existence of the multi-fragmentation process has been presented prior to this workshop.

This line of analysis which addresses the determination of the disassembly mechanism was introduced in a study of the event shape distributions produced from the reaction Ar + V at 35 MeV/n[8]. At that energy, which corresponds to 8 MeV/n of excitation energy for the combined system if one assumes complete stopping of the projectile participants by the target participants, the measured event shape distribution was best reproduced by a simulation modeling a sequential decay process. This conclusion is in agreement with previous studies which had explored lower excitation energies. In follow up experiment, the same system was studied for bombarding energies up to 85 MeV/nucleon. An early report on the results at these higher incident energies suggested that the sequential model failed to reproduce the experimental event shape distributions for energies above 35 MeV/nucleon[9]. This paper presents the final results of the event shape analysis for the higher energy data. As the incident energy is increased, the predictions from a model of a simultaneous multi-fragmentation process, which assumes isotropic emission of fragments, approach the experimental distributions.

The data were acquired using the MSU 4π Array[10]. Argon beams of 45, 55, 65, 75, and 85 MeV/nucleon were provided by the K1200 cyclotron. These data compliment an earlier set which was acquired using a 35 MeV/nucleon beam which was produced by the K500 cyclotron. For these experiments, the 4π Array consisted of 215 phoswich detectors and covered approximately **11** steradians solid angle. The detectors provided charge, mass and energy information for light charged particles (A from 1 to 12). The low energy threshold for detection of charged particles was 4 MeV/nucleon, however 20 MeV/nucleon was required to properly identify the fragments.

An estimate of the impact parameter was made for every event and only those from the most central collisions were used for this analysis. The estimate was made based on the charge detected with center of mass rapidity greater than 75% of that of the target and less than 75% of that of the projectile. This observable ostensibly measures the mass in the interaction region, which is directly proportional to the impact parameter. Spectator matter from either the target or the projectile should be rejected by the rapidity requirements. The distribution of impact parameters contained within the *central* bin is expected to range from 0 to 0.5 B_{max} and to be peaked around 0.3 B_{max}[11], where B_{max} is defined as R_{Ar} + R_V. This distribution of impact parameters produces an interaction region that contain 70 +/− 20 participants. The additional nucleons are assumed to be spectators and therefore are ignored for this analysis.

The data were analyzed using a sphericity/coplanarity analysis which was introduced by Fai[2] and applied to this problem by Lopez and Randrup[3]. In this analysis

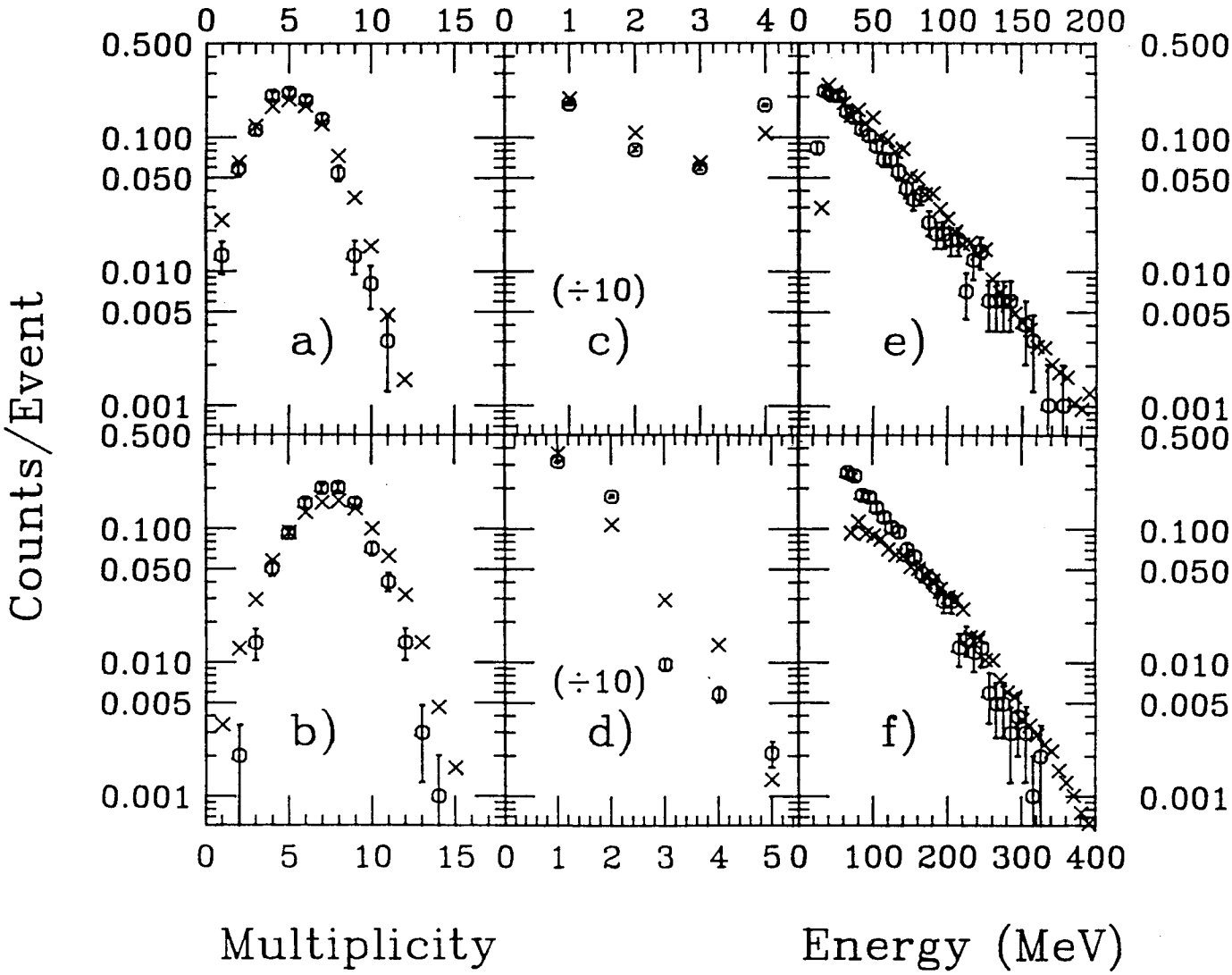

technique, one first defines a kinetic flow tensor

$$\mathbf{F}_{ij} = \sum_{n=1}^{N} \frac{\mathbf{p}_i^n \mathbf{p}_j^n}{2m_n} \tag{1}$$

The normalized and ordered eigenvalues (q_1, q_2, q_3) of this tensor are then used to define two shape parameters: **Sphericity** ($S = \frac{3}{2}(1 - q_3)$) and **Coplanarity** ($C = \frac{\sqrt{3}}{2}(q_2 - q_1)$). The data presented in this contribution are in the form of sphericity versus coplanarity distributions or their centroids.

A simulation that models a sequential decay process was developed. The primary constraint upon this simulation was that it reproduce the basic observables of the experimental data. The shape analysis is very sensitive to changes in these basic observables and a failure to match at this level would invalidate the more detailed analysis. Fig. 1 displays a comparison of the experimental data to the predictions of the simulation. The observables compared are a) multiplicity of identified particles, b) the total charged particle multiplicity, c) mass distributions, d) charge distributions, e) proton kinetic energy spectra, and f) helium kinetic energy spectra. The circles represent the simulation while the X's represent the experimental data. The figure presents data at 65 MeV/nucleon, the quality of the fit was similar for all of the other energies studied.

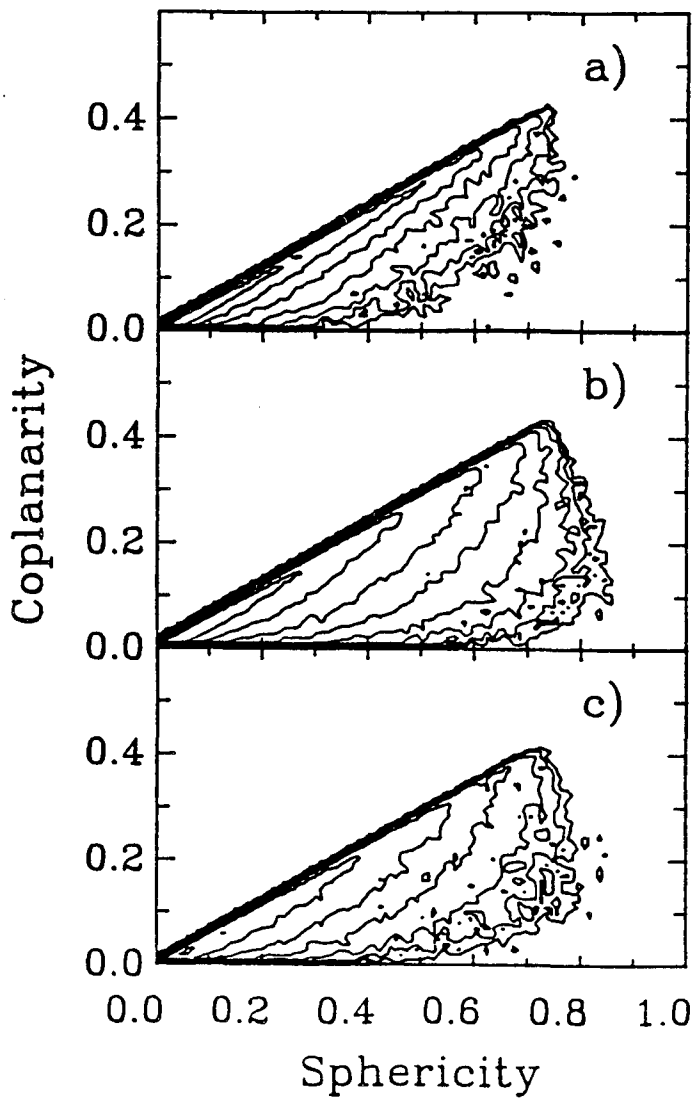

Fig. 2 displays contour plots of the shape distributions at 65 MeV/nucleon for a) the sequential simulation, b) the experimental data, and c) the simultaneous simulation. Events for the simultaneous simulation were generated from events from the sequential simulation. This constrained the basic observables of the two simulations to be identical.

Fig. 3 displays the centroids of the sphericity distributions for the experimental data and for the simulations as a function of incident energy. The diamonds represent the sequential simulation, the squares represent the experimental data, and the circles represent the simultaneous simulation. One can see from this plot that the data are reproduced extremely well by the sequential simulation at 35 MeV/nucleon. As the incident energy is increased, the data fall between the two predictions. Clearly between 35 MeV/nucleon and 65 MeV/nucleon

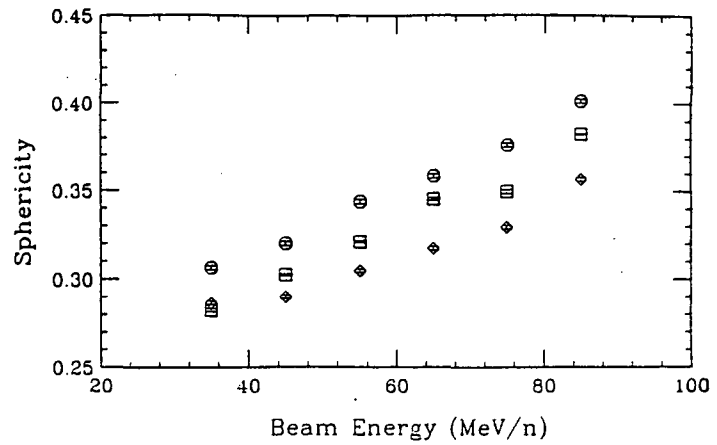

there is a progression from the sequential extreme to the simultaneous extreme. The data never reach the predictions of the simultaneous simulation, this may be because there are other effects that induce some elongations in the experimental data. For the purposes of this analysis, the definition of simultaneous has corresponded to completely isotropic emission, which is an unrealistic requirement.

The data described in this work suggest that the onset of simultaneous multi-fragmentation may occur at excitation energies above eight MeV/nucleon, which is the highest excitation energy for which a sequential model can still successfully reproduce the experimental data. The region from eight up to twenty MeV/nucleon may be a transition region where there is either a mixing of reaction processes, a mixing of events representing the alternate processes, or a transitory process. For the 35 MeV/nucleon case, the velocities are below the Fermi velocity in the center of mass. For this case one expects mean field effects to be strong and suggests that sequential decay may play an important role in the disassembly process.

This work was supported in part by the National Science Foundation under grant No. PHY-86-11210. The collaboration with Dr. Norbeck was supported by a grant from the Research Corporation.

a. Permanent address, University of Michigan, 4901 Evergreen Road, Dearborn MI, 48128.
b. Current address, GSI KPIII, Postfach 11 05 52, Planckstr 1, D-6100 Darmstadt 11, West Germany.

[1] J.P. Bondorf et al., Phys. Lett. **B150** 57 (1985).
[2] G. Fai and J. Randrup, Nucl. Phys. **A404** 551 (1983).
[3] J.A. Lopez and J. Randrup, Nucl. Phys. **A491** 477 (1989).
[4] J. Pochodzalla et al., Nucl. Phys. **A404** 353c (1989).
[5] R. Bougault et al., Nucl. Phys. **A404** 255c (1988).
[6] J. Pouliot et al., Phys. Lett. **B223** 16 (1989).
[7] B.A. Harmon et al., Phys. Lett. (in press).
[8] D.A. Cebra et al., MSUCL-704 (1989).
[9] D.A. Cebra et al., BAPS **34** 1826 (1989).
[10] G.D. Westfall et al., Nucl. Inst. Meth. **A238** 347 (1985).
[11] C.A. Ogilvie et al., Phys. Rev. **C40** 654 (1989).

Sequential Binary Decay and Multifragmentation in Light Projectile Breakup

Jorge Alberto López
Physics Dept., California Polytechnic State University,
San Luis Obispo, CA 93407

Among the possible mechanisms that lead to the production of fragments in intermediate energy reactions, binary sequential decay (BSD) and simultaneous production of fragments, or multifragmentation (MF), correspond to two viable extremes. Based on the fact that the Coulomb repulsion is drastically different for these two modes of nuclear decay, it was suggested [1] to use the kinematical signatures to distinguish between these two mechanisms. In this work we compare some kinematical properties of these two decays with those observed by Pouliout et al. [2] in the decay of ^{16}O at 32.5 MeV/A and of ^{20}Ne at 26.5 MeV/A. This work has been fully described elsewhere [3].

In the experiment, the projectiles (^{16}O, and ^{20}Ne) were excited peripherally by ^{197}Au, ^{27}Al, ^{12}C and ^{9}Be targets. The decay products were detected by an array of 34 phoswish detectors [3] that allowed determination, in some events, of energy, charge and direction of emission of all the particles. The resulting data were then compared to computer simulated results.

To simulate a sequential binary decay of an excited nucleus, a Montecarlo method based on an iterated Bohr-Wheeler treatment was used. The calculation was done as discussed in [1] except for the parametrization of the fission barriers [3]. This method produced mass distributions and velocity distributions characteristic of the SBD mechanism.

To produce multifragmentation events suitable for comparison, we again followed the prescription given in [1] that results in events with the same mass distribution and total energy as those of the SBD method. Briefly, in each event, we used the same particles obtained by the sequential decay, re-arrange them randomly in a volume at half the nuclear density, divided the total energy as Coulomb and kinetic energies and let the particles emerge along their Coulomb trajectories. Additionally, in both of these simulations we used the experimentally observed excitation energies for the decaying nucleus and the results were filtered through the experimental apparatus.

For comparison between the calculations and experimental data we look at the distribution of relative angles between emitted particles. Fig. 1 shows the filtered calculations for the two methods of decay used, normalized by the ratio of calculated events to experimental events (after filtering), as well as the experimental distribution for the case $^{16}O \rightarrow 4\,He$. The sequential decay appears to reproduce the observed distribution better than multifragmentation. Fig. 2 shows, not the mean angle between any two particles which is found not to be too relevant, but the standard deviation of the angle distribution for the experimental and calculated data for other various channels. Again, the sequential decay gives a somewhat better description of the experimental data.

As a second test, a sphericity-coplanarity analysis was used. Table 1 shows the average values of these coordinates for each channel. Again we observe a better agreement with the sequential decay calculation than with multifragmentation. The exception being the B-He-H Channel, presumably due to the small amount of particles present in that channel. Given these comparisons we conclude that the present exercise does not provide any evidence for multifragmentation of the projectile.

References

[1] J.A. López and J. Randrup, Nucl. Phys. **A491**, (1989) 477.
[2] Pouliot et al., Phys. Lett. **223**B, (1989), 16.
[3] B.A. Harmon et al., Phys. Lett., in print, (1990)

Table 1.

	B-He-H		He-He-He-He		He-He-He-H-H	
	Sph	Cop	Sph	Cop	Sph	Cop
MF	.138±.002	.068±.001	.291±.003	.14±.001	.231±.004	.094±.002
SD	.07±.002	.033±.001	.19±.003	.097±.002	.163±.005	.075±.003
EX	.122±.003	.055±.001	.191±.004	.101±.002	.168±.006	.08±.003

Fig. 1 Relative angle distribution for the ^{16}O -> 4 He channel

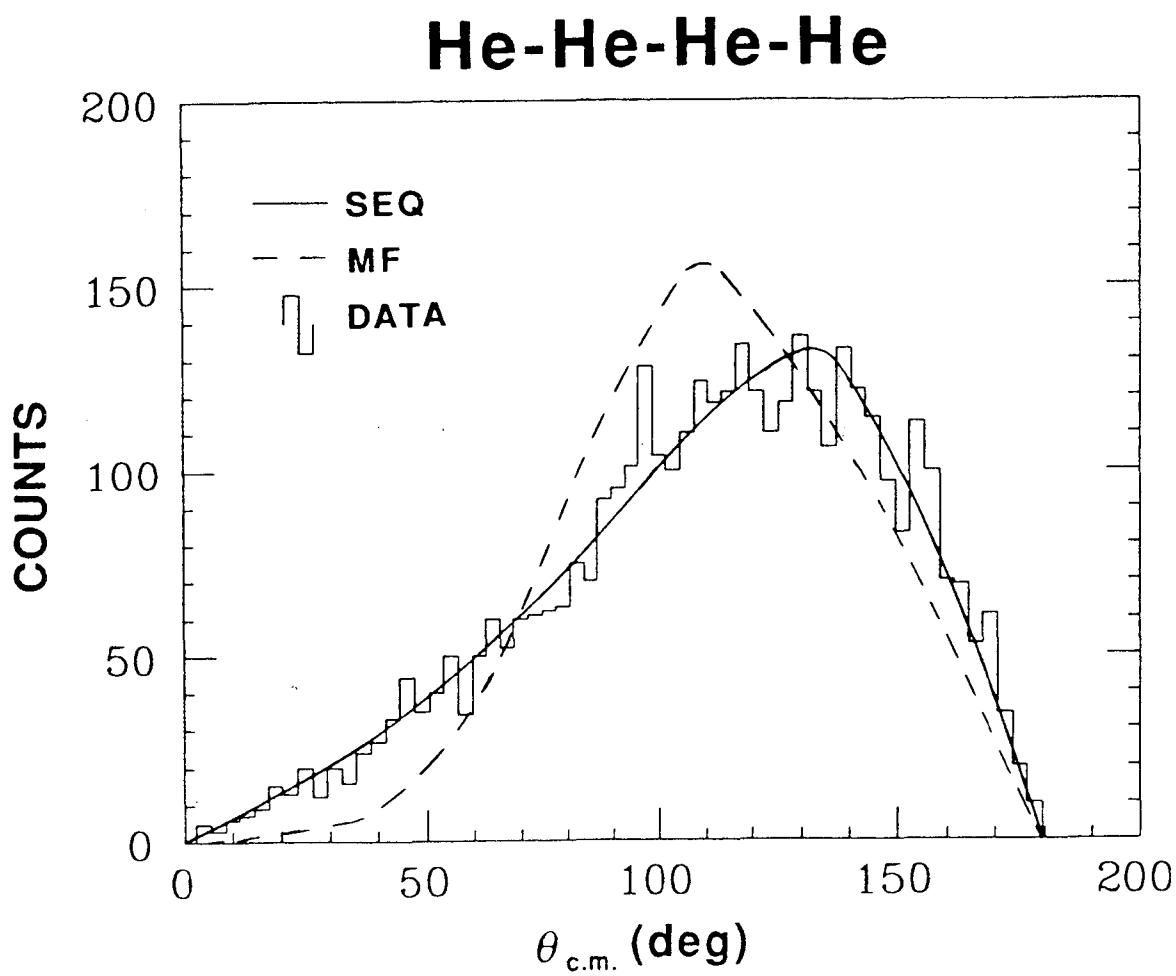

XBL 899-3291

Fig. 2 Standard deviations for the relative angle distribution of the decay of ^{16}O into several channels. The solid line represents the experimental results and the dashed lines the two calculations.

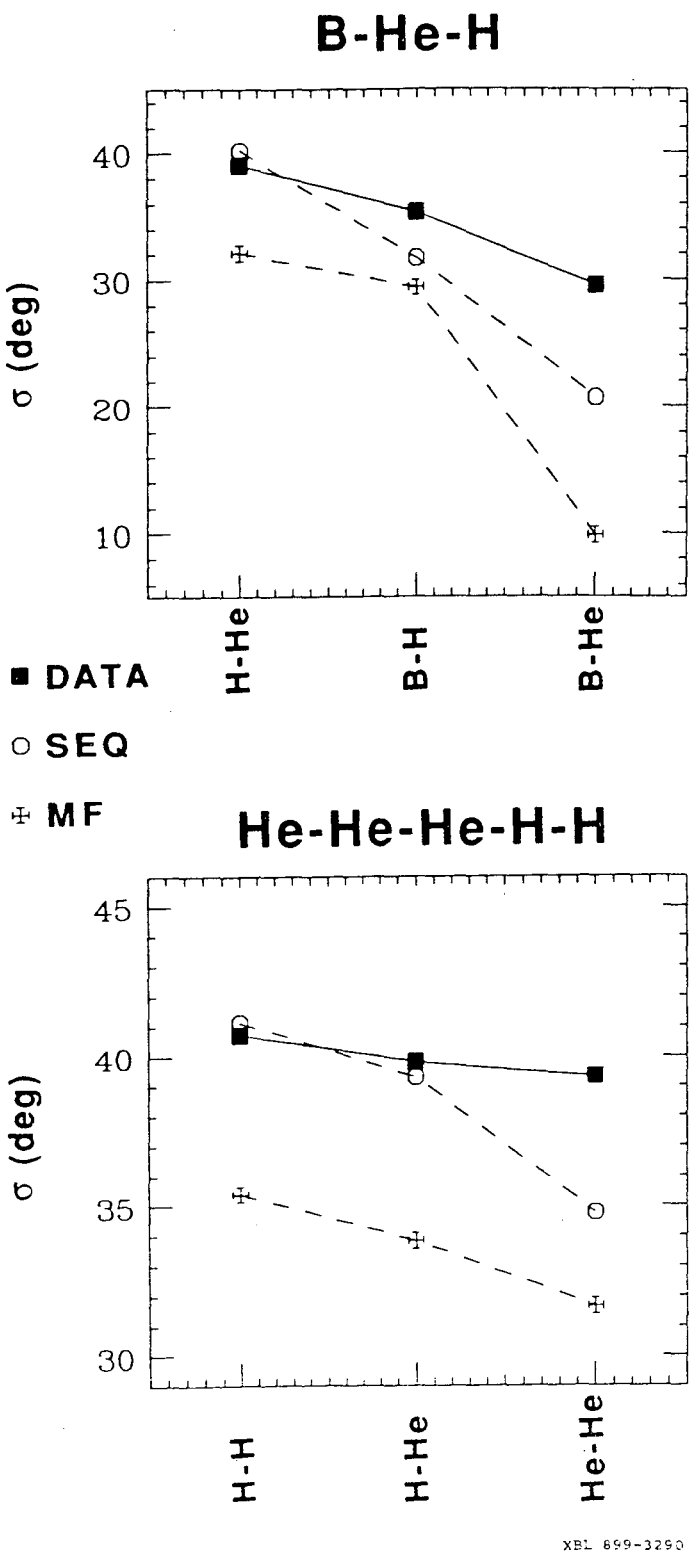

Towards a theoretical analysis of Ne on Ne at 45 MeV per nucleon

J. Gallego
Department of Physics, McGill University, Montréal, PQ, Canada, H3A 2T8

I. Introduction

In the present work we address the problem of solving the BUU equation

$$\frac{\partial f(\vec{r},\vec{p},t)}{\partial t} + \frac{\vec{p}}{m}\nabla_r f(\vec{r},\vec{p},t) - \nabla_r \mathcal{U}(\vec{r},t)\nabla_p f(\vec{r},\vec{p},t) = \mathrm{I_c}\,, \tag{1}$$

where $f(\vec{r},\vec{p},t)$ is the classical phase space density, $\mathcal{U}(\vec{r},t)$ is the self-consistent nuclear potential and $\mathrm{I_c}$ is the Boltzmann collision integral

$$\mathrm{I_c} = (2\pi)^3 \int \mathrm{d}^3p_3\,\mathrm{d}^3p_4\;\mathrm{d}\Omega\frac{\mathrm{d}\sigma_{\mathrm{NN}}}{\mathrm{d}\Omega}\,v_{12}\,\delta^3(\vec{p}_1+\vec{p}_2-\vec{p}_3-\vec{p}_4)$$
$$\times\,[f_1f_2(1-f_3)(1-f_4) - f_3f_4(1-f_1)(1-f_2)] \tag{2}$$

where the indices 1 and 2 refer to the incoming nucleons, 3 and 4 to the outgoing ones, σ_{NN} is the total nucleon-nucleon cross-section, v_{12} is the relative velocity of the incoming nucleons and f_i is the Pauli occupation factor around nucleon i.

The solution of (1) is often implemented by the test particle method (TPM),[1] and for many observables it gives very good results. In this paper we present a version that corrects some of its numerical inaccuracies. We are now investigating how well it can reproduce nuclear fragmentation. Even though this study is at present incomplete, we have some preliminary results for ^{20}Ne on ^{20}Ne at 45 MeV per nucleon, which we can compare with experimental data available.

II. Energy conservation - The Lattice Hamiltonian approach

We follow here the method of Lenk and Pandharipande [2] which guarantees energy conservation. Their approach is known as the Lattice Hamiltonian Method. The basic assumption is that test particles have finite density distributions $\rho_i(\vec{r}) = S(\vec{r}-\vec{r}_i)$. The density at a lattice site α centered at $\vec{r}_\alpha$ of volume $(\delta x)^3$ is

$$\rho_\alpha \equiv \rho(\vec{r}) = \sum_i^{N_{\mathrm{T}}A} S(\vec{r}_\alpha - \vec{r}_i)\,. \tag{3}$$

One can then define an *exact* lattice Hamiltonian as

$$\mathcal{H} = \sum_i^{N_{\mathrm{T}}A}\frac{p_i^2}{2m} + N_{\mathrm{T}}\,(\delta x)^3\sum_\alpha \varepsilon_\alpha\,, \tag{4}$$

where ε_α is the energy density computed at the center of the cell site. From (4) one can compute the equations of motion

$$\dot{r}_i^s = \frac{\partial \mathcal{H}}{\partial p_i^s} = \frac{p_i^s}{m} \quad , \quad \dot{p}_i^s = -\frac{\partial \mathcal{H}}{\partial r_i^s} = -N_{\mathrm{T}}\,(\delta x)^3 \sum_\alpha \mathcal{U}_\alpha \frac{\partial \rho_\alpha}{\partial r_i^s} \,. \tag{5}$$

The only constraint that the folding function $S(\vec{r}_\alpha - \vec{r}_i)$ must satisfy at all times is

$$(\delta x)^3 \sum_\alpha S(\vec{r}_\alpha - \vec{r}) = \frac{1}{N_{\mathrm{T}}} \,, \tag{6}$$

which guarantees that the sum of ρ_α over cell sites is equal to the number of nucleons. In our calculations we have used

$$S(\vec{r}_\alpha - \vec{r}_i) = N_{\mathrm{T}}{}^{-1} b^{-3} \prod_u \Theta\,(1 - |\Delta_{\alpha i}^u|) \,, \tag{7}$$

with $\Delta_{\alpha i}^u = (r_\alpha^u - r_i^u)\,/\,b$.

We stress once again the fact that energy conservation is built into the definition of the lattice Hamiltonian. Indeed, in numerical tests done with ^{2}H and ^{40}Ca moving through the lattice with beam energies of 4, 20 and 100 MeV per nucleon for 100 fmc^{-1}, energy was conserved to 1 part in 10^4 in single precision calculations, and to 1 part in 10^6 in double precision. Furthermore, for the ^{2}H system, no more than 20 test particles (of a total of 2000) escaped from the nucleus, with an even lower proportion for ^{40}Ca.

III. Fluctuations and the collision integral

The role of fluctuations in $f(\vec{r}, \vec{p}, t)$ as seeds for the onset of fragmentation was recognized long ago. In BUU codes, the collision integral is solved by cascade-type algorithms, where one considers the $N_{\mathrm{T}}A$ test particles as representing N_{T} ensembles of A nucleons, which suffer intra-ensemble two-body collisions. Considered separately, each ensemble gives rise to fluctuations, but the sum over all the ensembles produces averaged quantities, and the fluctuations are washed out.

Bauer, Bertsch and Das Gupta [3] reformulate the problem differently: they argue that fluctuations result from collisions between physical two nucleons, and thus each collision should change the momenta of $2N_{\mathrm{T}}$ test nucleons, not just those of the two that collided. Summing over all the collisions no longer washes out the fluctuations, and so each simulations represents a physical event.[4] Of course, one must now simulate many runs to calculate any physical observable.

IV. Some further considerations

In peripheral and grazing collisions, the nuclear surface plays an important role. If Yukawa-type interactions are included in the potential the stationary solutions naturally develop smooth surfaces. These solutions can be calculated using the Thomas-Fermi approximation[5] adjusting the depth and range of the Yukawa interaction to reproduce the surface depths and binding energies of intermediate-sized nuclei.

Since Coulomb forces play an important role in final state interactions between the emerging clusters, we have also included them in our calculation. Both the Yukawa and the Coulomb fields

are calculated at each time step by solving numerically the respective differential equations, with appropriate boundary conditions.

A final point about the code: statistical fluctuations in the Monte-Carlo sampling of the initial states gives rise to monopole and quadrupole oscillations of the nuclei. To reduce the effects of such oscillations, the sampling must be done carefully. Moreover, the discreteness of the grid gives rise to some initial deformation of the nuclei, resulting again in damped oscillations, so all the collision simulations started with the nuclei separated by 10 fm along the beam direction to allow these oscillations to die down before the nuclei collide.

V. Preliminary results

A collaboration between Michigan State, Toronto and Laval universities and Atomic Energy of Canada Ltd. is studying the fragmentation of medium-sized systems at intermediate energies. In the experiment they use a 4π detector, whose major components:

- TASCC forward array, with angular coverage from 2.5 to 17 degrees for the measuring charged fragments (for $E \geq 15$ MeV per nucleon).
- MSU 4π array, with angular coverage from 19 to 161 degrees, measuring charged fragment multiplicities and energies (for $E \geq 17$ MeV per nucleon).
- Si stack telescope located a 47 degrees, measuring the mass, charge and energy of charged fragments (for $E \geq 4$ MeV per nucleon).

As mentioned, we are studying ^{20}Ne on ^{20}Ne at 45 MeV per nucleon. In the code we have set $N_T = 100$, $(\delta x)^3 = 1$ fm^3, $b = 1$ fm, $\sigma_{NN} = 55$ mb, and the potential parameters $A = -250.18$ MeV, $B = 330.71$ MeV and $\sigma = \frac{7}{6}$ for the Skyrme interaction and $V_Y = -106.98$ MeV and $a = 0.45979$ fm for the Yukawa interaction.[5] The collisions were stopped after 200 fmc^{-1}, when clusters have stopped fragmenting. At the moment we have 650 simulations at impact parameters ranging from 0.1 to 6 fm.

One of our major problems we still have is the cluster identification. We have tried different approaches, but none of them are yet satisfactory. For the results presented in figures 1 and 2, we have used a rather simple algorithm: the test nucleons are grouped into nucleons according to their relative distances in phase-space, and we consider two nucleons to be bound if the distance between their average positions is less than 2 fm. This method has the advantage that it produces clusters with integer mass and charge.

VI. Conclusion

We believe that the code presented here is an improvement over traditional BUU codes, and that it is appropriate for the study of fragmentations since fluctuations are correctly put in. Our preliminary results we have are encouraging, but it is also clear that more work has to be put into the clustering analysis. Further extensions of the code, such as including momentum-dependent interactions, should allow us to study a wider variety of observables.

References

[1] G.F. Bertsch and S. Das Gupta, Phys. Rep. **160** (1988) 189.

[2]R. Lenk and V. Pandharipande, Phys. Rev. **C39** (1989) 2242.

[3]W. Bauer, G.F. Bertsch and S. Das Gupta, Phys. Rev **C29** (1984) 673.

[4]S. Das Gupta, Nucl. Phys. **A417** (1987) 417.

[5]S.J. Lee, H.H. Gan, E.D. Cooper and S. Das Gupta, Phys. Rev **C40** (1989) 2585.

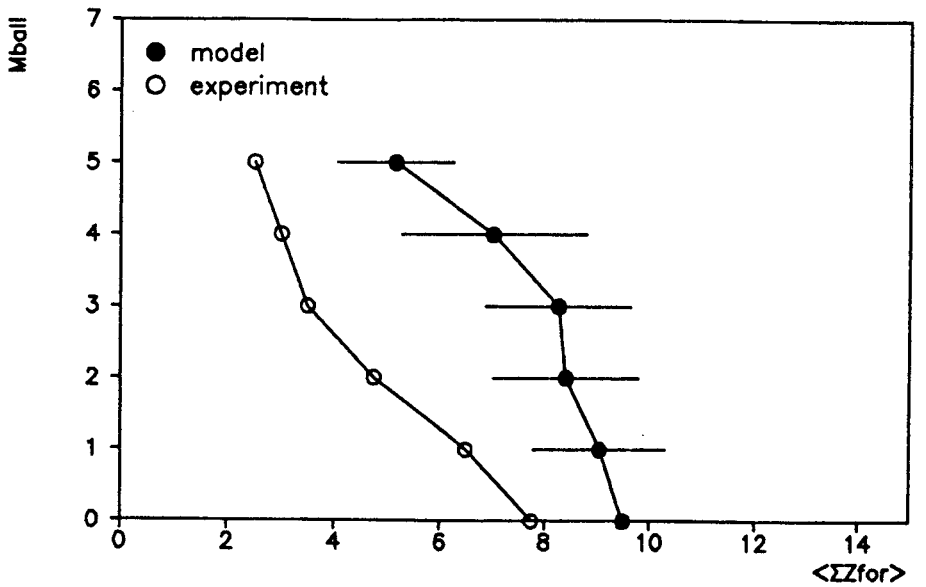

FIG. 1. Average charge in the forward array vs. charged fragment multiplicity in the 4π array. The discrepancy high ball multiplicites (≥ 3) due to low statistics.

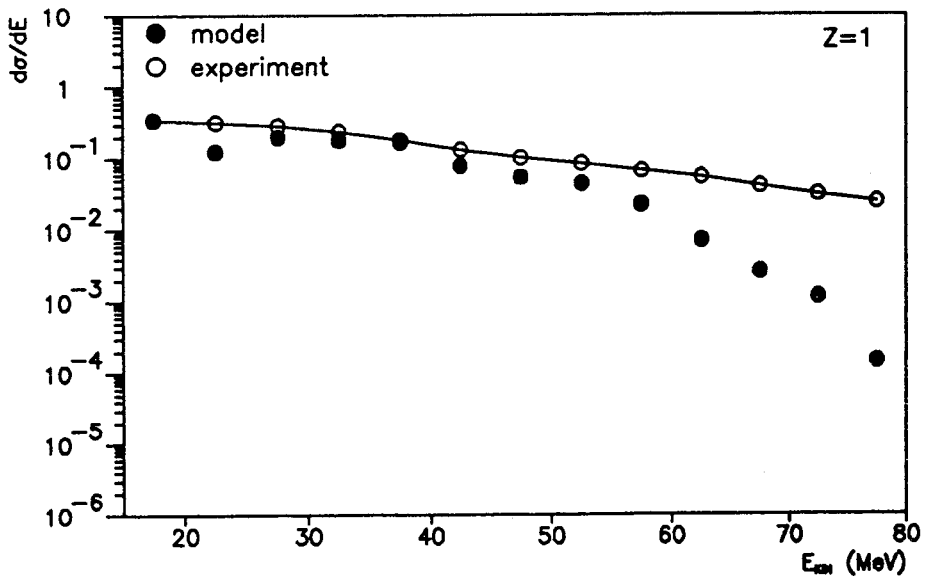

FIG. 2. Differential cross section for Z=1 fragments for $19 \leq \theta \leq 30$ in the lab frame. The discrepancies at the high-energy range are due to the low statistics we have. Harder to explain is the dip around 25 MeV.

A ONE-BODY TRANSPORT MODEL OF FLUCTUATION PROCESSES IN NUCLEAR COLLISIONS

S. Ayik*
Tennessee Technological University, Cookeville, TN 38505, USA

and

C. Gregoire, E. Suraud, J. Stryjewski, M. Belkacem
GANIL, B.P. 5027, F14021, Caen Cedes, France

1. INTRODUCTION

Many aspects of a many-body system can be described in terms of one-body transport models in which the system at any time is characterized by its single-particle density rather than by the full many-body information. In these one-body models, evaluation of the single-particle density is determined by a transport equation which contains the self–consistent mean-field potential and a collision term due to binary two-body collisions. Recently, this approach in a semi-classical limit with a Boltzmann-Uehling-Uhlenbeck (BUU) form of a collision term has been applied to nuclear collisions at intermediate energies [1]. Common to all one-body models, only the average effects of two-body collisions are retained in the equation of motion and higher order correlations are entirely neglected. This approximation corresponds to an ensemble averaging which is evident, for example, from the "molecular chaos assumption" introduced in derivation of Boltzmann equation. As a result, these one-body models determine the ensemble averaged single-particle density and cannot provide a description for the fluctuation processes in nuclear collisions. On the other hand, at low and intermediate energies dynamical fluctuations are substantial due to large available phase space for decay into many final states. Therefore, it is of great interest to improve one-body transport models by incorporating dynamical fluctuations due to high order correlations into the equation of motion.

2. STOCHASTIC BUU EQUATION

Recently, we proposed an extension of one-body transport theory by incorporating fluctuations into the equation of motion in a statistical approximation [2]. In a dilute system, dynamics is mainly determined by two-body collisions, which (i) produce dissipation by randomizing the single-particle momentum distribution and (ii) induce fluctuation by propagating correlations in phase-space. These two effects can be incorporated into the equation of motion for the single-particle density. This yields in semi-classical limit a stochastic BUU equation, or Langevin-Boltzmann equation, for the fluctuating single-particle density,

$$\left[\frac{\partial}{\partial t} + \frac{\mathbf{p}}{m} \cdot \nabla_r - \nabla_r U(f) \cdot \nabla_p\right] f(\mathbf{r},\mathbf{p},t) = K(f) + \delta K(\mathbf{r},\mathbf{p},t). \tag{2.1}$$

Here, K(f) has the form of the usual collision term in terms of fluctuating density,

$$K(f_1) = \frac{g}{(2\pi\hbar)^3} \int dp_2 dp_3 dp_4 W(12;34)[f_3 f_4 \tilde{f}_1 \tilde{f}_2 - \tilde{f}_3 \tilde{f}_4 f_1 f_2] \tag{2.2}$$

where g is the degeneracy factor, $f_j = f(r_j,p_j,t)$, $\tilde{f}_j = 1 - f_j$ and the spin-isospin averaged

*Work is supported in part by US–DOE grant DE–FG05–89ER40350.

transition rates are given in terms of N-N cross-section by

$$W(12;34) = \frac{1}{2m^2}\frac{d\sigma}{d\Omega}\delta(\mathbf{p}_1 + \mathbf{p}_2 - \mathbf{p}_3 - \mathbf{p}_4)\delta(\epsilon_1 + \epsilon_2 - \epsilon_3 - \epsilon_4). \tag{2.3}$$

The additional term δK in eq. (2.1) arises from correlations not accounted by the collision term K(f), and it is referred to as a fluctuating collision term. The fluctuating collision term varies rapidly in time with a characteristic time in the order of duration time of a two-body collision, and it is nearly impossible to calculate it explicitly. Therefore, it is assumed that eq. (2.1) describes a stochastic process in which the entire single-particle density is a stochastic variable and δK acts like a random force. The fluctuating collision term is characterized by a correlation function,

$$\overline{\delta K(\mathbf{r},\mathbf{p},t)\delta K(\mathbf{r}',\mathbf{p}',t')} = C(\mathbf{p},\mathbf{p}')\ \delta(\mathbf{r}-\mathbf{r}')\delta(t-t') \tag{2.4}$$

which is local in spatial coordinates due to localized two-body collisions. In a weak-coupling limit, the correlation function $C(\mathbf{p},\mathbf{p}')$ is explicitly evaluated and given by

$$\begin{aligned} C(\mathbf{p},\mathbf{p}') = & \int d\mathbf{p}_3 d\mathbf{p}_4 W(11';34)[f_1 f_1' \tilde{f}_3 \tilde{f}_4 + \tilde{f}_1 \tilde{f}_1' f_3 f_4] \\ & -2\int d\mathbf{p}_2 d\mathbf{p}_4 W(12;1'4)[f_1 f_2 \tilde{f}_1' \tilde{f}_4 + \tilde{f}_1 \tilde{f}_2 f_1' f_4] \\ & +\delta(\mathbf{p}-\mathbf{p}')\int d\mathbf{p}_2 d\mathbf{p}_3 d\mathbf{p}_4 W(12';34)[f_1 f_2 \tilde{f}_3 \tilde{f}_4 + \tilde{f}_1 \tilde{f}_2 f_3 f_4] \end{aligned} \tag{2.5}$$

where W is the same transition rate which enters into the collision term K(f).

The correlation function $C(\mathbf{p},\mathbf{p}')$ is entirely determined by the average properties of the single-particle density. The parameters such as the mean-field potential and N–N cross-section determining the average properties also describe the fluctuations in the framework of the stochastic BUU model. This result can be regarded as a consequence of a "fluctuation-dissipation theorem" which relates the fluctuation and dissipation properties locally in phase-space. The stochastic BUU equation describes the dynamical evolution as a diffusion process for the trajectories of single-particle density in an abstract space of all single-particle densities. This description is equivalent to a generalized FP equation in infinite dimensions for the probability distribution function of the single-particle density. In some situations, instead of the full probability distribution of the single- particle density, we may consider its first moment and second moment, i.e., variance and co-variances of density. For small fluctuations, the equation for the first moment is just the BUU equation describing the mean trajectory, and the equation for the second moment can easily be deduced from the stochastic BUU eq. (2.1) [2]. A similar equation for the second moment of density is derived using a somewhat different approach in reference [3].

3. APPLICATION TO NUCLEAR COLLISIONS

The stochastic BUU model summarized in the previous section provides an extended one-body transport description of many-body dynamics by incorporating dynamical fluctuations in a theoretically sound basis. It opens up a possibility for a dynamical description of multifragmentation processes in nuclear collisions at intermediate energies. By employing standard methods for solving a typical Langevin equation, we can obtain the numerical solutions of eq. (2.1) iteratively over short time intervals [4]. Starting with a definite density f(t) at time t, eq. (2.1) generates a set of densities $\{f(t+\Delta t)\}$ at time $t+\Delta t$. For the next step, we choose one of such possible states as the initial state, and eq. (2.1) generates a new set of states at the next time step, and so on. At each step the

generated states are randomly distributed around the initial state and their spread is determined by the correlation function $C(\mathbf{p},\mathbf{p}')$. In order to make this simulation numerically tractable, we project the fluctuations on a collective property $Q(\mathbf{p})$ and determine the spread of trajectories in terms of the collective variable, $Q=\int d\mathbf{p}Q(\mathbf{p})f(\mathbf{p},\mathbf{r},t)$. The reduced correlation function corresponding to the collective variable is given by

$$C_Q(t) = \int dp_1 dp_2 dp_3 dp_4 (\Delta Q)^2 \, W(12;34) f_1 f_2 \tilde{f}_3 \tilde{f}_4 \tag{3.1}$$

where $\Delta Q=Q(p_1)+Q(p_2)-Q(p_3)-Q(p_4)$. C_Q is proportional to the diffusion coefficient for the collective variable and it determines the rate of change of fluctuations in Q. Now, we can easily solve the Langevin process associated with Q by modifying it at each time step according to

$$Q \rightarrow Q + w \sqrt{\int_t^{t+\Delta t} dt' C_Q(t')} \tag{3.2}$$

where w is a normally distributed random variable. Once the fluctuations are inserted in Q, we can generate an event by renormalizing the momentum distribution to the new value of Q at each time step.

We performed numerical calculations based on the scheme presented here, in which the collective variable is chosen at the z-component of the quadrupole moment of the local momentum distribution along the beam axis, $Q(p)=2p_z^2-p_x^2-p_y^2$. Each event of eq. (2.1) is simulated with the help of the so-called Landau-Vlasov algorithm [5]. Fig. 1 shows the time evolution of the diffusion term together with the time evolution of the mean value of Q in a head-on collision of $^{12}C+^{12}C$ system at various energies. From Fig. 1, we can see that the fluctuations are large and peaked in time. There is a well–defined narrow peak just after touching. The peak in the fluctuations is an order of magnitude larger than the background which consists of numerical and thermal fluctuations. Consequently, large dynamical fluctuations are introduced during the early stages of the collision. As a first application, we study $^{40}Ca+^{40}Ca$ collision at bombarding energies E=20 and 60 MeV/nucleon. The collision at 20 MeV/nucleon is a typical low energy, incomplete fusion reaction. Fig. 2 shows the mass spectra obtained in both the BUU and the stochastic BUU approaches. Both calculations lead to a similar result, namely an incomplete fusion residue of mass $A\simeq45$ together with a large number of nucleons and a few very small fragments, $A\simeq2$–3. This result is very interesting for two reasons: (i) at low energies, the fluctuating theory does indeed lead to a fusion residue and not to an uncontrolled break-up of the nuclear system, (ii) as expected at low energies, the fluctuating theory gives essentially the same result as the average result of the BUU description. At higher energies, E/nucleon $\geq$ 50 MeV, multifragmentation is expected to occur. As can be seen from Fig. 3, the stochastic BUU calculations lead to a very reasonable mass spectrum of the produced fragments. The mass spectrum is an inclusive quantity which hardly discriminates between available theoretical descriptions. However, it provides a check on the reliability of our calculations. Investigation of more specific and sensitive observables is currently being performed.

1. G. F. Bertsch and S. Das Gupta, Phys. Rep. 160 (1988) 190.
2. S. Ayik and C. Gregoire, Phys. Lett. B212 (1988) 269, and submitted to Nucl. Phys. A (1989).

3. J. Randrup and B. Remaud, preprint LBL–25852 (1989).
4. H. Risken, The Fokker-Planck Equation, Springer (1984).
5. G. Welke, R. Malfliet, C. Gregoire, M. Prakash and E. Suraud, Phys. Rev. C40 (1989) 2611.

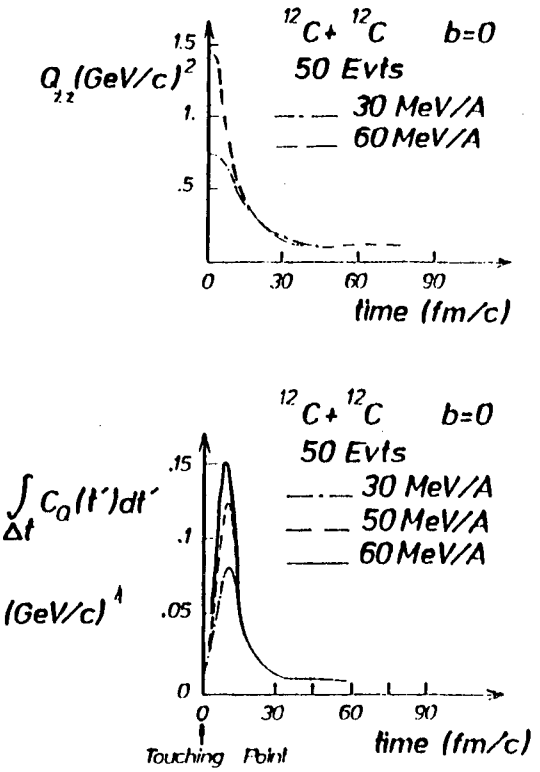

Figure 1

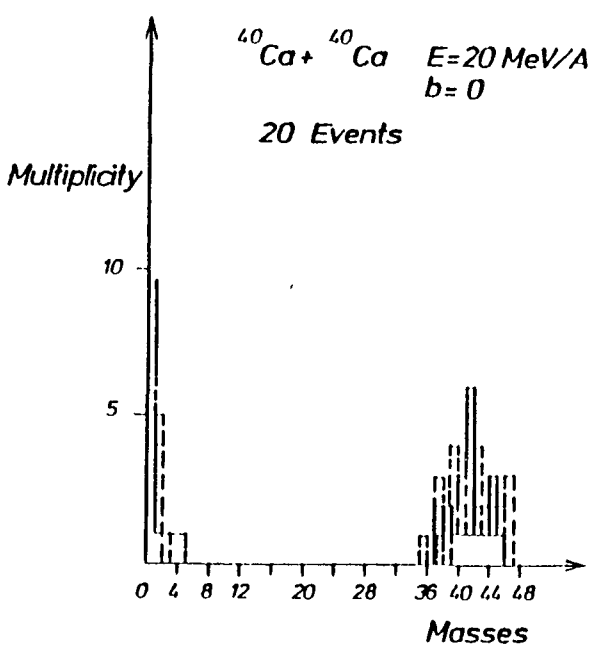

Figure 2

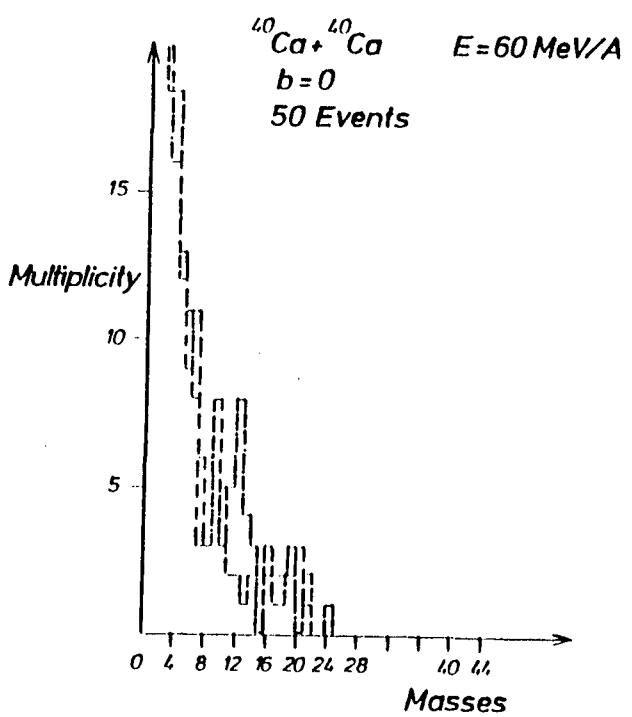

Figure 3

Energy and Mass Dependence of Collective Flow in Intermediate Energy Nucleus-Nucleus Collisions

G.D. Westfall, W. Bauer, D.A. Cebra, S. Howden, J. Karn,

D. Krofcheck, C.A. Ogilvie, A. Vander Molen, and W.K. Wilson
National Superconducting Cyclotron Laboratory and Department of Physics and Astronomy
Michigan State University, East Lansing, MI 48824-1321, USA

A. Nadasen
Department of Physics, University of Michigan at Dearborn, Dearborn, MI 48128, USA

Intermediate energy nucleus-nucleus collisions can provide information concerning the nuclear equation of state at excitations and densities not too far from the nuclear ground state.[1] In these collisions densities up to twice normal densities and excitations up to 50 MeV/nucleon can be produced.

Using the MSU 4π Array[2] we have measured interactions between Ar and V nuclei at energies ranging from 35 to 100 MeV/nucleon. We observe the disappearance of directed transverse momentum near an incident energy of 80 MeV/nucleon.[3,4] This disappearance corresponds to the balancing of the attractive and repulsive interaction and is generally reproduced by BUU calculations. We term the incident energy at which the attractive and repulsive interactions balance as $E_{balance}$. This observable is much less sensitive to the details of the experimental apparatus and the model calculations.

At Bevalac energies (above 200 MeV/nucleon), the interaction between two nuclei is dominantly repulsive. The interaction results mostly from nucleon-nucleon collisions. At low energies (around 10 MeV/nucleon), the two nuclei interact mainly through their mean fields. During the collision, the nuclei orbit or partially orbit each other. By convention, repulsive interactions are termed positive angle scattering and attractive interactions are called negative angle scattering. The observable used to study these interactions, the slope of the fraction of average transverse momentum in-plane versus the rapidity, is always a positive quantity when the reaction plane is determined from the data and is termed collective flow or directed transverse momentum. The experimental signature of the change-over from positive to negative angle scattering is that, as a function of incident energy, the slope decreases to zero and then begins increasing again. In a model calculation where the reaction plane is known, the collective flow changes sign. In both cases, the cross-over point is well defined. For models such as BUU that predict nucleon spectra exclusively, the problem of filtering the predictions through the acceptance of the apparatus is avoided. For the experimental data, the task of correcting the absolute value of the observed collective flow for the imprecise determination of the reaction plane is also not necessary.

The data presented in this paper were taken with the MSU 4π Array[2] using the K500 and K1200 Superconducting Cyclotrons at the National Superconducting Cyclotron Laboratory. In its current configuration, the MSU 4π Array consists of a main ball of counters and a forward array. The main ball is made up of 170 close-packed plastic phoswich detectors with 3 mm thick fast plastic ΔE and 25 cm thick slow plastic E scintillators.[2] The forward array consists of 45 phoswich counters similar to the ball counters but with 1.6 mm thick ΔE and 15 cm thick E scintillators. For the data presented here, the event trigger is one or more particles in the entire system which provides minimum bias data. The phoswich counters are capable of mass resolution for Z=1 fragments and provide Z resolution up to Z=4 in the main ball and up to Z=18 in the forward array at the higher energies. Impact parameter selection was accomplished by selecting on mid-rapidity charge and four impact parameter bins were selected.[7] The reaction plane was determined using a new method given by Wilson et. al.[6] which uses any kind of in-plane motion to determine the reaction plane.

Results for directed transverse momentum for five different fragment types (p,d,t,Z=2, and Z=3) and three impact parameter bins from Ar+V were produced for each of the energies of 35, 45, 55, 65, 75, 85, and 100 MeV/nucleon as function of the rapidity in the center-of-mass frame, y_{cm}, versus $< p^x/p^\perp >$ for midcentral collisions.[4] The use of the ratio $< p^x/p^\perp >$ rather than $< p^x/A >$ minimizes detector biases and reflects the fraction of observed transverse momentum that is in the reaction plane. The directed transverse momentum, or collective flow, is extracted by taking the slope of this curve as shown by the solid line in Fig. 1. The region is chosen to extend from y_{cm}=0 to about 75% of the projectile rapidity for all incident energies. In Fig. 1 the results for protons observed in mid-central collisions are shown. The values for the directed transverse momentum at different beam energies are compared in Fig. 2 for various observed particles from midcentral collisions of Ar+V. Note that the transverse momentum values decrease with increasing incident energy and reach a value of zero around

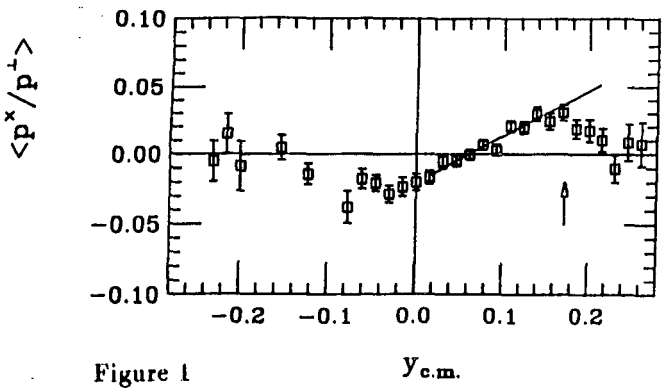

Figure 1

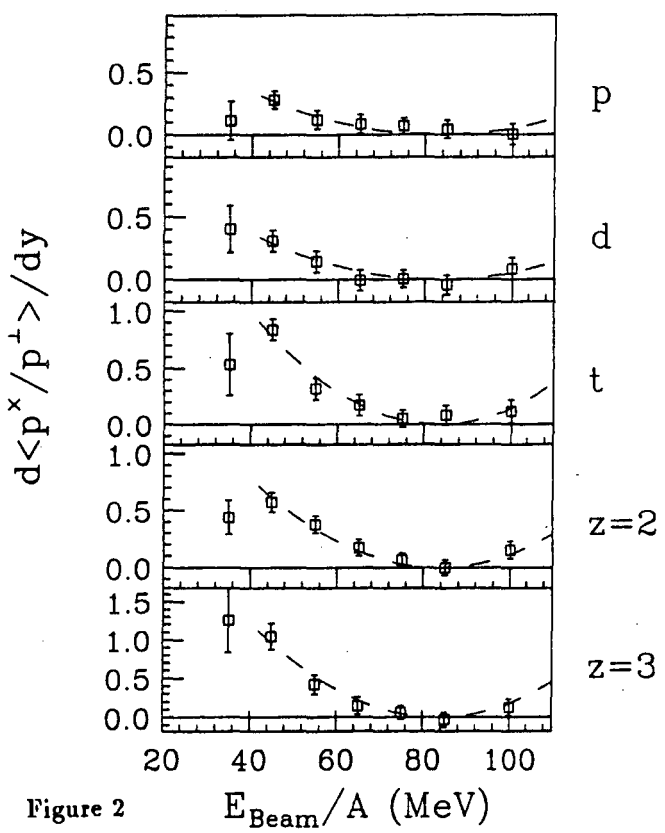

Figure 2

80 MeV/nucleon and then increase slightly. This disappearance of flow has previously been observed in La+La collisions to occur at or below 50 MeV/nucleon.[8] This decrease and reemergence with incident energy is interpreted to be the transition from negative scattering to positive scattering. This interpretation is reinforced by BUU calculations that reproduce this zero directed transverse momentum at energies around this value. Note that BUU calculations predict negative scattering angles at energies below 70 MeV/nucleon and positive angle scattering at energies above 90 MeV/nucleon.

The $E_{balance}$ predicted by BUU is sensitive to the parameters of the nuclear equation of state. In Fig. 3, BUU calculations are shown for Ar+V with two different values of the incompressibility, K, of 200 MeV and 380 MeV which correspond to soft and stiff equations of state respectively. For K=200 MeV, $E_{balance}$ is predicted to be 80 MeV/nucleon while for K=380 MeV, $E_{balance}$ is about 88 MeV/nucleon.

However, the nucleon-nucleon cross sections used in BUU are those for free scattering and it is possible that in-medium effects could alter these cross sections. To demonstrate the sensitivity of the BUU predictions to the nucleon-nucleon cross sections, we present calculations in Fig. 4 where the cross sections have been lowered by a constant fraction. If the in-medium cross sections are 80% of the free cross sections, $E_{balance}$ is predicted to be 108 MeV/nucleon while keeping the same parameters of the nuclear equation of state. If the in-medium cross sections are 70% of the free cross sections, $E_{balance}$ is predicted to be 122 MeV/nucleon. Thus the predictions of BUU for $E_{balance}$ are more sensitive to the assumed nucleon-nucleon cross sections than to parameters of the

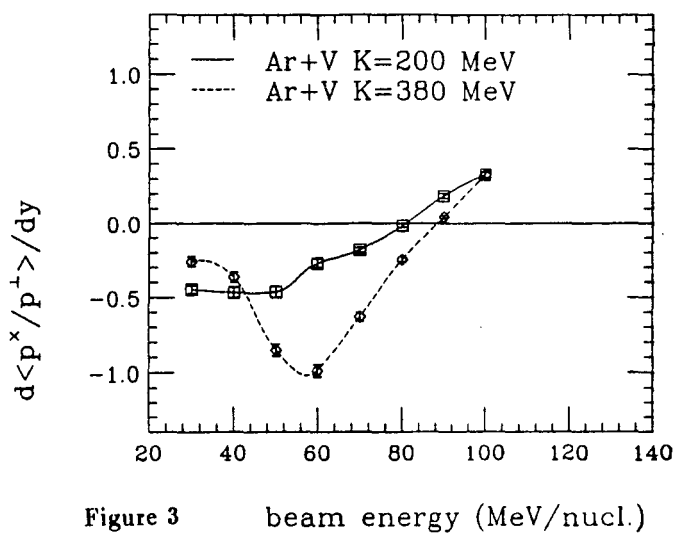

Figure 3

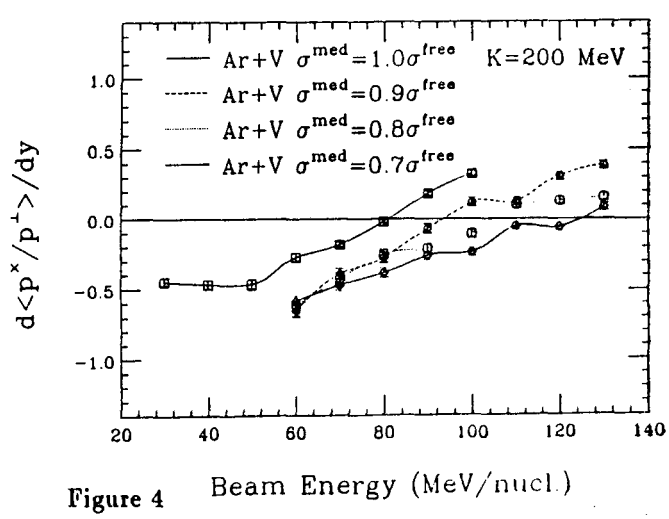

Figure 4

equation of state. Note that if the collisions are completely suppressed, then the scattering is always attractive.

If information concerning the nuclear equation of state is to be extracted from $E_{balance}$, then systematic data concerning the mass dependence of this observable is required. We have carried out the first steps in this direction by studying the disappearance of flow for Ar+V and La+La. We expect that there will be a mass dependence in $E_{balance}$ because the collisions should be proportional to the mass number of the one of the nuclei, A, while the mean field portion of the interaction scales with $A^{2/3}$ thus giving a dominance of the repulsive interaction in heavier systems. However, complete systematics will be needed to help determine the variables in BUU and enable the extraction of information concerning the nuclear equation of state.

This work was supported in part by the National Science Foundation under Grant No. PHY-89-13813.

---

[1]C.K. Gelbke and D.H. Boal, Prog. Part. Nucl. Phys., **19**, 33(1987).

[2]G.D. Westfall, J.E. Yurkon, J. van der Plicht, Z.M. Koenig, B.V. Jacak, R.Fox, G.M. Crawley, M.R. Maier, B.E. Hasselquist, R.S. Tickle, and D. Horn, Nucl. Inst. Meth. **238**, 347 (1985).

[3]C.A. Ogilvie, D.A. Cebra, J. Clayton, P. Danielewicz, S. Howden, J. Karn, A. Nadasen, A. Vander Molen, G.D. Westfall, W.K. Wilson, and J.S. Winfield, Phys. Rev. C **40**, 2592 (1989).

[4]C.A. Ogilvie, W. Bauer, D.A. Cebra, J. Clayton, S. Howden, J. Karn, A. Nadasen, A. Vander Molen, G.D. Westfall, W.K. Wilson, and J.S. Winfield, submitted to Rapid Communications, Phys. Rev. C, 1990.

[5]D.A. Cebra, S. Howden, J. Karn, A. Nadasen, C.A. Ogilvie,

Studies of Nuclear Collective Flow

DIOGENE Collaboration: J.-P. Alard[a], J. Augerat[a], R. Babinet[b], N. Bastid[a], F. Brochard[c], C. Cavata[b], P. Charmensat[a], M. Demoulins[b], P. Dupieux[a], H. Fanet[b], L. Fraysse[a], P. Gorodetzky[c], J. Gosset[b], M.-C. Lemaire[d], A. Le Merdy[b], D. L'Hôte[b], B. Lucas[b], J. Marroncle[a], G. Montarou[a], M.-J. Parizet[a], J. Poitou[b], A. Rahmani[a], C. Racca[c], Y. Terrien[b], O. Valette[b].

a- L.P.C., Clermont-Ferrand, B.P. 45, 63170 Aubière, France
b- DPhN, CEN Saclay, 91191 Gif-sur-Yvette cedex, France
c- C.R.N., B.P. 20 CR, 67037 Strasbourg cedex, France
d- LNS, CEN Saclay, 91191 Gif-sur-Yvette cedex, France

Speaker: M.-C. Lemaire
Laboratoire National Saturne

I - Introduction:

Collective hydrodynamical behaviour of nuclear matter compressed in relativistic nuclear collisions has been the topic of many theoretical and experimental works in these last years; a recent review has been written by K.H. Kampert [1]. First hints have been found in the 'shoulder arm' shape of the energy spectra[2] and the charged particle semi-inclusive angular distributions[3]. However these observations could be explained by more trivial effects; in particular, Coulomb effects may be partly responsible for the observed forward suppression of charged particles as this feature was not observed in neutron angular distributions[4]. These results stimulated the construction of 4π detectors, for studying emission patterns and event shapes could be studied as a function of the charged multiplicity of the event, which characterizes the centrality of the collision[5]. It has then been proposed to analyze these data with the sphericity tensor method[6]: after diagonilalisation, the event shape is characterized by the direction of the principal axis (flow angle) and two aspect ratios. Such an analyses has been carried out first for data taken by the Plastic -Ball group for symmetrical nucleus-nucleus collisions [7]; it exhibited a peak in the jacobian-free weighted flow angle distribution dN/d (cos θ) for the most the rsults are quite sensitive to finite particle-number distortions [8]. To overcome these difficulties, P. Danielewicz and G. Odyniec[9] proposed a new method: the transverse momentum analysis.

In this method, a vector $\mathbf{Q}_i$, which characterizes the reaction plane for each particle i is constructed as:

$$\mathbf{Q}_i = \sum_{i \neq j}^{M} \omega_j \, \mathbf{p}_j^{\perp}$$

where ω_j is a weighting factor taken as positive for particles emitted in the forward hemisphere of the center-of-mass system and negative for particles emitted in the backward hemisphere. Fragment i is removed from the summation in order to eliminate auto-correlations. Then, the tranverse momentum of each particle is projected onto this approximated reaction plane yielding the in-plane transverse momentum per unit mass $p_{x'}/m$. The ' superscript indicates values obtained in the estimated reaction plane. Reflecting event by event fluctuations due to finite number effects, the estimated and true reaction planes differin azimuth by $\Delta\phi$[9]; typical values of $\langle\cos\Delta\phi\rangle$ are 0.4-0.5[10] in our measurements. The quantities corrected for this effect are noted without the ' superscript. This method was first applied to Streamer-Chamber data, for the Ar + KCl system at E/A=1.8 GeV. The experimental values are much larger than the cascade predictions while fairly good agreement was claimed for VUU calculations with a stiff equation of state[11]. The dependence of $\langle p_x/m\rangle$ as a function of the rapidity y has been studied for a wide variety of systems[12]. For symmetric systems the slope around the c.m. rapidity has frequently been used as a measure of the flow F. Its systematic study shows that F peaks for semi-central collisions and scales roughly as $A^{1/3}$ between Nb and Au. As far as the energy dependence is concerned, it increases

up to E/A=400 MeV and saturates for higher bombarding energies. It has also been shown from Au + Au system that F increases with the mass of the detected fragment[13]. For asymmetric systems, such an analysis has been done for Ar + BaI_2 at E/A=1.2 GeV[14] . INC model predicts too low values , VUU predictions agree with the data, slightly favouring a stiff EOS. However, no error bars are put on the theoretical calculations, so that such conclusions are highly questionable[15] . The present paper deals with a summary of the DIOGENE results on the baryon and pion flows. For detailed reviews see refs. [16 17 18 19 20] in addition to the theses [5, 10].

I I - Flow analyses for DIOGENE results:

Triple differential cross-sections of pions and light fragments (p, d, t, ^{3}He and ^{4}He) have been measured with high statistics using the large solid angle detector DIOGENE[21] installed at LNS (Saturne National Laboratory). The DIOGENE central chamber acceptance allows to detect particles emitted in the angular range 20°<θ<132° with energies larger than 15 MeV for pions and 25 A.MeV for baryons. The heavy ion reactions studied are given in the following table:

Projectile	target	E/A (GeV)	Projectile	target	E/A (GeV)
Ne	NaF	.2 to 1.	Ar	Ca	.2 to .6
	Nb	.2 to 1.		Nb	.2 to .6
	Pb	.2 to 1.		Pb	.2 to .4

To characterize the centrality of the collision, the multiplicity of the pseudo-protons (free protons and those bound in light nuclei) have been used to calculate a reduced impact parameter b_r defined as : $b_r = b/(R_1 + R_2)$ where R_1 and R_2 are the projectile and target radii ($R = r_0 A^{1/3}$, $r_0 = 1.12$ fm)[22] .

As we were mainly dealing with asymmetric systems , for which the center of mass is not known a priori, the Danielewicz and Odyniec method has been slightly adapted : for each baryon of charge Z_μ, mass m_μ and rapidity y_μ, the weight used in the determination of the reaction plane is taken as : $(Z_\mu / m_\mu) .(y_\mu - \langle y\rangle)$ where $\langle y\rangle$ is the Z/m weighted average rapidity of all baryons of the event. Fig.1 displays an example of the dependence of $\langle p_{x'} /m\rangle$ as a function of the rapidity y for the pseudo-protons measured in Ar + Pb collisions at E/A=400 MeV and for different b_r. The flow parameter F defined as the slope of the straight line at the c.m. rapidity divided by $\langle\cos \Delta\phi\rangle$ has been studied versus b_r, target and projectile mass and incident energy. It displays a slight maximum at intermediate impact parameter, it is slightly higher for the heavier fragments. For Ne + NaF at a given b_r the pseudo-proton value decreases by 15% from E/A=400 to 800 MeV. It slightly increases as a function of the target or projectile mass. However, all these variations of F are quite small 10 - 25%. In addition, these values are overestimated by about a factor 2 as compared to those derived from the method described below (which allows to get rid of the influence of the acceptance geometry). With the same procedure INC calculations predict flow parameter F_{th} = (0.5-0.7). F_{exp}.

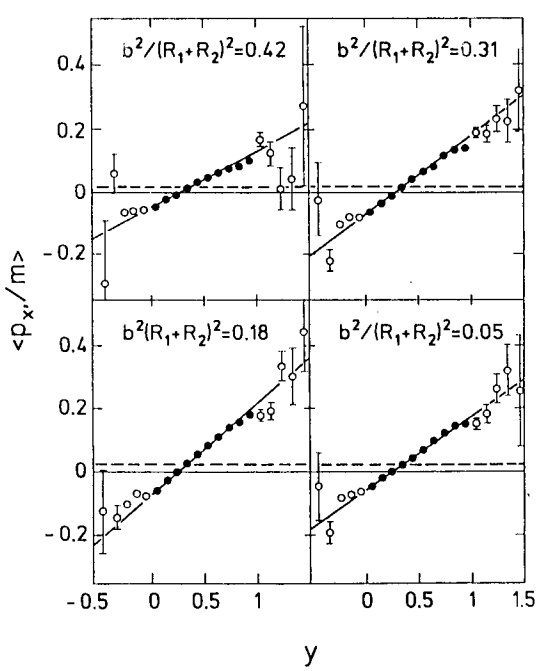

Fig.1 Average value of $\langle p_{x'} /m\rangle$ as a function of y (the rapidity), for pseudo-protons emitted in Ar + Pb collisions at E/A = 400 MeV and for different impact parameters. The straight lines display the linear adjustment performed on the black points, the dotted lines correspond to the average values of $p_{x'}$ /m calculated in the overall rapidity range.

Baryon Flow from Gaussian fits to triple differential cross-sections [23]

The method [10, 17, 23] consists in fitting the (p_z /m, $p_{x'}$/m) and (p_z /m, $p_{y'}$/m) two-dimensional cross-sections with two-dimensional Gaussian distributions. For each multiplicity cut, providing an estimated impact parameter, the cross-sections are evaluated in the center-of mass frame, p_z is the longitudinal momentum in this frame, and m is the proton mass.

The parameters given by the fits are θ and two standard deviations σ_3 and σ_1 for the in-plane cross-sections (p_z /m, $p_{x'}$/m) , one angle θ' and standard deviations σ_2 and σ for the out-of-plane cross-sections (p_z /m, $p_{y'}$/m) . These values are related as follows:

$$\sigma^2 = \sigma_3^2 \cos^2\theta + \sigma_1^2 \sin^2\theta$$

$$\theta' = 0° \ (\text{if } \sigma_2 < \sigma) \text{ or } 90° \ (\text{if } \sigma_2 > \sigma)$$

After corrections for finite number effects , one can deduce from these parameters the true flow angle Θ_F and the true variances $\sigma_1{}^2$, $\sigma_2{}^2$ and $\sigma_3{}^2$. On Fig. 2, are displayed the ellipses representing the 1/e contours of the Gaussian fits to the in-plane cross-sections for different impact parameters. The flow angle Θ_F increases when the impact parameter decreases to reach values as high as 60° for Ar + Pb at E/A=400 MeV. The size of the ellipses decreases when the impact parameter decreases; in agreement with the fact that the energy available per participant nucleon decreases. The variation of the flow angle Θ_F and aspect ratios :

$$\lambda_{31}^2 = \sigma_3^2 / \sigma_1^2 \quad \lambda_{32}^2 = \sigma_3^2 / \sigma_2^2$$

have been studied as a function of the centrality of the collision.

Except for Ne + NaF, Θ_F increases when the impact parameter decreases . The other trends of Θ_F are to increase with the target and projectile masses, all other conditions being the same; for Ne + (Nb,Pb) collisions Θ_F slightly increases between 400 and 800 MeV per nucleon.The squares of the aspect ratios vary linearly with the square of the reduced impact parameter, $\lambda^2{}_{31}$ varies more rapidly than $\lambda^2{}_{32}$. These aspect ratios are closer to 1, when the collisions become more centrals and for the heaviest targets; which just reflects that the systems become more equilibrated. These aspect ratios vary weakly with the incident energy. $\lambda^2{}_{31}$ is always larger than $\lambda^2{}_{32}$. In the plane:

$$\theta_F \ , \ r = 2\,\sigma_3^2 / (\,\sigma_1^2 + \sigma_2^2\,)$$

our results display the same behavior as the streamer chamber data group (Fig.3)[9].

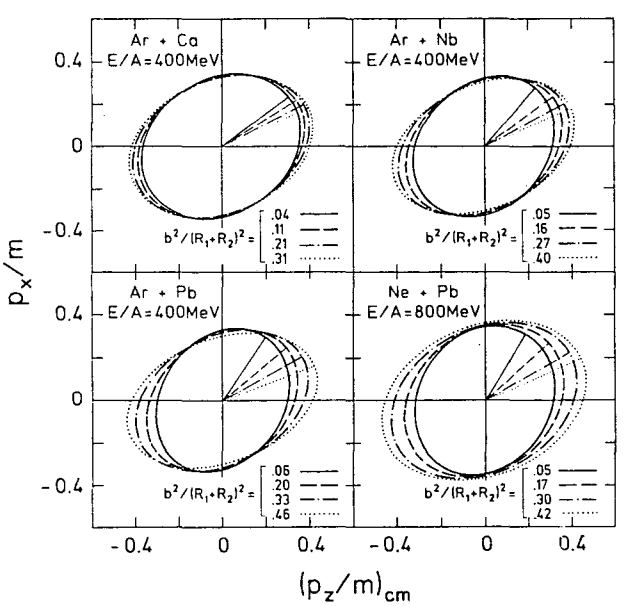

Fig. 2: Ellipses representing two-dimensional Gaussian fits to the in-plane cross-sections as a function of reduced impact parameter.

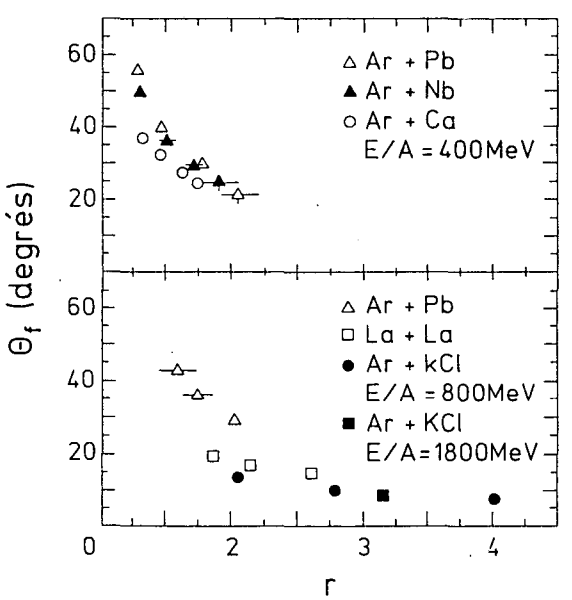

Fig. 3: Θ_F versus r defined in the text; DIOGENE results for pseudo-protons (top); Streamer chamber data for deuterons[9] (bottom).

A nice feature of the method described above is that the results seems independent of the DIOGENE acceptance cuts; indeed, it has been checked that introducing acceptance cuts more restrictive eliminating one third to half of the event statistics change the flow angle and aspect ratios respectively by less than 2° and 1%.

The theoretical flow angles derived with the same method from the intranuclear cascade calculations[24] are much too small (at least by a factor 2 for central collisions) as compared to the present experimental values.

Pion Flow measured in DIOGENE [25]

Pions play an important role in nucleus-nucleus collisions at relativistic energies: theoretical calculations [26 27], predict that their multiplicity is determined at the stage of high density and temperature. This property was first used to extract an equation of state from the difference between theoretical and experimental pion multiplicities, assuming the difference results from the lack of compression energy in the models[28]. However, different sources of diminution of the pion number have been suggested, like pion absorption[29], nuclear medium effects on the elementary cross-sections[30 31]; in addition, more elaborated models like BUU[32] / VUU[33], which include the mean field in addition to the two body collisions, claimed that the sensitivity of the pion multiplicity is not so obvious, especially, when momentum dependent forces are taken into account. As the theoretical situation, for the pion multiplicity is far from being clear, it is interesting to investigate another global observable like the pion flow.

Once the reaction plane is determined from the baryons, a transverse momentum analysis can be achieved for the pions as well as for the light fragments. The rapidity dependence of $\langle p_{x'}/m \rangle$ is diplayed in Fig.4 for protons and π^+ emitted in central collisions ($b_r^2 = 0.18$) of Ne + Pb collisions at E/A= 800 MeV. The center of mass rapidity y_0 is given by the value where the average proton transverse momentum goes through zero. The protons exhibit the usual behaviour of positive transverse momentum values for rapidities larger than y_0 and negative values for rapidities smaller than y_0. In contrast, to the protons the pions have always positive average in-plane transverse momentum values. The Intra-Nuclear-Cascade (INC) calculations predicts values compatible with zero over the whole range of rapidity.

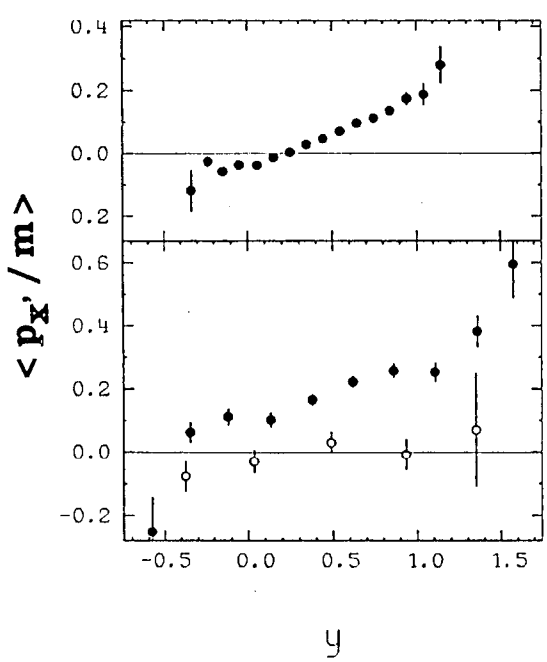

Fig. 4: Average value of $\langle p_{x'}/m \rangle$ for protons (top), and π^+ (bottom) for Ne + Pb system at E/A= 800 MeV, for a value of the reduced impact parameter of about 0.32; the open symbols correspond to INC predictions.

The experimental results can be summarized with two parameters: the flow parameter F taken as the slope of the rapidity (y) dependence of the average in-plane transverse momentum $\langle p_x/m \rangle$, (fairly well fitted by a straight line), and $\langle q_x \rangle$, the mean value of $\langle p_x/m \rangle$ averaged over y. The dependence of F and $\langle q_x \rangle$ has been studied systematically as a function of impact parameter, projectile and target mass, and incident energies, has been studied systematically . The results can be summarized as follows :

The pion flow F

- Its value is much smaller for than for the baryons: F ≅ 56 MeV/c for pions as compared to 375 MeV/c for protons for the exemple given in Fig. 4.

- For asymmetric systems at 600 and 800 MeV per nucleon, F increases when b decreases, at E/A=400 MeV with a slight maximum at intermediate impact parameters.

- INC calculations predicts F ≅ 0 in contradiction with the experimental observations.

The pion asymmetry $<q_x>$

-Its value is compatible with zero for Ne + NaF and Ar + Ca symmetric systems; for asymmetric systems its value is always positive, without systematic impact parameter dependence.

- $<q_x>$ is larger for π^+ than for π^-, all other conditions being the same.

-The fact that the azimuthal anisotropy of pion emission increases with the asymmetry of the system is clearly seen on Fig. 5, where $<q_x>$ is plotted as a function of A_c/A_p for the same range of reduced impact parameter ($0 \leq b_r^2 \leq 0.25$). These observations are consistent with an absorption effect since for non zero impact parameters and asymmetric systems, pions emitted from the participant zone have more matter to go through the heavy target than through the light projectile.

- QMD calculations [34] of $<q_x>$ (Fig.6) indicate that the introduction of the mean-field describes some of the experimental effect. The differences between π^+ and π^- is well described by the model which includes isospin dependence and Coulomb interaction. However, the model predicts less asymmetry than observed experimentally.

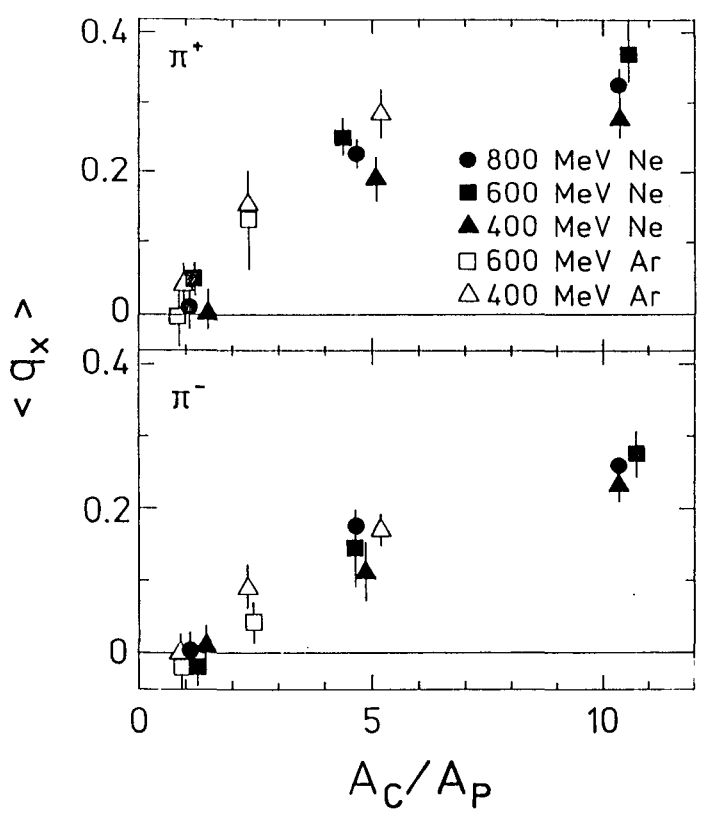

Fig.5: Pion average in-plane transverse momentum as a function of the system asymmetry at small impact parameter ($0 \leq b_r^2 \leq 0.25$).

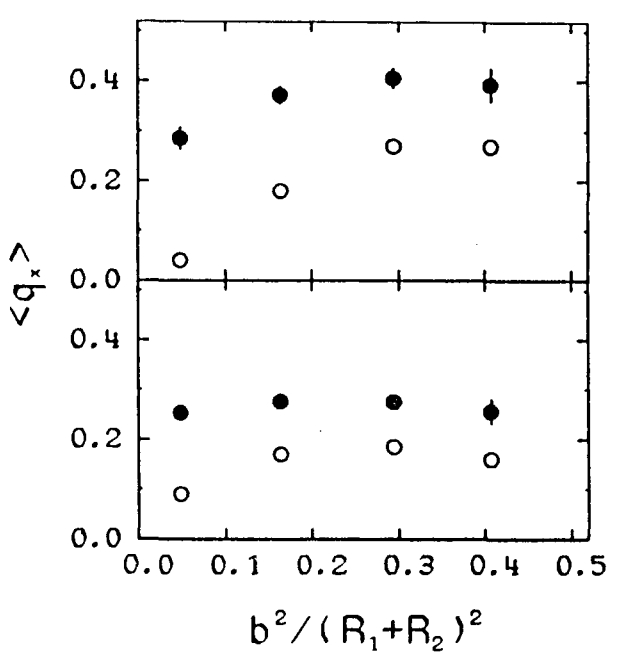

FIg.6 Experimental results (filled symbols) and QMD predictions for π^+ (top) and π^- (bottom) for Ne + Pb at E/A = 800 MeV.

- To be convinced that pion anisotropy is compatible with absorption, a simple semi-classical model has been derived . It assumes that the pions are emitted from the center of the participant zone and travel through average distances $\langle d_p \rangle$ and $\langle d_t \rangle$ in the projectile and target with an absorption mean free path λ. Assuming for the pion azimuthal distribution $dN/d\Phi = a_0 + a_1 \cos\Phi$, the ratio Ω is:

$$\Omega = \frac{\langle q_x \rangle}{\langle q_\perp \rangle} = \frac{1}{2} \, \mathrm{th} \left[\frac{\langle d_t \rangle - \langle d_p \rangle}{2\lambda} \right]$$

The experimental ratio Ω is plotted versus mass assymetry on Fig. 6; within the error bars, it is compatible with the calculations performed with a mean free path value of 4-6 fm. Such results are consitent with what is known from pion absorption cross-sections[35] and from phenomenological analysis of pion production in nucleon-nucleus collisions[36].

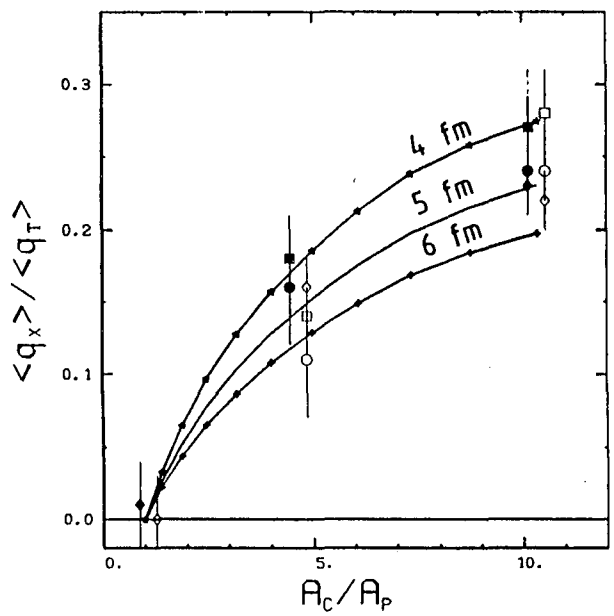

Fig. 7: Experimental values of $\langle q_x \rangle / \langle q_\perp \rangle$ for π^+ (open symbols) and π^- (closed symbols) at E/A=400 (circles), 600 (squares) and 800 (losanges) MeV. The curves correspond to different λ.

Conclusions:

For the baryons, an original method of fitting the in-plane and out-of-plane cross-sections by two- dimensional Gaussian distributions, provides flow angles and aspect ratios independent of geometrical detector biases. For asymmetric systems and the most central collisions investigated here, the flow angle raises up to 60°. Intra Nuclear Cascade calculations are unable to reproduce such large experimental values. Comparisons with more elaborated models are upon request.

For the pion flow, the preferential emission towards the projectile side is compatible with the absorption hypothesis, according to which the pions escape the participant region more easily towards the projectile side than on the target side. The pion mean free path extracted from a simple geometrical model varies between 4 to 6 fm; in agreement with the known pion absorption cross-sections. Intra Nuclear Cascade calculations predicts that the average in plane transverse momentum $\langle q_x \rangle$ is roughly zero. QMDcalculations provide positive values, but too small as compared to the experimental data.

From this systematic study of observables for different systems on a wide range of incident energies and impact parameters, theoreticians have a lot of informations available to test their models in quite different regions of densities and temperatures. Obviously, the models have to be sophisticated enough to include not only the equation of state but also the modifications of the particle properties when they travel through a dense and hot medium. Enough statistics are necessary in order to get relevant comparaison to the experimental data; this clearly calls for error bars on the calculated values, taking into account that often the theoretical observable is computed at one fixed impact parameter while the experimental data average on a certain range of impact parameters.

References:

[1] K.H. Kampert; J. Phys. G: Nucl. Part. Phys. 15 (1989) 691
[2] S. Nagamiya et al.; Phys. Rev. Lett. 45 (1980) 602
[3] R. Stock et al.; Phys. Rev. Lett. 44 (1980) 1243
[4] R. Madey et al.; Phys. Rev. 34 (1986) 347
[5] C. Cavata; thesis, Orsay (1989)
[6] M. Gyulassy et al.; Phys. Lett. 110B (1982) 185;
J. Cugnon et al.; Phys. Lett. 109b (1982) 167
[7] H.A. Gustafsson et al.; Phys. Rev. Lett. 52 (1984) 1590;
H. Ritter et al.; Nucl. Phys. A347(1986) 3c
[8] P. Danielewicz and M. Gyulassy; Phys. Lett. 129b (1983) 283
[9] P. Danielewicz and G. Odyniec; Phys. Lett. 157B (1985) 146;
P. Danielewicz et al.; Phys. Rev. C38 (1988) 120
[10] M. Demoulins, Thesis, ORSAY (1989)
[11] J.J. Molitoris and H. Stocker; Phys. Lett. 162B (1985) 47
[12] K.G.R. Doss et al.; Phys. Rev. Lett. 57 (1986) 302
[13] A.H. Gustafsson et al.; Mod. Phys. Lett. A3 (1988) 1323
[14] D. Keane et al.; Phys. Rev. C37 (1988) 1447
[15] J. Marroncle; Thesis, Clermont-Ferrand (1989)
[16] J. Gosset et al.; Balaton Conf. Nucl. Phys., Hungary (1987)
[17] O. Valette et al.; Hirschegg (1988) 133
[18] J. Poitou et al.; Hirschegg (1988)
[19] D. L'Hôte et al.; Nucl. Phys. A488 (1988) 457
[20] J. Gosset et al.; Phys. Rev. Lett. 62 (1989) 1251
[21] J.P. Alard et al.; NIM A261 (1987) 379
[22] C. Cavata et al.; submitted to publication in Phys. Rev.
[23] J. Gosset; Hirschegg (1990) and see ref. 10 and 17
[24] J. Cugnon et al.; Nucl. Phys. A379 (1982) 553;
J. Cugnon and D. L'Hôte; Nucl. Phys. A452 (1986) 738
[25] O. Valette; Piriac (1989) 146;
C. Cavata; Hirschegg (1990);
J. Poitou; Bormio (1990)
[26] J.J. Molitoris et al.; Phys. Rev. C36 (1987) 220
[27] R. Stock et al.; Phys. Rev. Lett. 49 (1982) 1236
[28] R. Stock, Phys. Rep. 135 (1986) 259
[29] J. Cugnon et M.-C. Lemaire; Nucl. Phys.; A489 (1988) 781
[30] B. ter Haar and R. Malfliet, Phys. Rev. C36 (1987) 1611; Phys. Rep. 149 (1987) 207
[31] M. Soyeur; Piriac (1989) 187
[32] C. Gale et al.; Phys. Rev. C35 (1987) 1666;
C. Gale, Phys. Rev. C36 ((1987) 2152
[33] J. Aichelin et al.; Phys. Rev. Lett. 58 (1987) 1926
[34] C. Hartnack et al.; Hirschegg (1988) 138
[35] T. Ericson and W. Weise; Pions and Nuclei (1988) 265
[36] D.A. Sparrow et al.; Phys. Rev. C10 (1974) 2215

Hydrodynamic Modeling of Heavy Ion Collisions

J.R. Wilson, C.T. Alonso, T.L. McAbee, and R. Vogt
Lawrence Livermore National Laboratory,
Livermore, California 94550

We are modeling heavy ion collisions treating the nucleons as a fluid described by an equation of state augmented by a Boltzmann equation for thermally produced particles such as pions. These calculations are fully dynamic (i.e. space- and time-dependent) and do not need to assume equilibrium, which is arrived at in a natural equilibration process. The particle-nucleon interactions are described by an absorption cross section and either a scattering cross section or a mean field. The goal of this project is to see if by matching experiments we can deduce some information about the nuclear equation of state.

We will first describe the results of calculations modeling the CERN 200 GeV/N ^{16}O + ^{197}Au experiments [1]. The pion-nucleon interaction for these calculations occurs via absorption and scattering cross sections. The cross sections, functions of baryon density and momentum, are fitted to data from π + A (with A > 12) experiments and extrapolated to above nuclear densities. For brevity we present here only on-axis two-dimensional collision calculations, though we have a full 3D capability.

Results of Dynamical 200 GeV/N Collision Calculations

We now present some of our results. Figure 1 shows the peak density, ρ_{max}, and the mean density ρ_{ave} (averaged over the region above nuclear density) as a function of time. We also plot the number of pions produced as a function of time. Note that pions are produced well after the peak high density, i.e. most pions are produced during the expansion phase. In fact, the pions that escape the nuclear fluid are produced at near normal nuclear density.

Figure 2 shows the total perpendicular energy E_T vs. pseudorapidity η. The E_T distribution resembles the measured distribution except that the calculated peak is at $\eta = 1.9$ while the observed peak is at $\eta = 2.2$. Near $\eta = 0$ our calculations agree well with the plastic ball data (we do see the observed bump at zero rapidity y). In Table I our calculations and experimental data are compared in more detail. While there is reasonable agreement between our model and the experimental calorimetry data, a principle discrepancy is that we calculate too few pions with too great an energy per particle. The total calculated pion energy agrees with the experimental results.

To investigate this pion discrepancy, we are modeling the pion interactions with the mean field model described by Ramona Vogt later in these proceedings.

We have also investigated internucleus penetration using a three fluid 1D hydrodynamical model. Our intent is to see if there is a possible justification for hydrodynamic modeling of heavy ion collisions. The results are presented in the next section.

Three-Fluid Hydrodynamical Model

The three fluids in this calculation are a left-moving nuclear fluid, a right-moving nuclear fluid, and what we will call an "energy fluid". The primary source of the energy fluid is the energy lost in the center of mass of a nucleon-nucleon collision. To calculate this process we use experimentally measured parameters. A secondary source for this energy fluid is its further interaction with the nuclear fluids. No experimental results or fundamental theories are available for this latter process, so we have parameterized it simply using a cross section and an energy exchange per collision. First we made a calculation with nucleon-nucleon interactions only. For this case Figure 3 shows the densities of the left- and right-moving nuclear fluids (solid curves) and the energy fluid (dashed) at a time after the nuclei have passed through each other. The density profiles of the nuclei are almost unchanged. The nuclei are slightly slowed down.

Figure 4 compares our energy fluid's energy density (solid curve) with the expected density from a one-fluid perfect gas calculation (adiabatic index = 4/3). Note that ninety percent stopping (meaning that 90% of the total energy in the center of mass frame is converted into the energy fluid) is achieved for the nuclei if the nucleon-energy fluid interaction is parameterized by a cross section per nucleon mass of the energy fluid equal to 0.6 fm^2 and an associated energy per collision of 1.5 GeV. If the energy fluid is treated as a gas of massless particles characterized by a temperature T, a cross section of $0.02 / T^2$ fm^2 (where T is in GeV) is sufficient to also produce 90% stopping.

The use of cross sections for the nuclear energy fluid interactions should be viewed only as a convenient parameterization of the interaction time scale and not as cross sections as usually measured or calculated. What we see, then, is the important point that a modest amount of interaction of the matter produced by nucleon-nucleon collisions, with nucleons following behind, is sufficient to mimic hydrodynamic behavior.

This research was performed at Lawrence Livermore National Laboratory under the auspices of the United States Department of Energy, contract No. W-7405-Eng-48. One of us (J.R.W.) is supported by NSF grant PHY 89-20710.

TABLE 1

Comparison of experimental data with our model for 200 A GeV $^{16}O + ^{197}Au$

Quantity	η Range	Experiment	Theory	Reference
Calorimetry:				
ZDC	-	0-100 GeV	52 GeV	WA80 [3,7]
Spectators:				
E_t / proton	$0.6 < \eta < 1$	175 - 225 MeV	280 MeV	WA80 [4]
E_t	$-0.1 < \eta < 2.9$	125 GeV	215 GeV	HELIOS [5]
Participants:				
E_t	$2.4 < \eta < 5.5$	80 - 100 GeV	117 GeV	WA80 [3,7]
E_t	$2.28 < \eta < 3.94$	115 GeV	115 GeV	NA35 [6]
E_t	$2.25 < \eta < 3.83$	75 GeV	115 GeV	NA35 [2]
E_t (mean)	-	$0.62 \pm .09$ GeV	0.61 GeV	NA35 [2]
Charged particles:				
p^{π}_t (mean)	$2.07 < y < 3.85$	0.35 GeV/c	0.63 GeV/c	NA35 [8]
N^{cp}	$-1.7 < \eta < 4.2$	360	250	WA80 [9]
N^{cp}	$2 < \eta < 4.2$	200	112	WA80 [9]
N^{cp}	$2.65 < \eta < 3.15$	120	34	WA80 [9]
E_t (mean)	$2 < \eta < 4.2$	0.55 GeV	0.71 GeV	WA80 [10]
η (peak π-)	-	2.2	1.9	NA35 [8]
$N^{\pi-}$	$0.45 < \eta < 4.55$	125	80	NA35 [8]

References:

1. T.L. McAbee, J.R. Wilson, and C.T. Alonso, Int. J. Mod. Phys. A 5, (1990) 543.

2. A. Bamberger et al. (NA35 Collaboration), Phys. Lett. B184, (1987) 271.

3. S. P. Sorensen et. al. (WA80 Collaboration), Z. Phys. C38, (1988) 3.

4. H. R. Schmidt et. al. (WA80 Collaboration), Z. Phys. C38, (1988) 109.

5. F. Corriveau et. al. (HELIOS Collaboration), Z. Phys. C38, (1988) 15.

6. W. Heck et. al. (NA35 Collaboration), Z. Phys. C38, (1988) 19.

7. R. Albrecht et al. (WA80 Collaboration), Phys. Lett. B199, (1987) 297.

8. H. Strobele et. al. (NA35 Collaboration), Z. Phys. C38, (1988) 89.

9. I. Lund et. al. (WA80 Collaboration), Z. Phys. C38, (1988) 51.

10. R. Albrecht et. al. (WA80 Collaboration) Phys. Lett. B202, (1988) 596.

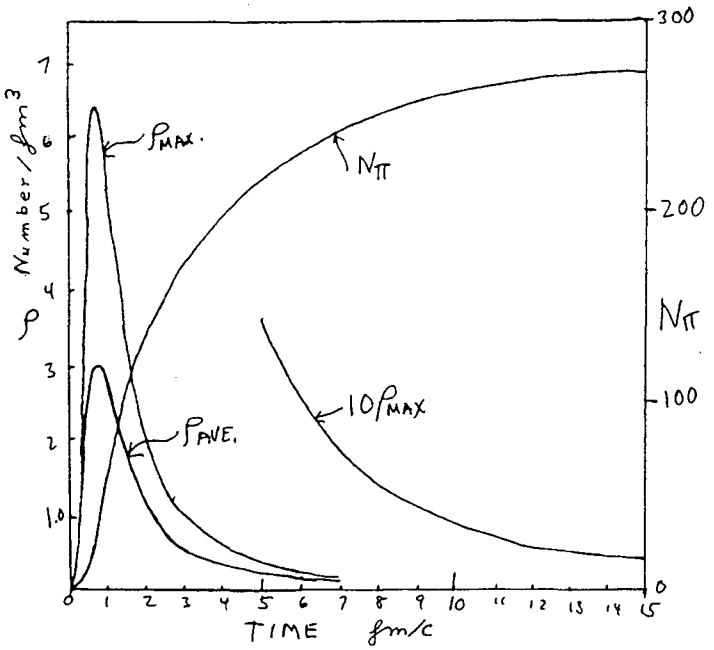

FIG 1

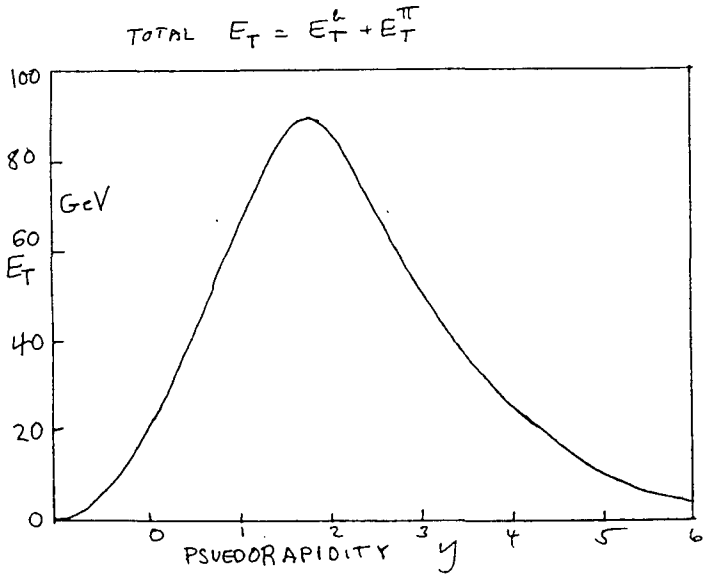

FIG 2

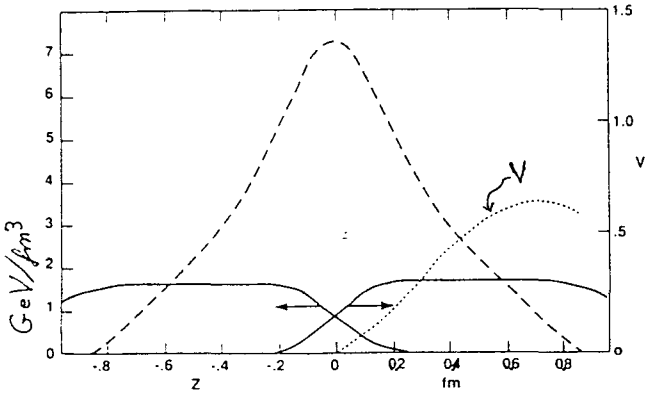

FIG 3

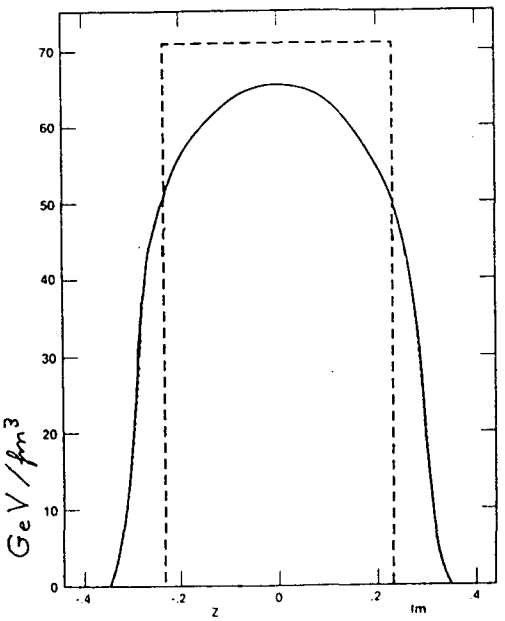

FIG 4

Transverse momentum in high energy heavy ion collisions and the nuclear equation of state*

Charles Gale†
Physics Department, McGill University, 3600 University St., Montréal, Qué., Canada, H3A 2T8

We discuss the mechanism for the production of transverse momentum in high energy nucleus–nucleus collisions. We argue that the transverse momentum observed experimentally reflects the nuclear equation of state indirectly only. It appears that the final state at high energies is mainly a consequence of the dynamics, in turn driven by the momentum dependent optical potential.

I. INTRODUCTION

In an effort to single out eventual signatures of the nuclear equation of state, several experimental observables have been proposed in high energy heavy ion collisions. Especially well known examples are flow angle distributions, obtained by adapting the thrust and sphericity analyses used in high energy physics to the heavy ion case[1], and transverse momentum distributions[2]. We will conduct a quantitative investigation of the latter variable for high energy heavy ion collision data obtained at the LBL Streamer Chamber.

II. THE BUU MODEL OF NUCLEAR REACTIONS AND MEAN FIELD PARAMETRIZATIONS

The BUU model has enjoyed some popularity over the recent years. One reason for this is that this model yields solutions of the Boltzmann equation through numerical techniques within reach of present day computers. These solution techniques are conceptually simple and appealing, even though the computational effort might be important. This approach has the desirable features a transport theory for nucleons in the nuclear medium should possess:

- Nucleons move on curved trajectories in the nuclear environment, owing to the interaction with the mean field (one–body scattering).
- Nucleons can undergo two–body scattering with suitable candidates.
- The Pauli blocking of final states is explicitly incorporated.

We do not give details on the Boltzmann–Uehling–Uehlenbeck equation. The interested reader is referred to the literature[3,4]. It suffices to say that the one–body phase space

density f is a solution of

$$\frac{\partial f(\vec{r},\vec{p})}{\partial t} + \{\mathcal{H}, f\} = I_c[f] , \tag{1}$$

where $I_c[f]$ is a collision integral which depends on the nucleon–nucleon scattering cross–section, $\{a, b\}$ is the classical Poisson bracket and $\mathcal{H}$ is the single–particle energy. In principle, σ_{NN} and the single particle potential U should be derived from a single interaction. Since the dense medium can modify the free cross sections in many ways, we adopt the attitude that our BUU model may be regarded as a "testing ground" for the effects of such modifications on experimental observables. In the discussions that follow, we have chosen $\sigma_{NN} = \sigma_{NN}^{free}$.

A determinant fraction of the physics in this scenario then enters in the choice of the mean field interaction that will be used. We have chosen a density–dependent interaction of the Skyrme type for the nuclear mean field, augmented by a momentum–dependent term. The features of our parametrization are described in detail in the literature[5,6] and we do not repeat them here. In a determinantal theory, the functional form of our momentum–dependent term would be obtained from the exchange term of a Yukawa force. Consequently, we refer to this interaction as the momentum–dependent Yukawa interaction (MDYI). It is quite pertinent to enquire if results of more microscopic calculations are reproduced by MDYI. Wiringa[7] has calculated the single particle potential in nuclear matter with the UV14 + TNI and UV14 + UVII interactions. Comparing with MDYI, we find the agreement quite good over a wide range of densities and momenta[6]. Similarly, the agreement with optical potential data is very good, both at low and high energies[8].

III. THE NUCLEAR EQUATION OF STATE AND TRANSVERSE MOMENTUM DATA

It is established that the transverse momentum technique proposed by Danielewicz and Odyniec[2] is sensitive to the flow characteristics of the nuclear system. It had been hoped early on that this experimental observable would be linked directly to the nuclear equation of state. This argument originates from the simple idea that, for a system in thermal equilibrium, one can simply relate the transverse momentum to the time integral of the pressure. However, this reasoning does not consider the possible nonequilibrium effects for which the relaxation times may be long on the time scales of nuclear collisions. Consequently, we have set out to investigate the sensitivity of the transverse momentum variable to the nuclear equation of state in the framework of the BUU model. It is a simple exercise in statistical mechanics to relate our MDYI interaction to its corresponding equation of state[6].

Comparing with data obtained by the Streamer Chamber collaboration for 800 MeV/n

nuclear collisions[9], we see that the agreement is quite impressive (Fig. 1).

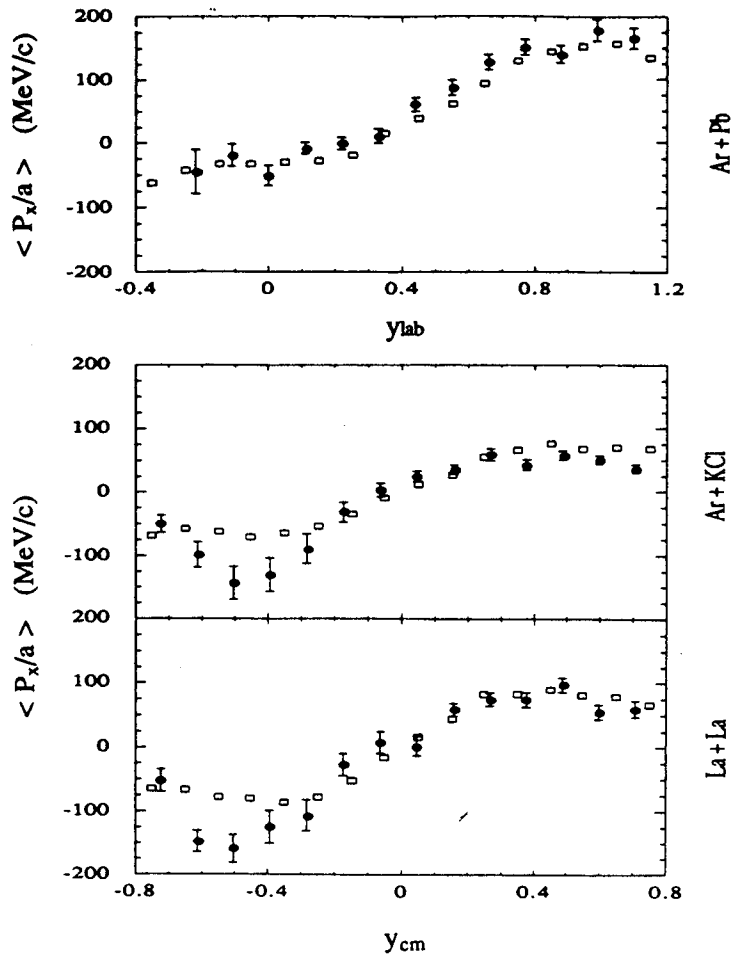

FIG. 1. Transverse momentum per nucleon as a function of rapidity in reactions of 800 MeV/n. Results of BUU simulations with the MDYI interaction (open squares) are compared with Streamer Chamber data (solid circles).

We can then ask the legitimate question: is this agreement sufficient to single out a possible nuclear equation of state, as characterized by its compressibility coefficient? The answer is: not quite. We in fact observe definite manifestations of nonequilibrium effects in the rapid rise of transverse momentum and we attribute this to the strong dynamical influence of the optical potential at these energies[6]. It is then clear that the transverse momentum generated need not reflect the equation of state directly at all, this being an equilibrium concept. To carry this argument to its logical conclusion, we display the effect of changing K from 215 MeV to 380 MeV (Fig. 2). The data clearly has little sensitivity to the precise

value of K.

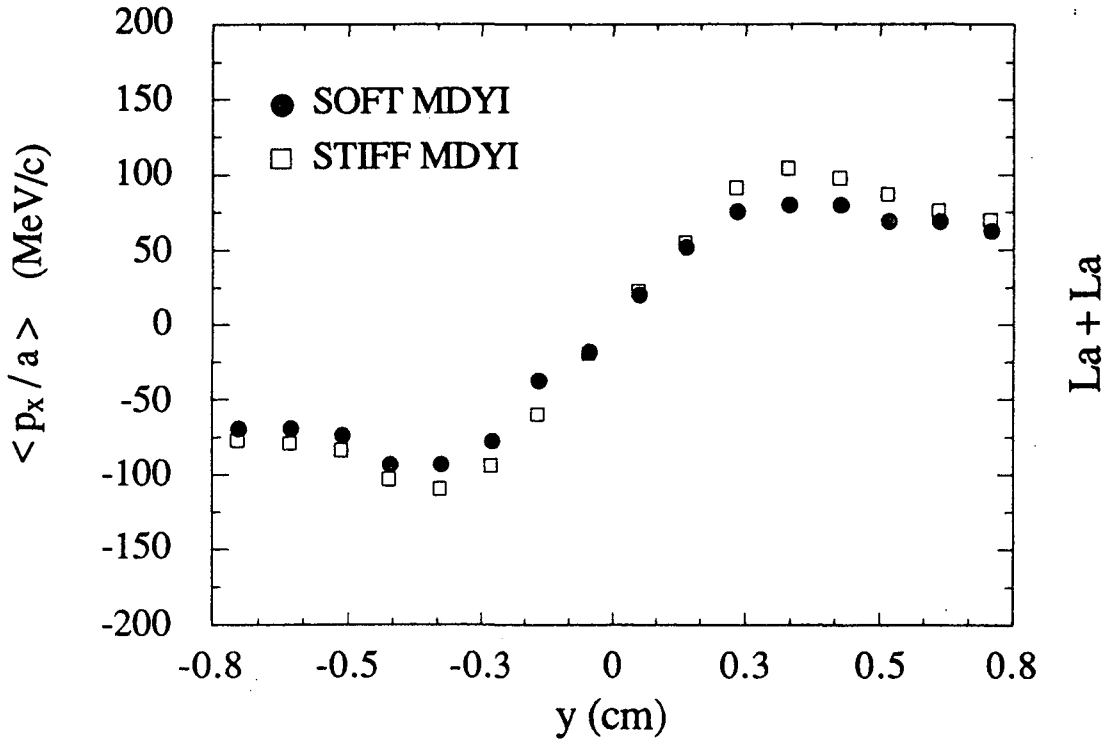

FIG. 2. Effect of the nuclear compressibility coefficient on transverse momentum generation. Effects of K = 215 MeV (solid circles) and K = 380 MeV (open squares) are shown.

IV. CONCLUSIONS

We have used the momentum–dependent BUU model to compare with streamer chamber measurements of the transverse momentum, and we have found that this observable is largely dependent on the nuclear mean field, not so much on the equation of state.This finding is in fact in accord with simulations in the relativistic Vlasov model[11]. Studies at lower energies will also be done, were the optical potential is smaller in magnitude. However smaller compressions will partly cancel this advantage for differentiating between equations of state. We plan to investigate the large body of data studied by the Plastic Ball as well as to study other observable such as azimuthal asymmetry[5] and out of plane squeeze–out[10].

It is a pleasure to acknowledge that much of the results discussed above were obtained in collaboration with S. Das Gupta, S. J. Lee, M. Prakash and G. M. Welke.

Critical Pion Opacity

Wolfgang Bauer
National Superconducting Cyclotron Laboratory
and Michigan State University
East Lansing, MI 48824-1321, USA

Abstract: The new effect of critical pion opacity is proposed. It is a reduction of the emission probability for central-rapidity pions in the vicinity of the critical point of the nuclear "liquid-gas" phase diagram. We show in a strongly simplified model how this effect can arise, and we discuss how it could be measured.

The classical phenomenon of critical opalescence is an increased scattering of electromagnetic radiation near to the critical point of a substance [1]. A particularly instructive example is found in Ref. [2] for the case of cyclohexane-aniline. Far away from T_c, there is no appreciable light scattering. As T_c is approached, however, the sample takes on a milky appearance. This is due to the scattering of light off the density fluctuations.

The density fluctuations are usually characterized by introducing the density-density correlation function

$$C(\vec{r}-\vec{r}') = \langle \rho(\vec{r})\rho(\vec{r}')\rangle - \rho^2. \tag{1}$$

Its relation to the isothermal compressibility is given by

$$\int d\vec{r} C(\vec{r}) = \rho \frac{\kappa_T}{\kappa_T^0}, \tag{2}$$

where the isothermal compressibility is defined as $\kappa_T = -V^{-1} \cdot (\partial V/\partial P)_{T,N}$ and its value for the ideal gas is $\kappa_T^0 = (\rho k_B T)^{-1}$. Since κ_T diverges at the critical point, the range of the correlation function has to increase near the critical point. Sufficiently close to T_c, the correlation length becomes as large as the wavelength of light. In this case, the density fluctuations scatter light strongly. This leads to the phenomenon of critical opalescence which was first explained in the classical theory of Ornstein and Zernicke [3]. The scattering intensity is given by

$$I(\vec{q}) = \frac{I^0(\vec{q})}{\rho} \int d\vec{r} e^{-i\vec{q}\vec{r}} C(\vec{r}), \tag{3}$$

where $\vec{q}$ is the momentum transfer, and $I^0(\vec{q})$ is the intensity for noninteracting particles.

We expect nuclear matter to have a phase diagram similar to a Van der Waals gas, because the nuclear interaction exhibits short range repulsion and long range attraction [4, 5]. It should be stressed at his point that there is no firm experimental evidence for the existence of a second order phase transition and a corresponding critical point as of yet. However, it is hoped that with the new heavy ion accelerators and 4π detectors this

interesting point of the nuclear phase diagram will be studied in detail. In a previous publication, we have pointed out methods to look for the critical point and to determine the critical exponents [6].

In this paper, we propose a new effect that should occur as we approach the critical point of nuclear matter from above as a function of the order parameter. It is the decrease of transparency of nuclear matter near the critical point for pions traversing it, and we have therefore dubbed it "Critical Pion Opacity".

We start out by noting that pion absorption is (at least) a two-nucleon process. The absorption of a pion on one nucleon is forbidden for simple kinematical reasons. The dominant channel for pion absorption is the so-called Delta process, in which a nucleon is excited to the isospin 3/2 Delta resonance state by the incoming pion. This Δ can then interact with a second nucleon via $\Delta + N \rightarrow N + N$ to complete the process of the pion absorption. This process has to take place at short inter-particle distances between the two nucleons of the order of [7]

$$d = \frac{\hbar}{\sqrt{M_N M_\pi}} \approx 0.5 \text{ fm}. \tag{4}$$

Thus the pion absorption cross section exhibits a dependence of $\sigma_{abs} \propto \rho^\lambda$, with $\lambda \geq 2$, and is therefore sensitive to the fluctuations in the density. If we could irradiate nuclear matter at its critical point with pions, we should see the effects of the density fluctuations in the pion absorption cross section. The following simple illustrative model is meant to demonstrate this effect.

We consider a system of nuclear matter at an average density of $\langle\rho\rangle = \rho_0/\alpha$ contained in a sphere of radius $R = r_0 A^{\frac{1}{3}} \alpha^{\frac{1}{3}}$ where A is the total number of baryons, the radius constant r_0 is given by 1.2 fm, and ρ_0 is the nuclear matter density. The constant α is in the range 2–4, such that the average density is at the critical value.

We take 2 limiting cases: One which contains no fluctuations in the density, $\rho(\vec{r}) = \rho_0/\alpha$, and one which contains maximum fluctuation, $\rho(r, \Omega_i) = \rho_0$, where Ω_i is an arbitrary solid angle with the constraint $\sum_i \Omega_i = 4\pi/\alpha$, and 0 otherwise (for the sake of analytical simplicity). In the homogeneous case, we obtain for the average absorption cross section for a pion escaping from the center of the distribution ($\lambda = 2$)

$$\begin{aligned} \sigma_{\text{hom}} &\propto \frac{1}{4\pi} \int_0^{4\pi} d\Omega \int_0^R dr \left(\frac{\rho_0}{\alpha}\right)^2 \\ &= r_0 A^{\frac{1}{3}} \rho_0^2 \alpha^{-\frac{5}{3}}, \end{aligned} \tag{5}$$

whereas the case with fluctuations yields

$$\begin{aligned} \sigma_{\text{inhom}} &\propto \frac{1}{4\pi} \int_0^{4\pi} d\Omega \int_0^R dr \rho^2(r, \Omega) \\ &= r_0 A^{\frac{1}{3}} \rho_0^2 \alpha^{-\frac{2}{3}}. \end{aligned} \tag{6}$$

We therefore obtain the result $\sigma_{\text{inhom}}/\sigma_{\text{hom}} = \alpha$, an increase in the absorption cross section by a factor of 2–4. For a general value of $\lambda \geq 2$, we obtain $\sigma_{\text{inhom}}/\sigma_{\text{hom}} = \alpha^{\lambda-1}$.

We now discuss if and how this effect could be observed in experiment. It is generally believed that there are in principle two ways in which the nuclear matter critical point can be reached. One would be in very asymmetric systems (proton + heavy target), in which for sufficiently high bombarding energies ($E_{\rm beam} > 5$ GeV) the spectator matter could be heated up to the temperature necessary to reach the critical point. The other way would be the central collision of symmetric heavy ion systems with $E_{\rm beam} \approx 100$ MeV/nucleon. The second one is preferred in our case, because of the simpler determination of the deposited excitation energy [8], and because in this case thermalization predominantly proceeds via elastic nucleon-nucleon collisions.

During the compression phase of this heavy ion collision, densities of 1.5 to 2 ρ_0 are reached and some pions are produced. The overall excitation function for these "sub-threshold" pions is well understood in this beam energy domain [9]. Even though there is a large amount of absorption during this high density phase of the collision, some pions escape from this high density phase. To experience the effect of density fluctuations near the critical point, the pions have to stay in the baryon matter long enough for it to expand to the critical point. We have estimated the time interval for this expansion in a simple manner.

We consider the case of isothermal expansion from a compressed spherically symmetric state at a temperature $T \approx T_c$. The equation to solve for the expansion is then

$$\frac{d}{dt}\vec{P} = \oint \mathcal{P} d\vec{s}, \tag{7}$$

where $d\vec{s}$ is a surface element of the sphere in which the baryons are contained, and $\mathcal{P}$ is the pressure. To obtain quantitative estimates for the expansion time, we chose the equation of state of Ref. [10],

$$\mathcal{P}(\overline{\rho}, \overline{T}) = 3.5\,(\overline{\rho}^3 - \overline{\rho}^2) + 1.825\,\overline{\rho}^{\frac{1}{3}}\,\overline{T}^2 \text{ MeV fm}^{-3} \tag{8}$$

with the dimensionless variables $\overline{\rho} = \rho(t)/\rho_0$ and $\overline{T} = T/T_c$, $T_c = 16.5$ MeV.

Instead of solving the full set of hydrodynamic equations, we obtain a simple estimate by computing the force on a circle which is obtained by cutting through the center of the nucleus. This leads to a simple second order differential equation initial value problem for the radius, $R(t)$ of the sphere containing the baryons,

$$\frac{d^2}{dt^2}R(t) = \frac{16\pi}{3\,A\,M_{\rm n}} R^2(t)\mathcal{P}(t) \tag{9}$$

We solve it using a standard Runge-Kutta method. For a system of $A = 300$ nucleons and an initial compression of $\rho_i = 2\rho_0$, for example, we calculated the time for the system to reach the critical density of $\rho_{\rm cr} = \frac{5}{12}\rho_0$ as $t_{\rm cr} = 21.4$ fm/c.

A pion which was created at $\rho = 2\rho_0$, $t = 0$, $R = 0$, can therefore have a maximum velocity of ≈ 0.5 c in the baryon center of mass frame, if it is required to be within the baryon sphere at $t = t_{\rm cr}$. This corresponds to a kinetic energy of $T^{\pi}_{\rm cr} = 22$ MeV.

Pions having less energy in the c.m. frame than this value will on average experience this effect, whereas the faster pions should not. The way in which we propose to test our

predictions is linked to this observation. We suggest to measure the ratio

$$\mathcal{R}_\pi(E_{\rm beam}) = \frac{\sigma_\pi(T^\pi < T^\pi_{\rm cr})}{\sigma_\pi(T^\pi > T^\pi_{\rm cr})} \tag{10}$$

for central collisions of symmetric heavy ion systems. We predict that this ratio will have a dip at the beam energy which leads to an expansion which goes through the critical point in the nuclear matter phase diagram. This dip should be superimposed on an otherwise smoothly rising function $\mathcal{R}_\pi(E_{\rm beam})$. The exact width and depth of this dip is not predictable within the simple framework developed here, but the experimental detection of this effect would indicate exiting new nuclear many-body physics.

It is a pleasure to acknowledge helpful discussions with G.F. Bertsch, V. Efimov, and P.J. Siemens.

References

[1] H.E. Stanley, "Introduction to Phase Transitions and Critical Phenomena", Oxford University Press, New York and Oxford (1971).

[2] R.A. Ferrell, in "Fluctuations in Superconductors" (eds. W.S. Goree and F. Chilton), Stanford Research Institute (1968).

[3] L.S. Ornstein and F. Zernicke, Proc. Sect. Sci. K. med. Akad. Wet. **17**, 793 (1914).

[4] L.P. Csernai and J.I. Kapusta, Phys. Rep. **131**, 223 (1986).

[5] P.J. Siemens and A.S. Jensen, "Elements of Nuclei", Addison Wesley, Redwood City (1987).

[6] W. Bauer, Phys. Rev. C **38**, 1297 (1988).

[7] G.E. Brown and P.J. Siemens, preprint.

[8] W. Bauer, Phys. Rev. Lett. **61**, 2534 (1988).

[9] W. Bauer, Phys. Rev. C **40**, 715 (1989).

[10] J. Kapusta, Phys. Rev. C **29**, 1735 (1984).

QUANTITATIVE PHENOMENOLOGY FOR THE e^+e^- PUZZLE, AND PREDICTED SHARP ANNIHILATIVE POSITRONS FROM U+Ta COLLISIONS

James J. Griffin
Department of Physics, University of Maryland,
College Park, Maryland 20742 (U.S.A.), and

Thomas E. Cowan
Physics Department(L-421), Lawrence Livermore National Laboratory
Livermore, California (U.S.A.)

ABSTRACT

Calculations based upon a Quadronium phenomenology of the "e^+e^- Puzzle" are reported. Here the U+Th lines (at 809, 760, and 608 keV) arise from from Free Annihilative Pair Emittive Decay (FAPE) of Q_o and the U+Ta (e^+e^-) lines (805, 748, and 620 keV), from decays of Quadronium bound to an emergent heavy ion, presumably Uranium (Bound Annihilative Pair Emittive Decay, BAPE). A good semi-quantitative description is obtained for the observed characteristics of these six lines. This description also implies a new process, Sharp Annihilative Positron Emission (SAPosE) in which the decay electron is captured, ejecting only a positron whose kinetic energy is equal to the total decay energy plus the electron binding energy. It follows that the U+Ta (e^+e^-), which appear to follow a bound decay, must exhibit such energetic positron lines, whose width and probability we estimate.

1. INTRODUCTION

Previously it has been noted[1,2] that the existence of a strongly bound state of Quadronium, ($e^+e^+e^-e^-$), could allow a *qualitatively* complete phenomenology[3-6] for the "e^+e^- Puzzle" posed by the data[7-11] on coincident e^+e^- pairs from high-Z heavy ion collisions. Our discussion is based upon the following spontaneous-creation/mass-inflation scenario[1-6] consequent to that conjecture.

In the super-Q critical field of the nuclear collision a leptonic Quadroniumatom (Q_o) is created spontaneously by an exothermic decay of the vacuum. This process is energetically possible because the Q_o atom is so strongly polarized by the nuclear Coulomb field that its isolated ground state energy of (~1.5MeV) MeV is reduced to a negative value. Then as the ions separate, and their effective Coulomb field diminishes, the Q_o is depolarized, absorbing from the ions the energy needed to attain its isolated ground (or excited) state energy (mass inflation).

As this process develops, the Q_o may be released, to decay as an isolated free particle, or it may be captured by an ion to decay from its bound state. In the latter case the decay leptons will acquire from the nuclear Coulomb field a positive difference energy, $\Delta = E_+ - E_-$. (Indeed we propose, and use, such a positive value of $\langle\Delta\rangle$ as the signature of bound decays.)

2. GLOBAL ASSESSMENT

Despite the success of this description, the specific calculations[12,13] which quantify it do not depend upon any structural features of the decaying particle itself, apart from its small radius, its capacity to bind to the nucleus, and its decay into (e^+e^-). Therefore the question whether this decaying object is in fact Quadronium, or something else, remains unresolved.

On the other hand, this Quadronium deciphering of the "(e^+e^-)-Puzzle" successfully encompasses the observations and suggests sharp questions for both theory and experiment. We expect these questions to lead either to further successful elaboration of the description or to some significant (and hopefully, indicative) failure. One can ask no more of a good phenomenology.

3. PHENOMENOLOGICAL CALCULATIONS

Our results[12-13] are summarized in Tables I, II, and III, as described in the captions. We here note only the central physical features which determine the implications of our description.

a) All widths arise from Lorentz transformation of the lepton energies from the rest frame of the Q_o to the lab frame: $\Lambda = \gamma\Lambda' + \gamma v_Q \lambda' \cos\theta'$, where $(\Lambda, \vec{\lambda})$ is a lepton energy-momentum 4-vector, or a sum or difference of them.

b) In the bound (BAPE) decay of Q_o, the sum energy width is dominated by the non-zero difference, $(p_+^{\prime} - p_-^{\prime})$. Also the average difference energy is positive, and the difference width is larger than that of the corresponding free decay due to the additional spread in the Coulomb potential energy for various decay sites of the Q_o. All of these features are due to the effect of the Coulomb field upon the decaying Q_o; also, their magnitudes are all fixed by the extension, R_o, of the Q_o wave function about the nucleus, which is here fit to the $\langle\Delta\rangle$- value of the 748 keV line. (The average lab velocity of the ion is taken equal to the maximum Epos-acceptable value, $v_U^{MAX} = 1.62 v_{CM}$, yielding an over-estimate, indicated by the $\gtrsim$ signs in Table II.)

c) For the free (FAPE) Q_o decays, there is no Coulomb field. Then $(p_+^{\prime} - p_-^{\prime})$ vanishes, and the (now unavoidably small) sum widths are determined by the spread of the small Q_o translational kinetic energy. Also, the difference energy is identically zero, and its width is entirely due to the Doppler broadening. (The speed of the free Q_o is assumed in our calculations to be distributed uniformly over the interval $(0, 2v_{CM})$.)

4 TABULATED THEORETICAL (& EXPERIMENTAL) RESULTS FOR FAPE, BAPE, AND SAPosE DECAYS.

The following three tables summarize the calculations and compare them with the corresponding experimental quantities (in parentheses) for the free, bound, and sharp positron pair emittive decays of Q_o.

Table I: The average difference energy and the widths of the sum and difference energy distributions calculated for the Free Annihilative Pair Emittive (FAPE) decay are compared with the experimental results (in parentheses) of Ref.10 for the U+Th collision (in keV). Good semi-quantitative agreement is evident, although the sum widths seem systematically too small.

TABLE I: U + Th, Free Annihilative Decays

K_T = $\langle\overline{K_+ + K_-}\rangle$	Sum Width $\langle\Gamma^F_\Sigma\rangle$ (Exp)	K.E. Diff. $\langle\bar{\Delta}\rangle$ (Exp)	Diff.Width $\langle\Gamma^F_\Delta\rangle$ (Exp)
608	6.2 (23)	0 (~-10)	96 (~166)
760	6.8 (<80)	0 (~+6)	110 (~140)
809	7.0 (42)	0 (~+25)	115 (~130)

Table II: The average difference energy and the widths of the sum and difference energy distributions are calculated for Bound Annihilative Pair Emittive (BAPE) decay and compared with the experimental data (in parentheses) of Ref. 10 for the U+Ta collision (in keV). The separate Coulomb and Doppler contributions to Γ^B_Δ are indicated. Good semi-quantitative agreement is evident. (The value (*) of $\langle\overline{\Delta^B}\rangle$ for the 748 keV line has been fit to experiment; also, the ≥ signs indicate overestimates.)

TABLE II: U + Ta, Bound Annihilative (BAPE) Decays

K_T	$\langle\Gamma^B_\Sigma\rangle \geq$(Exp)	$\langle\overline{\Delta^B}\rangle$ (Exp)	$\langle\Gamma^B_\Delta\rangle = \langle[\sigma_C^2+\sigma_D^2]\rangle^{1/2} \geq$(Exp)
620	27 ≥(20)	114 (~30)	$183=[102^2+153^2]^{1/2}$ ≥(~230)
748	26 ≥(26)	*150 (~150)	$239=[166^2+173^2]^{1/2}$ ≥(~450)
805	26 ≥(20)	163 (~220)	$265=[193^2+182^2]^{1/2}$ ≥(~280)

Table III: For each EPOS coincident (e^+e^-) line from the U+Ta reaction, the kinetic energies of the three most energetic sharp positrons are listed together with their estimated fractional (with respect to all Q_0 decays of the specified total energy) intensities, f_n. Also, the total positron fraction, f_+; the fraction of decays, f_R, which yield pairs with electrons of kinetic energy $K_- < 200$ keV (therefore) rejected by the EPOS e_- detectors; the fraction, f_P, which yields coincident pairs acceptable to EPOS; and the ratio, F, of (total) sharp positrons to the acceptable coincident pairs. Finally, the distances (in $\hbar/mc$) of the Q_0 from the nucleus which yield electrons of energies $E_1, E_2, \ldots E_\infty = 0$, and 200 keV, and which serve as the boundaries for calculating the fractions, f_i, are tabulated. The width of these lines are calculated to lie in the range, $60 < \Gamma_+ < 160$ keV, as discussed in Ref. 12.

TABLE III: SAPosE Lines in (U,Q_o) from U+Ta Reaction

EPOS (e^+e^-) Summed Energy $K_T = \langle K_+ + K_- \rangle$	Positron Lines Energy (fraction) (Distance, $\hbar/mc$) $K_+^1(f_1)$ $(<r_1)$	$K_+^2(f_2)$ $(<r_2)$	$K_+^3(f_3)$ $(<r_3)$	Total Positron Fraction $f_+ = \Sigma f_n$ $(<r\ )$	Electron Continuum Rejected Fraction f_R $(<d_{200})$	Pair Fraction f_P $(<\infty)$	Ratio: Positrons to Pairs $F = f_+/f_P$
805 keV	937(0.13)	837(0.03)	818(0.01)	0.17	0.14	0.69	0.25
Distance:	0.648	0.798	0.833	0.861	1.71	∞	
748 keV	880(0.14)	780(0.03)	761(0.01)	0.18	0.17	0.65	0.28
Distance:	0.684	0.854	0.894	0.927	1.99	∞	
620 keV	752(0.15)	652(0.04)	633(0.01)	0.21	0.28	0.51	0.41
Distance:	0.783	1.013	1.071	1.118	3.15	∞	

REFERENCES

1. J. J. Griffin, Proc. 5th Int. Conf.on Nucl.React.Mech., Varenna, Italy (6/88), ed. E. Gadioli (Physics, U.of Milano, Italia) p. 669.
2. J. J. Griffin, J. Phys. Soc. Jpn. 58 (1989) Suppl.p427.
3. J. J. Griffin, "Quadronium: Spontaneous Creation ...", U. Md. PP#89-053 (10/88), submitted to Phys.Rev.Lett.
4. J. J. Griffin, "Quadronium: Phenomenology for the e^+e^- Puzzle", U. of Md. PP#89-048, DOE/ER/40322-051 (9/88), submitted to Phys. Rev. C.
5. J. J. Griffin, in Microscopic Models...", ed. M.Guidry *et al.* (World Sci., Singapore, 1989), p 409.
6. J. J. Griffin, J. Phys.G:Nucl.Part.Phys.15,925 (1989).
7. We treat here the data of the EPOS group, from Refs. 8-11. Reviews, including the extensive work of the "Orange" group, can be found in Refs. 9,11.
8. T. Cowan, et al., Phys.Rev.Lett.54,1761(1985) and Phys. Rev. Lett. 56, 444 (1986).
9. T. E. Cowan, "Monoenergetic Positrons and Correlated Electrons from Superheavy Nuclear Collisions", Ph.D. dissertation, Yale Univ. (5/88).
10. H. Bokemeyer, *et al*, 8th Moriond Workshop, Les Arcs,France (1/89); and Rpt. GSI-89-49 (5/89) (GSI, Darmstadt, W. Germany).
11. In Physics of Strong Fields, ed. W. Greiner (World Science, 1987), one finds summaries by T. Cowan and J. Greenberg (p.111), H. Bokemeyer (p. 195), C. Kozhuharov (p.265), and W. Koenig (p.281). See also P. Kienle, Ann. Rev. Nucl.Part.Sci.36,605(1986).
12. J.J.Griffin and T. E. Cowan, U. of Md. PP#90-060, and PP#90-102, to be published.
13. J.J.Griffin, U. of Md. PP#90-063, to be published.

The Second Order Variation in Thomas-Fermi Theory

S. Das Gupta, S.J.Lee[1], R.K. Bhaduri[2], H.H. Gan[3] and E.D. Cooper[4]

Physics Dept., McGill University, Montreal, P.Q., H3A 2T8, Canada.

1. Now at Physics Dept., Rutgers University, Piscataway, NJ, USA.
2. Permanent address: Physics Dept., McMaster University, Hamilton, ON, Canada.
3. Now at Chemistry Dept., McGill University, Montreal, P.Q., Canada.
4. Now at Physics Department, Ohio State University, Columbus, Ohio, USA.

The energy E that one minimises in Thomas-Fermi theory consists of two parts; kinetic and potential. In three dimensions the density $n(\vec{r})$ is given by

$$n(\vec{r}) = \gamma 4\pi/h^3 \int_0^{p_F(\vec{r})} p^2 dp = \gamma 4\pi p_F^3(\vec{r})/3h^3 \tag{1}$$

Here γ is a degenaracy factor; 2 for electrons if one is doing atomic physics. In the nuclear physics case in which we are primarily interested , $\gamma = 4$ for N=Z nuclei if the Coulomb energy is neglected. The kinetic energy is given by $T = \int T(\vec{r})d^3r$ with

$$T(\vec{r}) = \gamma 4\pi/h^3 \int_0^{p_F(\vec{r})} \frac{p^4}{2m} dp = Cn^{5/3}(\vec{r}) \tag{2}$$

The potential energy may consist of several contributions. In the case of atomic electrons there is an external field due to the nucleus (this is absent in the nuclear physics case)

$$V^{(1)} = \int v_{ext}(r) n(\vec{r}) d^3r \tag{3}$$

There is finite range mutual interaction between nucleons (or electrons)

$$V^{(2)} = \frac{1}{2} \int v(\vec{r}, \vec{r}') n(\vec{r}) n(\vec{r}') d^3r d^3r' \tag{4}$$

It is customary to add other terms in the nuclear case to obtain saturation in nuclear matter:

$$V^{(3)} = \sum_i \int \frac{c_i}{\sigma_i + 1} (n(\vec{r}))^{\sigma_i + 1} d^3 r \tag{5}$$

Let us denote the equilibrium density by $n_0(r)$ and write $n(\vec{r}) = n_0(r) + \delta n(\vec{r})$. Provided $\int \delta n(\vec{r}) d^3 r = 0$ (we do not change the number of particles), we should find $E = E_0 + D(\delta n)^2$ with D positive if a minimum is reached. From eqs.(2),(3),(4) and (5), keeping terms upto second order in δn, we find

$$\begin{aligned} E = E_0 + \int \left(\frac{5}{3} C n_0^{2/3}(r) + v_{ext}(r) + \int v(\vec{r}, \vec{r}') n_0(r') d^3 r' + \sum_i c_i n_0^{\sigma_i}(r) \right) \delta n(\vec{r}) d^3 r \\ + \int \left(\frac{5}{9} C n_0^{-1/3}(r) + \frac{1}{2} \sum_i c_i \sigma_i n_0^{\sigma_i - 1}(r) \right) (\delta n(\vec{r}))^2 d^3 r \\ + \frac{1}{2} \int v(\vec{r}, \vec{r}') \delta n(\vec{r}) \delta n(\vec{r}') d^3 r d^3 r' \end{aligned} \tag{6}$$

The Thomas-Fermi density is found by requiring that in the region $n_0(r) \geq 0$ the density satisfies

$$\frac{5}{3} C n_0^{2/3}(r) + v_{ext}(r) + \int v(\vec{r}, \vec{r}') n_0(r') d^3 r' + \sum_i c_i \sigma_i n_0^{\sigma_i - 1}(r) = \lambda \tag{7}$$

where λ, the Fermi energy, is a constant (see ref. 1 for a numerical method for obtaining $n_0(r)$). Then the first order variation goes to zero explicitly from the condition $\int \delta n(\vec{r}) d^3 r = 0$. In addition we need

$$\begin{aligned} \int \left(\frac{5}{9} C n_0^{-1/3}(r) + \frac{1}{2} \sum_i c_i \sigma_i n_0^{\sigma_i - 1}(r) \right) (\delta n(\vec{r}))^2 d^3 r \\ + \frac{1}{2} \int v(\vec{r}, \vec{r}') \delta n(\vec{r}) \delta n(\vec{r}') d^3 r d^3 r' > 0 \end{aligned} \tag{8}$$

Eq.(10) is the stability condition for Thomas-Fermi approximation.

We will only consider examples where $n_0(r)$ goes to zero at some finite value of $r = r_0$. Several clarifying comments may be useful. The variation $\delta n(\vec{r})$ is restricted to be in

the region $r = 0$ to $r = r_0$ as outside of r_0, eq.(7) does not hold. We also require that $|\delta n(\vec{r})|/n_0(r) << 1$ as we have replaced the kinetic energy term $Cn^{5/3}(\vec{r})$, (eq.(2)) by $C(n_0(r) + \delta n(\vec{r}))^{5/3} \approx Cn_0^{5/3}(r) + O(\delta n) + O(\delta n)^2$. Further the variation of $\delta n(\vec{r})$ need to be such that $\int \delta n(\vec{r}) d^3r = 0$. Even with these restrictions there is, of course, an infinite number of choices of $\delta n(\vec{r})$ all of which must satisfy eq.(8). This can be ensured if, in the following eigenvalue equation,

$$\int S(\vec{r}, \vec{r}')g_i(\vec{r}')d^3r' = \epsilon_i g_i(\vec{r}) \tag{9}$$

where

$$S(\vec{r}, \vec{r}') = \left(\frac{10}{9} Cn_0^{-1/3}(r) + \sum_i c_i \sigma_i n_0^{\sigma_i - 1}(r) \right) \delta(\vec{r} - \vec{r}') + v(\vec{r}, \vec{r}') \tag{10}$$

all the eigenvalues ϵ_i are > 0. This is because $\delta n(\vec{r})$ can be expanded in terms of the eigenfunctions $g_i(\vec{r})$.

One may regard the Thomas-Fermi theory as a semi-classical approximation to Hartee-Fock theory. The analogy is quite deep. In the Hartee-Fock case one defines an RPA matrix. For stability the eigenvalues must all be real (ref.2). $S(\vec{r}, \vec{r}')$ is the corresponding matrix in semi-classical treatments. The experience in nuclear structure is that the lowest eigenfunctions of the RPA matrix are good representations of collective states, often identified in experiments. We find that this is true for eigenfunctions $g_i(\vec{r})$ as well. They closely represent results from incompressible and irrotational models of flow.

For practical purposes it is convenient to do a multipole expansion. Write $g(\vec{r}) = g_l(r)y_{lm}(\hat{r})$ and then $v(\vec{r}, \vec{r}') = \sum_{l,m} v_l(r, r')y_{lm}(\hat{r})y^*_{lm}(\hat{r}')$. The equation to solve now is $\int_0^{r_0} S_l(r, r')g_l(r')r'^2 dr' = \epsilon g_l(r)$. For $l > 0$, the condition $\int g_l(\vec{r})d^3r = 0$ is automatically satisfied. More care is needed in the $l = 0$ case.

Ref. 3 gives results from atomic physics as well as a summary of results from nuclear physics. Ref. 4 contains more details from nuclear physics and further establishes

connections with time dependent Vlasov equations.

The figure below shows the lowest solutions of the stability matrix for $l = 0, 1$ and2(solid lines)for the nucleus ^{40}Ca. The dashed line (which is indistinguishable from the solid line for $l = 1$) is given by $r^l \frac{\partial}{\partial r} n_0(r)$ for $l = 1, 2$ and for $l = 0$ by $\alpha^3 n_0(\alpha r) - n_0(r)$ with $\alpha \approx 1 + \delta\alpha$. The dotted line shows the calculated Thomas-Fermi density.

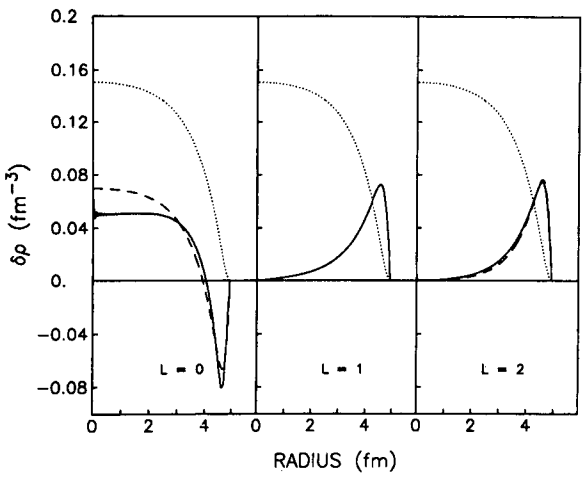

This work is supported in part by NSERC and in part by the Quebec Department of Education.

References

1) S.J.Lee,H.H.Gan,E.D.Cooper,S.Das Gupta, Phys. Rev C40,2585(1989).

2) D.J.Thouless,Nucl. Phys, 21,225(1960).

3) S.J.Lee,S.Das Gupta,R.K.Bhaduri, Phys Rev A(1990).

4) S.J.Lee,E.D.Cooper,H.H.Gan,S.Das Gupta, Phys Rev C41,706(1990).

Pion Production in Au+Au Collisions at 1.15 GeV/N from the Bevalac Streamer Chamber

S.I. Chase, P. Barnes, J.W. Harris, J. Miller, G. Odyniec, W. Rauch, L. Teitelbaum, S. Tonse
Nuclear Science Division, Lawrence Berkeley Laboratory,
University of California, Berkeley, CA 94720, USA
R.E. Renfordt
Fachbereich Physik, Universität Frankfurt, D-6000 Frankfurt, Germany
M.L. Tincknell
Physics Division, Oak Ridge National Laboratory, Oak Ridge, TN 37830

A complete picture of nuclear dynamics in the fireball regime is not possible without a detailed understanding of the expansion and freezeout which affect all hadronic participants in the reaction. The now well-established evidence for baryon flow provides an example of the effect of decompression on final-state distributions. Further information on these later stages of the collision may be found by studying pions, the other major hadronic constituent of the fireball. M.-C. Lemaire has shown at this meeting some suggestive results on pion flow in asymmetric systems from the Diogene collaboration but the mechanism that produces this effect is not yet well established. This paper concerns pion spectra in heavy systems in the collision energy range 500-1400 MeV/N. We suggest that some features of these spectra may shed some light on the dynamics of the later stages of fireball evolution.

The LBL-GSI Streamer Chamber collaboration analyzed the reaction Ar+KCl $\rightarrow \pi^-$ + X for central collisions at a variety of energies at the Bevalac[1]. Fig. 1 shows the π^- kinetic energy spectrum in the CM frame at beam energy 1.8 GeV/N at 90±10 degrees. The curve is a one-temperature Maxwell-Boltzmann distribution at T = 69 MeV. There is a clear excess in the data for E > 500 MeV. The data can however be fit with a two-temperature model. The main component is then consistent with the decay of deltas in thermal equilibrium at T = 118 MeV, the temperature extracted from a very good single-temperature fit of the proton kinetic energy spectrum. The second component, with roughly 5% of the total π^- yield, has a nearly isotropic angular distribution and a slope parameter T = 110±10 MeV. The authors suggested that the decay of higher resonances may be responsible for the second component. Alternatively, the 110 MeV temperature of the pions in the second component is suggests that they may be thermal pions from the 118 MeV fireball.

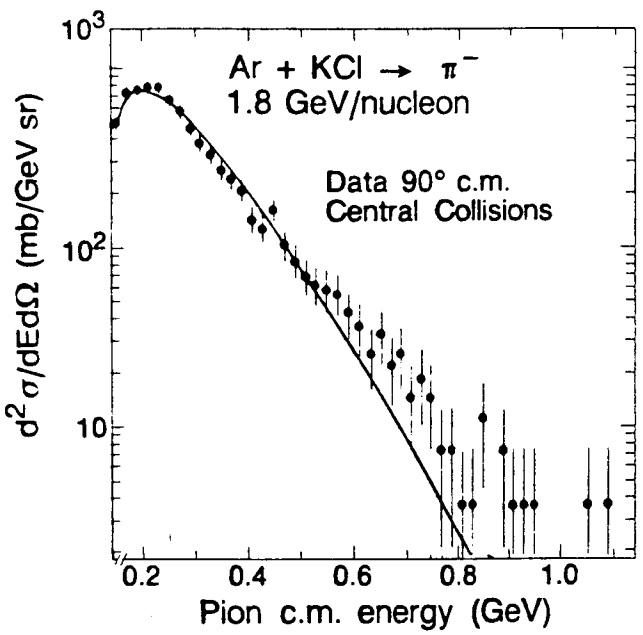

Fig.1: Energy spectrum of π^- at 90±10° in the C.M. with a Maxwell-Boltzmann fit with $T_\pi = 69 MeV$.

In a later experiment[2], La+La $\rightarrow \pi^- + X$ was studied at 530, 740, and 1350 MeV/N. Fig. 2 shows the π^- spectrum at the highest energy. The second component is now populated by the majority of the pions. At 530 and 740 MeV/N there is a small excess, less than 5%, for E > 400 MeV but in both cases the statistics are limited and the yield is not well known. Clearly there is a strong trend towards increasing yield in the second component with both increasing mass and beam energy. The mass dependence makes it more difficult to explain the excess in terms of higher resonances. One naively expects the yield of massive particles to be a function of temperature but not system volume. However, a "pumping" mechanism might follow these systematics. Due to the increase in the average number of collisions per participant in the more massive fireball, $\Delta + n \rightarrow N + n$ becomes more likely and, consequently, such higher resonances (N's and N*'s) are more abundant in the heavier fireball. Several authors[3] have also studied the effects of radial flow on the negative pion spectrum, with inconclusive results.

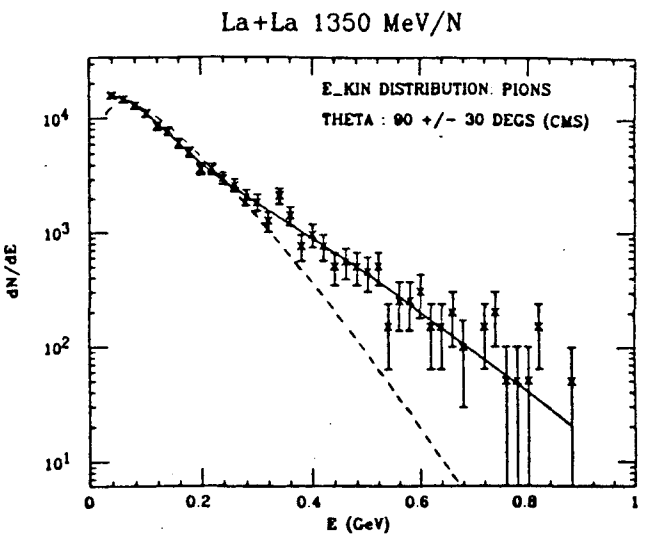

Fig.2: Kinetic Energy spectrum of π^- at 90±30° in the C.M. with one-temperature (dashed) and two-temperature (solid) fits.

The current experiment, Bevalac E902, by the LBL Streamer Chamber group and collaborators, extends the systematics to the very heavy Au+Au system at the highest available Bevalac energy for Au beam, 1.15 GeV/N. The streamer chamber was imaged with 3 image-intensified megapixel charge-coupled-device (CCD) cameras.[4] Our central trigger selects approximately 5% of the total inelastic cross-section, corresponding to impact parameters $\leq$ 3 fm in a clean-cut geometrical model. The resultant charged-particle multiplicity distribution and π^- yields are shown in Fig. 3. The x-intercept of the b = 0 line is at less than Z = 79 to account for measuring losses. The slope is determined by charge conservation and the other lines are computed relative to the b = 0 line assuming clean-cut geometry.

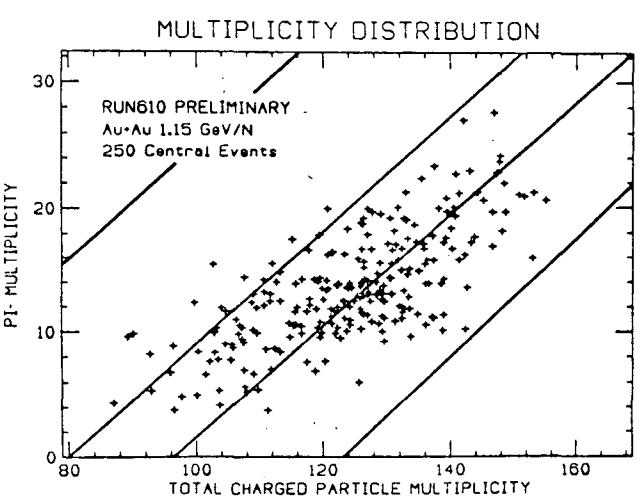

Fig.3: π^- and charged-particle yields for a central trigger of 5% $\sigma_{inelastic}$. Solid lines indicate variation of impact parameter, with b = 0, 1.8, 3.0, and 5.0 fm from right to left.

An estimate of $< N_\pi/A >$ can be derived from the raw data of Fig. 3. From the isospin excess of Au one can compute
$< N_\pi >= 2.64 < N_{\pi^-} >= 97. \pm 11.4$,
$< A >= 2.49 < N_{charge} >= 242. \pm 28.5$,
$< N_\pi > / < A >= .148 \pm .023$.
Now $< N_\pi > / < A >$ is not exactly $< N_\pi/A >$. With this caveat, Fig. 4 shows the published results[5] for Ar+KCl and La+La along with our estimate for Au+Au. The quoted errors reflect the ommission of three corrections: (1) removal of electrons from Bethe-

Heitler conversion, in the target, of photons from π^0 decay, (2) correct counting of Z>1 fragments in the participant charge, and (3) elimination of spectator charges now included in the participant charge estimate. This preliminary estimate is clearly consistent with previous results suggesting that pions are produced throughout the volume of the fireball, and not just at the surface. A complete analysis is forthcoming.

The preliminary π^- spectrum, Fig. 5a, clearly shows significant nonthermal behavior. Due to the low statistics in the data analyzed so far, quantitative estimates of slope parameters and yields are difficult to make at this time. No electron correction has been done but it is expected to be less than 10% everywhere. Comparison with the La+La π^- spectrum suggests that R1, the yield in the first component, is of comparable magnitude, which reflects the systematics previously observed, given the heavier mass but lower energy of the Au+Au system.

It is well known that cascade models with only the delta resonance predict an exponential spectrum. Fig. 5b shows a calculation with the Cugnon INC model, which is well described by a one-temperature fit of T = 61 MeV. The prediction of the VUU model, Fig. 5c, in constrast is not widely known. It is clearly concave, with R1 = 32.5%, i.e., it has a very large second component. (The La+La data of Fig. 2 has R1 = 42.9%.) For comparision, Fig. 5d gives the Au+Au data overlayed with both the normalized Cascade and VUU predictions.

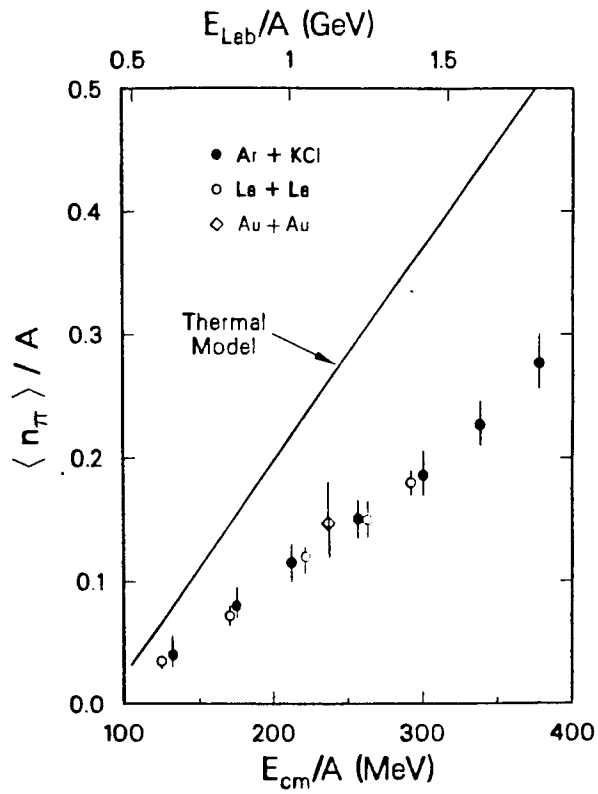

Fig.4: $< N_\pi >/A$ from Ref. 5 with the preliminary result for Au+Au from this work. $< N_\pi >$ scales with A at fixed E_{CM}, suggesting that pions are produced thoughout the fireball volume.

The success of VUU in predicting the concave shape of the spectrum suggests the possibility that the mean field is responsible for the spectral shape, perhaps through the effect of the baryon flow on the pions. Baryons in the flow plane receive an extra boost from decompression, and pions produced from these baryons may have an excess of kinetic energy relative to pions produced out of the flow plane. Furthermore, pions that scatter on these baryons may get 'caught in the baryon flow' and receive excess kinetic energy from the directed motion of the baryons.

Transverse-momentum analysis of full Au+Au events is necessary to determine if pions in the second component are correlated with the flow plane. The source of the second-component in the VUU data must also be identified. Future work also includes extension of the INC model to include higher resonances and a systematic study of VUU predictions for other avaiable data, i.e., Ar+KCl and La+La at all energies. Additional data reduction for Au+Au is proceeding, and the final statistics will more than double the current data.

None of the available models treat pion dynamics in a complete way. For example, the VUU model used above includes deltas in the mean field, but does not include free pions which interact only via hard collisions. Further understanding of this data will probably require careful comparisons to models such as VUU or QMD, and will be limited if these model difficiencies are not corrected.

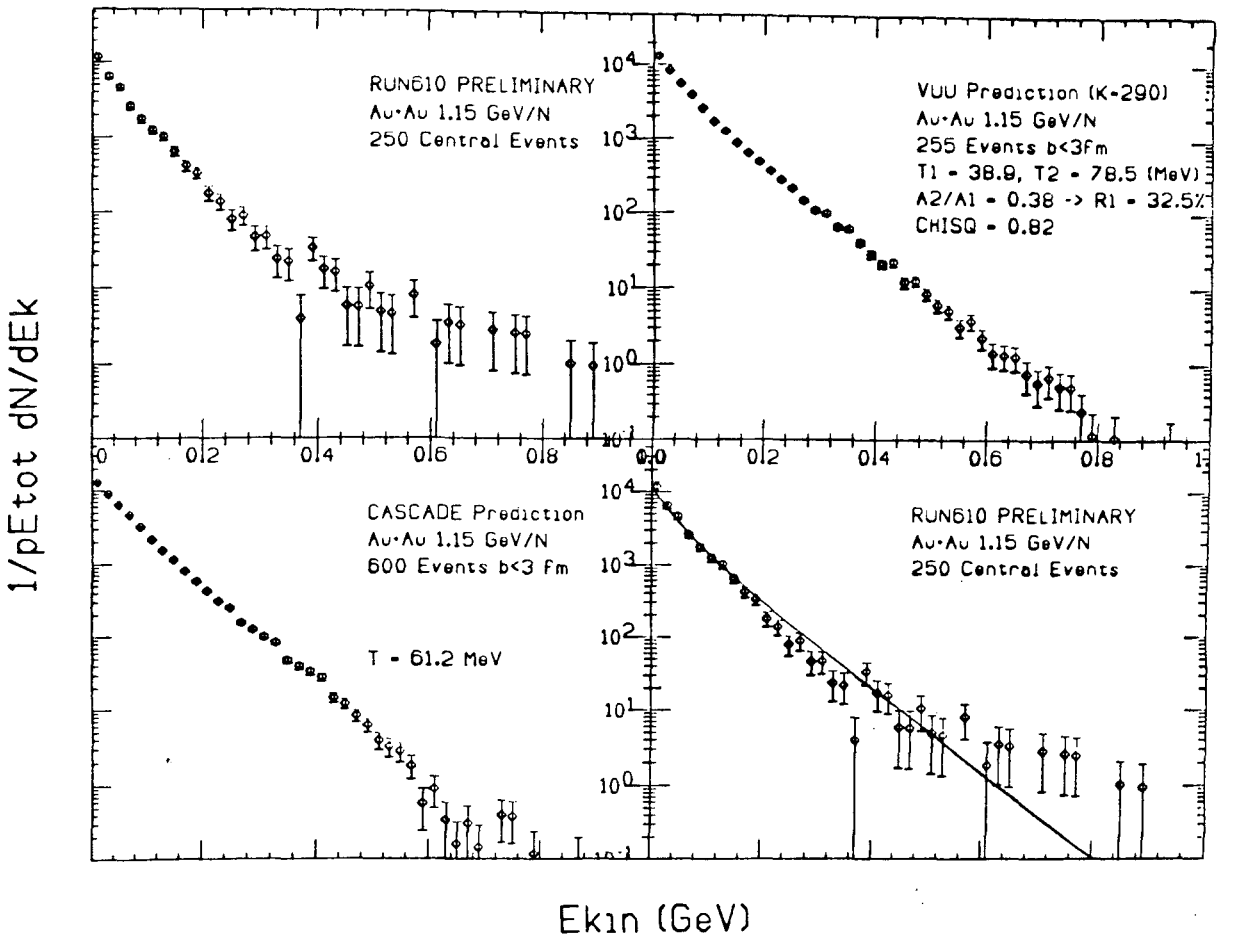

Fig. 5: (a) π^- Kinetic energy spectrum at $90 \pm 30°$ in the C.M. Note that unlike previous figures, this spectrum is weighted so that a one-temperature spectrum is a straight line. (b) VUU prediction for this system with parameters for a two-temperature fit. The event selection criterion is $b < 3fm$. (c) Intranuclear Cascade prediction. Unlike the VUU spectrum, this distribution is not concave. (d) Experimental data (same as (a)). The solid line is the two-temperature fit to the VUU spectrum.

[1]R. Brockmann *et al.*, Phys. Rev. Lett. **53**, 2015 (1984).

[2]G. Odyniec *et al.*, *Proceedings of the 8th High Energy Heavy Ion Study, Berkeley, CA 1987*, p.215.

[3]P.J. Siemens and J.O. Rasmussen, Phys. Rev. Lett. **42**, 880 (1979); D. Hahn and N.K. Glendenning, Phys. Rev. C **37**, 1053 (1988)

[4]M.L. Tincknell *et al.*, Optical Engineering, **26**, 1076 (1987).

[5]J.W. Harris *et al.*, Phys. Rev. Lett. **58**, 463 (1987).

Energy and Entropy Considerations in Nuclear Multifragmentation

William A. Friedman
Physics Department, University of Wisconsin, Madison, Wisconsin 53706

The decay of excited nuclei into several intermediate mass fragments (IMFs), larger than α-particles but smaller than fission fragments may occur by many mechanisms. While the simplest of these is that of evaporation, there are other more exotic processes. The term multifragmentation is often applied to all such events. In this work we wish to reserve the term "multifragmentation" for events which are qualitatively different from evaporation. Whereas the probability for producing several IMFs by evaporation is nonzero at nearly any energy, it is meaningful to consider energy thresholds for some of the other classes of events.

We will concentrate here on a process characterized by rapid massive cluster formation (RMCF). This process has been examined with the aid of a simple schematic model previously constructed for nuclear disassembly. The model, outlined in refs.1, involves an expanding-evaporating source of fragments. The RMCF process is revealed through the study of the evolution of sources which lose mass by evaporation while they expand.

In these studies, the instantaneous mass of the emitting source was determined as a function of density. A precipitous drop in the mass of the source at densities near, or below, $.4\rho_0$ is found in those cases with high initial temperatures. These sharp declines occur when the instantaneous temperatures are in the range of 5-6 MeV, and it is found that the mean mass of fragments emitted under these conditions rises abruptly. It is this rise in fragment mass and emission rate at low densities with which we associate the RMCF process. If the system contains too little energy to produce the low densities, RMFC does not occur. We explore here the features of the reaction which permit this process to occur.

It is convenient to use thermodynamic concepts to study the conditions leading to RMCF. We will be concerned with the qualitative features that lead to the production of the IMFs. For simplicity, we use the following schematic model for the excited system. We consider the heated expanding system to be a nucleus of density ρ excited above its ground state. The the energy of that ground state is taken to have the simple dependence on ρ, $E_{gs}/A = 8((1-\rho/\rho_0)^2 - 1)$. This interpolates between the two known limits at $\rho = \rho_0$ and $\rho = 0$. The density of energy states at the excitation above the ground state is assumed to be the same as that of a finite temperature Fermi gas, with a Fermi energy, ϵ_f, that varies with the density of the system as $\rho^{2/3}$. This dependence follows from the assumption that the expansion is isentropic. Using this model we can determine the instantaneous free energy, F, for any density and excitation energy (temperature) of the expanding system, since all of the functions associated with excitation can be treated in the finite temperature Fermi gas model.

Next we consider the conditions under which the low density system might condense into normal density clusters (IMFs). Toward this end we compare the free energy/particle of the homogeneous system with the free energy/particle of the cluster. We assume that clusters will form when their free energy is equal or less than that of the constituents in the source. The cluster free energy is found from F_c $(= -TlnZ + E_{gs})$, where the partition function Z is associated with the motion of the cluster center-of-mass. It includes a factor for the volume in

which the cluster moves, and this is a crucial factor in determining F_c. For cluster formation on the surface of the system, with motion outward, we have shown[2] that this volume is intimately related to the evaporation decay rate itself. In ref.2 we demonstrated that the volume occupied by that flux of the clusters which come from the surface of the source during the mean life-time for the statistical emission is exactly that volume required for the free energy of the evaporated cluster to equal to the free energy of its constituent nucleons in the source. Consequently IMF emission by surface evaporation can occur at any excitation energy, but the rate may be slow.

To determine when clusters will form *internally* we must consider a different volume in the calculation for the cluster free energy. In this case we take the volume to be that occupied by the A nucleons which join to form the cluster ($V = A/\rho$), i.e., the volume of the cavity produced by the formation of the cluster. With this choice the cluster free energy may be calculated at each density. We now can calculate the cross-over condition (density, temperature) at which the free energy of the cluster becomes lower than the free energy of particles in the homogeneous source. It is the *internal* formation of fragments due to the cross-over of free energies that we find associated with RMCF. Indeed, the observed RMCF behavior evident in the expanding-evaporating source model is found to occur precisely when conditions approach those of the cross-over.

In the foregoing we have been concerned with the conditions at which the clusters form. It is equally important to examine the physics leading up to these conditions. This is especially important in appreciating the differences among various models which study multifragmentation. We must carefully consider the concept of "freeze-out". This generally refers to the condition under which the fragments cease interacting strongly with one another. We might associate the situation of RMCF with such a stage of disassembly.

It is crucial to introduce a second, different, "freeze-out" condition. We shall call this one the *entropy*-freeze-out condition. By contrast, we will refer to the the previously mentioned condition as the *force*-freeze-out condition. These distinct conditions are roughly analogous to the "saddle" and "scission" conditions in transition-state fission theory. Both of these two conditions are important to the multifragmentation process.

In the microcanonical approaches to disassembly the two freeze-out conditions are the same. Entropy is assumed to increase as the system expands to the large volume in which the breakup occurs. In the expanding-evaporating source model, on the other hand, the two conditions are very different. The entropy-freeze-out condition is taken at normal nuclear density, whereas the force-freeze-out, for example the condition for RMCF, is at a much lower density. Intermediate models, in which the entropy increases up to a given density between normal nuclear density and the force-freeze-out, are also possible.

To illustrate the significance of the two freeze-out conditions, we next consider three sample cases, all with the same force-freeze-out condition, but with different entropy-freeze-out conditions and different conditions leading to force-freeze-out. We take a density of $.2\rho_0$ and a temperature temperature of 5.8 MeV as the force-freeze-out condition for all three cases . This condition corresponds to a specific cross-over condition and is associated with a thermal energy/particle of 5.18 MeV, and entropy/particle of 2.07 at the RMCF point.

We next work backwards in time for each of the cases to determine the conditions which

prevailed at normal nuclear density, prior to the expansion which results in the force-freeze-out condition. For case I) let us assume that the entropy-freeze-out point is at normal density, ρ_0. Then for this case the entropy per particle at ρ_0 is 2.07 (the same as at the force-freeze-out condition), while the temperature is 16.96 MeV, and the thermal energy per particle is 15.16 MeV. For cases II) and III), we assume that the entropy-freeze-out is at the force-freeze-out condition given above. For case II) we assume that the system must work against a force associated with the density dependence of the ground state. We then find that at ρ_0 the entropy per particle would be 1.75 (less than 2.07); the energy per particle would be 10.305 (if there is no collective kinetic energy at ρ_0), and the temperature would be 13.1 MeV. Finally for case III) we assume the system does no work against any attractive potential in progressing from normal density to the force-freeze-out condition. Then we find that at ρ_0 the entropy per particle would be 1.28, with the thermal energy 5.18 MeV (the same as at the force-freeze-out condition), and the temperature would be 8.654.

This illustration clearly demonstrates the importance of considering the *two* freeze-out conditions, and also the importance of the conditions leading to the freeze-out points. If case III) were to hold, an energy of about 5 MeV/particle would lead to the same type of final freeze-out, as would require 15.16 MeV/particle if case I) were to hold. This big difference may account for large differences in predictions of the energy which must be reached in order to achieve multifragmentation.

No particle loss from the source between the freeze-out conditions was considered in the previous three cases. If one is to quantitatively determine what excitation energy is required for a system to achieve the conditions for multifragmentation, one must also take into consideration the particles which are emitted between the two conditions. With the emission of particles, presumably from the surface of the the expanding system, their kinetic energy and separation energy are removed from the source. A portion of the original excitation energy is also taken by the collective compressional energy corresponding both to the reduction of the density and to the loss of source mass. Finally, the expanding source source acquires a collective kinetic energy. In addition to the minimal excitation energy required to achieve RMCF at the force-freeze-out condition, all of these components of energy must be supplied by the initial excitation energy,

The expanding-evaporating source model is especially well suited for studying the evolution of the system between the two freeze-out conditions. It has been used for this purpose with a system having $A = 190$ and $Z = 76$ which has an entropy-freeze-out at normal nuclear density, ρ_0, with a temperature, at that point, of 15 MeV. We take the condition for RMCF, force-freeze-out, to be a density of $.30\rho_0$ with a temperature of 5.89 MeV. During the time the system progresses from the entropy-freeze-out to the force-freeze-out we calculate that it loses about 45 units of mass and about 17 units of charge. These carry away about 836 MeV of energy in kinetic energy, and about 182 MeV in separation energy. The compressional energy of the system grows from 0, at the entropy-freeze-out point, to 574 MeV, at the force-freeze-out point. The collective kinetic energy (expansion) goes from 0 to 136 MeV. From an original excitation energy of about 2400 MeV ($E^*/A = 12.6MeV$) the excitation energy at the force-freeze-out has dropped to about 675 MeV ($E^*/A = 4.66$). This significant change further demonstrates

that the dynamics of the process between the two freeze out conditions has a crucial bearing on determining what excitation energy is required to achieve multifragmentation.

Signs for the onset of multifragmentation have been sought in recent experiments. One study, by a group from GSI, Frankfurt, and Heidelberg[3], looked for a rapid increase in the mean multiplicity of IMFs with increasing excitation energy.

We have used our model to calculate the mean multiplicities for fragments relevant to these measurements. These calculations were performed for systems with starting masses of 190 units (Z=76) and 100 units (Z=44), to reflect reactions involving gold and silver targets. We find that the calculations for *both* the light and heavy targets represent the data remarkably well. The models used by the authors of ref.3 where not successful in accounting for both light and heavy targets. Contrary to the observation, the microcanonical model of Bondorf anticipated a sharp multiplicity rise in both sets of data at relatively low excitation energy. This anticipation may stem from the fact that the Bondorf model is one in which the entropy- and force-freeze-out conditions are the same, and it does not explicitly deal with the physics occurring between the two. In other microcanonical calculations by Gross the cracking mode (multifragmentation) emerges at 4-5 MeV/A, consistent with the sharp rise predicted by Bondorf model. In the calculations of Gross both freeze-out conditions have the density about $.2\rho_0$ and the temperature is about 5-6 MeV. These conditions are indeed similar to those at RMCF conditions but not to the initial conditions of our calculations.

We find that, in the region explored by the experiments in ref.3, low densities are not found. The multiplicities calculated without expansion are essentially the same as those calculated with expansion. Thus according to the model, the IMFs which are measured appear to come from surface evaporation. In the energy region above that discussed in Ref.3, we do find a sharp rise in IMF multiplicity and evidence for RMCF. This occurs at approximately 1500 MeV for the mass 190 system, while the exact location of this rise is sensitive to the restoring force (equation of state).

It thus appears that a sharp rise with energy in IMF multiplicity would be a good and simple feature to signal the onset of multifragmentation. The slope of this rise should, however, be greater than that associated with the surface evaporation process. It appears, at this time, that such a signature has not been seen.

This work was supported in part by a grant from the U.S. National Science Foundation.

1. W.A. Friedman, Proceedings of the Eleventh Oaxtepec Symposium on Nuclear Physics, Notas de Fisica Vol.11, No.1, 71 (1988);
W.A. Friedman, Phys.Rev.Letts.60, 2125 (1988).

2. W.A. Friedman, in *Nuclear Dynamics and Nuclear Disassembly, Proceedings of the Symposium, Dallas, Texas April 1989*, Edited by J.B.Natowitz,(World Scientific,Singapore,1989) p.349;
W.A. Friedman, Phys.Rev.C40, 2055(1989).

3. R. Trockel, et.al., Phys.Rev.C39, 729 (1989).

Nuclear Collisions at 200 GeV/Nucleon from WA80 Experiment at CERN

WA80 Collaboration

F. Plasil,[a] R. Albrecht,[b] T. C. Awes,[a] C. Baktash,[a] P. Beckmann,[c]
F. Berger,[c] R. Bock,[b] G. Claesson,[b] G. Clewing,[c] L. Dragon,[c] A. Eklund,[d]
R. L. Ferguson,[a] A. Franz,[e,f] S. Garpman,[d] R. Glasow,[c]
H. A. Gustafsson,[d] H. H. Gutbrod,[b] J. Idh,[d] P. Jacobs,[e] K. H. Kampert,[c]
B. W. Kolb,[b] P. Kristiansson,[e] I. Y. Lee,[a] H. Löhner,[c] I. Lund,[b]
F. E. Obenshain,[a,f] A. Oskarsson,[d] I. Otterlund,[d] T. Peitzmann,[c] S. Persson,[d]
A. M. Poskanzer,[e] M. Purschke,[c] H. G. Ritter,[e] S. Saini,[a] R. Santo,[c]
H. R. Schmidt,[b] T. Siemiarczuk,[b] S. P. Sorensen,[a,f] K. Steffens,[c]
E. Stenlund,[d] D. Stüken,[c] M. L. Tincknell,[a] and G. R. Young[a]

Each major CERN experiment that has made use of the 200-GeV ^{16}O and ^{32}S projectiles available during 1986 and 1987 has concentrated on one specific method by which the possible formation of the quark-gluon plasma (QGP) can be studied. Our WA80 collaboration has emphasized the measurement of direct photons. Thermal, directly radiated photons provide us, in principle, with an excellent means to study the QGP since they are essentially uninfluenced by the hadronization process because of their electroweak interaction. However, in the case of nucleus–nucleus collisions, spectra of direct photons are extremely difficult to deduce from photon measurements due, primarily, to the dominating effect of the combinatorial background arising from the decay of the multitude of neutral pions which are produced in these reactions. WA80 has measured photons with a single-arm lead-glass photon detector (SAPHIR) of limited acceptance and limited resolution. The procedure used to deduce spectra of direct photons relies on our ability to account for all photons impinging on the surface of SAPHIR that result from known hadronic decays. The difficulties associated with this task can be appreciated when we consider the uncertainties associated with SAPHIR's efficiency (in a high-multiplicity environment), its limited acceptance (making certain invariant-mass reconstructions impossible), and the unknown transverse momentum distributions of the other hadronic decays that contribute to the background (η, ω, and η') in addition to the dominant neutral pions.

In mid-1988, we reported preliminary results on direct photon emission from reactions induced with ^{16}O projectiles at 200 GeV/nucleon.[1] Subsequent work on the evaluation of SAPHIR efficiency and acceptance, however, has led to a revision of our preliminary findings. The current status of direct photon emission results obtained by the WA80 collaboration is discussed here. One important by-product of our efforts to determine direct photon spectra is a set of distributions of neutral pions which, in themselves, provide us with interesting information on the nature of the compressed and highly excited reaction zone. These distributions are also presented here.

In order to place our neutral-pion and direct-photon findings into the proper context, we review briefly previously discussed conclusions on the general and global aspects of nucleus–nucleus collisions at CERN energies. First, it was found that multiplicity distributions of charged particles, transverse energy distributions, and residual energy measured at zero degrees are all strongly correlated with each other. Any one of the above experimentally determined quantities can serve as a guide to the impact parameter associated with any given event. We prefer to make use of the total energy measured in the Zero-Degree Calorimeter, E_{ZDC}, and we will use this quantity as a measure of collision centrality. Second, it has become apparent that the global features of the reactions are determined by the collision geometry. Specifically, transverse energy and E_{ZDC} distributions are determined by the number of participants which can be determined on the basis of a "clean-out" tube geometry.[2] Quantitatively, we have determined that in our pseudorapidity range ($2.4 < \eta < 5.5$), the transverse energy per participant at 200 GeV/nucleon is about 2 GeV and that it does not depend either on the target–projectile combination or on collision centrality. There is, however, a strong dependence on bombarding energy, and the equivalent value of E_T/participant at 60 GeV/nucleon is only about 1 to 1.2 GeV.

From the transverse-energy conclusions outlined above, it is possible to estimate attained energy densities and to extrapolate these findings to systems, such as Pb+Pb, that have not been investigated. The most widely used method by which energy-density estimates are made is due to Bjorken.[3] Strictly speaking, this method applies only to the extreme relativistic limit, where $dE_T/d\eta$ distributions exhibit a plateau. This situation is not reached at CERN energies. Furthermore, the Bjorken approach involves a formation time τ which is not known and which is usually taken to be 1 fm/c. This method involves boost invariance and allows us to obtain differential energy-density estimates valid for each local rest frame. While we have estimated energy densities under various alternative assumptions which do not rely on the existence of a plateau at midrapidity,[4] the Bjorken approach provides us with a means of making system-to-system comparisons that is not surpassed at the present time. Using our experimental, preliminary $dE_T/d\eta$ distributions, we found the standard Bjorken volume-averaged energy densities to vary from about 1.0 GeV/fm^3 for ^{16}O+^{12}C to about 2.5 GeV/fm^3 for ^{16}O+^{197}Au. In addition, by making use of the E_T/participant values described above, we estimate that the volume-averaged energy density attained in a central Pb+Pb collision will be about 2.7 GeV/fm^3. The two points to note are that the above values of energy density (2-3 GeV/fm^3) are within the range of values estimated to be required for QGP formation, and that Pb+Pb collisions do not involve much higher volume-averaged energy densities than O+Pb collisions.

In addition to the average E_T values/participant determined in the WA80 experiment, it was also found that $dE_T/d\eta|_{max}$ per participant is about 1 GeV for reactions at 200 GeV/nucleon. This finding makes it possible to estimate energy densities as a function of the radial profile of the colliding system. This result was first discussed in Ref. 4. It was brought out that in the central core of a head-on S+Au collision at 200 GeV/nucleon, the energy density is expected to reach 3 GeV/fm^3, while in a head-on Au+Au collision the central energy density may reach a value as high as 4 GeV/fm^3. Since, in addition to the higher core energy densities, large colliding nuclei may involve a larger volume of QGP formation, the development of heavy beams at the CERN SPS should be pursued. It should be stressed, however, that the most effective way of increasing the energy density is by increasing the collision energy; and it is possible that sufficiently high energy densities for QGP formation may not be attained until the Relativistic Heavy-Ion Collider is built at BNL.

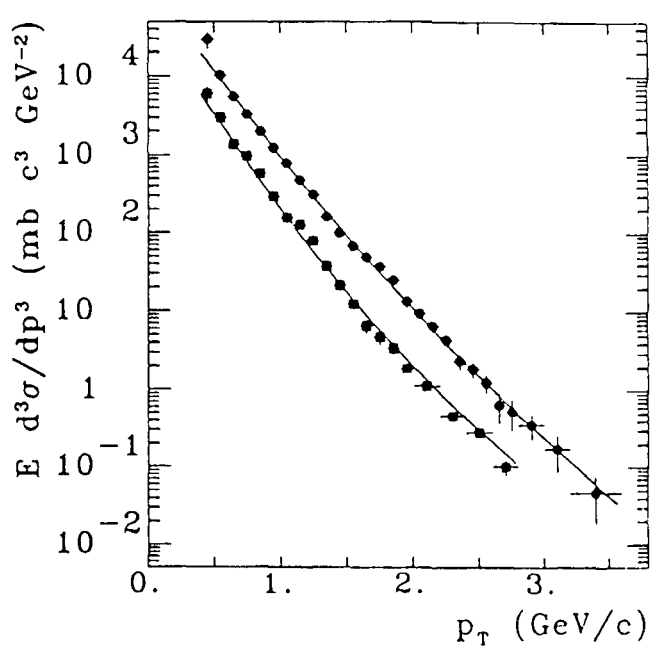

Fig. 1. Invariant π^0 cross sections from central (circles) and peripheral (squares) collisions of ^{16}O projectiles with an Au target at 200 A GeV measured in the pseudorapidity range $1.5 \leq \eta \leq 2.1$. The lines represent fits to the data with Eq. (1) and parameters of Table 1.

The investigation of the π^0 spectra presented here covers a p_T region up to 3.6 GeV/c and involves the selection of data according to collision centrality. The results cover the full data set of the 1986 ^{16}O+Au run and extend the subset of data published in Ref. 5. They are described together with data analysis and efficiency and acceptance corrections in a forthcoming publication.[6] Only selected highlights are presented here. In Fig. 1 invariant π^0 cross sections are shown for central and peripheral 200 A GeV ^{16}O+Au events. Attempts to fit the spectra with a combination of two thermal distributions did not give reliable results since the two extracted temperatures turned out to be sensitive to both the relative normalization and to statistical fluctuations. Following Hagedorn[7] the spectra were parametrized by:

$$E\frac{d^3\sigma}{dp^3} = \begin{cases} A\ \exp(-m_T/T) & \text{for } p_T \leq 0.8 \text{ GeV/c} \\ C\ \left(\frac{p_0}{p_T+p_0}\right)^n & \text{for } p_T \geq 0.8 \text{ GeV/c} \end{cases} \tag{1}$$

where A, T, C, p_0, and n are parameters and m_T is the transverse mass, $m_T = (p_T^2 + m^2)^{1/2}$. The first expression is an approximation to a thermal distribution, while the second expression is empirical and based on QCD considerations. Two parameters are eliminated by the requirement that the values and slopes of the two expressions match at $p_T = 0.8$ GeV/c. The fit values of the remaining three parameters, A, T, and n, are given in Table 1 for the data of Fig. 1 and also for minimum bias p+Au and ^{16}O+Au data at 200 GeV/nucleon. The fitted curves are also shown in Fig. 1. The two points to be noted are that the value of the parameter T remains constant (within experimental errors) for all data sets, and that the parameter n varies from one data set to another, indicating differences in the spectra at p_T values above 0.8 GeV/c. The differences in the high p_T region become more apparent when comparisons are made to data from $p+p$ collisions and when ratios of spectra are plotted as a function of p_T. A marked change of slope at higher values of transverse momentum is seen in the p+Au case and has previously been ascribed to the onset of hard QCD scattering.[8] This effect is also found in our peripheral-collision ^{16}O data, but not in results from central collisions where, presumably, the effect is obscured by nuclear effects.

Table 1. Parameters obtained from fitting Eq. (1) to experimental data of Fig. 1 and to minimum bias data from p+Au and ^{16}O+Au reactions at 200 GeV/nucleon.

System	A (mb c^3 GeV^{-2})	T (MeV/c)	n
200 GeV p+Au	$(1.3 \pm 0.5)10^4$	180 ± 16	37.6 ± 3.9
200 A GeV O+Au			
minimum-bias	$(3.6 \pm 1.3)10^5$	184 ± 16	25.9 ± 2.4
peripheral	$(6.6 \pm 2.9)10^4$	174 ± 18	16.8 ± 1.9
central	$(1.7 \pm 0.8)10^5$	194 ± 22	26.0 ± 3.1

In Fig. 2, the γ/π^0 ratio is shown for central and peripheral ^{16}O+Au reactions at 200 GeV/nucleon as a function of p_T. The Monte Carlo calculations depicted in the figure give the contribution of all decay photons. The Monte Carlo procedure and its assumptions are described elsewhere.[9] Within the limits of uncertainties, all of the observed photons are accounted for by known hadronic decays. Given all sources of uncertainties, we set un upper limit of about 15% for the contribution of direct photons to the γ/π^0 ratio in our p_T range. With better statistics, it should be possible to set a limit at the 5% level.

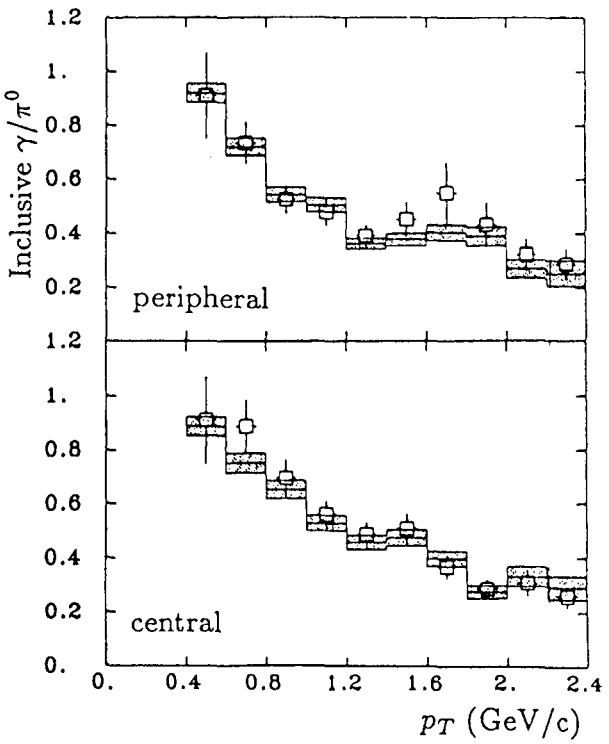

Fig. 2. Ratio of inclusive photon cross section to π^0 cross section as a function of transverse momentum for central and peripheral ^{16}O+Au reactions at 200 GeV/nucleon. The squares indicate data, and the shaded histograms are Monte Carlo results representing hadronic decays. The difference between the data and the histograms can be attributed to the contribution of direct photons.

References

a. Oak Ridge National Laboratory,* Oak Ridge, Tennessee 37831.
b. Gesellschaft für Schwerionenforschung (GSI), D-6100 Darmstadt, West Germany.
c. University of Münster, D-4400 Münster, West Germany.
d. University of Lund, S-22362 Lund, Sweden.
e. Lawrence Berkeley Laboratory, Berkeley, California 94720.
f. University of Tennessee, Knoxville, Tennessee 37996.
* Operated by Martin Marietta Energy Systems, Inc., under contract DE-AC05-84OR21400 with the U.S. Department of Energy.

1. R. Santo *et al.*, Proceedings, Seventh International Conference on Ultrarelativistic Nucleus-Nucleus Collisions, Lenox, Massachusetts, September 26-30, 1988; Nucl. Phys. **A498**, 391c (July 1989)
2. R. Albrecht *et al.*, Phys. Lett. B **199**, 297 (Dec. 1987).
3. J. D. Bjorken, Phys. Rev. D **27**, 140 (1983).
4. T. C. Awes et al., pp. 485-90 in Proceedings, XXIV Recontres de Moriond, Les Arcs, Savoie, France, March 13-19, 1989, Les Editions Frontieres, 1989
5. R. Albrecht *et al.*, Phys. Lett. B **201**, 390 (Feb. 1988).
6. R. Albrecht et al., "Transverse Momentum Distributions of Neutral Pions from Central and Peripheral ^{16}O+Au Collisions at 200 A GeV," to be submitted to Zeitschrift fuer Physik A
7. R. Hagedorn, Rivista del Nuovo Cimento **6**, 1 (1983).
8. M. A. Faessler, Phys. Rep. **115**, 1 (1984)
9. L. Dragon, "Produktion neutraler Pioinen und direkter Photonen in ultrarelativistischen Schwerionenreaktion," Dissertation, Institut fuer Kernphysik, WWU Muenster, 1989.

Collision Dynamics and Particle Production in Relativistic Nucleus-Nucleus Collisions at CERN

John W. Harris
Nuclear Science Division, Lawrence Berkeley Laboratory,
University of California, Berkeley, CA 94720, USA
and the
NA35 Collaboration

1. Introduction

The possibility of forming a quark-gluon plasma is the primary motivation for studying nucleus-nucleus collisions at very high energies. Various "signatures" for the existence of a quark-gluon plasma in these collisions have been proposed. These include an enhancement in the production of strange particles,[1] suppression of J/Ψ production,[2] observation of direct photons from the plasma,[3] event-by-event fluctuations in the rapidity distributions of produced particles,[4] and various other observables. However, the system will evolve dynamically from a pure plasma or mixed phase (of plasma and hadronic matter) through expansion, cooling, hadronization and freezeout into the final state particles. Therefore, to be able to determine that a new, transient state of matter has been formed it will be necessary to understand the space-time evolution of the collision process and the microscopic structure of hadronic interactions, at the level of quarks and gluons, at high temperatures and densities. In this talk I will review briefly the present state of our understanding of the dynamics of these collisions and, in addition, present a few recent results on particle production from the NA35 experiment at CERN.

2. Collision Dynamics

2.1 Geometry

Information on the geometry of nucleus-nucleus collisions can be obtained from measured interaction cross sections, multiplicity distributions, rapidity distributions and the distributions of energy in the transverse and longitudinal directions in an event. The interaction cross sections are found to have a geometrical dependence on the radii of the colliding nuclei and are observed to be independent of incident energy for energies from 2 GeV/n to 200 GeV/n.[5,6] The transverse energy distributions are observed to be impact parameter dependent and support a "clean-cut" geometrical overlap of the colliding nuclei.[7,8] For the nucleus-nucleus case of A_P projectile nucleons incident on A_T target nucleons the transverse energy distributions can be reproduced by an A_P-fold convolution of proton-nucleus(A_T) collisions over the same range of impact parameters.[7,8] The first and second moments of multiplicity distributions for nucleus-nucleus collisions are well described by a superposition of proton-nucleus collisions,[5] rather than a superposition of pp collisions. The rapidity distributions of produced particles have been measured and are observed to peak at the rapidity of the center-of-mass of the geometrical overlap of the colliding nuclei.[9] This information provides support for the important role that geometry plays in the dynamics of these collisions.

2.2 Freezeout Characteristics

Hanbury Brown and Twiss (HBT) correlations[10] between negative pions have been measured for various systems by the NA35 Collaboration. The approach involves a Gaussian parameterization[11] of the pion-emitting source, at the time when interactions cease (freezeout), with R_T the transverse radius, R_L the longitudinal radius and Λ the chaoticity parameter. Another parameterization[12] of the source distribution which is Lorentz-covariant and incorporates the inside-outside cascade for the collision dynamics determines the parameters R_T, Λ and the source lifetime τ_0. A value of $\Lambda = 1$ corresponds to chaotic emission from the source. Values of $\Lambda < 1$ correspond to decreasing chaoticity, with $\Lambda = 0$ total coherence. In 200 GeV/n O + Au reactions, pions at $2 < y < 3$ near midrapidity in the effective ^{16}O + Au center-of-mass ($y_{cm} = 2.5$) originate from a large ($R_T \simeq 8$ fm), relatively chaotic ($\Lambda \simeq 0.8$), long-lived ($\tau_0 = 6.4$ fm/c) source.[13]

This picture suggests the formation of a thermalized fireball at midrapidity. Considering the large number of produced particles, mostly pions, near midrapidity in central collisions of O + Au at 200 GeV/n (approximately 120 - 140 per unit rapidity[9,13]) and the $\pi\pi$ strong interaction cross sections, one predicts a similar size ($R \simeq 8$ fm) for a thermalized system of pions at freeze-out. Preliminary NA35 results on HBT correlations for negatively-charged pions from central 200 GeV/n S + Ag and S + Au collisions exhibit this same effect, a large source of midrapidity pions. Examining these data as a function of the pion multiplicity of the event it is found that for pions at midrapidity the source radius increases with the multiplicity. For the lighter S + S system at midrapidity and for the heavy target systems away from midrapidity the transverse size is near that of the incident projectile, the longitudinal size is smaller and the chaoticity parameter is low similar to that observed in HBT measurements in e^+e^- and hadron-hadron collisions.

2.3 Thermalization and Nuclear Stopping

As stated in section 2.1, the locations of the peak positions of the rapidity distributions of produced particles are consistent with a simple geometrical overlap picture of the collision process. The distributions are Gaussian in shape and are broader than expected for emission from an isotropic fireball. Whether the rapidity distributions represent a large degree of stopping in the Landau[14] sense or partial stopping as predicted by string mechanisms in the Lund/FRITIOF model[15] is still undetermined. Up to now, the Landau and string models both predict the measured rapidity distributions of produced particles at CERN energies. The talk by Prakash in this Workshop addresses the subject of the proper use of the Landau model and how its results compare to the data.

Rapidity distributions of protons are not yet available from experiment for nucleus-nucleus collisions at CERN. The NA35 Collaboration has measured rapidity distributions of "charge flow", which can be associated with protons, by subtracting all negative from positive particles to obtain the "protons" displayed in Fig. 1. Also shown are the rapidity distributions of negative particles and Λ's, both of which peak at midrapidity. These data are for 200 GeV/n S + S central reactions. Also displayed for comparison are the negative particle rapidity distribution for 200 GeV p + p

minimum bias data, arbitrarily normalized to be able to compare to the S + S data. The S + S data are reflected about $y = y_{cm} = 3$. The rapidity distributions for negative particles from the minimum bias p + p and central S + S reactions are nearly identical in shape, suggesting the same production mechanism with little or no rescattering in the two cases. The rapidity distributions of "protons" from the S + S reaction is spread out in rapidity and exhibits significantly more stopping than predicted in the Lund/FRITIOF model which underpredicts the "proton" yield at $y = y_{cm} = 3$. Another string model VENUS 2 [16] has been successful in predicting the "proton" rapidity distribution using breakup of leading diquarks.

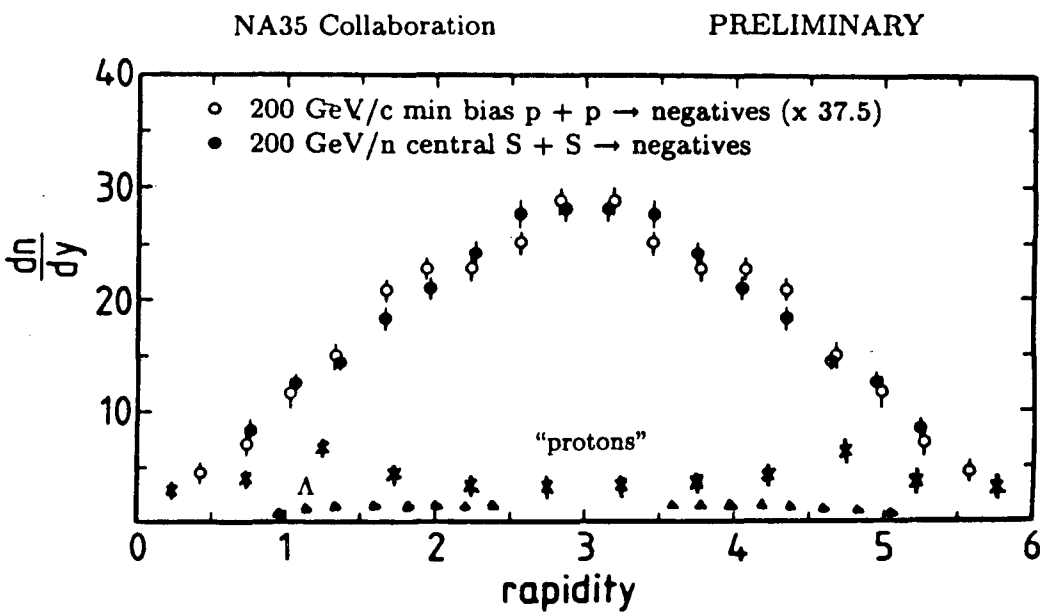

Fig.1. Rapidity distributions of negative particles, "protons" and Λ particles for central collisions of 200 GeV/n S + S and negative particles for minimum bias collisions of 200 GeV/c p + p (arbitrarily normalized for comparison). The data are reflected about $y = y_{cm} = 3$.

The degree of nuclear stopping and details of the energy densities reached in nucleus-nucleus collisions at CERN energies, both derived from transverse energy distributions, are described in the talk of Plasil in this Workshop.

3. Particle Production

3.1 Strange Particle Production

The NA35 Collaboration has measured the production of strange particles in 60 and 200 GeV/n p + Au and O + Au and in 200 GeV/n S + S collisions.[17,18] Displayed in Fig. 2 is the mean number of Λ particles per event as a function of the mean charged particle multiplicity of the events for S + S reactions. The Λ production increases with centrality of the collision at a rate faster than that predicted by the Lund/FRITIOF model and faster than a superposition model of nucleon-nucleon

data. The same dependence is also observed for $\bar{\Lambda}$ and K^0 production. For central collisions the Λ yield is more than a factor of two larger than predicted by any of the models, including a hadron gas model, with the exception of a parton gas model. For details of the models and comparisons see Ref. 19. The ratios of $< \Lambda > / < \pi^- >$, $< \bar{\Lambda} > / < \pi^- >$ and $< K^0 > / < \pi^- >$ also increase with centrality of the collision. These enhanced strange partice production yields have yet to be explained in terms of simple nuclear phenomena.

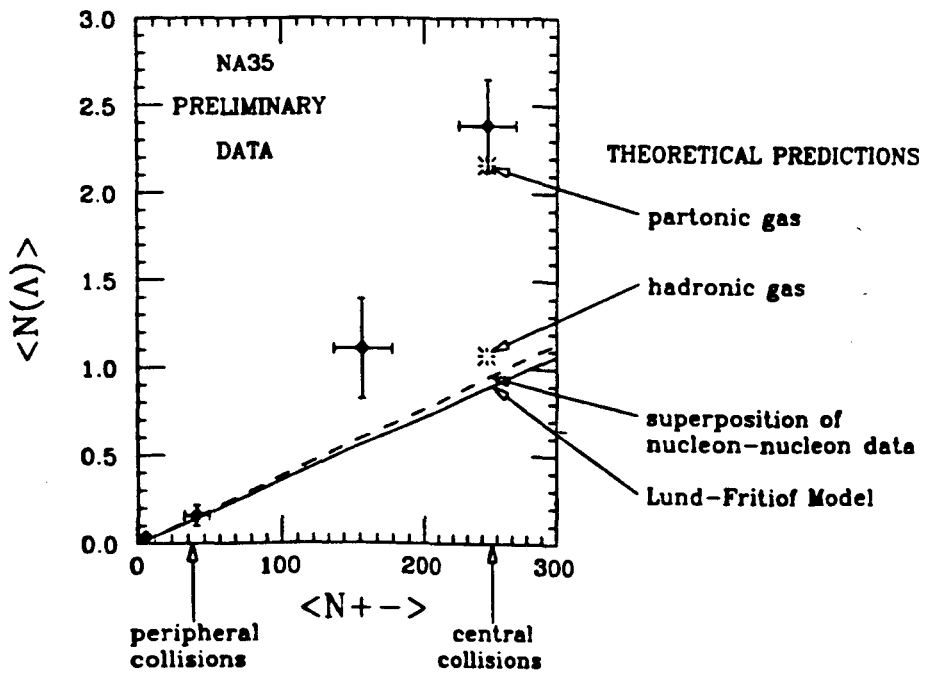

Fig.2. The mean multiplicity of Λ particles as a function of the mean charged particle multiplicity for 200 GeV/n S + S collisions. See text for model descriptions.

3.2 Transverse Mass and Momentum Distributions

The transverse momentum distributions of produced particles have the potential of providing information on the freezeout temperature, hydrodynamical flow effects and possibly the primordial, critical temperature of the system prior to expansion and freezeout. In the absence of flow effects the lower $p_\perp$ part of the spectrum should reflect the freezeout conditions. However, flow effects would distort this part of the spectrum and these effects might be identified in the $p_\perp$ distributions for various detected particle types and systems. Displayed in Fig. 3 are transverse mass ($m_\perp$) distributions, where $m_\perp = (p_\perp^2 + m^2)^{1/2}$, of various particles at midrapidity for central collisions of 200 GeV/n O + Au and S + S. Plotted are $m_\perp^{-3/2} dn/dm_\perp$ as a function of $m_\perp$. Using relativistic thermodynamics as developed by Hagedorn[20] for a single isotropic fireball, a Boltzmann distribution after integration over rapidity gives $dn/dm_\perp$ = constant $m_\perp^{3/2}\, e^{-m_\perp/T}$ for large $m_\perp/T$. Thus $m_\perp^{-3/2} dn/dm_\perp$ plotted as a function of $m_\perp$ should be a negative exponential for large enough $m_\perp$. This appears to be the case for the measured Λ, K^0 and "proton" distributions as well as the large $m_\perp$ end of the π^- spectra. The straight lines correspond to $dn/dm_\perp$ = constant $m^{3/2}$

$e^{-m_\perp/T}$ with T = 200 MeV. Is this the critical transition temperature?

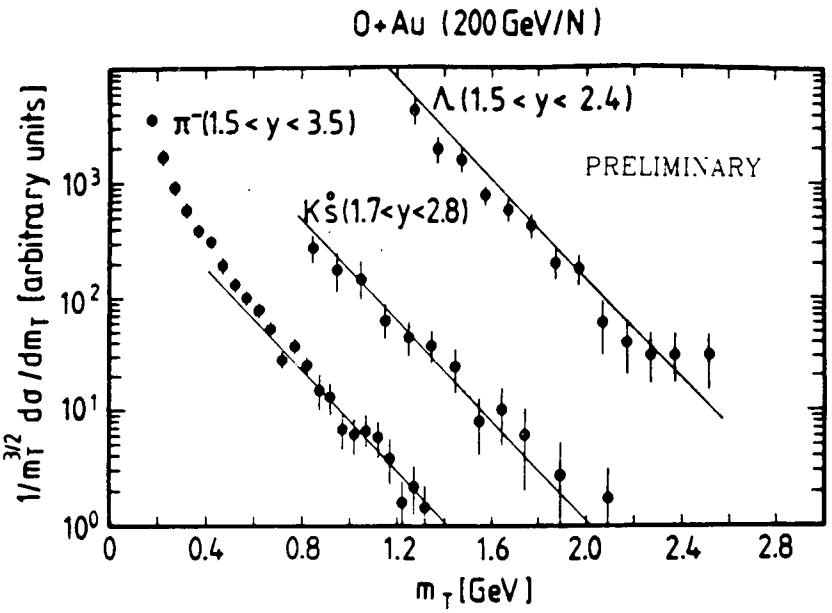

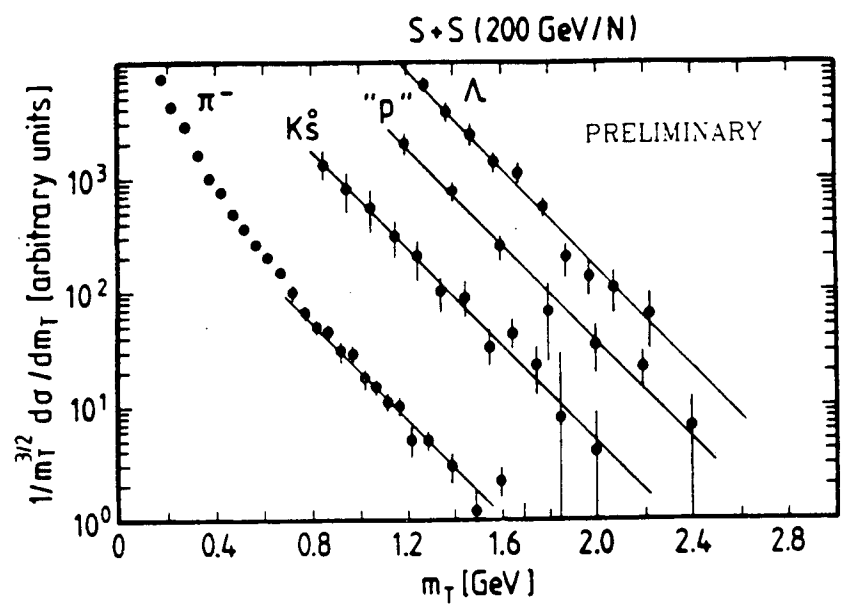

Fig.3. Transverse mass distributions for various particles in central collisions of 200 GeV/n a) O + Au and b) S + S. The rapidity intervals for a) are on the figure while those for b) are $0.8 < y < 2.0$, $1.5 < y < 3.0$, $1.4 < y < 2.7$ and $1.5 < y < 3.5$ for Λ, p, K^0 and π^-, respectively. The straight lines correspond to a temperature of 200 MeV in the Hagedorn fireball model.

The measured $m_\perp$ distributions of pions are generally nonthermal in shape and may be a complicated mixture of the effects of freezeout, flow and possibly a critical temperature. Using the velocity of sound in an ultrarelativistic gas, $c/\sqrt{3}$, we can estimate the $m_\perp$ regime where hydrodynamic flow will have a large effect. Hydrodynamic flow would have its greatest effect in the lowest $m_\perp$ part of the spectrum where $m_\perp < 1.22$ m. Recent analysis[21] of this data and that for π^0 production from WA80 in a radial flow model concludes that the spectra can be fit with an average radial flow velocity of approximately c/2 and a freezeout temperature of 100 MeV. The initial temperature in this model before expansion is 200 MeV, similar to that derived from the high $m_\perp$ part of the particle spectra of Fig. 3. Another analysis of the measured pion $p_\perp$ distributions in terms of hydrodynamical flow appears in the talk of Ruuskanen in this Workshop.

4. Acknowledgements

This work was supported by the Director, Office of Energy Research, Division of Nuclear Physics of the Office of High Energy and Nuclear Physics of the U.S. Department of Energy under contract DE-AC03-76SF00098.

References

1. R. Hagedorn and J. Rafelski, Phys. Lett. 97B (1980) 180.
2. T. Matsui and H. Satz, Phys. Lett. B178 (1986) 416.
3. L.D. McLerran and T. Toimela, Phys. Rev. D31 (1985) 545.
4. L. Van Hove, Z. Phys. C27 (1985) 135.
5. A. Bamberger et al., Phys. Lett. B205 (1988) 583.
6. P. Barnes et al., Phys. Lett. B206 (1988) 146.
7. A. Bamberger et al., Phys. Lett. B184 (1987) 271.
8. L.P. Remsberg et al., Z. Phys. C38 (1988) 35 and W. Heck et al., Z. Phys. C38 (1988) 19.
9. H. Ströbele et al., Z. Phys. C38 (1988) 89.
10. R. Hanbury Brown and R.Q. Twiss, Nature 177 (1956) 27 and Nature 178 (1956) 1046.
11. F.B. Yano and S.E. Koonin, Phys. Lett. B78 (1978) 556.
12. K. Kolehmainen and M. Gyulassy, Phys. Lett. B180 (1986) 203.
13. A. Bamberger et al., Phys. Lett. B203 (1988) 320.
14. L.D. Landau, Collected Papers, No. 88, Izv. Akad. Nauk, Ser. Fiz. 17 (1953) 51.
15. B. Andersson et al., Nucl. Phys. B281 (1987) 289.
16. K. Werner, BNL Preprint BNL-42 435 (1989).
17. A. Bamberger et al., Z. Phys. C43 (1989) 25.
18. J. Bartke et al., U. Frankfurt Preprint (1990).
19. M. Gazdzicki et al., Nucl. Phys. A498 (1989) 375c.
20. R. Hagedorn, CERN 71-12 (1971); GSI-Report 81-6 (1981) 236;
    Proceedings of Quark Matter 84, ed. K. Kajantie, Springer-Verlag (1985) 53.
21. K.S. Lee and U. Heinz, Z. Phys. C43 (1989) 425.

Are We Closer to Pion Condensate or Quark-Gluon Plasma?

P.V. Ruuskanen and M. Kataja

Department of Physics, University of Jyväskylä
SF-40100 Jyväskylä 10, Finland

Introduction

If the pions which are observed in the recent heavy-ion experiments [1] at CERN and Brookhaven are extrapolated backwards close to the collision time, one finds densities which are clearly above the thermal densities at the transition temperature, commonly estimated to be of order 200 MeV. At this temperature the thermal density of pions is ~ 0.3 fm^{-3}. E.g. in S+S collisions the pion multiplicity[2] is $dN/dy \simeq 90$ for all charge states. Taking $R_A = 3.5$ fm and the initial time $\tau_i = 2$ fm/c, one gets $n \simeq 1.2$ fm^{-3}, which is several times the thermal density at $T = 200$ MeV.

One can obtain such a high density of quanta in several ways. We would like to convince ourselves that the observed increase of quanta is due to the phase transition to quark-gluon plasma (QGP) with roughly 10 times the number of pionic degrees of freedom. Higher density can also be achieved raising the temperature. At $T \simeq 320$ MeV, pions reach the density 1.2 fm^{-3}. It is not completely ruled out that such a state of overheated pion gas could be formed in the collision process. In a static situation we believe, e.g. from lattice calculations, that QGP is the stable state at such a temperature. In the short production time and rapid initial expansion this static argument is not necessarily applicable. However, all calculations starting from an initial state of such a high temperature lead to p_{T}-distributions which are much wider than the observed ones.

At the presently observed densities another quite plausible possibility[3] — instead of strong heating of pions over the transition temperature — is the formation of dense pion gas far from chemical equilibrium. If pions with momenta of the order or less than the thermal momenta are added to thermal pion gas, their number will not immediately adjust to chemical equilibrium. The rate of reactions which reduce the pion number compared to two-body reactions which affect the momentum distribution is expected to be low[4]. What happens then is, that the gas rapidly reaches thermal equilibrium but not necessarily chemical equilibrium because the time scale for the latter can exceed that of the expansion.

The rapid increase of the pion density above the equilibrium value can be a consequence

of the production dynamics. If the final density of produced particles does not reach or exceed the density of quanta in QGP at transition temperature (expected to be of order 2–5 fm^{-3}), the nucleus-nucleus collision might be described in terms of hadronic degrees of freedom. One can think of (almost) independent, numerous NN-collisions to produce pions with momenta, which are independent of the total number of pions. If the dense state lasts long enough, the system would evolve to a stable state, e.g the mixed phase of QGP and hadron gas. In the case of rapid expansion the density can drop, however, to normal hadronic densities before the transition takes place.

If, on the other hand, plasma is formed initially, we still do not know whether the phase transition leads to hadron gas in chemical equilibrium since the details of the phase transition in the rapidly expanding system are not known. It could happen, that the last remnants of plasma are small droplets[5], which decay into numerous low momentum pions. In summary, there does not seem to be any obvious reasons to believe that the final hadrons should be initially in chemical equilibrium, even though they might well be in thermal equilibrium.

As has been pointed out earlier[4], the expanding gas of massive pions will fall off the chemical equilibrium as a result of the small rate of pion number reducing reactions. We have performed numerical calculations of this effect by assuming conservation of pion number and using the equation of state of free gas of massive pions. Even though the increase of chemical potential from zero is considerable (up to 100 MeV), it does not seem to lead to values which are close enough to the mass to change the shape of the spectrum (cf. Fig.1 below).

Results

Let us first consider the properties of the distribution function of pions

$$f(x,p) = \frac{g}{(2\pi)^3} \frac{1}{\exp((E-\mu)/T) - 1},$$

with nonzero chemical potential μ.* A positive value of μ means excess of pions and as $\mu \to m_\pi$, the excess piles up at low momenta and the system approaches the condensation point. E.g., the density of 1.2 fm^{-3} is the condensation density ($\mu = m_\pi$) at temperature $T = 220$ MeV.

Fig. 1a shows the dependence of the distribution function on chemical potential for $T/m = 1$. When μ is not close to m, say $\mu/m \leq 0.75$, chemical potential essentially affects only the normalization of the distribution. As μ approaches m, the number of pions with low momenta increases, making the distribution function concave. When $\mu = m$ the distribution function becomes singular behaving like p^{-2} at small momenta. Since $\mu \leq m_\pi$, a further increase of pions leads to formation of condensate. The distribution

* Note that we assume the conservation of pion number. In charge symmetric pion gas μ has the same value for all charge states

function of massless particles is also shown. It also has a concave shape with a p^{-1} singularity.

The effect of μ on p_T-distribution is illustrated in Fig. 1b in the case of no transverse flow. As μ increases, the low p_T part of the spectrum is enhanced and the distribution becomes concave. With proper choice of μ, the shape becomes similar to that of massless pions. With transverse flow the two cases usually lead to different behavior as will be seen below.

An example of a fit with $\mu \neq 0$ but without flow is given in Fig. 2a, where the measured spectrum of negative particles in S+S collisions at 200 GeV/nucleon[2] is shown together with the calculated spectrum for $T = 164$ Mev and $\mu = 118$ MeV. The quality of the fit is good ($\chi^2/NDF = 1.7$), even though there might be slight indication of flattening of the data at largest values of p_T. A slightly better fit ($\chi^2/NDF = 1.0$) is obtained for the O+Au data with $T = 169$ MeV and $\mu = 126$ MeV.

The possibly concave shape of the p_T-spectrum for p_T above 1 GeV has been interpreted[6] as an indication of flow. This might be the case. The evolution of flow presupposes (at least roughly) thermal behavior of the system. The low p_T pions represent a large fraction of all pions and come from the dense part of the final state. If the flow interpretation of the high p_T part of the spectrum (representing order of 1% or less of the final pions) is correct, one should expect typical thermal features also in the low p_T region. With zero chemical potential, thermal spectrum always starts with zero slope at zero transverse momentum[7] and flow can lead even to formation of a dip in the spectrum at $p_T = 0$[8].

The latter feature tends to persists even with nonzero chemical potential as is shown in Fig. 2b. In this Figure, results from a hydrodynamic calculation with conservation of massive pions are plotted for different decoupling conditions together with the same data as in Fig. 2a. The initial conditions, $T_i = 230$ MeV, $\mu_i = 130$ MeV, $\tau_i = 2.0$ fm/c and $R_A = 3.5$ fm, produce the observed final multiplicity. The dotted line is the calculated p_T-spectrum when the decoupling surface is taken to be a constant number density surface, $n_{dec} = 0.04$ fm^{-3}, in the expanding pion gas. The tail of the distribution is well reproduced, but ~ 3 pions are missing from the low p_T peak. **This is 10 % of all the negative particles.** They have been shifted to the mid p_T values around ~ 0.5 GeV, and are almost unnoticeable there. The overall quality of the fit is poor.

The solid curve corresponds to decoupling at fixed time, $t = 5$ fm/c. In this case The temperature of the inner region is ~ 160 MeV and the chemical potential ~ 120 MeV. The overall representation of the data is better and it could be improved by specifying a variable initial chemical potential with large values at small r. As $\mu \to m$ the numerics becomes complicated and we have not tried to push for perfect fits. The dotted curve is a calculation for massless pions with $T_i = 290$ MeV at $\tau_i = 2.0$ fm/c. For massless particles the final spectrum always has a concave shape.

To conclude, we have shown that the whole range of measured transverse momentum spectrum of pions can be understood within a single thermal distribution if the assumption on chemical equilibrium of pions is relaxed. In the rapidly evolving situation of a heavy

ion collision, this appears as a likely explanation of the observed spectra, especially of the low p_T feature. The behavior of the large p_T tail of the spectrum gives a slight indication of transverse flow. Including the flow effects tends to lead to depletion of small momentum pions even in the case of nonzero chemical potential.

References

1. For a review, see G. Baym et al. (eds.) *Proceedings of Quark Matter 88*, Nucl. Phys. A498 (1989) and presentations of experimental results in these Proceedings.
2. J.W. Harris et al., LBL–26528, to be published in Nucl. Phys. A
3. M. Kataja and P.V. Ruuskanen, University of Jyväskylä preprint, 1/90, January, 1990; M. Kataja, P.V. Ruuskanen, E. Sarkkinen and H. von Gersdorff, in preparation.
4. G. Baym, Nucl. Phys. A418 525c (1985); S. Gavin, Nucl. Phys. A435 826 (1985) and University of Illinois Thesis, 1987.
5. L. Van Hove, Z. Phys. C27, 135 (1985).
6. K.S. Lee and U. Heinz, Z. Phys, C43, 425 (1989); R. Venugopalan and M. Prakash, SUNY at Stony Brook preprint.
7. D. Kusnezov and G. Bertsch, Phys. Rev. C40, 2075 (1989).
8. M. Kataja, P.V. Ruuskanen, L. McLerran and H. von Gersdorff, Phys. Rev. D34, 2755 (1986); P.V. Ruuskanen, Acta Phys. Pol. B18, 551 (1987)

Figure Captions

Fig. 1. (a) Thermal distribution function for $T/m = 1$ and different values of μ/m. The distribution function for $m = 0$ is shown in the same figure. In this case the argument is p/T. (b) The p_T-spectrum for matter at rest is plotted for different values of μ/m and for massless particles at $T = 140$ MeV.

Fig. 2. Transverse momentum data on negative particles in S+S collisions with various fits. (a) The curve is calculated from thermal distribution with $T = 164$ MeV and $\mu = 118$ MeV and assuming no flow. (b) Results from hydrodynamic calculations. The solid and the dotted line represent a calculation with conserved massive pions and nonzero chemical potential. For the solid line the decoupling is assumed to happen at fixed time, $t = 5$ fm/c, and for the dotted line at constant density, $n = 0.04$ fm^{-3}. The dashed-dotted line is the case of massless particles. Initial conditions are chosen to reproduce the observed multiplicity.

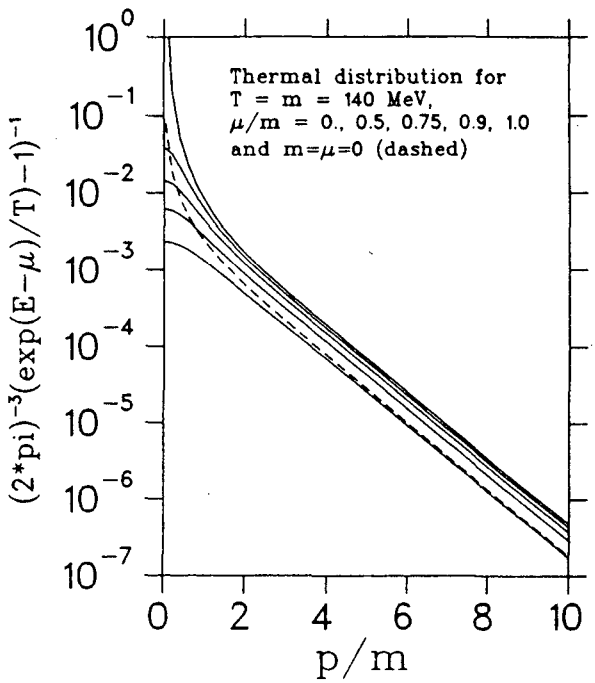

Fig. 1a

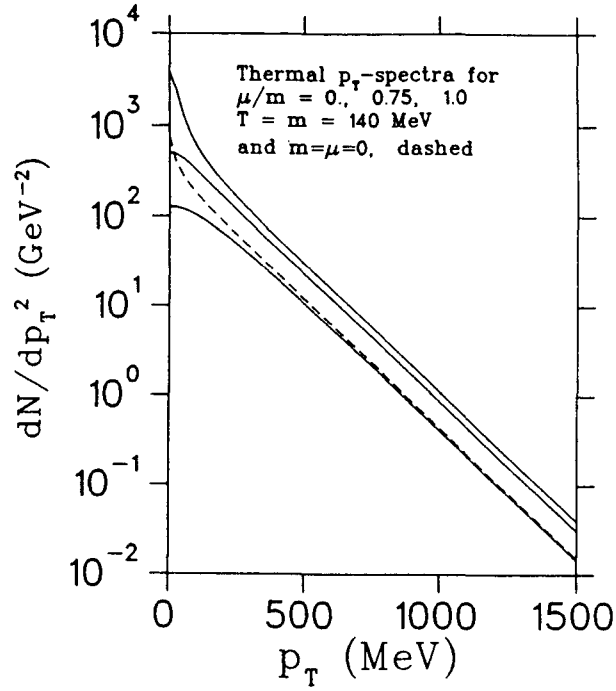

Fig. 1b

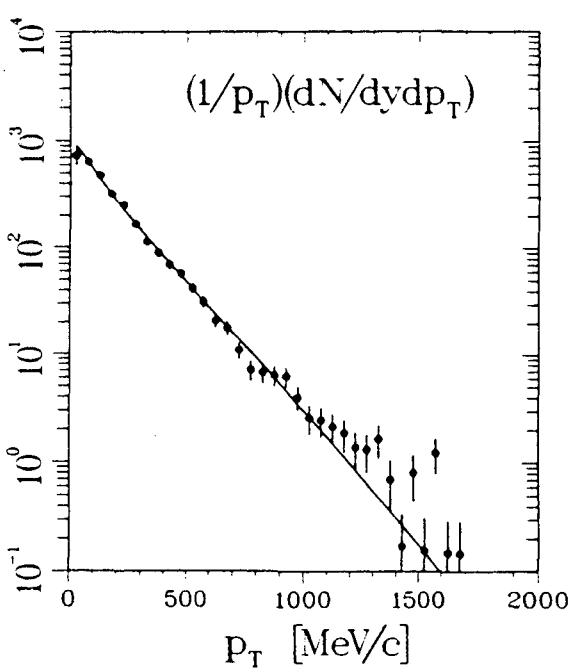

Fig. 2a

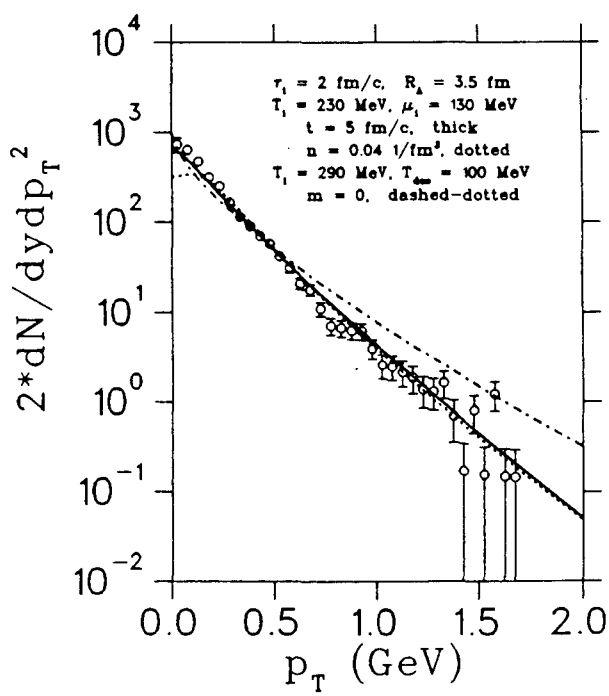

Fig. 2b

Rapidity Spectra of Secondary Particles from Nuclear Collisions at Ultrarelativistic Energies

Raju Venugopalan and Madappa Prakash

Physics Department, State University of New York at Stony Brook
Stony Brook, New York 11794-3800

The rapidity and/or pseudorapidity spectra of pions produced in nuclear collisions at beam energies of 14.5, 60 and 200 GeV are fit well by gaussian distributions.[1] The centers of these gaussians occur at $y_c \sim \ln\gamma(1+\beta)$, where β is the relative velocity between the nucleon-nucleon center of mass and the laboratory frames. The heights grow approximately according to $2E_{lab}^{1/4}$ while the widths increase with E_{lab}. Indeed, these spectra seem to follow the trend observed in hadronic collisions at ISR energies.[2]

The many attempts to model ultrarelativistic collisions can be broadly classified into two groups: (i) hydrodynamic models, and, (ii) sequential scattering models. Typical examples of the first category are the Landau-Milekhin[3,4] approach at one extreme and the Bjorken[5] approach[1] at the other. The Lund model[6] based on string dynamics exemplifies the second category. Both of these approaches roughly reproduce the essential features of the rapidity spectra. Whether the similarities of the final results from these two different approaches is due to the smooth behaviour of multi-particle final states alone or whether the two approaches are related at a deeper level is a topic presently under scrutiny.[7] Some vexing questions remain for both models. Two examples of these in the hydrodynamic model are the apriori justification of local equilibrium and the appropriateness of boundary conditions. In the string picture, on the other hand, interactions between the strings remain to be included.

Here we seriously entertain the idea that hydrodynamics is applicable and discuss the predictions of the Landau model. Curiously, the discourse regarding the interpretation of the rapidity spectra in the Landau model is somewhat confusing, given its apparent simplicity. We shall discuss how one might draw erroneous conclusions regarding the predictions of the rapidity spectra as well as the quality of fits predicted by the model. We discuss concurrently how Milekhin's[4] reformulation of Landau's original model makes predictions about these spectra which are potentially interesting.

We initially consider only the stage of one dimensional hydrodynamic flow in central collisions of symmetric nuclei. The more general three dimensional case will be discussed later. From energy-momentum conservation, $\partial_\mu T^{\mu\nu} = 0$, and the continuity equation $\partial_\mu(nu^\mu) = 0$, one obtains[8]

$$\frac{\partial^2\chi}{\partial\eta^2} + (c_0^2 - 1)\frac{\partial\chi}{\partial y} - c_0^2\frac{\partial^2\chi}{\partial y^2} = 0 \tag{1}$$

[1]The scaling assumption inherent in this approach leads to flat rapidity distributions observed only at much higher energies than considered here.

where $\chi \equiv \chi(\eta, y)$ is a potential function of fluid flow. The independent variables are $\eta = \tanh^{-1} v$ and $y = \ln(T/T_i)$. The fluid velocity is $u^\mu = \gamma(1, v)$, T is the proper temperature and T_i is the same at the beginning of fluid flow. The physical properties of the fluid, with the chemical potential assummed to be zero, are contained in the sound speed $c_0 = (dp/d\epsilon)_S^{1/2}$, where S is the entropy which is conserved during the flow.

We emphasize that the Khalatnikov potential equation is valid for a hot excited system undergoing longitudinal expansion (provided that it is bounded by outward bound progressive waves) irrespective of the dynamics of its past history. Following Milekhin, we shall term such a hot expanding region, initially confined to a region of width l, the non-trivial region. Guided essentially by the above viewpoint, Milekhin[4] derived the following exact solution of the Khalatnikov equation for constant c_0,

$$\chi = -(l/2c_0)e^y \int_{\eta/c0}^{-y} dy' \exp\left[-\frac{1+c_0^2}{2c_0^2}y'\right] I_0\left[\frac{1-c_0^2}{2c_0^2}(y'^2 - c_0^2\eta^2)\right] \tag{2}$$

With this expression for χ one then obtains[4] the distribution of entropy in pseudorapidity

$$\frac{dS}{d\eta} = S_i \cdot \frac{1-c_0^2}{4c_0} \exp\left(\frac{1-c_0^2}{2c_0^2}y\right) \cdot \left[I_0(z) + \frac{|y| I_1(z)}{(y^2 - c_0^2\eta^2)^{1/2}}\right] \tag{3}$$

Above, $y = \ln(T_k/T_i)$ where T_k is the temperature at the end of one dimensional flow, $z = (y^2 - c_0^2\eta^2)^{1/2} \cdot (1 - c_0^2)/2c_0^2$ and I_0 and I_1 are imaginary modified Bessel functions. The height of the distribution depends on S_i and c_0, where S_i is the initial entropy, while the width depends on T_k/T_i and c_0. One may further observe that the range of physically permissible rapidities is limited to $\eta_{max} = |y|/c_0$.

For $|y| >> c_0\eta$, asymptotic expansions of Eq. 3 lead to gaussians with the variance squared $L_0 = 2\ln(T_i/T_k)/(1-c_0^2)$. Fig. 1 shows a comparison of results from Eq. 3 and the gaussian distributions. The gaussian approximation is inapplicable for $c_0^2 = 1/3$ contrary to what is widely believed, but becomes valid for $c_0^2 \to 0$. The reason Landau obtained the asymptotic result to Eq. 3 for $c_0^2 = 1/3$ is because of a number of approximations[2] he made to Eq. 2 which are unlikely for physically plausible temperatures.

Curiously though, the distribution in Eq. 3 is extremely well fit by a gaussian of larger variance $L \to \alpha L_0$ for a wide range of T_i/T_k and c_0^2. The bottom right panel in Fig. 1 shows α vs T_i/T_k for c_0^2=1/3 and 1/7. The constraint that Milekhin's exact solution for the entropy distribution fit the heights and widths of the experimentally observed gaussians results in specific predictions for $S_i, c_0^2, T_i/T_k$ and the initial width l of the expanding system within the model.

The viewpoint stated earlier enables one to exploit the experimental spectra most effectively. For one, the above conclusions do not presume full stopping. In as much as the one dimensional expansion governs the rapidity spectra, gaussian profiles of the rapidity spectra are insensitive to the degree to which the projectile nuclei are stopped. Indeed, our minimal assumptions are better served by having only part of the energy density in the non-trivial region. Secondly, Landau's detailed geometrical assumptions (which, in our current theoretical understanding, are questionable) are completely absent from our

picture. Thus our conclusions regarding the fewer physical variables are theoretically on firmer grounds.

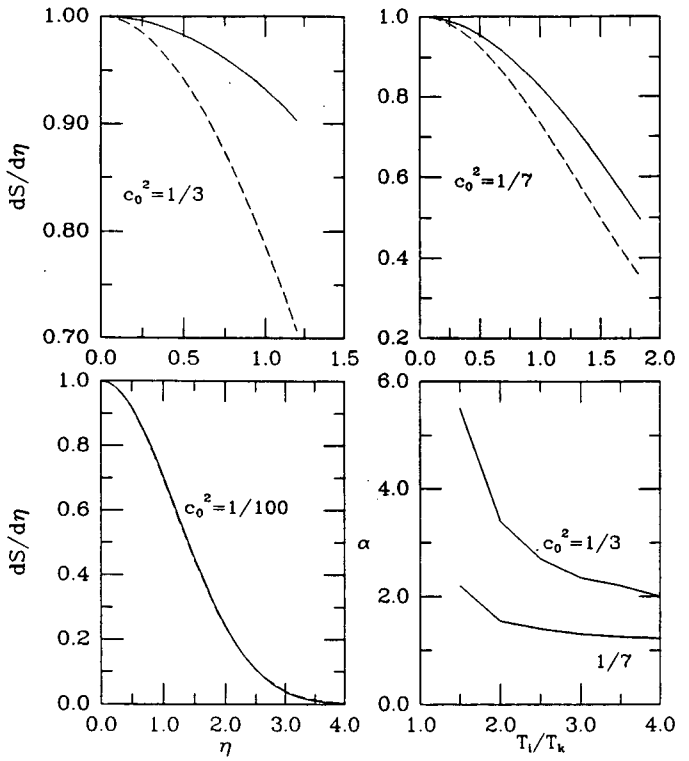

Fig. 1. Entropy distributions vs pseudorapidity for constant speed of sound squared c_0^2 and $T_i/T_k = 2$. Solid lines are Milekhin's exact results (Eq. 3) and dashed lines are gaussian approximations with squared variances $L_0 = 2\ln(T_i/T_k)/(1-c_0^2)$. to Eq. 3. The bottom right panel shows the scale factor in $L \rightarrow \alpha L_0$ by which L_0 should be increased to fit the results of Eq. 3 by gaussians.

We turn now to our present understanding of c_0^2 given the constituents of the expanding region. It is well known that $c_0^2 = 1/3$ only for massless non-interacting particles. Fig. 2 shows c_0^2 vs T for massive non-interacting pions and for a free gas containing also heavier resonances. The limit $c_0^2 = 1/3$ is reached only for $T >> 200$ MeV. Using the results of recent work[9] on effective chiral lagrangian theories of interacting hadrons at finite T, we have calculated c_0^2 for interacting pions for $T \leq 190$ MeV. These are shown by the dashed lines in Fig. 2. The attractive $\pi-\pi$ interactions reduce c_0^2 from its non-interacting values. This feature may also be understood from the fact that interacting pions behave like a system of non-interacting pions and $\rho-$mesons. While the inclusion of interactions when many resonances are present remains a challenging task, the important point is evident

- even in the absence of phase transitions c_0^2 is considerably less than 1/3.

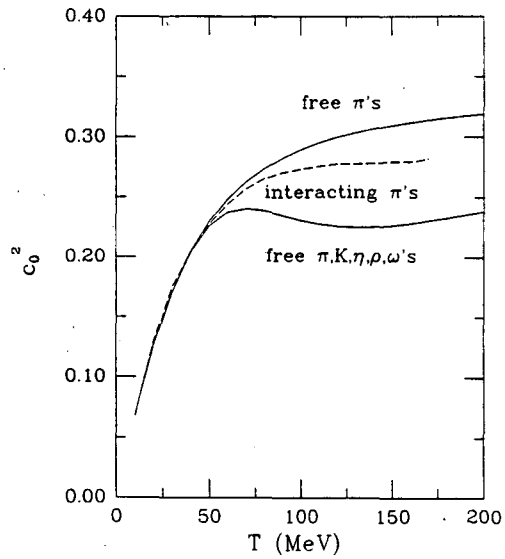

Fig. 2. Sound speed squared vs temperature for massive hadrons. Interactions between pions are based on the chiral perturbation theory results of Ref.[9]

In the absence of a phase transition and with parametrized forms of $c_0 = c_0(T)$ it has been shown[10] that the rapidity spectra are mostly sensitive to the initial c_0 for a 1+1-dimensional flow and our conclusions remain valid. With a phase transition and for lattice simulations of $c_0(T)$, the spectra for 1+1-dimensional flow acquires oscillations which vanish however in a 2+1-dimensional model.[11] Further investigations of the extent to which rapidity and transverse momentum spectra are sensitive to different equations of state, or equivalently $c_0(T)$ vs T, is therefore a promising direction for further study.

This work was supported by the Department of Energy under Grant No. DE-FG02-88ER40388.

References

[1]H. von Gersdorff et al., Phys. Rev. **C39**, 1385 (1989).
[2]S. Chadha, C. S. Lam and Y. C. Leung, Phys. Rev. **D10**, 2817 (1974).
[3]L. D. Landau, Izv. Akad. Nauk SSSR, Ser. Fiz. **17**, 51 (1953).
[4]G. A. Milekhin, Jl. Exptl. Theoret. Phys. **8**, 682 (1959).
[5]J. D. Bjorken, Phys. Rev. **D27**, 140 (1983).
[6]B. Andersson, Nucl. Phys. **A498**, 93c (1989).
[7]B. Andersson, [private communication].
[8]I. M. Khalatnikov, Jl. Exptl. Theoret. Phys. **27**, 59 (1954).
[9]P. Gerber and H. Leutwyler Nucl. Phys. **B321**, 387 (1989).
[10]K. Wehrberger and R. M. Weiner, Phys. Rev. **D31**, 222 (1985).
[11]U. Ornik, F. W. Pottag, and R. M. Weiner, Phys. Rev. Lett. **6339**, 2641 (1989).

Fast Pulsars, Strange Stars

Norman K. Glendenning
Nuclear Science Division, Lawrence Berkeley Laboratory
University of California, Berkeley, California 94720

1 Introduction

The initial motivation for this work was the reported discovery in January 1989 of a 1/2 millisecond pulsar in the remnant of the spectacular supernova, 1987A. The status of this discovery has come into grave doubt as of data taken by the same group in February, 1990. At this time we must consider that the millisecond signal does not belong to the pulsar. The existence of a neutron star in the remnant of the supernova is suspected because of recent observations on the light curve of the remnant, and of course by the neutrino burst that announced the supernova. However its frequency is unknown.

I have had a second motivation for some time, which now becomes the single one, and it is quite strong. Spectacular advances in technology in the last few years have revolutionized all sciences, and perhaps no one more dramatically than astronomy. These include both space based and ground observation. Of particular relevance to my topic is the rapidity with which millisecond pulsars are being discovered. It was only twenty three years ago that the first pulsar was discovered, and for many years thereafter the fastest one known was the Crab, with a period of 33 ms. Then in 1982, at a time when about three hundred pulsars had been found, the first truly millisecond pulsar was discovered, with period $P = 1.56$ ms. Since then there have been eight additional discoveries and altogether 18 with periods $P < 100$ ms, that is to say in the extreme tail of the distribution whose mean is about 0.7 seconds, as shown in Fig.1. The discovery frequency is therefore between one and two a year and increasing. Why am I so excited by these prospects? Because I can make a strong case that a pulsar rotation period of about 1 ms divides those that can be understood quite comfortably as neutron stars, and those that cannot. What we will soon learn is whether there is an invisible boundary below which pulsar periods do not fall, in which case, all are presumably neutron stars, or whether there exist sub-millisecond pulsars, which almost certainly cannot be neutron stars. Their most plausible structure is that of a self-bound star, a strange-quark-matter star. The existence of such stars would imply that the ground state of the strong interaction is not, as we usually assume, hadronic matter, but rather strange quark matter. Let us look respectively at stars that are bound only by gravity, and hypothetical stars that are self-bound, for which gravity is so to speak, icing on the cake.

2 Stars bound only by gravity

Fast rotation places a limit on the mean density of a star, and conversely for any given star, or equation of state, there is an absolute upper limit on the rotation frequency imposed by stability to mass loss at the equator, the Kepler frequency. Other general relativistic instabilities lower the limit to about 90 percent of the Kepler frequency. I have carried out a general study of the attributes of the equation of state and star that will allow it to rotate very rapidly. A full report of this work has been given elsewhere [1]. A grided search over more than 1400 models of the equation of state in a very flexible parameterization, which included the possibility of a first or second order phase transition was performed. Here I merely summarize the results. As general attributes of the equation of state it must be soft at low or intermediate density and very stiff at high density, at or near the causal limit. Such equations of state seem unphysical in the sense that physical systems exploit processes that lower the energy [2, 3] ie. which soften the equation of state, such as would be achieved in this context by conversion of nucleons to hyperons at high density, or a phase transition to quark matter, both of which lower the energy by an increase in the number of degrees of freedom. Yet we are forced to equations of state that stiffen rather than soften, by our insistence that the star is bound only by gravity, and then

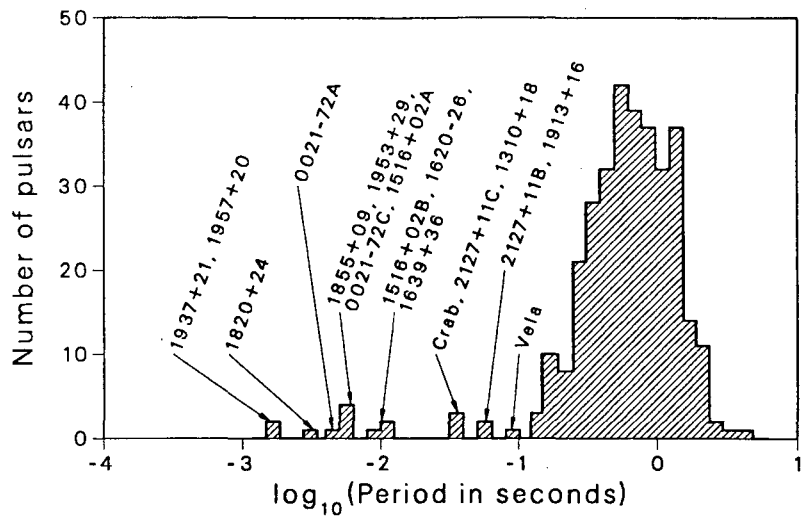

Figure 1: Distribution of pulsar periods.

looking for a central density that is low enough to make a description in terms of hadrons seem plausible. Moreover, the minimum central density of a star that is bound only by gravity and can withstand fast rotation at 1/2 ms is 13.2 ϵ_0 if GR instabilities are ignored, and 16 ϵ_0 if account of them is taken. It is implausible that matter at such a high multiple of nuclear density can consist of individual hadrons!

2.1 Generic relations for neutron stars

Let us examine generic relationships for neutron stars, which like all others we know of are bound only by gravity. This we do for several models computed in relativistic nuclear field theory, which includes both nucleons and hyperons [2]. In Fig.2 we show the mass-radius relationship that is typical of a neutron star, whose only binding force is gravity. This is the typical and inevitable relationship when gravity alone binds the star; for small mass, gravity is weak and the star large, for large mass, gravity is strong and the star small. The termination point for collapse to a black hole is marked by a dot. Note that the mass of the neutron star, or in other words its baryon number, $A \sim M/m$, must be very precisely tuned to achieve the fastest rotation while remaining stable to mass loss at the equator.

2.2 Hybrid stars

We have learned that to satisfy the double constraint of fast rotation and the mass of known pulsars, the central density of the star, if bound only by gravity, must be very high. The plausible state of matter at high density is quark matter. Could the star be a neutron star with a quark matter interior, the two states of matter being in equilibrium at their interface?

The equation of state of quark matter, because of asymptotic freedom, is expected to be soft. For example, in the bag model, $\epsilon \approx 3p + 4B$, $v_s^2 = 1/3$. In contrast, to satisfy the double constraint the models in my study were stiff at high density; many had reached the causal limit, $v_s^2 = 1$, in the star. Such stars seem to be incompatible with the findings of this study. Since the binding of the star is provided by gravity alone, the mass-radius relation has the generic form discussed before (see Fig.3).

2.3 Conclusions for stars bound only by gravity

To satisfy the double constraint of sufficient limiting mass and stability to fast rotation we are led to conclude that;

1. The equation of state must be soft at low density and stiff at high.

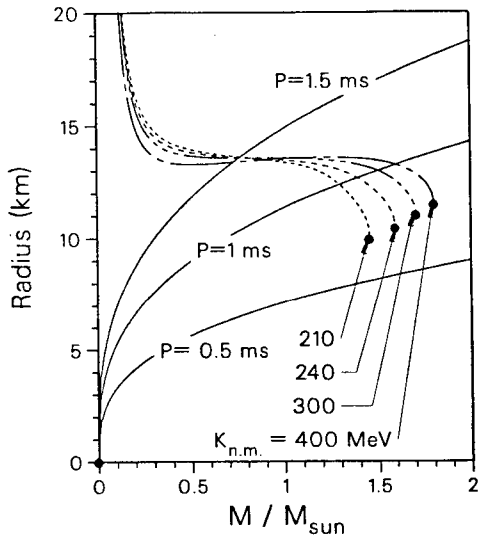

Figure 2: Generic relation for neutron stars for several equations of state as labeled according to compression of *nuclear matter*. The limits imposed by a 1.5, 1.0 and 0.5 ms pulsar are shown. Stars below these curves are stable for still shorter periods.

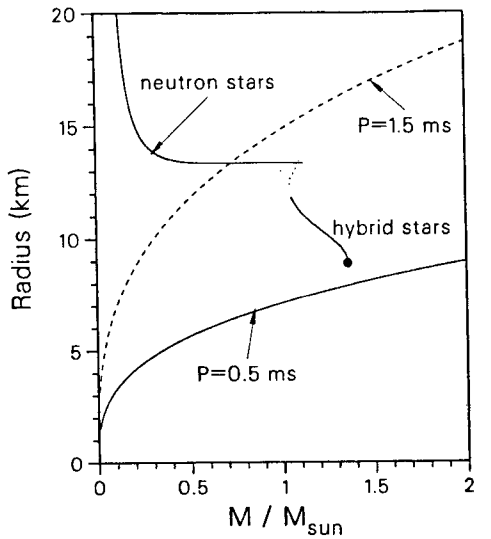

Figure 3: Hybrid stars with a first order phase transition between hadron and quark phases (dotted region between solid lines are unstable mixed phase).

2. This requirement seems to be incompatible with hybrid stars, those with a quark matter core and neutron star exterior.
3. The central energy density must be very high, $> 13\epsilon_0$, for those models for which the star profile is like that of a star bound by gravity alone under the least stringent assessment of relativistic instabilities, and still higher, $> 16\epsilon_0$, under the conservative assessment.
4. Only stars in a very narrow window in mass, or equivalently in baryon number, $A \sim M/m$, those on the verge of collapse to a black hole, can withstand fast rotation.
5. The star profiles that are obtained by minimizing the central energy density are not those of neutron stars, but rather of self-bound systems, which are bound at zero pressure with density $\sim 5\epsilon_0$ or more.

To account for a collapsed star with sub-millisecond period that is bound only by gravity we arrive at an impasse. Perhaps the assumption that the star is bound only by gravity leads us into all these difficulties!

3 Self-Bound Stars

Usually we assume that strange quark matter (u,d,s quarks), which is a lower energy state of quark matter (u,d), is also unbound. On the contrary, Witten has suggested [4] that strange matter may actually be bound and also be the absolute ground state. In this case strange matter, from nuggets with sufficiently large A to overcome finite number and surface effects, all the way to strange stars are stable. All other states of matter would be only metastable. Since ordinary nuclei would have an expected lifetime exceeding the age of the universe by far, Witten's hypothesis does not violate our experience. However, it is not possible to decide on theoretical grounds whether ordinary matter or strange matter is stable. Lattice QCD cannot be solved with sufficient accuracy. For example, to decide whether the energy per baryon in strange matter is less than it is in Fe^{56} (930.4 MeV) or greater than the proton mass (938.3 MeV) requires an accuracy of less than one percent. At best theory can give us guidance at the ten percent level (100 MeV)! Since neither assumption contradicts any known fact, we must look to experiment and astrophysical observation for the answer,

The structure of strange stars, if strange matter is stable, is entirely different from that of neutron stars. This shows up most dramatically in the mass-radius relationship [5, 6]. Because strange matter is self-bound, say at energy density ϵ_b, the mass of a small spherical strangelet is $M = (4\pi/3)R^3\epsilon_b$ and, just as for a nucleus, the radius scales as $M^{1/3}$, in contrast to neutron stars, where for small masses, the radius is very large because of the weak gravitational field. The generic form of the mass-radius relation for a self-bound star is *independent* of any particular model of binding. If such a self-bound state exists, then there are two distinct families of collapsed stars, neutron stars and stars made of the self-bound phase, most plausibly strange matter. The two cases are contrasted in Fig.4. We show three

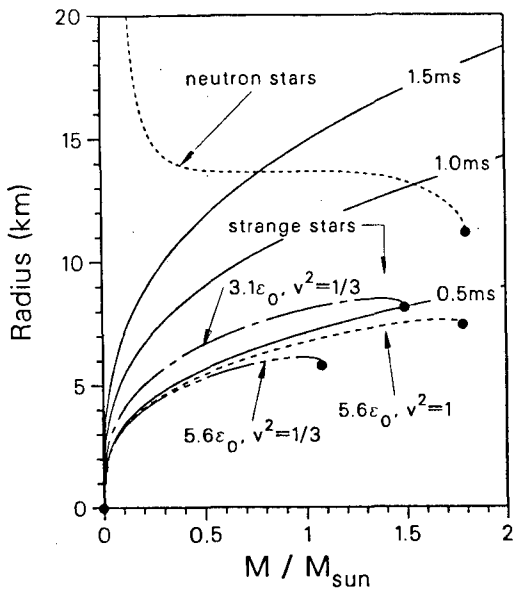

Figure 4: The mass-radius relation for a typical neutron star equation of state and for strange quark matter cases. The solid lines denote limits for the 1.5, 1.0 and 0.5 ms pulsars. Stars below these lines respectively are stable for shorter periods of rotation. [7, 8]

strange star sequences marked according to the value of the self-binding energy density ϵ_b. If $\epsilon_b > 5.4\epsilon_0$ the whole family of strange stars can rotate at $P = 1/2$ ms. In addition to this energy we need to postulate an equation of state for strange quark matter which has a self-bound state. This we take, for illustration, as $\epsilon = p/v^2 + \epsilon_b$. A value $v^2 = 1/3$ corresponds to a soft quark-matter equation of state, and $v^2 = 1$ to a stiff one. We see that it is quite possible to account both for compact stars of masses greater than any so far observed and also for sub-millisecond rotation.

We have come to some remarkable conclusions [7, 8]! In addition to those enumerated earlier,

6. All known pulsar masses and periods can be understood in terms of plausible neutron star models in which neutron stars of masses up to $\sim 1.5M_\odot$ and rotational periods as short as 1 ms are achieved at central densities of 3-4 ϵ_0 [1].

7. The hypothesis that most comfortably would fit a submillisecond pulsar is that it is made of matter in a phase that is absolutely stable at somewhat more than five times nuclear energy density. The likely candidate for such matter is strange-quark-matter. If another plausible state of matter which fits the above description can be found and for which the lifetime of hadronic matter is greater than the age of the universe with respect to decay to such a state, then it is also a candidate for describing the fast pulsar.

(a) A strange star does not have to be fine tuned in A, to be *the* one at or very near the end of the sequence that can spin fast.

(b) Possibly the whole family of stars can spin fast, not just those near the limit. This depends on whether the energy density of strange matter in its ground state is greater than about $5.4\epsilon_0$.

4 Cosmological considerations

If strange-quark matter is the true ground state, why have we not known about it? In fact when one looks in detail at this question one finds that the universe would be imperceptibly different whether the ground state is hadronic or quark matter. Virtually no primordial nuggets are expected; strange-quark-matter would have evaporated at the high temperatures of the early universe. Strange stars, if

sub-millisecond pulsars are discovered would indicate that strange matter is the ground state as would the discovery of stable strange nuggets in laboratory relativistic collisions. Here I look at cosmological evidence. If strange matter is the ground state and if the density in the heavier neutron stars is high enough to convert the core to quark matter, the entire star will rapidly convert to strange- quark-matter. About 1/100 compact stars are in binaries in which both partners are compact. Since all orbits decay by gravitational radiation (eg. PSR1913+16), these compacts will ultimately collide, and some material may be expelled into the galaxy. In mildly relativistic head on collisions of compact stars it is expected that 1/10 of the mass will be expelled. This provides an extreme upper limit for decay of a binary. Taking account of the frequency of type II supernova ($\sim$ 1/40/year), the age of the galaxy (10^{10} yr), and the fraction of compacts that are in binary compacts, we can estimate the amount of such debris in the galaxy as $10^5 M_\odot$, a surprisingly large fraction of the mass of the galaxy ($10^{11} M_\odot$). The corresponding density of debris is about 10^{-30} g/cm^3. (The volume of the galaxy is about 10^{68} cm^3). As an extreme overestimate we can assume that all debris is in strange nuggets and that all nuggets produced in star collisions have the minimum mass while remaining massive enough to be stable ($A \sim 1000$). We find 10^{59} nuggets. With a typical galactic velocity of 10^7 cm/sec, we can calculate a flux, and find the number/cm^2 striking the earth over its lifetime. Matter mixes to a considerable depth over geologic times. Assume a mixing depth of 1 km. We find a density of nuggets of $\sim 10^7$/cm^3, or a ratio of nuggets to nucleons of 10^{-17}. This is an extreme upper limit, which lies below the upper bound presently imposed by experiment (10^{-14}) [9], and it is problematical that a sufficiently sensitive experiment can be designed to detect such a feeble ratio. In this way we see how imperceptibly different the galaxy would appear, whichever is the ground state, hadronic or strange quark matter!

5 Outlook

Given the present discovery rate of millisecond pulsars, within the next few years we can anticipate sufficient data to provide evidence concerning the fundamental question as to the nature of the true ground state. The accumulated evidence will either provide a statistical basis for doubting that sub-millisecond pulsars exist, or one or more such pulsars will be discovered. Laboratory searches for strange debris from star collisions seem impractical unless samples can be identified that would be enriched, such as perhaps moon rock. Searches in relativistic collisions are underway, but the production of cold strange nuggets depends on fluctuations. It appears that the best chance of deciding this arcane but fundamental issue is through the search for fast pulsars.

This work was supported by the Director, Office of Energy Research, Office of High Energy and Nuclear Physics, Division of Nuclear Physics, of the U.S. Department of Energy under Contract DE-AC03-76SF00098.

References

[1] N. K. Glendenning, *Strange-Quark-Matter Stars*, invited paper, Rio de Janiero International Workshop on Relativistic Aspects of Nuclear Physics, August 1989, (to be published by World Scientific Publishing Co) (LBL-27959).

[2] N. K. Glendenning, Astrophys. J. **293** (1985) 470.

[3] H. A. Bethe, Ann. Rev. Nucl. and Part. Sc. **38** (1988) 1.

[4] E. Witten, Phys. Rev. D **30** (1984) 272.

[5] C. Alcock, E. Farhi and A. V. Olinto, Astrophys. J. **310** (1986) 261.

[6] P. Haensel, J. L. Zdunik and R. Schaeffer, Astron. Astrophys. **160** (1986) 121.

[7] N. K. Glendenning, Phys. Rev. Lett. **63** (1989) 2629.

[8] N. K. Glendenning, J. of Phys. G, **15** (1989) L225.

[9] M. Brugger et al., Nature **337** (1989) 434.

Fission Reactions with Intermediate Energy Heavy Ions

M. Begemann-Blaich[2], T. Blaich[2], H.C. Britt[1], Y.D. Chan[3], A. Dacal[3], D.J. Fields[1], M.M. Fowler[2], Z. Fraenkel[5], L.F. Hansen[1], A. Harmon[3], S. Kaufman[4], R.G. Lanier[1], J. Leyba[3], D.J. Massoletti[1], M.M. Namboodiri[1], J. Pouliot[3], B.A. Remington[1], T.C. Sangster[1], R.G. Stokstad[3], G.L. Struble[1], F. Videbaek[4], M.L. Webb[1] and J.B. Wilhelmy[2]

[1]Lawrence Livermore National Laboratory, Livermore, CA 94550
[2]Los Alamos National Laboratory, Los Alamos, NM 87545
[3]Lawrence Berkeley Laboratory, Berkeley, CA 94720
[4]Argonne National Laboratory, Argonne, IL 60439
[5]Weizmann Institute of Science, 76100 Rehovot, Israel

I Introduction

We have made a systematic study of heavy ion reactions in the energy range of 50–100 MeV/nucleon using medium mass projectiles on medium and heavy mass targets. This intermediate energy range is of particular interest since it represents a transition region from low energies where collective effects dominate and the mean field plays a dominant role to energies well above Fermi energy where heavy ion reactions can be described to a first approximation as a series of nucleon-nucleon collisions (intranuclear cascade picture).

The experiments were performed at the low-energy beam-line of the Lawrence Berkeley Laboratory BEVALAC accelerator using the PAGODA(1) detector system. This detector system consists of eight identical units of gas detectors and plastic scintillators arranged as a "logarithmic array" of an unusually wide dynamic range, which are capable of detecting from 200 MeV protons down to 0.1 MeV/nucleon heavy ions. The eight units covered a total solid angle of 13.5% of 4π. The PAGODA detection system is described in greater detail in Reference 1.

We measured the reactions of Ne, Fe and Nb projectiles on targets of Nb, Ta, Au and Th at 50, 75 and 100 MeV/nucleon. However, we report here only the results for the reaction of Fe projectiles on Ta, Au and Th targets and Nb projectiles on Au targets. Moreover, in the present paper we will discuss mainly the analysis of the fission decay channel. Since fission is a collective phenomenon, its measurement in the intermediate energy region is a convenient way of studying the change in the collective properties of the nucleus in this transition region.

II Experimental Results

The PAGODA detector system is capable of identifying the charge of ions up to $Z \simeq 15$ and with a Z-resolution of 2 units up to $Z \simeq 47$. The velocity of the detected ions is measured with a resolution of 0.05 cm/ns in the range 0.10–2.30 cm/ns. We show in Fig. 1 the excitation functions for the reaction products with $Z \geq 6$ for the reaction of Fe projectiles on Au targets at 50 and 100 MeV/nucleon and for Nb+Au at 50, 75 and 100 MeV/nucleon. The reaction products have been divided into three groups which roughly correspond to three reaction channels which have been measured in the present experiment: (1) Reactions in which one or more *intermediate mass* ($Z = 6 - 25$) *fragments* (IMF) are emitted; (2) reactions in which ions in the *fission fragment* (FF) mass region ($Z = 25 - 47$) are emitted, and (3) reactions in which a single target-like *heavy residue* (HR) ($Z \geq 47$) is emitted. From the figure we can draw qualitative but nevertheless important conclusions: (1) Despite the difference in the dynamics of the three types of reactions (IMF, FF and

HR) (which will be discussed in greater detail in forthcoming publications) the excitation functions for the three fragment ranges are quite similar in shape; (2) they show little change in the energy range of 50–100 MeV/nucleon (except perhaps for Fe+Au yielding IMF's), and (3) show little projectile dependence, except for an overall increase in cross section with increasing projectile mass. Altogether, we see surprisingly little change in the reaction cross sections in a bombarding energy range in which the underlying reaction mechanism is expected to change quite dramatically.

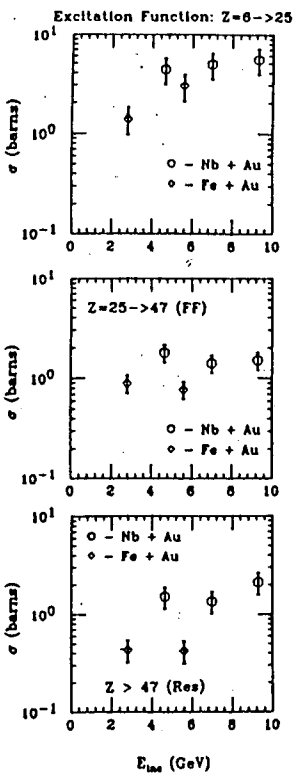

Figure 1

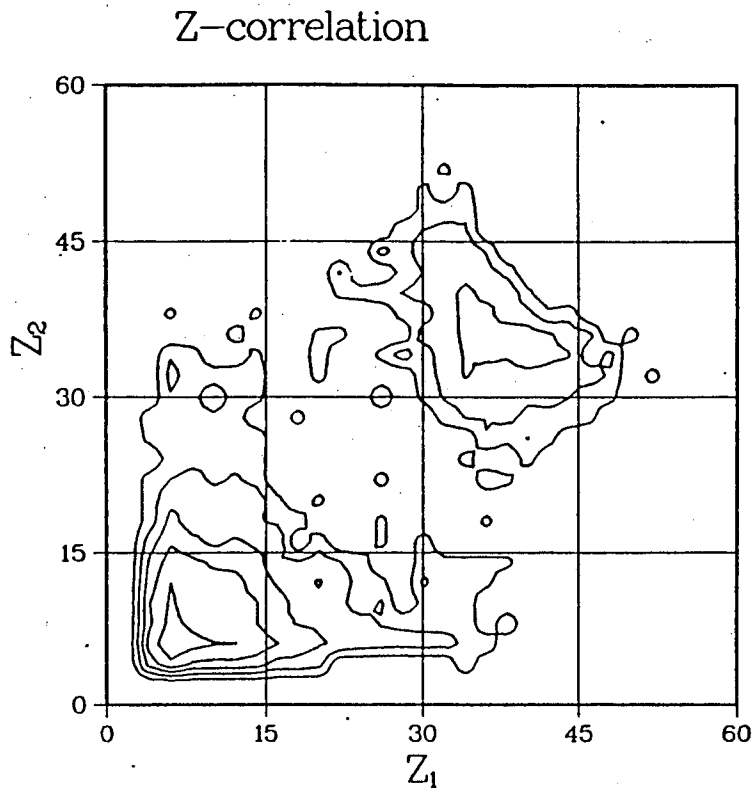

Figure 2

We show in Fig. 2 a contour plot of Z_1 vs. Z_2 for Nb+Au at 100 MeV/nucleon for reactions in which two heavy fragments are detected. We can clearly separate two regions. One region contains the events of very asymmetric charge distribution in which at least one fragment has a charge of $Z \leq 20$ and the summed charge of the two fragments is substantially below that of the target, implying that the reaction was not binary and that additional particles were emitted. The second region contains the events in which each fragment has roughly the one half of the charge of the target and it has a symmetric mass distribution. The events in this Z_1 vs. Z_2 region satisfy three other criteria for binary fission events: The vector sum of their velocities is roughly that given by the Viola systematics for fission[2], their summed azimuthal angular distribution $(\phi_1 + \phi_2)$ is centered at 180° and very narrow and their net perpendicular momentum is small. We thus are justified in associating these events with binary fission events. In the rest of this paper we will confine ourselves mainly to events of this type.

Since the Intranuclear Cascade (INC) model (see below) predicts a very good correlation between the linear momentum transfer (LMT) to the fissioning nucleus (which can be readily measured with the PAGODA detector) and its excitation energy, we have chosen to present our results as a function of the LMT. Figure 3a shows the LMT distribution for Fe and Nb projectiles on an Au target, whereas Figure 3b shows this distribution for Nb projectiles on three heavy targets at 100 MeV/nucleon. We find little projectile dependence in Fig. 3a, whereas Fig. 3b shows that the LMT distribution (and hence the excitation energy distribution) for thorium is centered at much lower values than for the Ta and Au, indicating that most of the thorium events are very low energy fission events presumably originating from very peripheral reactions, as would be expected given the low fission barrier of thorium. There is little difference between the LMT distributions for the Ta and Au targets.

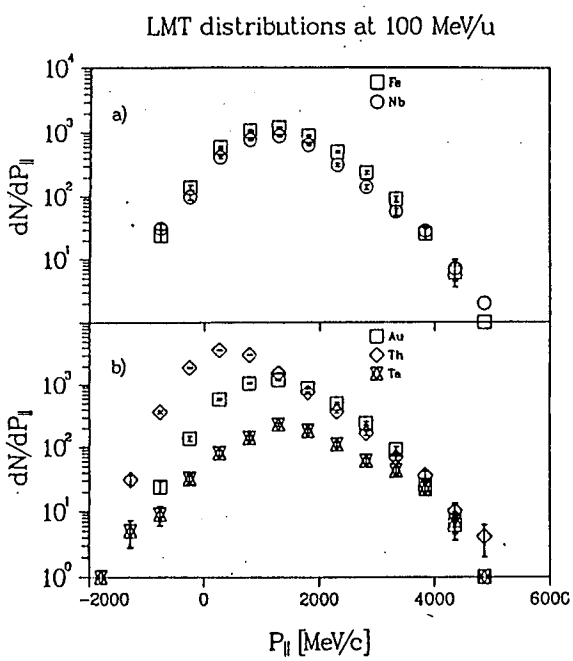

Figure 3

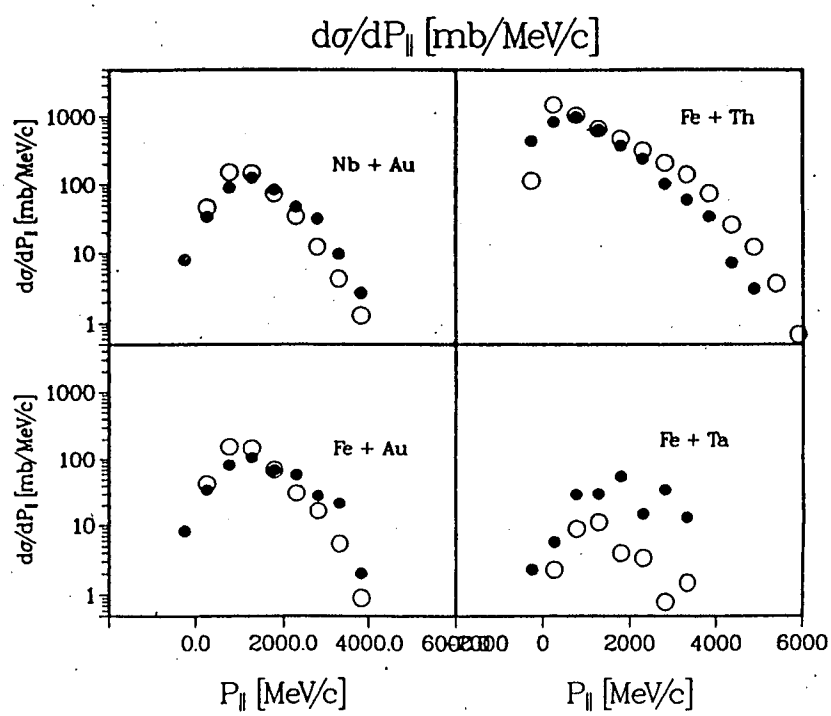

Figure 4

III Calculations

We have chosen to compare our experimental results for fission at 100 MeV/nucleon with the predictions of a model which assumes the reaction to consist of an intranuclear cascade (INC)[3] followed by statistical decay of the excited nuclei which allows for competition between particle evaporation and fission. For the calculation of the fission-particle evaporation competition we used the PACE[4] code which uses the Bohr-Wheeler formulation for the fission width with the angular-momentum dependent fission barriers of Sierk[5].

However, in order to take into account the fact that fission is a relatively slow reaction channel governed by dissipation processes which cannot compete with particle evaporation at very high excitation energies (which is not taken into account by the Bohr-Wheeler theory) and we have arbitrarily restricted fission to excitation energies below 150 MeV. Also, in order to save computer time, we have discarded all residual nuclei of the INC with excitation energy larger than 1000 MeV (since these nuclei will have emitted so many particles that fission is highly unlikely once their excitation energy is reduced to 150 MeV) and for the excitation energy range from 1000 to 300 MeV we have replaced the PACE code by a simplified evaporation cascade having a Maxwellian spectrum with a slope parameter of 15 MeV[6]. We assume that the angular momentum removed by the particles in this stage of the evaporation process is the maximum allowed value given by tangential emission from the surface of the nucleus. With these assumptions our calculation is able to reproduce the fission cross sections for other intermediate energy reactions[7,8].

We show in Figure 4 a comparison between the experimental parallel momentum distribution of the fissioning nuclei for four reactions at 100 MeV/nucleon (solid circles) with the results of our calculation (open circles). We see that the calculation reproduces very well the experimental distributions for the Th and Au targets in both shape and absolute value. For the Fe+Ta reaction the shape of the parallel momentum distribution is well produced by the calculation but the calculation is substantially lower in absolute value.

IV Summary

Heavy ion reactions between medium and heavy mass projectiles and heavy mass targets in the intermediate energy (50-100 MeV/nucleon) range can readily be separated into a binary fission part, into a part which involves the emission of one or more intermediate mass fragments and a part in which a target-like heavy residue is emitted. All three reaction channels show surprisingly little bombarding-energy dependence, nor are the reactions strongly dependent on the projectile and target masses. The experimental LMT distribution of the fissioning nuclei is well reproduced for the Au and Th targets in both shape and absolute value by a calculation based on a simple INC-statistical evaporation model in which the fission channel is restricted to excitation energies less than 150 MeV.

Acknowledgment

This research was supported in part by the US-Israel Binational Science Foundation.

References

1. M.M. Fowler *et al.*, Nucl. Instrum. Methods **A281**, 517 (1989).
2. V.E. Viola, Nucl. Data **1**, 391 (1966).
3. Y. Yariv and Z. Fraenkel, Phys. Rev. **C20**, 2227 (1979); Phys. Rev. **C24**, 488 (1981).
4. A. Gavron, Phys. Rev. **C21**, 230 (1980).
5. A.J. Sierk, Phys. Rev. **C33**, 2039 (1986).
6. Z. Chen *et al.*, Phys. Rev. **C36**, 2297 (1987).
7. U. Lynen *et al.*, Nucl. Phys. **A378**, 129c (1982)
8. F.D. Becchetti *et al.*, Phys Rev. **C28**, 276 (1983).

Characteristics of Intermediate Mass Fragment Emission from Ne+Ag and Ne+Au at 60 MeV/u *

G.Bizard[1], Y. Cassagnou[2], R. Dayras[2], H. Delagrange[3], R. Legrain[2], M. Louvel[1], S. Motobayashi[1], A. Péghaire[3], J. Péter, E.C. Pollacco[2], E. Rosato[4], F. Saint-Laurent[3], C. Volant[2], and J.P. Wieleczko[2]

1) LPC, Caen Esplanade de la paix F-14032 Caen CEDEX
2) DPhN/SEPN CEN Saclay F-91191 Gif sur Yvette CEDEX
3) GANIL, Caen BP n°5027 F-14021 Caen CEDEX
4) INFN, Universita di Napoli, I-80125 Napoli

abstract

In order to characterize intermediate mass fragment (IMF) production, six ionization chambers were used as a trigger for an almost 4π charged particle detector. The IMF trigger at large angles selects the more violent collisions and is equivalent to requiring a high multiplicity of light charged particles at back angles. The Z-distributions are function of this multiplicity. Global variables analysis is in progress.

For sufficiently energetic collisions between heavy ions, a number of theoretical studies [1] predict the existence of a multifragmentation process where the system disintegrates into massive and numerous fragments. Experimental work in this domain has been quite vigorous and a number of systems have been studied [2-4], principally in inclusive mode. What is particularly disturbing is that data is well described by different models. Thus assumptions as widely varying as transition between liquid-gas phases, cold break-up, statistical decay of hot nuclei and simple consideration of the available phase-space yield very similar observables. We have set an objective to perform measurements where it might be possible to choose between the different mechanisms. In this contribution we report on preliminary results on the reactions Ne+Au and Ne+Ag at 60 MeV/u using the Neon beam provided by the GANIL facility.

The experimental set up consisted of six telescopes (ΔE gas, E silicon) located at 35, 45, 57.5, 70, 110 and 160° and devoted to identification and energy measurements of the medium mass fragments ($4<Z<18$).Their angular location was chosen in order to favour the observation of IMF's emitted through evaporation of quasi compound nuclei and from the so-called intermediate velocity sources. In this way contributions from the peripheral collision were reduced and the more violent collisions were selected. These telescopes were used as a trigger of the multiparticle detector installed in the large vacuum chamber NAUTILUS at GANIL. It consists of a wall of 96 plastic scintillators at forward angles (3 to 30°) [5] and of a barrel of 72 staves made of plastic scintillators covering the larger angles (30 to 150°) [6]. The energy loss, time of flight and the direction of emission of particles are measured in a large solid angle so that the spatial and energy distributions were determined for the major part of the emitted fragments up to Z=9. Runs were also recorded with the multidetector alone (systematic triggering) in order to obtain data with minimal constraints and compared to the former IMF trigger data.

Preliminary results are shown in fig 1: a comparison

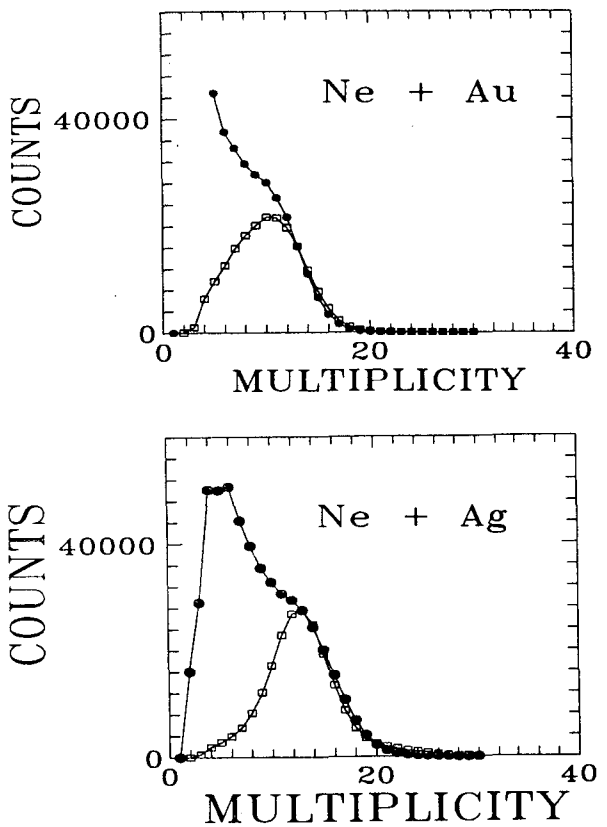

Figure 1

of the multiplicity distributions for the two triggering conditions is shown for the Ne+Ag and Ne+Au systems. The distribution without constraint except multiplicity >1 (open squares) exhibits two components whereas the triggering by the telescopes amounts to select events of higher multiplicity. The low multiplicity component for the systematic triggering corresponds to peripheral reactions. These events probably suffer from incomplete measurements since fast particles could escape undetected in the forward angle free space (<3°). The telescope trigger selects more violent collisions which manifest themselves by high multiplicity of light particles. Several mechanisms can contribute to these events: evaporation, fission, multifragmentation. At first glance it appears that higher multiplicities are selected in the Ne+Ag system than in the Ne+Au system. This can be related to the higher available energy per nucleon in the lighter system.

Another aspect is seen by looking at the multiplicity into two angular ranges: Θ_M<30° (wall) and Θ_M>30° (barrel). The two selection modes act differently: when requiring the presence of a fragment (Z>2) in one of the telescopes, only a very small increase in the multiplicity is observed for the forward part. In contrast, for the backward angles a strong change is observed particularly for the Ag target; this selection in the multiplicity distribution when triggering with a fragment in the telescopes is, on the other hand, weaker for the Au target due to the presence of a larger number of fission fragments associated with small multiplicities.

Thus, the IMF detection or the charged particle multiplicity at backward angles (Θ_M>30°) select the more violent collisions. This ability of the backward multiplicities to favour observation of central collisions has also been pointed out in experiments using the fission fragments correlation technique [7]. The major part of the forward angle multiplicity is less affected by the IMF selection since it results most likely from projectile break-up.

In agreement with ref. [4], where a more detailed analysis using two moving sources was done, the invariant IMF cross section velocity plots ($\beta_{//}$, $\beta_{\perp}$) reveal two sources of IMF production (besides the projectile one which is negligible at the measured angles): the slower one has a velocity close to the center of mass velocity whereas the other has a velocity slightly lower than half beam velocity. For the Au target, the small velocity component appears enhanced with respect to the midrapidity source contribution when selecting on the lowest

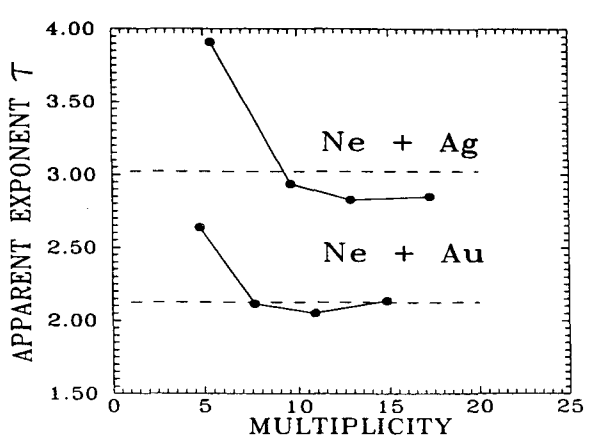

Figure 2

multiplicities.

The angle integrated Z-distributions were further analysed and fitted to a power law distribution $Z^{-\tau}$ for four different multiplicity bins. The values obtained for the apparent exponent τ are plotted in fig. 2, versus the mean multiplicity for each bin. For both targets, the τ values are larger for the low multiplicity bin and remain rather constant for the three other bins. The dashed lines indicate the τ values resulting from fits to the total Z-distributions without multiplicity gating; these values agree with the findings of ref. [4] at the same bombarding energy and also exhibit a target mass dependence since a lower τ value is obtained for the heavier system.

Investigating further the Z-distributions gated by multiplicity bins for the Au target, the multiplicity cuts have the same consequence at forward and backward angles: namely the slope becomes steeper for lower multiplicities. In contrast for the Ag target, this trend is still seen at forward angles whereas the very steep slope does not change with the multiplicity selection at larger angles. Therefore for the Ag target, the equilibrated source dominates the back angle emission. For the Au there is no such clean division and the evaporative and non-equilibrated components are present over the whole angular range.

An interesting observation is the ability of the multiplicity data to extract the evaporative component. Thus for Ag where the evaporative component is difficult to extract in singles mode, it is easily removed by placing a low multiplicity filter. On the other hand the excitation function studied in ref. [4] shows similar selectivity as for the charge multiplicity. We note that at low available energy E^* the Au data are marked by a strong evaporative component and show higher τ values. The same result is obtained via the low multiplicity filter. With high E^*, τ is essentially constant, which again is reproduced by imposing high multiplicity windows.

Fig 3 shows a contour plot of the detected parallel momentum in the 4π detector (mainly light charged particles) versus multiplicity when one IMF is

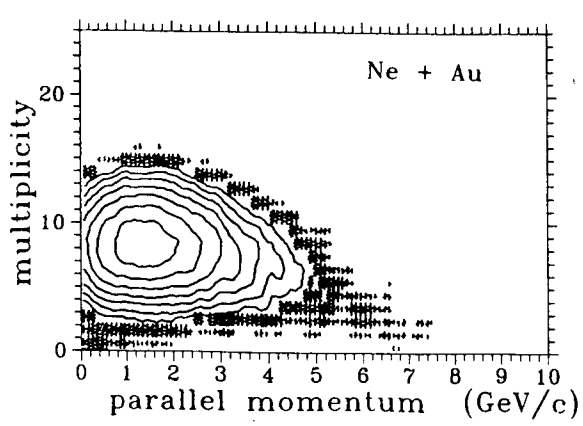

Figure 3

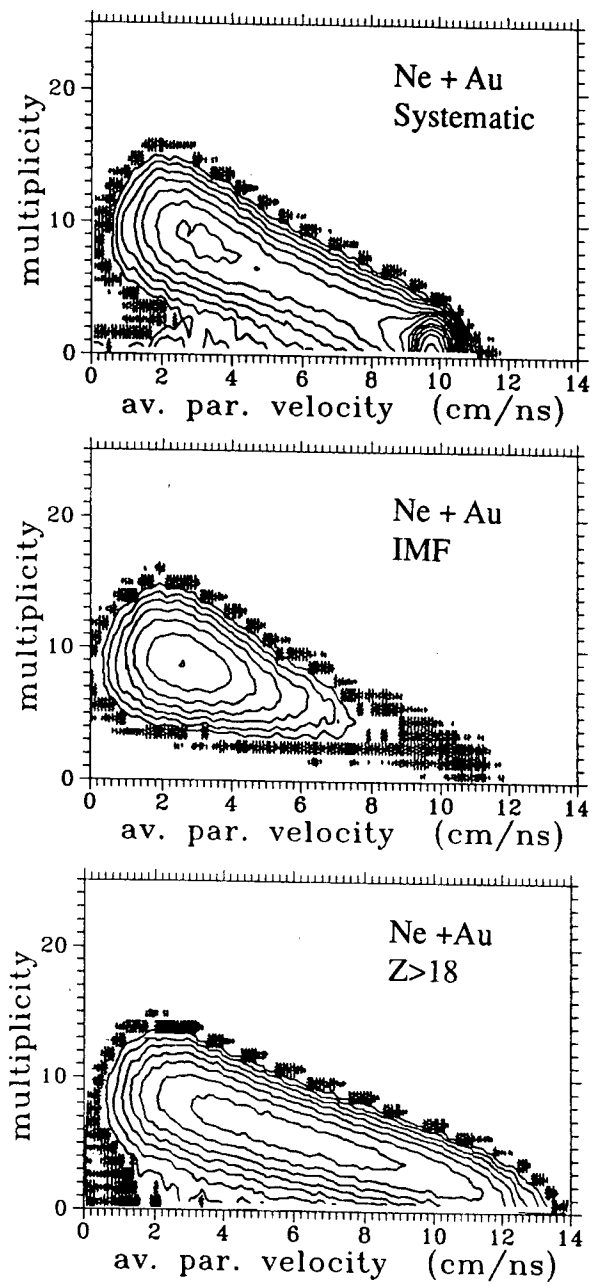

Figure 4

detected in a telescope for the gold target. The incident projectile momentum being 6.8 GeV/c, all these high multiplicity events are incomplete. The missing momentum may arise from undetected preequilibrium particles or from one or several undetected (because of thresholds) heavier fragments. A global variables analysis of these incomplete events may be difficult.

Nevertheless the average parallel velocity [8] of the detected nucleons in the 4π detector is defined as $V_{av}=\Sigma m_i V_i \cos\theta_i / \Sigma m_i$ where m_i is the mass, V_i the laboratory velocity and θ_i the laboratory polar angle of the detected products. Fig. 4 shows contour plots of the average parallel velocity versus multiplicity in three different cases for the gold target. In the case of the systematic trigger a peak at low multiplicity and velocity close to the projectile velocity (10.3 cm/ns) is observed. When requiring the detection of one IMF in the telescopes lower average parallel velocity (close to the center of mass velocity 1cm/ns) are selected. For the detection of fragments of charge Z>18 (mainly fission fragments) intermediate velocities are observed. The average parallel velocity seems to be a reasonable variable to select central collisions, but a complete simulation of the response of the detector system is necessary to relate the average parallel velocity to the impact parameter.

In summary, for the Ne+Ag and Ne+Au systems at 60 MeV/u, IMF detection selects the higher multiplicity events. The more violent collisions are also correlated with high muliplicities at backward angles (Θ_M>30°). The IMF Z-distributions are sensitive to multiplicity cuts, the lower multiplicity bin, selecting the equilibrated component. But the major origin of the IMF is from a midrapidity source associated with higher multiplicity. The average parallel velocity of the detected products seems to be a good variable to delimit central collisions.

Further analysis of the present data and simulations are in progress to complement these preliminary results.

* Experiment performed at the GANIL national laboratory.

references

[1] Proceedings of the 7th high energy heavy ion study,
GSI, Darmstadt October 1984,
Report GSI-85-10.
P.J. Siemens, Nature (London) 305, 410 (1983).
J. Aichelin et al., Phys. Rev. C30, 107 (1984).
J.P. Bondorf et al.,
Nucl. Phys. A387, 25c(1982).
D.H.E. Gross et al., Z. Phys. A309, 41 (1982).
L.G. Sobotka et al.,
Phys. Rev. C31, 668 (1985).
W. Bauer et al., Nucl. Phys. A452, 699 (1986).
X. Campi, Phys. Lett. 208B, 31 (1988).

[2] D.E. Fields et al.,
Phys. Lett. B220, 356 (1989)

[3] R. Trockel et al.,
Phys. Rev C39, 729 (1989)

[4] N.P. Vodinas et al.,
St Malo contributed papers p.67 (1988).
Y. Cassagnou et al.,
St Malo contributed papers p.101 (1988).
G. Imme et al.,
St Malo contributed papers p.107 (1988).
N.H Papadakis et al., to be published.

[5] G. Bizard et al., NIM A244, 483 (1986).

[6] A. Péghaire et al., Report GANIL P89/24
to be published.

[7] M.B. Tsang et al.,
Phys. Lett. B220, 492 (1989).

[8] J. Péter et al.,
to be published in Phys. Lett.

SEARCH FOR MULTIFRAGMENTATION NEAR THRESHOLD IN THE ^{3}He + ^{nat}Ag SYSTEM[§*]

S.J. Yennello, K. Kwiatkowski, N.R. Yoder, V.E. Viola, R. Płaneta[†], J.L.Wile and D.E. Fields; Departments of Chemistry and Physics and Indiana University Cyclotron Facility; Indiana University; Bloomington, IN 47405;

E.C. Pollacco, C. Volant, R. Dayras, Y. Cassagnou, S. Harar[**] and R. Legrain; DPhN/BE CEN Saclay, F-91191 Gif-sur-Yvette Cedex, France;

E. Hourani, IPN, BP no. 1, F-91406 Orsay, France; and

E. Norbeck, University of Iowa, Iowa City, IA

Central collisions between energetic projectiles and heavy target nuclei permit investigation of the thermal properties of nuclear matter over the full range of internal excitation up to the vaporization limit. An important signature of such hot systems is the emission of intermediate-mass fragments (IMF: $3 \leq Z \lesssim 15$). At relatively low excitation energies ($E^{*} \lesssim 100$ MeV) the formation of IMFs can be understood in terms of emission from a fully equilibrated compound nucleus. At projectile velocities in the vicinity of Fermi velocity, non-equilibrium processes which resemble pre-equilibrium nucleon emission become an increasingly important component of the IMF yields at forward angles, while equilibrium-like emission predominates at backward angles. At still higher energies, the existence of multifragmentation has also been reported, indicating the onset of violent nuclear collisions which generate a high degree of chaos in the system during a very short interaction time.

The possibility of observing the threshold for multifragmentation poses an important physics question. The onset of this phenomenon should be characterized by a change in reaction observables when the deposition energy becomes sufficiently large. Previous inclusive studies of protons incident on a Xe target have provided evidence for such a mechanism change in the vicinity of 2-10 GeV bombarding energy [1]. Taken in context with coincidence studies [2] this result has been associated with the onset of multifragmentation and interpreted in terms of a liquid-gas phase transition model.

In the present study, we have sought to extend earlier investigations of the evolution of equilibrated and non-equilibrated IMF emission mechanisms [3] and to search for evidence of multifragmentation in the ^{3}He + ^{nat}Ag system. The experiments were performed at the SATURNE II accelerator at the Laboratoire National Saturne in Saclay, France with beams of total energy 480, 900, 1800, 2700 and 3600 MeV. The experimental objectives in these measurements have been (1) to obtain a highly systematic set of inclusive data for IMF emission over a range of projectile energies from the target-projectile Coulomb barrier region up to relativistic energies and (2) to perform exclusive measurements of complex fragment ($Z>2$) multiplicities. In order to identify changes in the reaction mechanism, emphasis has been placed on defining complete fragment energy spectra from well below the Coulomb energy up to the maximum possible energy over as large a range of angles and ejectile Z-values as possible. Complex fragments were measured with an array of gas-ionization/silicon ΔE-E telescopes.

Fig. 1 illustrates the evolution in the energy spectra for carbon fragments

as a function of ^{3}He bombarding energy at a backward angle. These data are representative of the behavior of other fragments as well. At 480 and 900 MeV the spectra strongly resemble those obtained at lower energies [3]. For the higher energy bombardments the forward angle spectra (not shown) all appear quite similar, with perhaps somewhat flatter spectra at the three higher energies. Most striking, however, is the comparison at 140°, where a transition in the spectral character appears to occur between 900 and 1800 MeV. Further, the spectra for a given angle at 1.8, 2.7 and 3.6 GeV are virtually identical. Thus, analysis of the exponential slopes of the high-energy portion of these spectra suggests that at incident energies up to 900 MeV, the data evolve systematically, in accord with lower energy results [3]. However, above this energy, the spectra at backward angles indicate a distinctly different character which appears to be nearly independent of bombarding energy.

Another aspect of the energy spectra that suggests a mechanism change above 900 MeV bombarding energy is found in the behavior of the Coulomb peaks associated with these spectra. Two systematic features emerge as a function of increasing bombarding energy: (1) the most probable peak energy decreases, and (2) the width of Coulomb peak increases, extending the spectra down to significantly lower energies at 3.6 GeV than at 900 MeV and below. This behavior is similar to previous studies with protons [1] and is consistent with a mechanism in which the Coulomb field of the emitting system is strongly modified by multiple charged-particle (fragment) emission either prior to or simultaneous with the fragment in question.

The systematic behavior of the elemental yield distributions parallels that of the energy spectra; i.e., a change in character is observed between 900 MeV and 1.8 GeV. A power-law fit to the charge distribution data, $\sigma(Z) \propto Z^{-\tau}$, has been performed at each energy and angle, as well as for the total yield. In Fig. 2 the power-law parameter τ is plotted as a function of bombarding energy for both lower-energy data [3] and the present results. The dependence of τ on bombarding energy in Fig. 4 shows a smooth decrease with incident energy at both forward and backward angles up to 1.8 GeV, after which the power-law parameter becomes essentially constant at $\tau = 2.1 \pm 0.1$ for all cases. This value is similar to that found for proton-induced reactions [1,4]. Thus, examination of the bombarding energy dependence of both the IMF kinetic-energy spectra at backward angles and the power-law parameters τ suggests a change in reaction mechanism between 900 MeV and 1.8 GeV for complex fragment production from the ^{3}He + ^{nat}Ag system. Similar arguments have been proposed for the p + Xe system, although at somewhat higher incident energies but comparable values of the average linear momentum transfer [1].

In Fig. 3 the angular distributions for carbon fragments obtained at 900 MeV and 3.6 GeV are compared with lower energy ^{3}He + ^{nat}Ag data, where IMF emission has been shown to occur by both statistical decay from a fully equilibrated source and precompound emission on a fast time scale [3]. Most evident in this plot is the strong increase in cross section (~x100) as a function of bombarding energy, depending on angle of emission. This increase becomes more pronounced as the atomic number of the IMF increases. In contrast, the increase in the <u>average</u> excitation energy deposited in central collisions increases much more slowly ($\lesssim$ a factor of 3) over this energy interval, as deduced from linear momentum transfer systematics [5] and intranuclear cascade calculations [6].

In order to estimate the excitation energy and temperature associated with these ^{3}He + ^{nat}Ag results, the ISABEL cascade code has been run for a full range of impact parameters, b, as a function of ^{3}He bombarding energy. These calculations indicate that for the total reaction cross section ($\sigma_R \approx 1800$ mb), the increase in the average excitation energy of the residual nucleus is a relatively weak function of bombarding energy above 200-300 MeV. However, for the central collision component ($b \leq 2.6$ fm, $\sigma_c \cong 200$ mb) the average excitation energy increases rapidly with bombarding energy. The region above 1 GeV bombarding energy corresponds to an average excitation energy in the residual nucleus of about 300 MeV, or a nuclear temperature of $T \approx 4.5$ MeV (assuming a $= A/8$ MeV^{-1}). This temperature range corresponds to values predicted by several models of multifragmentation and is consistent with experimental estimates of limiting temperatures for hot nuclei [7].

While the inclusive data are suggestive of a transition toward multifragmentation between 1 and 2 GeV in the ^{3}He + Ag system, exclusive experiments are required for confirmation. Such data are also essential to determine whether this process is sequential or instantaneous. To this end we have recently performed an experiment in which we have studied the ^{3}He + Ag reaction at 900 MeV and 3.6 GeV using a 36-telescope detector array with approximately 2 steradians of solid angle coverage.

The detector configuration was arranged so that an approximately random coverage of the total solid angle was attained. In Fig. 4 preliminary data from the 3.6 GeV experiment show the raw multiplicity distribution for events with $Z \geq 4$, i.e. only Be and heavier fragments are included in M_{IMF}. These results, uncorrected for solid angle and angular distribution, confirm the presence of multifragment events up to $M_{IMF}=5$, accounting for over 40 percent of the total charge in the reaction. Proper simulations must be performed in order to estimate the true multiplicities.

---

§ This work was performed at the Laboratoire National Saturne.
* Research supported by the US Department of Energy grant no. DE.FG02-88ER.40404.A000 and NSF grant no. PHY-87-14406.
† Present address: Institute of Physics, Jagellonian University, Reymonta 4, Kraków, POLAND
** Present address: GANIL, BP5027 F-14021 Caen, Cedex, France

References

1. A.S. Hirsch et al., Phys. Rev. C29 (1984) 508;
   N.T. Porile et al., Phys. Rev.C 39 (1989) 1914.
2. A.I. Warwick et al., Phys. Rev. C27 (1983) 1083.
3. K. Kwiatkowski, et al., Phys. Lett. B171 (1986) 41;
   M Fatyga et al., Phys. Lett. B185 (1987) 321.
4. S.J. Yennello et al., Phys. Rev. C. 41 (1990) 79.
5. F. St. Laurent et al., Phys. Lett. B 110 (1982) 372;
   V.E. Viola, Nucl. Phys. A 471 (1987) 53c.
6. Y. Yariv and Z. Frankel, Phys. Rev. C 24 (1981) 488.
7. Proc. Symp. on the Formation and Decay of Hot Nuclear Matter, (Dallas, TX, April, 1989), J. B. Natowitz, ed., World Scientific, New Jersey, 1989.

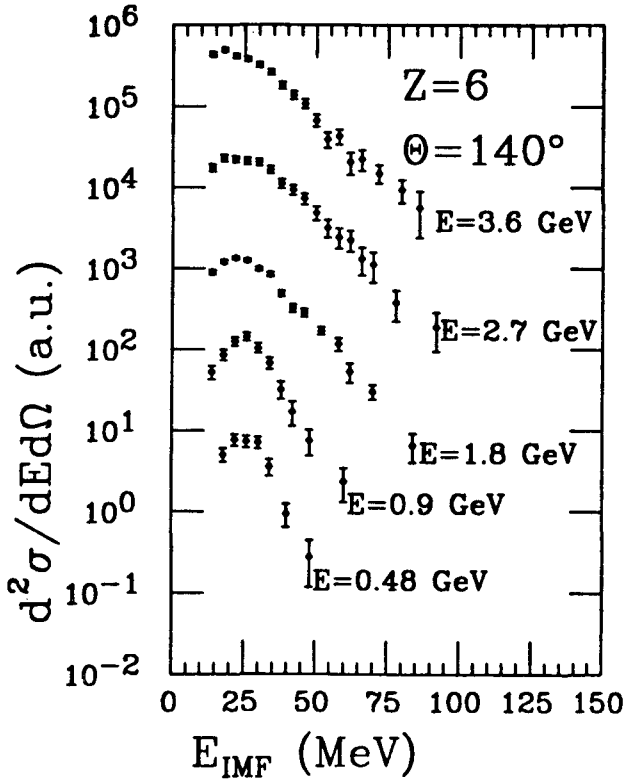

Fig. 1 Kinetic energy spectra for carbon fragments observed at bombarding energies indicated on figure.

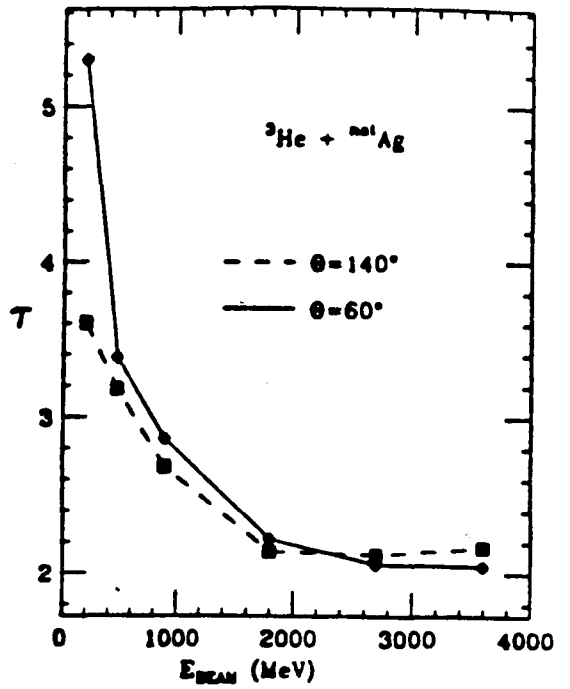

Fig. 2 Power-law parameter τ for the ^3He + ^{nat}Ag system as a function of total bombarding energy.

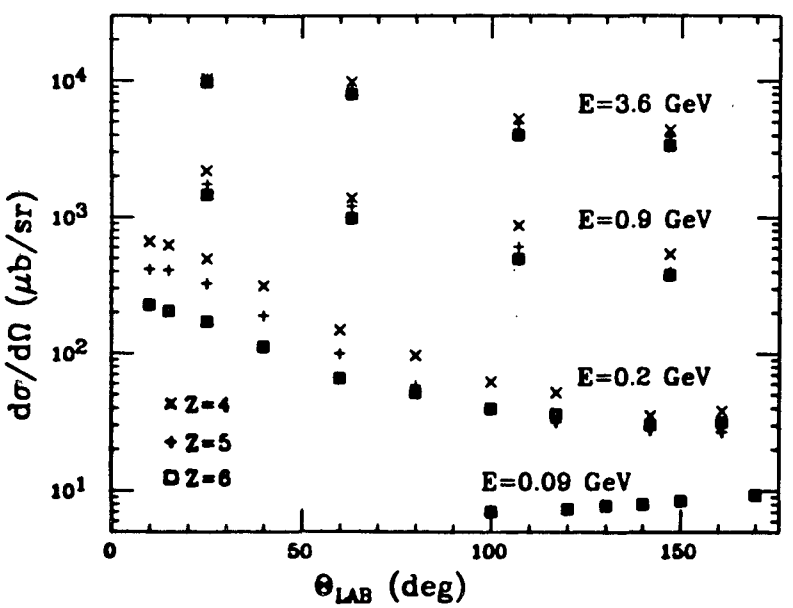

Fig. 3 Angular distributions of carbon fragments emitted from the ^3He + ^{nat}Ag system at bombarding energies indicated.

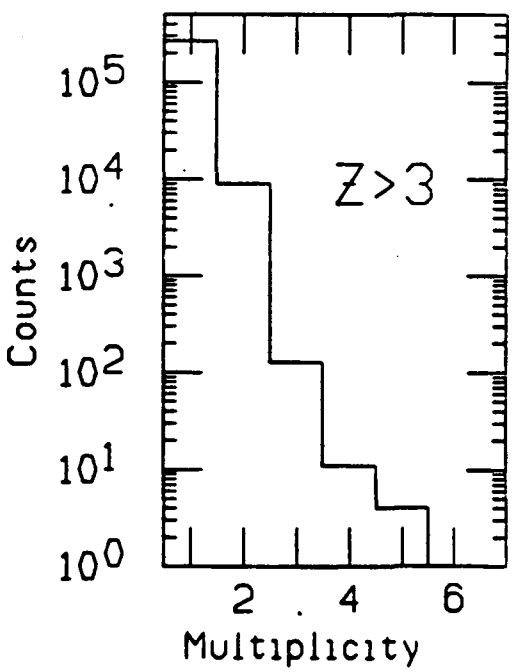

Fig. 4 Raw multiplicities for fragments with $Z \geq 4$ formed in the bombardment of a silver target with 3.6 GeV ^3He ions.

Sources of Light Particles in Peripheral Collisions

P.L. Gonthier, B. Bouma, P. Harper, D. Bleitz, M. Vonk and T. Koppenol
Department of Physics, Hope College, Holland, MI 49423

D.A. Cebra, Z.M. Koenig, D. Fox, K. Wilson, S. Howden, A. Nadasen,
A. Vander Molen, J.S. Winfield and G.D. Westfall
National Superconducting Cyclotron Laboratory, East Lansing, MI 48824-1321

The emission of light particles in peripheral collisions has been associated with various production mechanisms such as the formation of hot spots[1,2], Fermi jets[3], piston effect[4], quasi-free knockout[5], and projectile breakup.[6,7] Such prompt emission is expected to take place during the early stages of the collision, thereby providing a probe of the reaction mechanism which yields information on the dissipation of the energy during the collision. However, the projectile and target nuclei can be excited to particle unbound states which are long lived. Decay of such states leads to sequential processes. Sequential emission is the decay of statistically equilibrated projectile-like fragments (PLFs) and target-like fragments (TLFs) which have been accelerated by the Coulomb field of the two interacting nuclei.

We probe the heavy ion reaction mechanism by first selecting peripheral collisions. We accomplish this by detecting the remnants of the projectile after it has suffered a collision with the target nucleus. During the reaction, the kinetic energy of the projectile is dissipated into collective and internal modes of excitation then both the PLFs and TLFs de-excite by emitting light particles. By studying the energy and angular correlations of the emitted light charged particles in coincidence with PLFs, we focus on the reaction dynamics. The main sources of light particles are the sequential decay of the PLFs and TLFs, prompt decay of the projectile during the collision and emission from the interaction zone where the nuclear densities overlap.

We performed two experiments at the National Superconducting Cyclotron Laboratory in which we measured the energy and angular correlations of α particles in coincidence with PLFs in the reactions of 35 MeV/nucleon ^{16}O with ^{nat}Ni. One experiment involved Si detectors backed by fast/slow plastic scintillators. In the second experiment the 4π detector was triggered by a forward array of 45 fast/slow scintillators.

The signature for the sequential decay of PLFs has been seen best in the energy correlation of the α particles observed close to the PLFs. A plot of the laboratory energy of the α particles, E_α, versus the laboratory energy of the carbon ions, E_C is displayed in Fig. 1 for α particles at the indicated angles in coincidence with carbon detected at $\theta_C = +10^\circ$. The data at $\theta_\alpha = +15^\circ$ reveal a pattern of two high intensity regions with a pronounced valley in between them. This pattern of two lobes is typical of sequential decay of PLFs. At $\theta_\alpha = -15^\circ$ there is only one broad high intensity region, and the

separation of sources at this angle is not apparent.

We present in Fig. 2 energy spectra of α particles in coincidence with carbon corresponding to the projections of the distributions in Fig. 1 unto the E_α axis. The two prominent bumps in the energy spectrum at $\theta_\alpha = +15°$, which is closest to the observed PLFs at $+10°$, correspond to the two lobes seen in Fig. 1 at $\theta_\alpha = +15°$. Most of the yield at this angle results from the decay of the projectile as shown in the figure by model calculations. Also included in the model is a component of fast, beam velocity α particles. This component is parameterized by Gaussian functions for the laboratory velocity distribution and angular distribution. These calculations are shown in Fig. 2 as dashed curves (the narrower dashed curves) for sequential decay of TLFs and dotdash curves for the decay of PLFs. On the opposite side of the beam from the detected PLFs at $\theta_\alpha = -15°$ there is an excess of beam velocity α particles which has been observed in other studies at various bombarding energies.[8,9,10] This beam velocity component of α particles has been fitted by the model and is shown as dotted curves. This fast component of α particles presumably arises during the initial moment of interaction and seems to be independent of the later stages of the collision as one also finds this component in coincidence with fusion-like residues.[8,9]

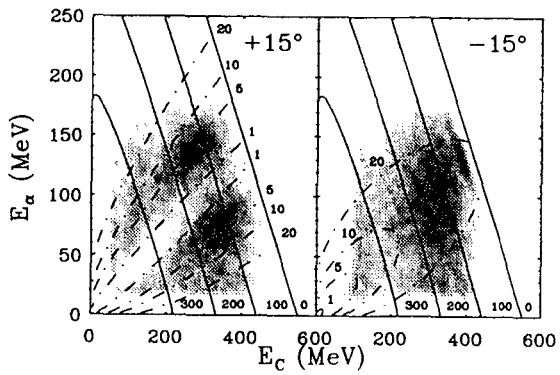

Figure 1 Density plot, with the intensity varying linearly, for α particles at the indicated angles in coincidence with carbon at $\theta_{PLF} = +10°$. Curves represent three body kinematic calculations. The dotdash curves correspond various values of the relative energy (MeV) between ^{12}C and α particle assuming the breakup of ^{16}O into $^{12}C + \alpha$. The solid curves correspond to the total excitation energy, Q_3 (MeV).

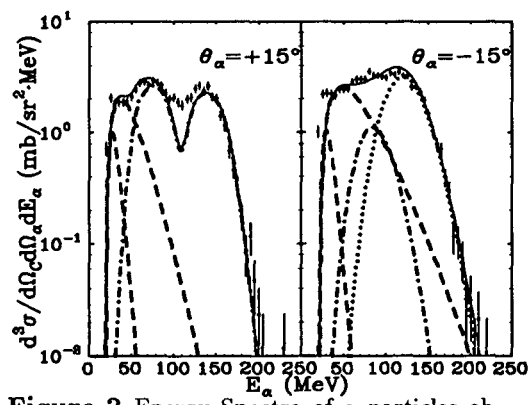

Figure 2 Energy Spectra of α particles observed at the indicated angles in coincidence with carbon ions at 10°. Model calculations represented by curves; see text. Positive angles represent the same side of the beam as the observed PLFs, while negative angles indicate the opposite side.

In order to understand the production of particles, we examine the correlation of atomic numbers from multiplicity=2 events from the data taken with the forward array detector system, Fig. 3 presents the atomic number Z_2 of ions detected between $\theta_{Z_2} = -(7° \rightarrow 18°)$ on the opposite side of the beam from Z_1 detected at $\theta_{Z_1} = +10°$. The numbers correspond the the total number of counts for a fixed amount of beam time. As can be seen the $^{12}C + \alpha$ is the dominate channel of the breakup of the ^{16}O.

There is a substantial number of events for the proton pickup but many fewer for the α particle pickup. The distribution in this figure suggests that most of these fragments come from the projectile breakup. Similar indications are obtained fom triple coincidence events.

In order to understand the production of particles, we examine the correlation of atomic numbers from multiplicity=2 events from the data taken with the forward array detector system, Fig. 3 presents the atomic number Z_2 of ions detected between $\theta_{Z_2} = -(7^o \rightarrow 18^o)$ on the opposite side of the beam from Z_1 detected at $\theta_{Z_1} = +10^o$. The numbers correspond the the total number of counts for a fixed amount of beam time. As can be seen the $^{12}C+\alpha$ is the dominate channel of the breakup of the ^{16}O.

There is a substantial number of events for the proton pickup but many fewer for the α particle pickup. The distribution in this figure suggests that most of these fragments come from the projectile breakup. Similar indications are obtained fom triple coincidence events.

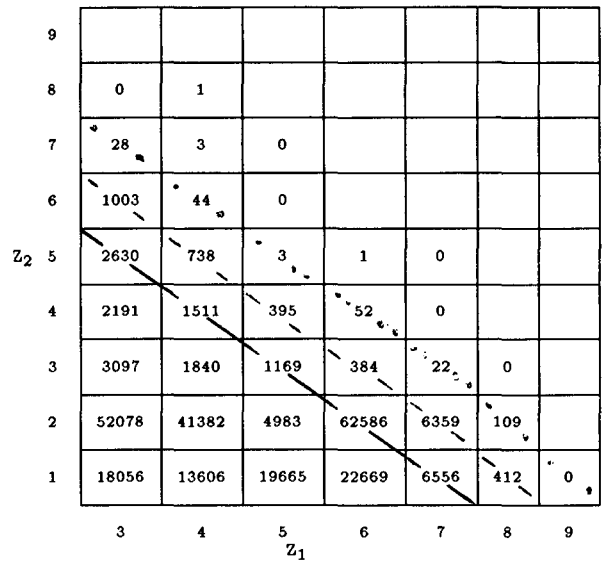

Figure 3 Coincidences between ions of atomic number Z_1 in coincidence with ions Z_2 observed on the opposite side of the beam from the detected Z_1. Solid, dashed and dotted lines indicate events in which the sum of $Z_1 + Z_2$ is equal to the atomic number of the projectile, Z_{PRO}, is equal to $Z_{PRO} + 1$ and is equal to $Z_{PRO} + 2$, respectively. The events along the dashed line result from the proton pickup channel while the events along the dotted line result from the α particle pickup channel.

We reconstruct the ^{16}O by detecting an α particle in the vicinity of a ^{12}C using the forward array detector of the 4π detector system. From Fig. 2, we can see that the majority of the $^{12}C - \alpha$ yield at $\theta_\alpha = +15^o$ results from the breakup of ^{16}O. With the large energy thresholds, the contribution from the decay of TLFs as seen by the forward array at this angle pair is of the order of a few percent.

In coincidence with the reconstructed projectile we select events where α particles appear on the opposite side of the beam from the projectile. The histogram in Fig. 3 represents energy spectrum of the multiplicity=2 events for α particles in coincidence with ^{12}C on the opposite side of the beam. The data are arbitrarily normalized to each other. Comparison of the energy spectrum from $(C - \alpha) - \alpha$–multiplicity=3 events with the energy spectrum for $(C - \alpha)$–multiplicity=2 events, indicates conclusively that the fast, beam velocity component of α particles which tends to be focused on the opposite side of the beam from the PLFs, arises from the breakup of the projectile. When nitrogen is reconstructed by demanding a proton in the vicinity of the ^{12}C, the multiplicity=3 events tend to select the proton pickup channel mentioned earlier.

This α particle energy spectrum from $(C - p) - \alpha$ events is very similar to the α energy spectrum (histogram) from $(C - \alpha)$–multiplicity=2 events. The $(Be - \alpha) - \alpha$ and $(Li - \alpha) - \alpha$ events result from the direct, multiple decay of the projectile without the necessity of picking up nucleons from the target. These spectra (not shown) have the same

shape as the multiplicity=2 spectra. These studies provide very conclusive evidence that the projectile is the source of the fast, beam velocity component focused on the opposite side of the beam from the detected PLFs.

Looking back at the dashed curve in Fig. 3 for the $(C - \alpha) - \alpha$–multiplicity=3 events, we can draw the conclusion that the TLF is definitely the source of the intermediate component of α particles. Since for these events the projectile is reconstructed, the Fermi jet model cannot explain the data. The model that seems most amenable to explain the data is a knock-out picture in which the projectile scatters off an α particle cluster on the surface of the target nucleus. During this process the α particle is removed from the target and the projectile is excited to an α particle unbound state. The Fermi momentum distribution of the α particle in the target nucleus broadens the energy spectrum of the α particle, thereby smearing out the correlation between it and the reconstructed projectile on the opposite of the beam.

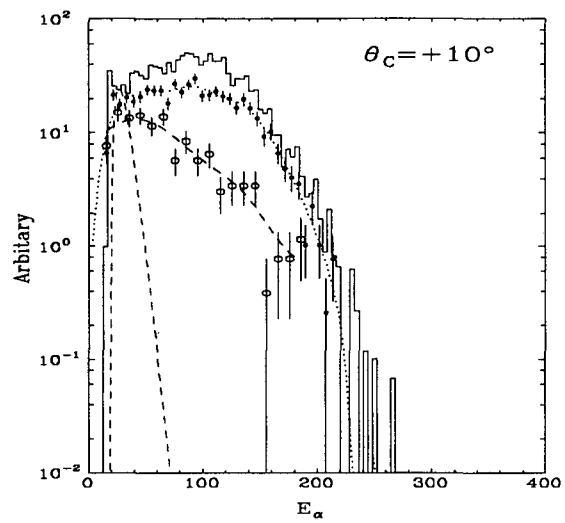

Figure 4 Energy spectrum of α particles (histogram) in coincidence with carbon ions detected on the opposite side of the beam. Open circles with the dashed curve to guide the eye represent the energy spectrum of α particles detected on the opposite side of the beam from the reconstructed ^{16}O (triple coincidences). Solid circles with the dotted curve to guide the eye represent the energy spectrum of α particles detected on the opposite side of the beam from the reconstructed ^{13}N (triple coincidences).

References

[1] H. Ho *et al.*, Z. Phys. A283, 235 (1977).

[2] P.A. Gottschalk and M. Weström, Nucl. Phys. *A314*, 232 (1979).

[3] J.P. Bondorf, J.N. De, G. Fái, A.O.T. Karvinen, B. Jakobsson, and J. Randrup, Nucl. Phys. *A333*, 285, (1980); M.C. Robel, Ph. D. thesis, Lawrence Berkeley Laboratory Report LBL-8181, (1979).

[4] D.H.E. Gross and J. Wilczyński, Phys. Lett. *67B*, 1 (1977).

[5] R.K. Bhowmik et al., Phys. Rev. Lett. 43, 619 (1979).

[6] A. Gamp et al., Phys. Lett. *74B*, 215 (1978).

[7] R. Billerey, C. Cerruti, A. Chevarier, N. Chevarier, B. Cheynis, and A. Demeyer, Z. Phys. A292, 293 (1979).

[8] H. Ho *et al.*, Phys. Lett. 96B, 51 (1980).

[9] P. Gonthier, H. Ho, M.N. Namboodiri, L. Adler, J.B. Natowitz, S. Simon, K. Hagel, R. Terry, and A. Khodai, Phys. Rev. Lett. 44, 1387 (1980).

[10] H. Ho, P.L. Gonthier, G.-Y. Fan, W. Kühn, A. Pfoh, L. Schad, R. Wolski, J.P. Wurm, J.C. Adloff, D. Disdier, A. Kamili, V. Rauch, G. Rudolf, F. Scheibling, and A. Strazzeri, Phys. Rev. C27, 584 (1983).

Intermittency in high energy collisions

Sergei Voloshin

Theoretical Physics Institute, University of Minnesota
and
Moscow Engineering Physics Institute, Moscow, USSR

The study of intermittency in high energy collisions has attracted in the recent years an increasing interest. It started in 1986 when Bialas and Peschanski[1] proposed a new method for analysis of multiparticle production processes. In this approach the whole rapidity window should be divided in M equal bins. The multiplicity factorial moments averaged over all bins as a function of M are under study.

$$F_i(M;\Delta) = \frac{1}{M}\sum_{m=1}^{M} M^i \frac{\langle k_m(k_m-1)\cdots(k_m-i+1)\rangle}{\langle N(N-1)\cdots(N-i+1)\rangle} . \tag{1}$$

where k_m is the number of particles in the m-th interval, and N is the number of particles in the rapidity window. The important result of Ref.1 is that the factorial moments would depend on M raised to a power if there is any intermittency in multiparticle production process. Such power behavior was observed in different experiments (such as[2,3] and others). It is likely that the intermittency is present at the Collider energy[4]. The question arose if these data indicated some new physics. It was shown in Ref.5 and other papers that it is possible to account for the data within standard framework of multiparticle phenomenology and further study is necessary. In this work attention will focus on the role of resonance decays and multi-chain production and particularly on the possibilities of its revelation. We also propose using split-bin correlation functions to avoid influence of some experimental errors (such as double counting) exhibiting power-law divergences as the bin size diminishes which may mask signals of intermittency and to extend this approach to transverse energy experiments.

In our calculations we used simple version of quark-gluon string model[6] where the total multiplicity distribution is represented as a convolution of the distribution in the number of Pomeron showers and the distribution in the number of particles in a single shower. The so called "quasi-eikonal" approximation was used to obtain the probabilities of production several Pomeron showers, which result in approximately 1.8 showers per inelastic collision at the energies of interest ($s \approx 20GeV$). Following Ref.6 we choose the rapidity distribution for each shower in the form:

$$\frac{dn}{dy} = D[1-\exp(\frac{y-y_{max}}{2})][1-\exp(\frac{y_{max}-y}{2})]. \tag{2}$$

Here D is the normalization factor and y_{max} is defined by shower energy.While the energy per shower is large enough the rapidity distribution corresponding bigger number of showers grows at $y = 0$ and become more narrow. The factorial moments are very sensitive to such changes. We used simplest suggestion of equal energy distribution among showers. A Poisson distribution with the mean value determined by the

rapidity distribution was used for the probability of producing N particle within the rapidity interval Δy.

Below we present results of calculations for hadron-hadron collisions at the energy $E = 250GeV$ and rapidity interval $-2 < y < 2$, the same conditions as in the experiment[2]. The experimental data are presented in fig.1. The solid lines are linear fits to the data for $\delta y = \Delta y/M < 0.1$ which we use below for the convenience of comparison with the results of calculations.

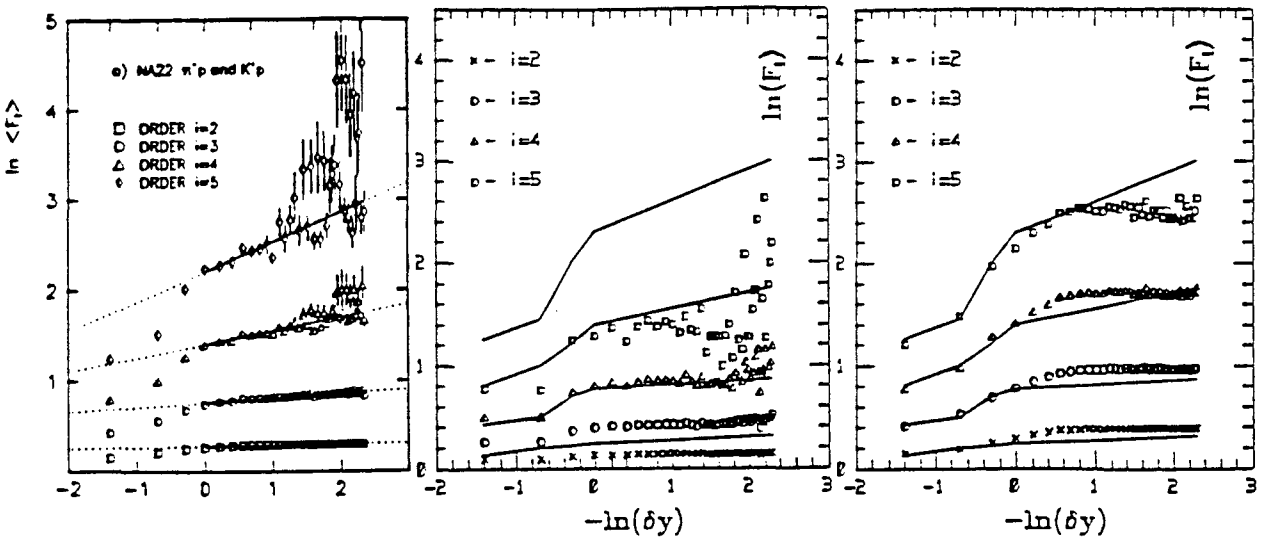

Fig.1 Fig.2 Fig.3

Fig.2 presents the results when only multi-Pomeron exchanges have been taken into account but not resonances. Note, that if we used only one-Pomeron exchange all moment would be very close to unity. The model[6] describes the KNO-function better (really excellent) if one uses a Poisson distribution not for the number of particles but for the number of pairs of produced particles. It is likely that in this way resonance production and decays are effectively taken into account.If we try to calculate on this assumption we will have power increase of the moments. That is because for the distribution in pairs of particles with mean value $\bar{n} = \bar{N}/2$ (for the flat rapidity distribution) in the bin δy

$$F_2 = \frac{1}{4\bar{n}^2}\sum_{n=1}^{\infty} 2n(2n-1)e^{\bar{n}}\frac{\bar{n}^n}{n!} = 1 + \frac{1}{2\bar{n}}. \tag{3}$$

But $\bar{n} = \bar{n}_{total}/M$ and we have F_2 a linear function of M! Note that the double counting results in the same way. Even 10% of such pairs results to bigger growth of factorial moments then have been seen experimentally. If we assume that pairs have fixed rapidity separation $2\Delta y$ the moments will have a fall at $\delta y = 2\Delta y$. The real resonances have some distribution in their products rapidity separation. We used simplest one corresponding isotropic two particle decays. Fig.3 presents the results for two kinds of resonances, one with probability 0.75 and $\Delta y_{max} = 1.5$ and the other with probability 0.1 and $\Delta y_{max} = 0.2$.

There are some possibilities to study the role of multi-Pomeron exchanges and resonance decays[7]. So one can take into account only particles with the same sign

of charge (only positive or negative particles) and in this way diminish the role of resonances. The other possibility is to try to enhance the contribution of longitudinal decays by choosing particles with $p_t < p_{cut}$ and study the moments decrease at $\delta y \approx \Delta y_{max}$. The effect can be seen in spite of smoothing due to the resonance p_t distribution. Fig.4 presents the predictions for $p_{cut} = 0.1GeV$ and 75% of resonances with $\Delta y = 0.5$ among all particles. The distribution function for transverse momenta of direct particles (both stable hadrons and resonances) is taken to be

$$P(p_T) \sim p_T \exp(-p_T^2/2\tilde{p}^2)\ , \qquad \tilde{p} = 0.3GeV. \tag{4}$$

The role of multi-Pomeron exchanges can be studied, for example, by choosing non-symmetric rapidity windows or imposing additional condition for other rapidity window[7]. This technique is also useful for hadron-nucleus collisions.

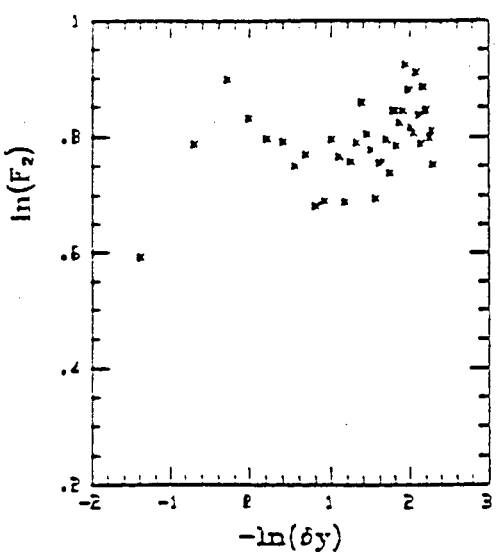

Fig.4

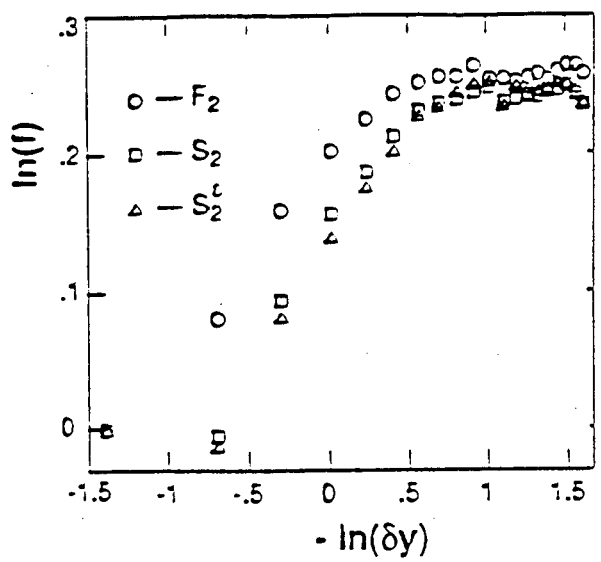

Fig.5

In addition, we propose the use split-bin correlation functions[8] which are free of some disadvantages of factorial moments and can be constructed using continuous variables such as transverse energy. The simplest split-bin correlation function is

$$S_2(M) = M \frac{\langle \sum_{m=1}^{M} n_m^L n_m^R \rangle}{\langle N^L N^R \rangle}\ , \tag{5}$$

where the rapidity window is divided into M bins, $n_m^{L(R)}$ is the number of particles in the left (right) half of the m-th bin, and $N^{L(R)}$ is the number of particles in the left (right) half of the rapidity window.$S_2(M)$ will exhibit a power-law divergence as $M \to \infty$ if intermittency occurs, just as F_2 does. We can also construct a split-bin correlation function using transverse energy $\mathcal{E}^T = \mathcal{E} \sin\theta$, where $\mathcal{E}$ is the energy in a bin and θ is the angle with respect to the beam direction, measured from the primary

interaction vertex. This construction gives us

$$S_2^{\mathcal{E}}(M) = M \frac{\langle \sum_{m=1}^{M} \mathcal{E}^T_{m,L} \mathcal{E}^T_{m,R} \rangle}{\langle E^T_L E^T_R \rangle}, \tag{6}$$

where $\mathcal{E}^T_{m,L(R)}$ is the transverse energy in the left (right) half of the m-th bin, and $E^T_{L(R)}$ is the transverse energy in the left (right) half of the rapidity window. In Fig.5 we compare $S_2^{\mathcal{E}}$ with S_2 and F_2.

The split-bin correlation function can be used to study correlations in other variables than rapidity, such as azimuthal angle ϕ. The ϕ-distribution of particles is very flat for most event samples (because of the high degree of symmetry of the collisions), so searches for intermittency in ϕ are also interesting. The simplest correlation function of such type is one constructed by splitting each of the rapidity bins into two equal ϕ sub-bins and assuming that $n_m^{L(R)}$ in (5) is the number of particles in the m-th bin with $\cos\phi > (<) 0$.

In particular, measurement of split-bin correlation functions for events with high $\mathcal{E}^T$ might yield valuable information about the hadronization process. We believe that the use of split-bin correlation functions will open up new approaches to the study of the intermittency in multi-particle processes.

I am grateful to J. Kapusta and D. Seibert for helpful discussions. I furthermore thank Larry McLerran for hospitality at the Theoretical Physics Institute of the University of Minnesota.

References

1. A. Białas and R. Peschanski, Nucl. Phys. **B273** (1986) 703; Nucl. Phys. **B308** (1988) 857.

2. I. V. Ajinenko *et al.* (EHS/NA22 collaboration), Phys. Lett. **B222** (1989) 306.

3. R. Holynski *et al.* (KLM collaboration), Phys. Rev. Lett. **62** (1989) 733; Phys. Rev. **C40** (1989) R2449.

4. I. Sarcevic and H. Satz, preprint AZPH-TH/89-58.

5. A. Capella, K. Fialkowski and A. Krzywicki, Phys. Lett. **230B** (1989) 149.

6. A. B. Kaidalov and K. A. Ter-Martirosyan, Phys. Lett. **117B** (1982) 247; Sov. J. Nucl. Phys. **39** (1984) 979.

7. S. A. Voloshin, preprint TPI-MINN-89/37-T, submitted to Z. Phys. C.

8. S. Voloshin and D. Seibert, preprint TPI-MINN-90/5-T, submitted to Phys. Rev. Lett.

Microscopic Field Theoretical Approach to Ultrarelativistic Nucleus-Nucleus Collisions

A. J. Sierk, R. J. Hughes, and J. R. Nix
Los Alamos National Laboratory, Los Alamos, New Mexico 87545

In nucleus-nucleus collisions at AGS, CERN, and RHIC energies, the interaction time is extremely short, and the nucleon mean free path, force range, and internucleon separation are all comparable in size. These conditions are very different from those that would be required to make valid most of the approximations and models that have been used previously to describe such collisions. To satisfy *a priori* the basic conditions that are present, a fully microscopic many-body treatment that allows for nonequilibrium phenomena, interactions with correlated clusters of nucleons, and particle production appears necessary. Furthermore, the approach must be manifestly Lorentz covariant, or problems with causality immediately arise. On the other hand, at bombarding energies of many GeV per nucleon, the reduced Compton wavelength of projectile nucleons is sufficiently small that quantal coherence effects are negligible and the classical approximation for nucleon trajectories is valid. A natural approach that satisfies all these requirements is a classical relativistic field theory corresponding to the exchange of massive particles.

Massive fields have been with us since the 1930s. Independently of Yukawa's seminal realization[1] that the nuclear force is related to meson exchange, Proca[2] had proposed field equations corresponding to the exchange of massive vector (spin-1) particles to study the possibility that the photon's mass is nonzero. The classical equations for treating the motion of a point nucleon in a massive vector field were derived soon thereafter by Bhabha.[3] More recently, Serot and Walecka[4] have introduced a relativistic quantum field theory corresponding to the exchange of scalar σ mesons and vector ω mesons, solving it in the mean-field approximation for the properties of both nuclear matter and finite nuclei. Attempts have been made to apply this σ-ω model to relativistic heavy-ion collisions, but computational difficulties have led to such drastic simplifications as the local-density approximation[5] or the complete neglect of radiation.[6]

In our work, we are trying to solve the classical equations of motion *exactly* for a simplified Lagrangian corresponding to the exchange of vector ω mesons. We neglect pseudoscalar and scalar mesons because contributions from their exchange decrease by the factor $1/\gamma = (1 - v^2)^{1/2}$ relative to those arising from the exchange of vector mesons. (Here and throughout this paper we use units in which the speed of light $c = 1$, as well as in which the reduced Planck constant $\hbar = 1$.) For N nucleons of mass M interacting through the exchange of vector mesons of mass m with coupling constant g, the Lagrangian density is

$$\mathcal{L} = -M \sum_{i=1}^{N} \int d\tau_i \delta^{(4)}[x - x_i(\tau_i)] - \frac{1}{16\pi} F_{\mu\nu} F^{\mu\nu} + \frac{1}{8\pi} m^2 A_\mu A^\mu - A_\mu J^\mu \quad . \tag{1}$$

Here the field strength tensor is $F^{\mu\nu} = \partial^\mu A^\nu - \partial^\nu A^\mu$ and the four-current is

$$J^\mu = g \sum_{i=1}^{N} \int d\tau_i \delta^{(4)}[x - x_i(\tau_i)] u_i^\mu \quad , \tag{2}$$

with four-velocity $u_i^\mu = dx_i^\mu(\tau_i)/d\tau_i$. We use the Einstein summation convention that repeated covariant and contravariant Greek indices are to be summed over from 0 to 3, with the diagonal metric specified by $g_{\mu\nu} = g^{\mu\nu} = \mathrm{diag}(1, -1, -1, -1)$. The quantity $x^\mu = (t, \boldsymbol{x})$ is the contravariant spacetime four-vector consisting of time t and position $\boldsymbol{x}$, and $\partial^\mu = \partial/\partial x_\mu$ is the contravariant four-gradient. The spacetime trajectory of nucleon i as a function of its proper time τ_i is denoted by $x_i(\tau_i)$.

The covariant equations of motion for the N nucleons that result from the Lagrangian density (1) are[3]

$$M a_i^\mu = g F_{\mathrm{ext}}^{\mu\nu} u_{i\nu} + \frac{2}{3} g^2 \left(\frac{da_i^\mu}{d\tau_i} + u_i^\mu a_i^\nu a_{i\nu} \right) + f_i^\mu \quad , \tag{3}$$

with four-acceleration $a_i^\mu = du_i^\mu(\tau_i)/d\tau_i$. The three contributions to the four-force appearing on the right-hand side of Eq. (3) represent, respectively, the external retarded Lorentz force on nucleon i due to the other nucleons, the radiation reaction, and the self-interaction due to the nonzero meson mass, which is given by

$$f_i^\mu = g^2 m^2 \left[\int_{-\infty}^{\tau_i} d\tau_i' \left(s_i^\mu u_i^\nu - s_i^\nu u_i^\mu \right) \frac{J_2(m s_i)}{{s_i}^2} \right] u_{i\nu} \quad . \tag{4}$$

The four-vector separation is $s_i^\mu = x_i^\mu(\tau_i) - x_i^\mu(\tau_i')$, with interval $s_i = (s_i^\mu s_{i\mu})^{1/2}$, and J_2 is a second-order Bessel function of the first kind. The integration over the particle's past trajectory in Eq. (4) reflects the ability of the particle to catch up with its own earlier disturbance, portions of which travel slower than light because of the nonzero meson mass. The covariant equations of motion for the four-potential A^μ are solved in terms of a retarded Green function.[3]

We convert the differential equations (3), which are numerically unstable in that form, into the integral equations[7]

$$a_i^\mu(\tau_i) = \int_{\tau_i}^{+\infty} d\tau_i' \left[\frac{3}{2g^2} \left(g F_{\mathrm{ext}}^{\mu\nu} u_{i\nu} + f_i^\mu \right) + u_i^\mu a_i^\nu a_{i\nu} \right] \exp\left[-\frac{3M}{2g^2} (\tau_i' - \tau_i) \right] \quad , \tag{5}$$

which satisfy the boundary conditions that a_i^μ are bounded as $\tau_i \to +\infty$. Because the integrations in Eq. (5) are over *future* proper times, we solve these equations iteratively, with the positions and four-velocities that enter determined by use of a finite-difference method.

For the mass of the ω meson we use the new result[8] $m = 782.0$ MeV, which corresponds to a Yukawa interaction range of $a = 0.2523$ fm. For the coupling constant

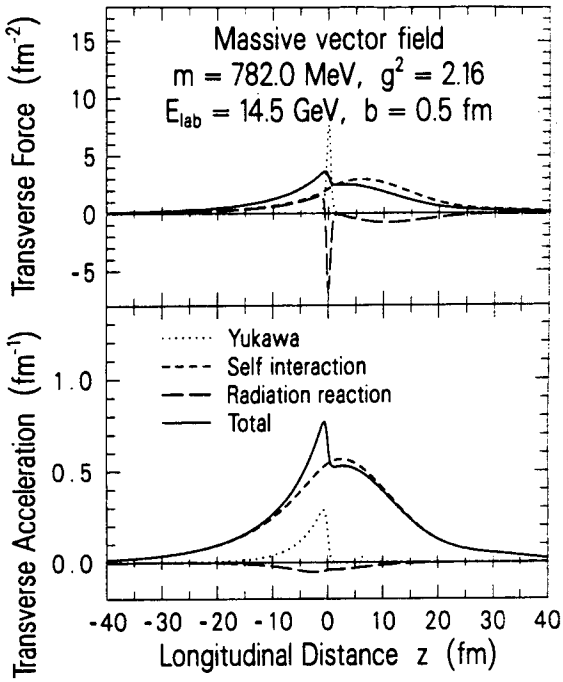

Figure 1. Contributions to the transverse four-force and transverse four-acceleration.

we started with the value $g^2 = 10.81$ that is required to properly saturate symmetric nuclear matter in the mean-field treatment of the relativistic σ-ω model.[4] Because of large nonlinearities associated with both the radiation reaction and the self-interaction, we have thus far been unable to obtain converged solutions corresponding to these values. We have obtained solutions both for a massless vector field with the full value of g^2 and for a massive vector field with a value of g^2 that is 20% of the original value.

Figures 1 and 2 are examples of the latter for a single nucleon incident on a scattering center that remains fixed in the laboratory system. Whereas the Yukawa contribution to the transverse force is a narrow spike near the position of the scattering center, the contributions from the radiation reaction and self-interaction extend over large distances on both sides of the scattering center. On the other hand, the Yukawa contribution to the transverse acceleration extends over a large distance only in front of the scattering center, which can be understood from the integration in Eq. (5) of an exponential times a narrow spike. Because the range of the exponential is proportional to g^2, the extension will be much larger for a realistic value of g^2.

As seen in Fig. 2, both the transverse kinetic energy imparted to the projectile and the radiated energy increase rapidly with decreasing impact parameter. The radiated energy, which is calculated from energy conservation since Larmor's formula does not apply to massive fields, is in the form of ω mesons. Because ω mesons subsequently decay into π^+, π^-, and π^0 with 89.3% probability, into π^0 and γ with 8.0% probability, and into π^+ and π^- with 1.7% probability,[8] our Lagrangian density (1) provides a definite mechanism for the production of pions and photons, or alternatively quark-antiquark pairs and photons. For a realistic value of g^2, both the transverse kinetic

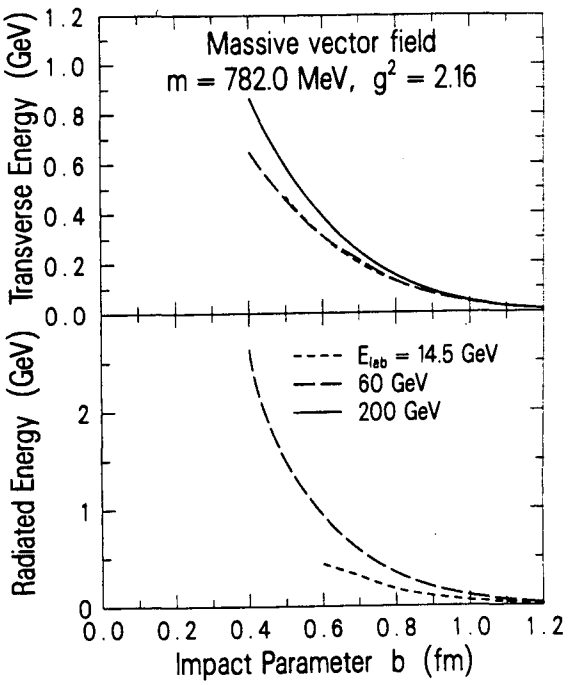

Figure 2. Dependences upon impact parameter of the transverse kinetic energy and total radiated energy.

energy imparted to the projectile and the radiated energy will be larger than that shown in Fig. 2.

In summary, a classical relativistic field theory corresponding to the exchange of vector ω mesons provides a logical approach for studying the effects of relativistic retardation, nonequilibrium phenomena, interactions with correlated clusters of nucleons, and particle production in ultrarelativistic nucleus-nucleus collisions, but some formidable computational difficulties must be overcome before these virtues are realized.

We are grateful to F. H. Harlow for stimulating discussions during the early phases of this investigation. This work was supported by the U. S. Department of Energy.

References

1. H. Yukawa, Proc. Phys. Math. Soc. Japan **17**, 48 (1935).
2. A. Proca, J. Phys. Radium **7**, 347 (1936).
3. H. J. Bhabha, Proc. Roy. Soc. London **A172**, 384 (1939).
4. B. S. Serot and J. D. Walecka, Adv. Nucl. Phys. **16**, 1 (1986).
5. B. Blättel, V. Koch, W. Cassing, and U. Mosel, Phys. Rev. **C38**, 1767 (1988).
6. H. Feldmeier, M. Schönhofen, and M. Cubero, Nucl. Phys. **A495**, 337c (1989).
7. G. N. Plass, Rev. Mod. Phys. **33**, 37 (1961).
8. G. P. Yost *et al.*, Phys. Lett. **204B**, 1 (1988).

Collective Flow at Ultra-relativistic Energies

Espen F. Staubo, Alv K. Holme, László P. Csernai
Physics Department, University of Bergen,
Allègaten 55, N-5007 Bergen, Norway

and

Daniel Strottman
Theoretical Division, Los Alamos National Laboratory
Los Alamos, New Mexico, 87545, USA

AGS and SPS experiments indicate that normalized pseudorapidity distributions of charged secondaries are strongly peaked at mid rapidities for 14.6, 60, and 200 GeV/nucleon O+Ag/Br collisions and do not show any development of a central plateau as shown by the KLM collaboration. The present data from WA-80 and NA-35 also indicate that the stopping of baryons is strong at energies up to 200 GeV/nucleon. At the lower energies (14.5 and 60 GeV) there is evidence for complete stopping in central collisions where no energy is detected around zero degrees in calorimeters.

Thus it is not illogical to attempt a description of these latter two reactions in terms of a one-fluid hydrodynamical model in which there is complete stopping. The of these calculations and experiments is to determine under what conditions a quark-gluon plasma (QGP) is formed in heavy ion collisions. However, all three-dimensional calculations so far have used an equation of state (EOS) without any phase transition. Also, the breakup mechanism of the fluid cells is important if we intend to describe observable quantities, because the random thermal motion of particles is not negligible. The phase transition in baryon-rich matter has been considered only in one dimensional calculations up to now. Thus a clear prediction of the type of fluid-dynamical flow signal does not really exist so far. All *predictions* are based on essentially one-dimensional calculations. The essence of these predictions is that the transverse flow should decrease in the presence of a phase transition in a given energy region. This is due to the fact that the pressure is strongly decreased by the latent heat of the deconfinement phase transition in the mixed phase region.

Equation of State. For our numerical fluid dynamical study we have selected a phenomenological EOS reproducing the characteristic phase diagram of the QGP phase transition [1]. It is composed of a nuclear part which is described by the Sierk-Nix parametrization, a QGP part which is given by the bag model EOS, and a mixed phase which is obtained by Maxwell construction. Nucleons and pions as well as nonstrange quarks and gluons were considered.

The selected EOS has a first order phase transition. The critical temperature at $n = 0$ is $T_c = 216$ MeV, consistent with recent lattice QCD results: $T_c = 177 - 276$ MeV. The energy density increases monotonously with T until T_c is reached where the critical energy density is $e_{cH}(n = 0) = 280$ MeV/fm^3.

The EOS used in the fluid dynamical calculations was tabulated, in 10000 points, giving the pressure and temperature as a function of the baryon density and energy density. For comparison we performed two sets of fluid dynamical calculations with EOS's with and without a phase transition to QGP. The details of the EOS are discussed in ref. [1].

Fluid Dynamical Model. The equations of relativistic perfect fluid dynamics were solved numerically by the PIC method on CRAY-XMP computers in Trondheim and Los Alamos. Here we present results of numerical calculations for ^{32}S+^{208}Pb at 14.5 and 60 GeV/nucleon beam energy. The calculational grid was chosen to have 10 cells along the transverse diameter of the ^{32}S nuclei. The size of the fluid cells at $E_{Lab} = 14.5$ (60) GeV/nucleon was $\Delta z = 0.43$ (0.32) fm,$\Delta x = \Delta y = 0.75$ fm. The number of marker particles per cell was two in the z and three in the transverse directions, so that the total number of marker particles is 18 per cell. The calculations were performed in reference frames that optimized the numerical accuracy (the width of the Lorentz contracted projectile and target were approximately the same in this frame).

The numerical solutions satisfied energy and momentum conservation to machine accuracy of

the CRAY's. Symmetries in symmetric collisions like A+A and in $b = 0$ collisions were maintained in the calculations although they were not explicitly enforced. The results of the calculations for equal mass target and projectile were and stayed completely reflection symmetric about the c.m. point and about the z axis (where the z-axis is chosen along the beam). The symmetries were also reflected by the fact that in exactly central collisions the transverse momentum, $< p^x >$, was zero. The presence of symmetries provides a sensitive test of the numerical procedure.

In the calculations presented here we studied the breakup dependence of the results by choosing several breakup times one after the other. At these breakup times the fluid was frozen out globally everywhere at the same time. The calculation was stopped at around $t = 10 - 15$ fm/c in the calculational frame.

The phase transition to QGP contributes to an appreciable increase of the maximum density and to a longer expansion time. In case of the QGP EOS at energies, 14.5 and 60 GeV/nucleon the average density reached a maximum of 4.3 (9) n_0 at 3.5 (1.6) fm/c, while it dropped below $2n_0$ at 6.7 (8.5) fm/c. The densities reached were higher than in case of a pure hadronic EOS. QGP was formed for a period of about 3.5 (6.5) fm/c with a maximum volume of 13 (40) fm^3. The volume average of the QGP temperature had a maximum value of 205 (265) MeV. At 60 GeV/nucleon with the QGP EOS, where the mixed phase did not decay completely even at 15 fm/c. At this time the calculation has to be stopped because the volume of the expanding matter reached the limits of the maximum possible calculational grid on a CRAY-XMP. The low density, $\approx n_0$, and high temperature, ≈ 210 MeV, mixed phase domains persisted for a long time because the pressure in this state is extremely low, ≈ 100 MeV/fm^3 (see ref. [1]). By this time the spectator and participant regions were completely separated.

At 14.5 GeV/nucleon the mixed phase domains decayed smoothly because their temperature stayed considerably below 210 MeV, and so the pressure was large enough [1] to maintain a rapid expansion.

Measurables. We can calculate the baryon and pion distributions, assuming a thermal emission at the breakup inside each cell. This is consistent with our EOS where thermal pions were also considered. We also assume that the pion chemical potential vanishes, in accordance with the one fluid model where local thermodynamical equilibrium is assumed for all particles.

At the breakup the local pion momentum distribution at a space-time point x is assumed to be a relativistic Bose distribution: $f_\pi(x, p; U^\mu, T)$, while baryons followed a Jüttner distribution. The pions are emitted in their own local rest frame (LR), and their number is proportional to this volume V_{LR} as well as to T^3. At the breakup each fluid cell is moving with the velocity $U^\mu = \gamma(1, \beta_{||}, \beta_\perp) = \gamma_\perp(\cosh(y_0), \sinh(y_0), v_\perp)$, where y_0 is the rapidity of the fluid cell and the other variables provide the usual decomposition of the four velocity.

At 60 GeV/nucleon the phase transition to QGP yields a total pion multiplicity of 245, while the hadronic EOS yields about 235 at 10 fm/c breakup time. Earlier breakup times yield a higher pion multiplicity for the hadronic EOS, but in case of the plasma the mixed phase is still decaying at this time and the pion multiplicity is still increasing. At this time the "breakup" densities are still 1.5 (1.3) n_0 for the QGP (hadronic) EOS. At this energy the decay of the mixed phase still continues at 15 fm/c, and by then the pion multiplicity increases to 300.

The breakup probably depends on the temperature also. The pion multiplicity is proportional to T^3 and so it is extremely sensitive to the breakup condition. Also, the number of fluid cells filled with matter is important: a dilute system corresponds to a larger source volume. Furthermore, if the dilute system is also expanding faster the local rest (LR) volume of the pion source, $V_{(LR)} = \gamma V_{cell}$, is further enhanced. Due to these competing mechanisms and to the long lifetime of the mixed phase at higher energies, it is not possible to draw a unique conclusion regarding how the phase transition affects the pion multiplicities quantitatively. Breakup conditions play an essential role in determining pion multiplicities, and these conditions are outside the predictive power of fluid dynamics.

Pion and baryon observables were evaluated from the model at different breakup times. The contribution of a fluid cell to the final pion or baryon rapidity distribution was defined as:

$$\frac{dN_{\ cell}}{dy} = \gamma V_{cell} \int \frac{d^3p}{p^0} \frac{d}{dy} \left(p^\mu U_\mu f(x,p) \right). \tag{1}$$

The final rapidity distribution is then obtained by summing up the contributions from all the fluid

cells. For pions only the *hot* cells, $T >$ 15 MeV, were taken into account. For central symmetric collisions the width of the pion rapidity distribution calculated in this model agrees with the prediction of the Landau model and with experiments in the 10 - 60 GeV/nucleon energy range.

The calculated dN_π/dy functions for an $S + Pb$ reaction at 14.5 GeV/nucleon beam energy are shown in ref. [2].

For this reaction at the energy of 60 GeV/nucleon, the rapidity distribution at 10 fm/c the peaks at $y = 2.0$ (1.4) for QGP (hadronic) EOS, The smaller pressure in the plasma case leads to a much sharper cut between participants and spectators, and consequently to less participants from the target. This causes the much higher peak rapidity for QGP. At 10 fm/c the peak of rapidity distribution is still strongly increasing, while for hadronic matter EOS it is slightly decreasing.

The participant peak of baryon rapidity distribution shows the same behaviour. The normalization of the cold target peak indicates that the shift of the participant rapidity is due to the smaller (QGP) or larger (Hadronic EOS) target participation (Fig. 1).

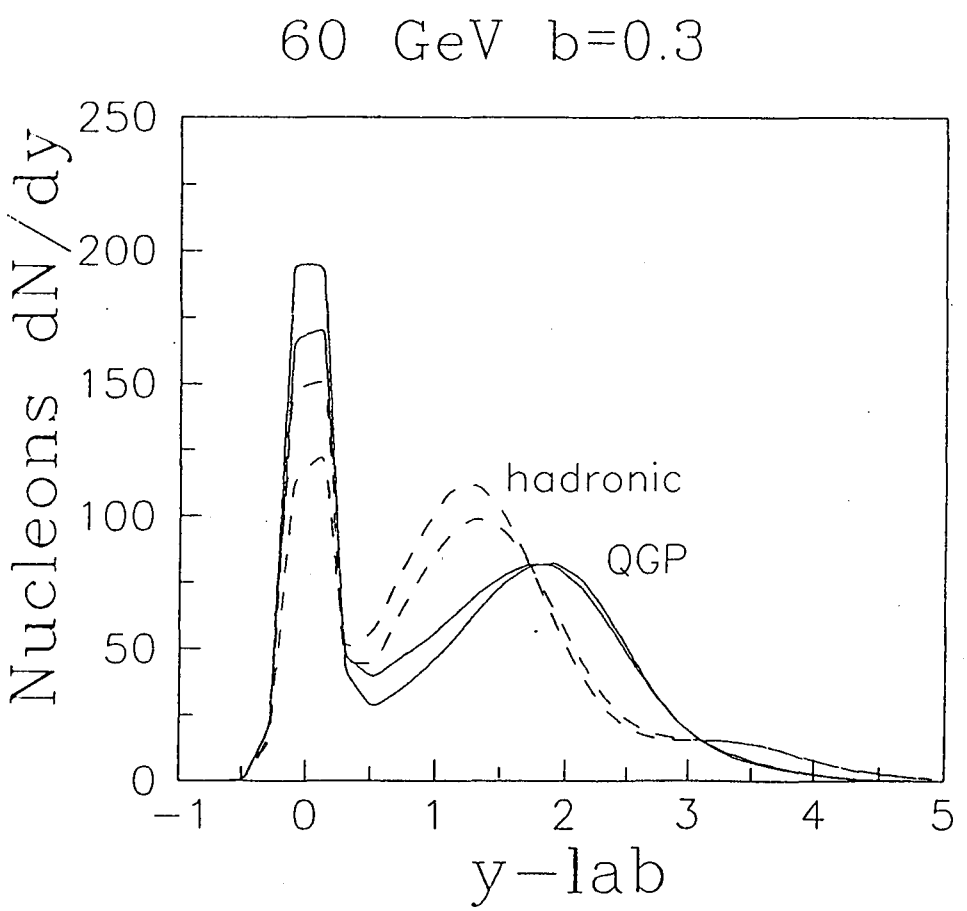

The total baryon rapidity distribution dN_B/dy from the relativistic three – dimensional one – fluid dynamical model for the reaction S+Pb at E_{Lab} = 60 GeV/nucleon, at impact parameter $b = 0.3(R_p + R_t)$. The breakup times are 7.6 and 10 fm/c. QGP (hadronic) EOS's are indicated by full (dashed) lines. Increasing breakup times yield more particles at mid rapidity. With the QGP EOS the participants are less but they move with higher rapidity.

A consequence of these results is that pion azimuthal correlations are unlikely to be observed at ultra-relativistic energies because $p_\perp \gg p^x$, so thermal fluctuations and limited statistics will wash out the signs of the small transverse flow projected to the reaction plane.

Following the same basic lines as presented by Ruuskanen earlier the pion transverse momentum distribution arising from a fluid cell can also be evaluated. After a straightforward calculation we

arrive at the result

$$\frac{dN_{\pi,cell}}{p_\perp\, dp_\perp} = \frac{\gamma V_{cell} g_\pi\, T}{(2\pi\hbar)^3} \sum_{j=1}^{\infty} [aK_1(ja)I_0(jb) - bK_0(ja)I_1(jb)], \tag{2}$$

where $a = \gamma_\perp m_\perp/T$, and $b = \gamma_\perp v_\perp p_\perp/T$. The resulting spectra are shown in ref. [2]. There is a clear deviation from the straight exponential shape in all cases. The formation of QGP decreases both the temperature and the transverse flow so the $p_\perp$ spectra are steeper. The observable effective temperature or slope parameter is higher than the average temperature of the fluid cells at the same time.

The important feature is that the spectrum shows a concave shape which is a consequence of the collective expansion. This shape, (also seen in several experiments, is connected to transverse radial flow as pointed out by Atwater, Freier, and Kapusta using a model with idealized cylindrical geometry. The fact that the same shape can be obtained from a one-fluid dynamical calculation shows that the concave shaped $p_\perp$ spectrum is a consequence of the collective flow but it is not necessarily related to complete transparency and the Bjorken scaling expansion. In our calculations the spectra with hadronic EOS are more concave indicating a larger transverse flow. The QGP causes a reduced flow in the transverse direction and a broader width in the longitudinal direction. This can be explained by the fact that the QGP is much softer, leading to a more compressed and flat shape before the expansion of the matter starts. Then the expansion starts dominantly in the beam direction due to the larger pressure gradients in this direction. At the same time the transverse flow is reduced.

Summary. Thus in the stopping energy region, which is expected to include the phase transition threshold, one can make use of a phenomenological EOS if the matter is not too far from local thermal equilibrium. The one-fluid dynamical model as one extreme, assuming local thermalization, yields a flow pattern depending on the EOS.

The fact that the width of the pion rapidity distribution of O+Ag/Br reactions is reproduced by the model at 14.5 GeV /nucleon energy [3] suggests that models assuming strong or complete stopping may be used to describe the dynamics of nuclear collisions in the $10 - 60$ GeV/nucleon energy range.

With a phenomenological EOS describing the phase transition to QGP in a $S + Pb$ collision at 60 GeV/nucleon a QGP was created in a volume which reached 18% of the rest volume of the projectile. For a period of 2 fm/c the plasma occupied more than 10% of the initial nuclear volume. At 14.5 GeV/nucleon pure plasma was created in a small volume only, (max. 6% of the projectile), and it existed for a very short time. Thus, the modification of the flow pattern was caused by the mixed phase mainly.

The main effects of the QGP formation are increased longitudinal and reduced transverse flow. At 60 GeV/nucleon these effects are stronger, while at the lower energy the small amount of the plasma produced and the uncertainties in breakup time make it difficult to observe a clear change in the flow experimentally.

Acknowledgement. This work was supported by the US National Science Foundation, and the Norwegian Research Council (NAVF).

References

[1] A. K. Holme, E. F. Staubo, L. P. Csernai, E. Osnes and D. Strottman,Phys. Rev. **D 40** (1989) 3735.

[2] E. F. Staubo, A. K. Holme, L. P. Csernai, M. Gong and D. Strottman, Phys. Lett. **B 229** (1989) 351.

[3] L. P. Csernai, M. Gong and D. Strottman, Nucl. Phys. **A 495** (1989) 403c.

High Energy Gamma-Ray Production in Heavy Ion Collisions

James E. Clayton
National Superconducting Cyclotron Laboratory and
Department of Physics and Astrononmy, Michigan State University
East Lansing Michigan 48824

High energy gamma-ray production from heavy ion collisions has been studied extensivly by many groups in the last six years.[1-6] The discovery of these photons created much excitement as a new probe of the reaction dynamics in heavy ion collisions. The earliest explanation of these high energy gamma-rays came from Vasak, Muller and Greiner[5] who attributed the photons to coherent bremsstrahlung. The mechanism was thought to be coherent since the wavelength of the emitted photon was long compared to the dimensions of the colliding nuclei. The predictions of coherent bremsstrahlung are that in the emitting frame, namely the nucleus-nucleus center-of-mass frame, the angular distribution is quadrupolar, and that the production cross section would be proportional to the square of the total charge for the colliding system. However, in all the subsequent measurements the data could be explained by incoherent neutron-proton bremsstrahlung. In this model it is the individual neutron-proton collisions in the reaction that give rise to the high energy gamma-rays. Proton-proton collisions, which would also be quadrupolar in the emitting frame, are reduced by about 25% relative to the neutron-proton yield.

First, we report on results from an experiment[7] performed at Lawrence Berkeley Laboratories to search for coherent bremsstrahlung with a high-mass projectile and target. A natural self supporting Sn foil was irradiated with a ^{136}Xe beam from the Bevalac at incident beam energies of E/A= 89 and 124 MeV respectivily. The high gamma-rays were detected in a plastic Cerenkov detector. We detected photons from 30 MeV up to 160 MeV in the laboratory. For both beam energies measurements were made at angles of 30°,60°,90,^{o}120°, and 150° in the laboratory. The data taken at E/A= 89 MeV also included measurements at 45°, 75°,105°,and 135°. The increased number of points at E/A=89 MeV ensured that the angular distribution was accurate enough to observe a possible quadrupole contribution to the angular distribution. Since the data at both energies were taken with the same target and projectile the energy dependence for heavy systems could be examined.

A systematic analysis was performed to extract various quantities of interest such as slope parameters and the angular dependence in the emitting frame. A least-squares fit to the data was made with a moving source model which allowed the normalization, slope parameter, strength of the dipole component, and the source velocity β to be free parameters. The exact details of the fitting procedure is given in Ref 7. Figure 1 shows the angular distribution in the nucleon-nucleon center-of-mass system; the line is an isotropic fit to the data. The data sets are consistent with isotropic emission from a source moving with the nucleon-nucleon center-of-mass velocity. We find no significant signature for coherent emission of gamma-rays in heavy ion collisions at these incident energies.

The second subject that we will address is a recent prediction by Prakash et al.[8] regarding the influence of the delta isobar degree of freedom in high energy gamma-ray production. Using a thermal model Prakash et al. studied the

impact parameter dependence of high energy gamma-ray production. They chose to use detailed balance and make the prediction regarding high energy gamma-ray production based on photo-absorption cross sections. They felt that this approach did not suffer from the long wavelength approximation used by other models in the prediction for bremsstrahlung gamma-rays from heavy ion collisions. The photo-absorption cross section can be separated into three regions:

1. $E_\gamma < 40$ MeV: Here the dominant mechanism is the giant dipole resonance.
2. $40 < E_\gamma < 140$ MeV In this region photo-absorption is dominated by the formation of the quasi-deutron. This process is the inverse of incoherent neutron-proton bremsstrahlung.
3. In the region of photon energies $140 < E_\gamma < 500$ MeV the absorption cross section is dominated by the excitation to the first excited state of the nucleon, the $\Delta(1232)$ resonance.

Using the photo-absorption cross sections and detailed balance in their thermal model, Prakash et al. found that in the region above 140 MeV the cross section for gamma-ray emission would be enhanced by a factor of 5-10 times the yield from incoherent bremsstrahlung.

This prediction was investigated with the K-1200 Cyclotron at Michigan State University. We studied the gamma-ray emission in the reaction ^{14}N + Zn at E/A=75 MeV with a 5" x 9" BaF_2crystal placed 75 cm from the target. Neutrons and charged particles were elimanated by a combination of three methods. The major background reduction came from the gate on the time of flight versus energy spectrum. We also placed a 20 cm nylon bar in front of the crystal to reduce the background from the target. Muons and charged particles were further reduced by a plastic scintillator anticoincidence shield that surrounded the detector. We used the energy loss from cosmic rays to calibrate the detector full scale energy. Comparing the energy loss from the cosmic ray data to tagged photon data from the Saskatchewan Accelerator Laboratory we found that the muon energy loss corresponds approximately to an 83 MeV gamma-ray. With this information we conclude that the full scale for our measurement is about 180 MeV. The spectra that we measured for the reaction ^{14}N + Zn at E/A= 75 MeV is shown in Fig. 2, and one can observe that there is no significant enhancement in the gamma-ray spectra in the region above 140 MeV. The data can be explained in the framework of incoherent neutron-proton bremsstrahlung.

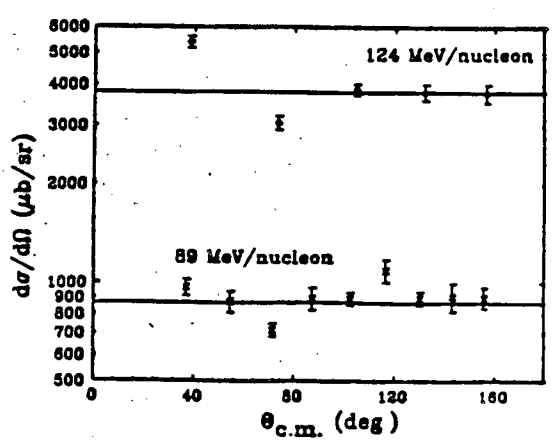

FIG. 1. The angular distribution for gamma rays with $E_\gamma \geq 50$ MeV in the nucleon-nucleon center-of-mass frame. The straight lines are based on fits to a simple isotropic moving source model to the data at all measured angles as described in the text.

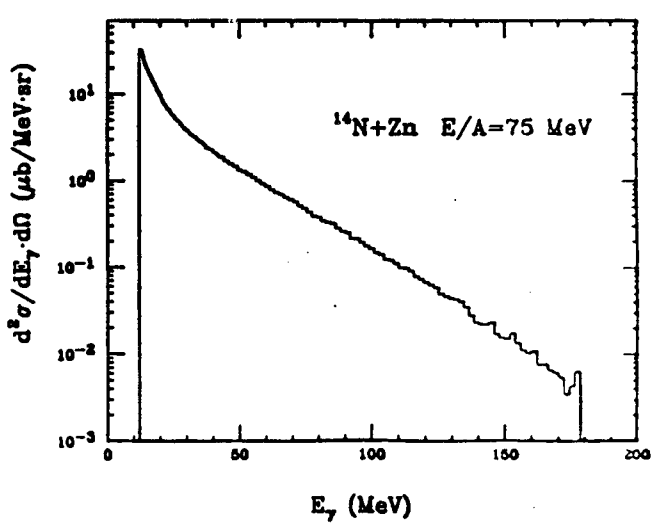

FIG. 2: The measured energy spectrum for high-energy gamma rays from the heavy-ion reaction $^{14}N+Zn$ at E/A=75 MeV.

In order to compare the systematics of all the various target and projectile systems measured to date Nifenecker and Bondorf[9] proposed a model based on the number of first neutron proton collisions. In this first collision hypothesis, the total gamma-ray cross section is given by a simple relation, $\sigma_\gamma = \sigma_r \langle N_{np} \rangle P_\gamma$, where $\langle N_{np} \rangle$ is the impact parameter-averaged number of first neutron-proton collisions. The total reaction cross section σ_r is given by the geometrical cross section, and P_γ is the probability of gamma-ray emission in a neutron-proton collision. With this scaling, a comparison between data sets can be made, and the results are shown in Fig. 3. Here the probability for gamma-ray emission above 50 MeV in the laboratory is plotted against the Coulomb corrected incident beam energy. The values for ^{136}Xe + Sn at both beam energies and the ^{14}N + Zn are plotted along with all the other data measured to date. The systematics are such that a smooth curve could be drawn through all the data points, and the trend is that the bremsstrahlung probablilty increases as the incident beam energy increases. A plot of the cross section for subthreshold pion production shows a similar dependence on the incident beam energy.

The final subject we wish to address at this meeting is the Proton + Nucleus measurements of Edgington and Rose[10] made in the 1960's. They studied bremsstrahlung from proton nucleus collisions at E=140 MeV. The measurements were made with large lead glass detector, and they looked at bremsstrahlung from targets as light as deuterium to as heavy as Pb. The first indication that there may be a problem with this data set came in 1988 when Kwato Njock et al.[11] made a measurment of proton-nucleus bremsstrahlung at 72 MeV. They found that the total cross section measured by Edgington and Rose was low compared to their value by a factor 2-3. Later Pinston et al.[12] made a similar measurement at E=168 and 200 MeV and found similar results to the E=72 MeV data.

We proposed to check the validity of the two measurements by studying proton + nucleus bremsstrahlung reactions at incident energies of 104, 145 and 195 MeV on targets of C, Zn, Pb, CD_2. The measurements were made with two 5"x9" BaF_2 crystals at angles of 45°, 60°, 90°, 120°, and 135° in the laboratory. The result for the comparison to the data of Edgington and Rose is shown in Fig. 4 for the data at E=145 MeV. Although this analysis is in the preliminary stages, we can conclude that there is discrepancy regarding the magnitude of the cross section measured by Edgington and Rose. We have compared the total cross section for gamma-rays above 40 MeV in the nucleon-nulceon center-of-mass and find a result roughly 2-3 times greater than the value reported by Edgington and Rose. This is consistant with the measurements by Kwato Njock[12] and Pinston.[13] In the measurement of the system P + CD_2 we hope to be able to extract the P + deutron bremsstrahlung cross section at incident proton energies of 145 and 195 MeV. We can do this by subtracting out the C contribution to the spectra by normalizing the two spectra via the 15.1 MeV gamma ray transition in C. The CD_2 spectra is also shown in Fig. 4 (it is multiplied by a factor of 100 for display purposes).

In summary we have made a series of measurements in search of interesting predictions regarding high energy gamma-ray production. We found no evidence for coherent bremsstrahlung from very heavy systems. Instead the data could be described within the framework of incoherent neutron-proton bremsstrahlung. The search for the enhancement of the photon yield from direct decays of the Δ resonance was unsuccessful. We found no compelling evidence the direct photons arising from Δ decay was the dominant production mechanism at E/A=75 MeV. However, it may be that we must go to higher energies in order to see the effect. Recent calculations by Bauer et al.[14] predict that it maybe possible to observe the photons from Δ decay at incident energies near E/A 200 MeV. Finally we have performed a measurement to check the data of Edgington and Rose and we confirm that the discrepancy reported by Pinston and Kwato Njock is correct.

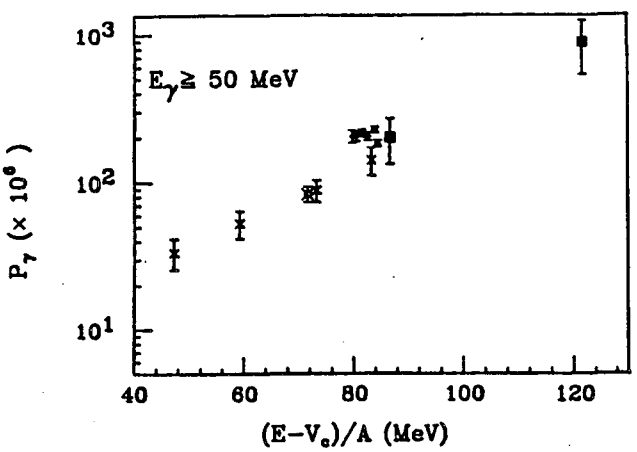

FIG. 3: Plot of probability of gamma ray emission P_γ, from (1) for gamma rays with $E_\gamma \geq 50$ MeV in the laboratory versus the Coulomb corrected bombarding energy. The open circle is the present data. Other values are from Ref. 1, solid diamonds, Ref. 4, crosses; Ref. 7, solid squares.

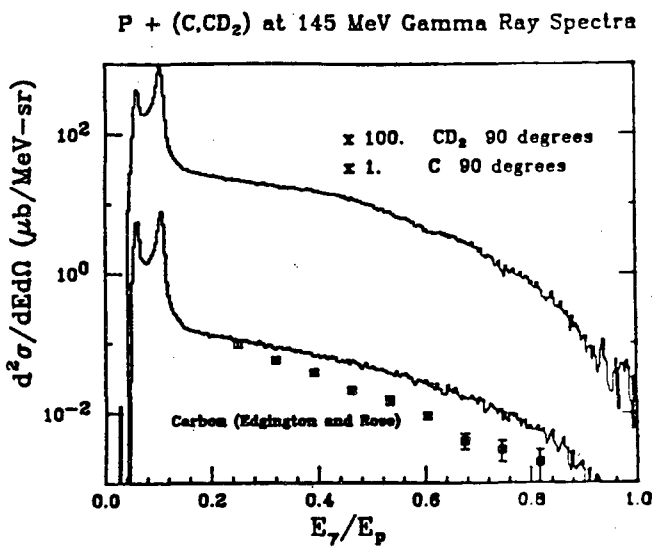

Fig 4. The measured energy spectra for high energy gamma-ray emission from p + (C,CD$_2$). The carbon spectra is also compared to the proton data of Edgington and Rose.

REFERENCES

1. J. Stevenson et al., Phys Rev. Lett.57, 555 (1986).
2. M. Kwato Njock et al., Phys Lett.175B, 125 (1986).
3. N. Alamanos et al., Phys. Rev. Lett.173B, 392 (1986).
4. E. Grosse et al., Europhys. Lett.2, 9 (1986).
5. D. Vasak et al., J. Phys. G 11, 1309 (1985).
6. W. Bauer et al., Nucl. Phys. A456, 159 (1986.)
7. J. Clayton et al., Phys. Rev. C40, 1207 (1989.)
8. M. Prakash et al., Phys. Rev. C37, 1959 (1988).
9. H. Nifenecker et al, Nucl. Phys. A442, 478 (1985)
10. J.A. Edgington, and B. Rose Nuc. Phys. A89, 523 (1966).
11. M. Kwato Njock et al., Nucl. Phys. A489, 368 (1988)
12. M. Kwato Njock et al., Phys. Lett B207, 269 (1988).
13. J.A. Pinston et al., Phys. Lett. B218, 128 (1989).
14 W. Bauer et al., Phys. Lett. B229, 16 (1989).

Production of e^+e^- Pairs at the Bevalac

Howard. S. Matis
Lawrence Berkeley Laboratory, University of California, Berkeley, CA 94720 U.S.A.

(for the DLS collaboration)

During the last several years, the Dilepton Spectrometer (DLS) collaboration[1,2,3,4,5] has studied the production of dileptons in both proton-nucleus collisions and nucleus-nucleus collisions. This paper summaries the results of previous publications and provides a preliminary glimpse of some new data.

When nuclei collide, a hot hadronic fireball is created. From this fireball, hadrons and real and virtual photons are produced. Hadrons, which are created in the the center of the fireball such as pions and protons, will then rescatter or annihilate with the fireball. These hadrons will strongly react as they pass through the fireball until they leave the surface. Therefore, we can say that these hadronic processes generally probe the surface of a nuclear collision. Moreover, when a virtual photon is produced in the interior of a fireball, it will decay into a lepton pair. Both the virtual photon and the lepton pair only interact weakly with the quarks and gluons of the fireball, so that for all purposes they are unaffected after their production. Consequently, measurement of the virtual photon will provide a direct measurement of the interior of a nucleus-nucleus collision. As the electromagnetic decay of a virtual photon is well known, calculations are much easier for dileptons compared to hadron production. Virtual photon production should be much better understood than hadrons and should be a superior probe of hot hadronic matter.

Furthermore, much current theoretical work has shown that dileptons can be a signal for the production of the quark-gluon plasma. If quark deconfinement occurs, then effects such as the changing of the width or position of the ρ meson could happen. In addition to these processes, the rate of production of the continuum could increase. However, processes such as pion annihilation, which could occur at Bevalac energies, could obscure a signature of the quark-gluon plasma. Consequently, one must understand the low energy behavior of dileptons before any claim for the detection of a phase transition can be made in the dilepton channel.

There is much unknown about dileptons. The low mass behavior of pairs are not understood very well. The mass and p_t behavior of dileptons seems to be universal from experiments with 12 GeV proton beams to those done at ISR energies. However, there appears to be an excess of events at low mass. Before the DLS, there was no pair data below 12 GeV and the heaviest projectile that was used to produce a pair was a proton.

Recently, there has been considerable theoretical interest in dilepton production. Goldman[6] *et al.* and Gale and Kapusta[7] have studied the process of pion annihilation. Gale and Kapusta have shown that in a static calculation, dilepton production is sensitive to the interior density of a nucleus-nucleus collision. Furthermore, they demonstrated that the measurement of dileptons produced by pion-pion annihilations should give information on the pion dispersion relationship in nuclear matter. This calculation has been extended to a dynamical model[8] by Xia *et al.*

---

[1]G. Roche *et al.*, Phys. Rev. Lett., **61**,1069 (1988).

[2]C. Naudet *et al.*, Phys Rev. Lett., **62**, 2652 (1989).

[3]A. Letessier-Selvon *et al.*, Phys. Rev. **C40**, 1513 (1989).

[4]G. Roche *et al.*, Phys. Lett. **B226**, 228 (1989).

[5]H. S. Matis, contribution to the *Winter Workshop on Nuclear Dynamics V*, LBL-25019 (1988).

[6]T. Goldman *et al.*, Phys. Rev. **D20**, 619 (1979).

[7]C. Gale and J. Kapusta, Phys. Rev. **C35**, 2107 (1987) .

[8]L. H. Xia *et al.*, Nucl. Phys **A485**, 721 (1988).

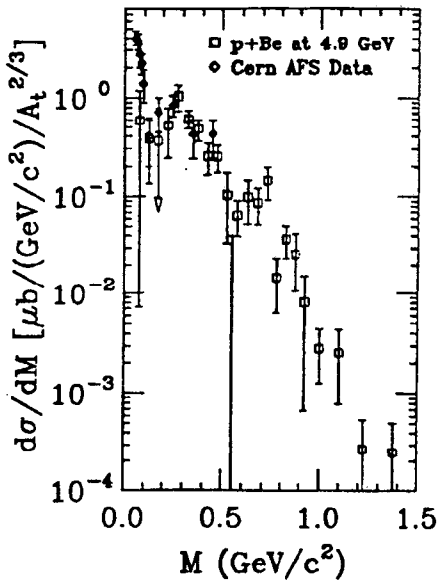

Fig. 2. The DLS 4.9 GeV and CERN e^+e^- data plotted together. The ISR data was normalized to the DLS data.

The integrated cross section is shown in Fig. 3. Note, that the Dalitz contributions to the total cross section *are not* subtracted from these data points and may affect the magnitude of the 1 GeV data. Also, shown on that figure are arbitrary scaled one and two pion cross section production curves. The shape of the one pion cross section curve is much flatter than the data while the shape of the two pion cross section curve resembles our data much better.

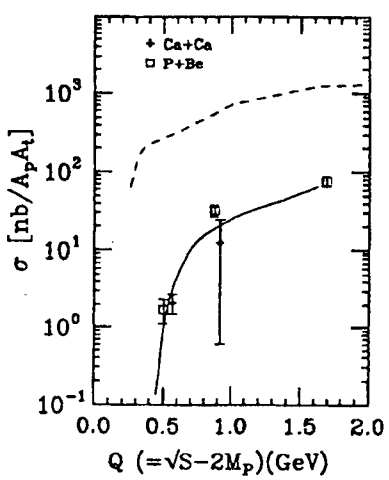

Fig. 3. Total cross section for DLS data. The upper curve is the scaled one pion cross section curve; while the lower curve is the scaled two pion cross section.

Our dilepton data are measured in three variables, m, y, and p_t. For convenience we integrate over y and have two dimensional data. To compare a calculation to our data, it is most appropriate to fit to this two dimensional data. Fig. 4 shows a simple fit with the phenomenological KSS model. Note, that even though the data is two dimensional, we only show

To measure dileptons, our collaboration has designed a two-arm spectrometer to detect electron pairs. Electrons were chosen because it is feasible, at Bevalac energies, to separate them from pions at better than 10^5 with Cerenkov counters. The apparatus used in this experiment has been described in a recent publication.[9]

Fig. 1. shows the mass spectra at several energies measured by the DLS in p-Be collisions. Shown in that figure is a calculation of the dileptons produced by Dalitz decay. From these data, one can clearly conclude that direct dileptons have been detected at 2.1 and 4.9 GeV. As Dalitz decay is appreciable for the 1.0 GeV data, direct dilepton production (production other than by Dalitz decays) can not confidently be claimed. The major uncertainty in the Dalitz calculation is the knowledge of the π^0 cross section at 1.0 GeV.

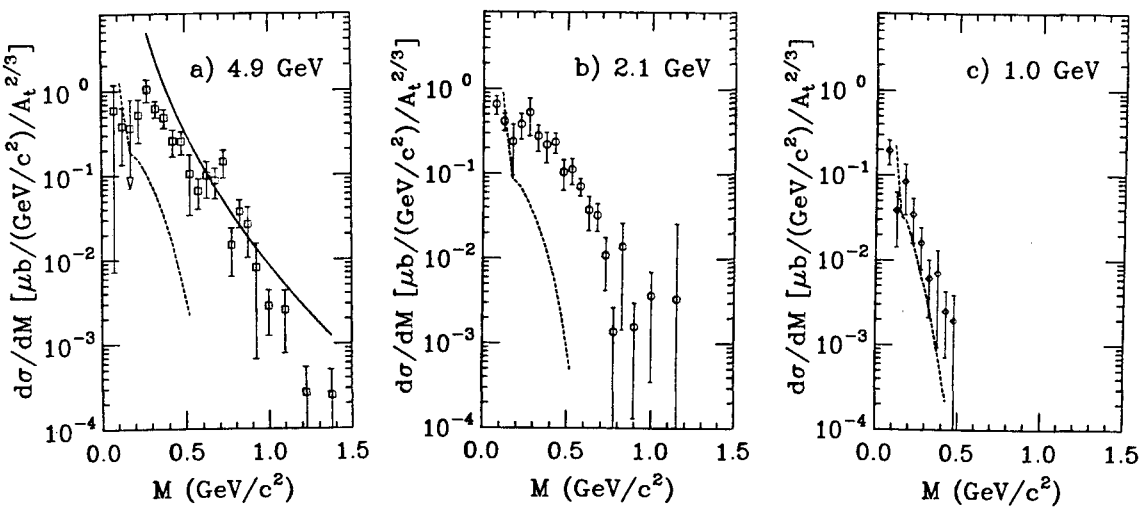

Fig. 1. Invariant Cross section for p-Be collisions at 4.9, 2.1 and 1.0 GeV. The dashed line shows the calculated background due to Dalitz decay of pions and other mesons; while the solid line shows a fit to 12 GeV KEK data.

An enhancement around the ρ mass can be seen in the 4.9 GeV data. The shape of the mass distribution is remarkably similar to those measured at much higher energies as shown by the solid curve. The contribution below 100 MeV is probably due to Dalitz decays. Because of uncertainty with the measured pion production cross section, it is not possible to separate the hadron-bremsstrahlung cross section in this region.

A rise in the cross section at about 300 MeV is observed in both the 2.1 and 4.9 GeV p-Be data. Pion annihilation in nuclear matter can produce such a behavior. However, Kapusta and Lichard[10] have recently shown that their model cannot explain this structure. Fig. 2 shows that e^+e^- data[11] taken at the ISR has a similar dependence. Also, the DLS acceptance and the unlike sign background are smooth in this region and appear unlikely to produce a bump in the data. We are currently doing a careful study of our detector performance to further rule out any instrumental effect.

---

[9] A. Yegneswaran *et al.*, to be published in Nucl. Instr. Meth., (1990).

[10] J. Kapusta and P. Lichard, Phys Rev. **C40**, R1574 (1989).

[11] V. Hedberg, Ph. D. Thesis, LUNDFD6/(NFFL-7037) (1987); W. Willis, Nucl. Phys. **A478,** 151c (1988).

the fit in the m and p_t projection. The KSS[12] model is fit with the DLS acceptance filter. Note, that the KSS model deviates significantly from the region where the structure is observed. We have found models in which the mass spectrum is fit well and yet the model fails to reproduce the p_t spectrum. Therefore, all comparisons should be made with both the mass and p_t data.

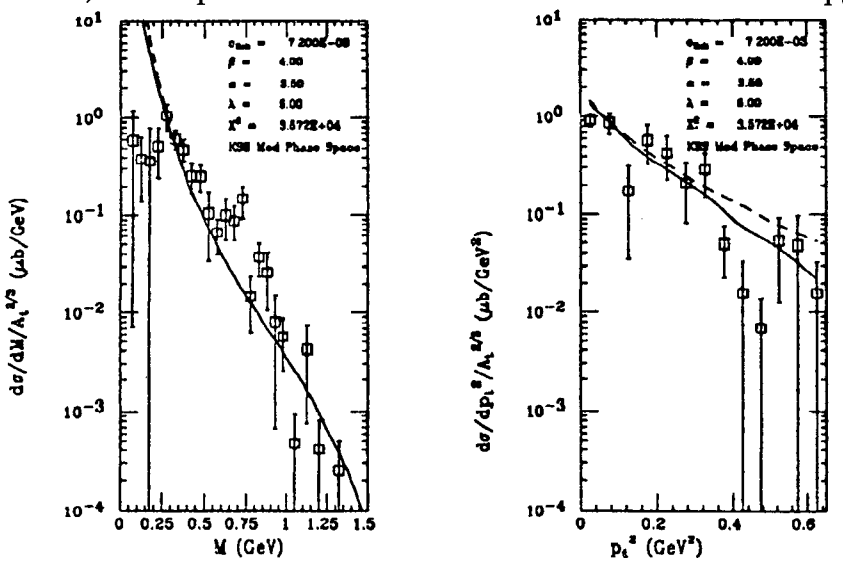

Fig. 4. A simultaneous fit using the KSS model to the 4.9 GeV data. The solid line shows the curve that was used to do the fit. The dashed curve shows the fit without the DLS acceptance filter included.

Our previous publications have shown the results of the Ca-Ca collisions at 1.0 and 2.1 GeV/n. For both energies, there is a significant direct dilepton signal. Because of low statistics, it is not possible to conclude whether there is a structure at 2.1 GeV/n. Plotted in Fig. 3 is the measured total cross sections scaled by A_pA_t for the Ca data points. In order to account for Fermi momentum inside the nucleus, Q, the maximum energy available to make a pair, is calculated with the average value of the Fermi momentum. Note, that in a more realistic calculation it would be necessary to weight the average value of Q with the shape of the total cross section. From this total cross section plot, it appears that the scaling from p-Be to Ca-Ca is approximately A_pA_t.

A test run has recently been made with Nb-Nb at 1.0 GeV/n. At an early stage of analysis, there appears to be a direct dilepton signal. However, careful checks must be made such as examining the reconstruction at high pion multiplicities. Analysis of this data is proceeding so that our experiment will be able to make quantitative statements.

In summary, direct dileptons have been definitely measured for p-Be collisions at energies of 2.1 and 4.9 GeV. The shape of the distributions, above 300 Mev, are similar to that measured at higher energies. The excitation curve for the total cross sections follows the same as the one found for $pp \rightarrow \pi\pi x$. There exists a structure at a mass of about $2m_\pi$ whose origin is unexplained. In addition, direct pairs have been observed for Ca-Ca collisions at both 1.0 and 2.1 GeV/n. The scaling from p-Be to Ca-Ca is roughly A_pA_t. Preliminary results show that there is a measurable cross section at 1.0 GeV/n for Nb-Nb collisions.

In preparing this paper, I would like to thank my colleagues of the present DLS collaboration: G. Krebs, A. Letessier-Selvon, C. Naudet, J. Panetta, L. Schroeder, and P. Seidl (LBL); P. Kirk and Z. F. Wang (LSU); S. Beedoe, J. Carroll, J. Gordon and G. Igo (UCLA); T. Hallman, L. Madansky and R. Welsh (Johns Hopkins); D. Miller and A. Yegneswaran (Northwestern); and P. Force and G. Roche (Clermont II). This work was supported by the Director, Office of Energy Research, Office of High Energy and Nuclear Physics, Division of Nuclear Physics of the U.S. Department of Energy under Contract DE-AC03-76SF00098.

---

[12]K. Kinoshita *et al.*, Phys. Rev. **D17**, 1834 (1978).

DILEPTON PRODUCTION THEORY

Joseph Kapusta
School of Physics and Astronomy
University of Minnesota
Minneapolis, MN 55455

Bitnet: FVS6269@UMNACVX

Whenever charged particles collide they radiate real and virtual photons, the virtual ones decaying into lepton pairs. The advantage of observing electromagnetic signals from a strongly interacting many-body system is that they travel relatively unscathed from the production point to the detector. Since production rates are rapidly increasing functions of temperature and density these electromagnetic signals are good probes of the early high temperature and density stage of heavy ion collisions. The purpose of this talk is to provide an exploratory study[1] of electron-positron radiation from finite temperature and density nuclear matter, and to make some corresponding comparisons with the p(4.9 GeV) + Be measurements of the DLS group[2].

In the nuclear many-body environment there will be a profusion of micro-processes leading to dilepton production. Let us focus on just two of them. At Bevalac, SIS and AGS energies the nuclei essentially stop in the center of mass frame leading to a compression of baryon density. Among baryon-baryon scatterings np will be the most important for radiation, since pp contributions are suppressed in the dipole limit, and nn can only contribute via magnetic dipole couplings. At temperatures of order 100 MeV pions are rather abundant. Annihilations of π^+ with π^- into e^+e^- will be another important contribution. For very high temperatures relevant to the formation of quark-gluon plasma, quark-antiquark annihilation into dileptons has long been considered a possible probe. However, in a heavy ion collision the quarks and gluons must eventually hadronize, primarily into pions, and these pions can annihilate to provide a background to the quark-antiquark annihilations. At the energies relevant to the accelerators mentioned above, quark-gluon plasma formation is not expected. Then pion annihilations are actually a process of primary interest, not a background, since these annihilations may yield information on the properties of pions in the hot and dense system.

A first estimate of thermal rates is based on relativistic kinetic theory. The rate for the reaction a + b to produce a dilepton pair plus anything else is

$$\frac{dR_{ab}^{e^+e^-}}{dM^2} = \int \frac{d^3k_1}{(2\pi)^3} \; f_a(\vec{k}_1) \int \frac{d^3k_2}{(2\pi)^3} \; f_b(\vec{k}_2) \; \frac{d\sigma_{ab}^{e^+e^-}}{dM^2} \; v_{rel}$$

where the f's are the momentum distributions, v_{rel} is essentially the relative velocity of a and b, and the elementary cross section to produce a pair of mass M must be known. The rate has the dimensions of number of such reactions per unit time per unit volume per unit invariant mass. As an example, if we use thermal momentum distributions then we get the rates as shown in figure 1. We see that two-pion annihilation dominates np bremsstrahlung for masses exceeding the two-pion threshhold.

The rate for two-pion annihilation is proportional to the square of the pion number density and so informs us of the number of pions produced when nuclear matter is very hot and dense. This number may very well be different than the number of pions observed asymptotically in the detectors. In addition it is expected that the pion dispersion relation is softened in nuclear matter. The

energy of the pion may even have a local minimum at nonzero momentum due to p-wave attraction to nucleons (delta resonance) and this could drastically alter the pion annihilation rate into dileptons. The rate for pion annihilation into dileptons with zero total momentum (back-to-back) in the nuclear matter frame, including a modified pion dispersion relation $\omega = \omega(k)$, is

$$\left.\frac{dR^{e^+e^-}_{\pi\pi}}{d^3q\,dM}\right|_{\vec{q}=0} = \frac{\alpha^2}{3(2\pi)^4}\frac{|F_\pi(M)|^2}{(e^{\omega/T}-1)^2}\sum_{\substack{k\\ \text{such that}\\ 2\omega(k)=M}}\left(\frac{k}{\omega}\right)^4\left|\frac{d\omega}{dk}\right|^{-1}$$

Here $F_\pi(M)$ is the pion electromagnetic form factor. The rate involves a Jacobian of the transformation from momentum to energy, namely the group velocity $d\omega/dk$. The rate is inversely proportional to the group velocity, and at a local minimum $d\omega/dk$ vanishes, hence the rate diverges. An example is plotted in figure 2 as well as the rates for pions with their free space dispersion relation and the contribution from np bremsstrahlung. There is a big enhancement of the dilepton production rate due to the softening of the pion dispersion relation. More importantly there is now some interesting structure to the spectrum, which is important in heavy ion measurements.

Scott Pratt argued that since the current is proportional to the group velocity, the rate should be proportional to the group velocity rather than inversely proportional to it. Although this is an argument valid only in the infinite wavelength limit and hence not applicable in this context,it does raise the question as to what the exact expression for dilepton production is. It turns out that the following expression is exact with respect to the strong interactions, and correct to lowest order in e with respect to the electromagnetic interactions:

$$E_+E_-\frac{dR^{e^+e^-}}{d^3p_+d^3p_-} = \frac{2e^2}{(2\pi)^6}\frac{1}{M^4}\left(p_+^\mu p_-^\nu + p_+^\nu p_-^\mu - p_+\cdot p_- g^{\mu\nu}\right)\,\mathrm{Im}\Pi^R_{\mu\nu}$$

Here Π^R is the retarded photon self-energy at finite temperature and density. To compute it in the context of self-interacting pions alone requires knowledge of both the pion self-energy (which gives the pion dispersion relation) and the pion electromagnetic vertex. One can show that the most general form of the latter involves three scalar functions each of which depends on five variables. The vertex is related to the propagator by the Ward-Takahashi identity. Unfortunately this identity is only one scalar equation and cannot be used to determine the vertex from the propagator. Recently Korpa and Pratt[3] have used a simple version of the delta-hole model to compute the vertex at finite density. When this modified vertex is used to compute the rate the curve shown in figure 2 is obtained. There is no longer a big enhancement of the rate above 300 MeV. However, the Jacobian peak is still present at threshhold, and this leads to an important structure in the spectrum. Observation of a bump or similar structure in heavy ion collisions below the free space two-pion threshhold would be important information of the behavior of pions in high density nuclear matter.

The DLS has reported a bump in the dilepton mass spectrum around 275 MeV in p + Be collisions at 4.9 GeV.[2] Previous calculations have shown that this bump cannot have its origin in nucleon-nucleon bremsstrahlung nor in the Dalitz decay of the delta resonance.[4] Peter Lichard and I attempted to explain this bump by considering the annihilation of two pions produced in the collision.[5] We used the experimentally observed cross-sections for the production of 2, 3, 4 or 5

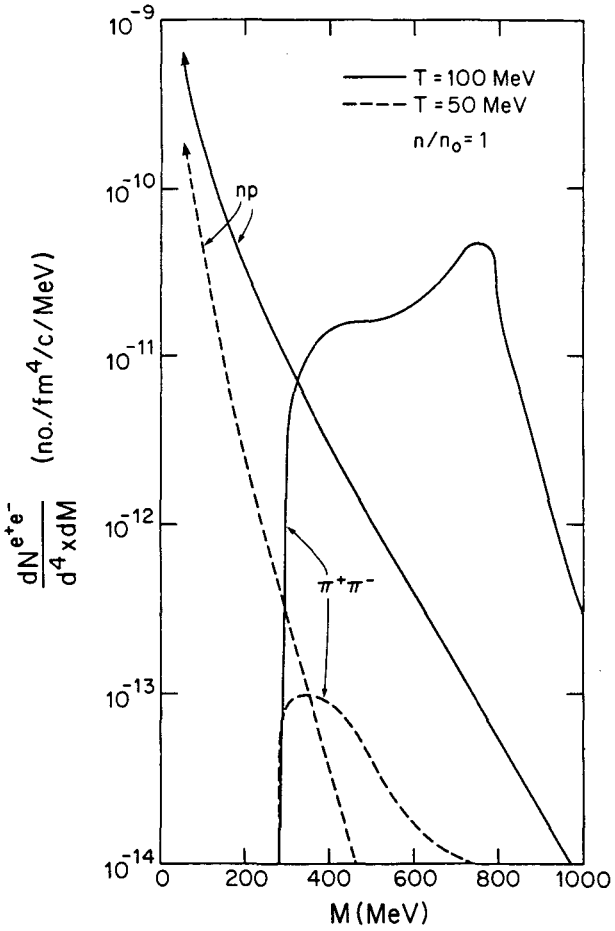

Figure 1

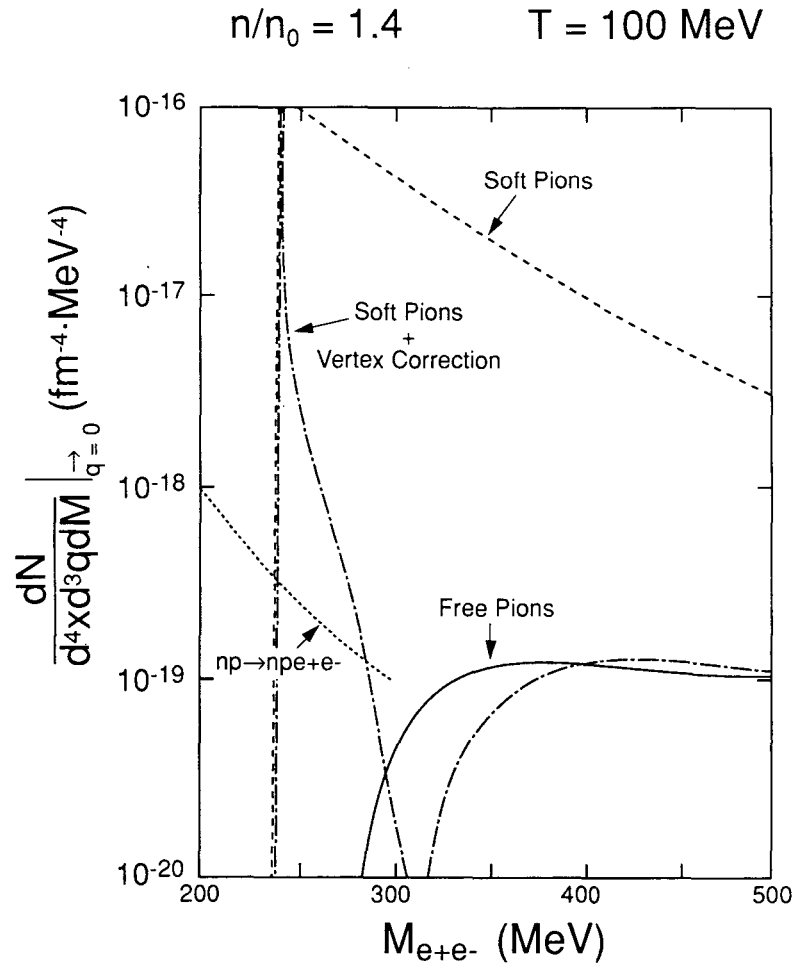

Figure 2

pions in a pp collision at essentially this energy. We used a phase space generator which included transverse momentum cut-off and leading particle effects, and from it obtained the momentum-correlated two-pion distributions. We assumed that these pions were created independently in a region of position space modelled by a Gaussian of width 1 fm. Once created the pions were assumed to follow straight-line trajectories out to the detectors. Of course, once in a while the pions' trajectories overlap, and when that happens they may annihilate into e^+e^-. The number of pairs produced is

$$N_{e^+e^-} = \int_0^\infty dt \int d^3x \int d^3k_1 d^3k_2 \; W(\vec{k}_1,\vec{k}_2,\vec{x},\vec{x},t) \; \sigma_{\pi^+\pi^-}(M) v_{rel}$$

where W is the two-pion phase space density. Invariant mass and momentum cuts can be introduced in the integration. Our result is shown in figure 3. The absolute rate is not too bad for large mass, but in fact the yield is inversely proportional to the square of the Gaussian radius, so there is some freedom in the absolute normalization. Most importantly there is no enhancement of the yield near threshhold; it misses the data by more than an order of magnitude. The nuclear system studied is so small one could hardly believe that many-body effects of the type described before would come into play. Therefore the origin of this bump remains a puzzle. We anxiously look forward to accurate measurements of the yields in heavy ion collisions!

This work was supported by Department of Energy Grant No. DE-FG02-87ER40328.

1. C. Gale and J. Kapusta, Phys. Rev. C35, 2107 (1987); ibid. 38, 2659 (1988).
2. G. Roche et. al., Phys. Rev. Lett. 61, 1069 (1988).
3. C. Korpa and S. Pratt, preprint 1989.
4. C. Gale and J. Kapusta, Phys. Rev. C40, 2397 (1989).
5. J. Kapusta and P. Lichard, Phys. Rev. C40, R1574 (1989).

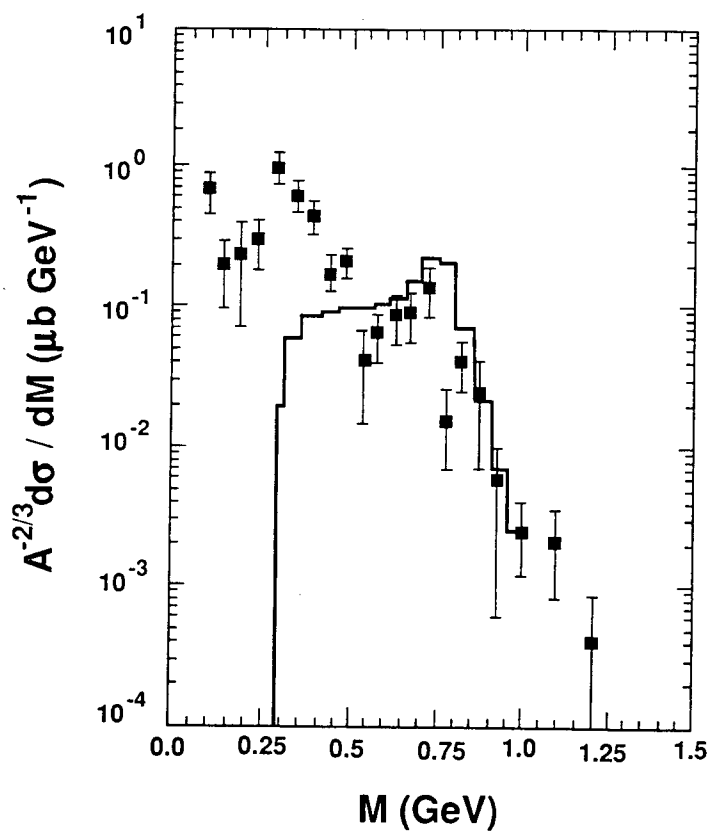

Figure 3

The Production of Soft Dileptons from a Hot Quark–Gluon Plasma

Eric Braaten
Department of Physics and Astronomy
Northwestern University
Evanston, Illinois 60208

The production rate for soft dileptons in a hot quark-gluon plasma has recently been calculated using a resummation of perturbation theory with surprising results.

QCD, the field theory of strong interactions, predicts that at high temperature, hadronic matter will undergo a phase transition to a quark-gluon plasma. At extremely high temperature T, the running coupling constant $g_s(T)$ of QCD becomes very small, and many properties of the plasma can be calculated using perturbation theory. At the temperatures that may be accessible in heavy ion collisions, $g_s(T)$ is not small. Nevertheless, I believe that the most promising approach to understanding the properties of the plasma is to develop a systematic treatment of hot QCD, and then extrapolate down to the temperatures of interest.

By hot QCD, I mean hadronic matter at a temperature T much larger than the phase transition temperature and the masses of the relevant quarks (u, d, and s) and also large enough so that $g_s(T) << 1$. Then the only important energy scales are the well-separated scales T, g_sT, g_s^2T, etc. The scale T is quite simple; it can be handled by perturbation theory. The scale g_s^2T is very complicated; nonperturbative effects are known to arise at this energy scale. Considerable progress has recently been made in understanding the intermediate scale g_sT. Naive perturbation theory is not sufficient, but it is possible to treat this scale systematically using a resummation of perturbation theory[1].

The first concrete application of the resummation methods developed in Ref. 1 has been a calculation of the spectrum of soft dileptons emitted by a quark gluon plasma[2]. By soft dilepton, I mean a lepton pair with total energy on the order of g_sT. The spectrum of hard dileptons (with energies on the order of T) can be calculated using straightforward perturbation theory. The dominant production mechanism is quark-antiquark annihilation into a virtual photon. For back-to-back dileptons with total energy E and total momentum $\vec{p} = 0$, the rate is

$$\frac{dW}{dE\, d^3p}(\vec{p}=0) \;=\; \frac{5\alpha^2}{36\pi^3}\left(\frac{1}{1+e^{E/2T}}\right)^2, \tag{1}$$

The first perturbative corrections are down by $g_s(T)^2$, and were recently computed explicitly by Altherr and Aurenche[3].

It was pointed out by Kapusta[4] that the rate for soft dileptons can differ from the above prediction by orders of magnitude. One reason is that light quarks in a thermal medium develop an effective mass[5] $m_q = g_s T/\sqrt{6}$, so the threshold for the $q\bar{q}$ annihilation process is at $2m_q$. At finite temperature, the quark also develops an extra propagating degree of freedom which can be interpreted as a coherent excitation of a hard gluon and an antiquark hole with almost equal and opposite momentum. We label this mode q_- to distinguish it from the ordinary quark mode q_+. The dispersion relations for the two modes were first calculated by Klimov and Weldon[5], and are shown in Fig. 1. As $k \to 0$, both dispersion relations approach the effective quark mass m_q. Note that the minimum for $\omega_-(k)$ occurs not at $k = 0$, but at some nonzero momentum $k = .408m_q$. A complete calculation of the spectrum of soft dileptons must take into account not only m_q, but the nontrivial momentum dependence of $\omega_+(k)$ and $\omega_-(k)$.

The annihilation of the soft quark modes q_+ and q_- with their antiparticles is not the only mechanism that can produce soft dileptons at leading order in g_s. Surprisingly, there are also scattering processes that produce soft dileptons at the same order. An example is the process $Gq_\pm \to Q\gamma^*$, where G and Q represent a hard gluon and a hard quark and γ^* is a soft virtual photon. While the rate for this process is proportional to g_s^2, explicit calculation shows that it is compensated by a factor of T^2/E^2, so that the rate is indeed of leading order in g_s when $E \sim g_s T$.

Using the resummation methods of Ref. 1, a complete calculation to leading order in g_s of the production rate for soft dileptons with $\vec{p} = 0$ has recently been carried out by Braaten, Pisarski, and Yuan[2]. The processes that contribute are those listed below, together with their charge conjugates. The sum of the partial rates from the processes involving only soft particles is shown as the lower curve in Fig. 2. Note that this curve has sharp peaks at $E = .470m_q$ and $E = 1.856m_q$, separated by a gap. The individual processes are:

$q_+ \to q_-\gamma^*$: A q_+ decays into a q_- with the same momentum k. The spectrum from this process terminates at $E = .470m_q$ with a sharp peak. The peak is a Van Hove singularity, and is due to a divergence in the density of states that contribute to this process.

$q_-\bar{q}_- \to \gamma^*$: The q_- annihilation process turns on with a Van Hove singularity at $E = 1.856\ m_q$. At this energy, the q_- particles are produced with momentum $k = .408m_q$ at the minimum of the dispersion relation $\omega_-(k)$.

$q_+\bar{q}_+ \to \gamma^*$: This is the normal quark-antiquark annihilation process, which turns on at the threshold $E = 2m_q$. For $E > 7m_q$, this contribution dominates, approaching the naive prediction (1).

$q_+\bar{q}_- \to \gamma^*$: This process also turns on at the normal threshold $E = 2m_q$.

The remaining processes that produce soft dileptons at leading order in g_s involve scattering of hard particles. The sum of the partial rates for these processes are shown as the upper curve in Fig. 2. This curve displays little structure except that it grows dramatically at low energies. The individual processes are

$q_\pm G \to Q\gamma^*$, $q_\pm \bar{Q} \to G\gamma^*$: These involve scattering of one hard particle and grow like $1/E^2$ at small energy.

$QG \to GQ\gamma^*$, $Q\bar{Q} \to GG\gamma^*$, $GG \to Q\bar{Q}\gamma^*$: These involve scattering of two hard particles, and grow like $1/E^4$ for small E.

As shown in Fig. 2, these processes completely overwhelm the dramatic structure in the partial rate from the annihilation and decay of soft quark modes. However what is lost in structure is gained in the overall rate. For energies on the order of m_q, the rate is orders of magnitude larger than the naive prediction (1), which is shown as a dashed line in Fig. 2.

In conclusion, progress is being made in our understanding of the high temperature limit of a quark-gluon plasma. The energy scale g_sT can now be treated systematically using a resummation of perturbation theory. A complete calculation to leading order in g_s of the production rate of soft dileptons has revealed that the dominant production mechanism involves scattering of hard particles, and that the rate is orders of magnitude larger than naive predictions.

This work was supported in part by the Department of Energy under contract DE-AC02-76-ER022789.

References

1. R.D. Pisarski, Phys. Rev. Lett. **63**, 1129 (1989); E. Braaten and R.D. Pisarski, Brookhaven preprint BNL-43293, to appear in Nucl. Phys. B.; E. Braaten and R.D. Pisarski, Phys. Rev. Lett. **64**, 1338 (1990).

2. E. Braaten, R. D. Pisarski, T. C. Yuan, Brookhaven preprint BNL-43941.

3. R. Baier, B. Pire, and D. Schiff, Phys. Rev. D. **38**, 2814 (1988); T. Altherr, P. Aurenche, and T. Becherrawy, Nucl. Phys. B315, 436 (1989); T. Altherr and P. Aurenche, Annecy preprint LAPP-TH-237/89; Y. Gabellini, T. Grandou, and D. Poizat, Nice preprint NTH 89/1.

4. J. Kapusta, Phys. Lett. **136B**, 201 (1984).

5. V.V. Klimov, Sov. J. Nucl. Phys. **33**, 934 (1981); H.A. Weldon, Phys. Rev. D. **26**, 1394 (1982); Phys. Rev. D. **40**, 2410 (1989).

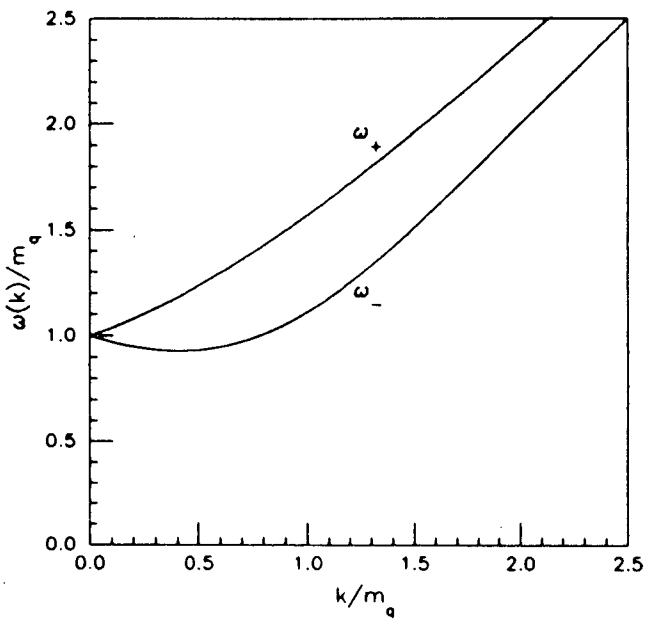

Figure 1. The quark dispersion relations $\omega_+(k)$ and $\omega_-(k)$.

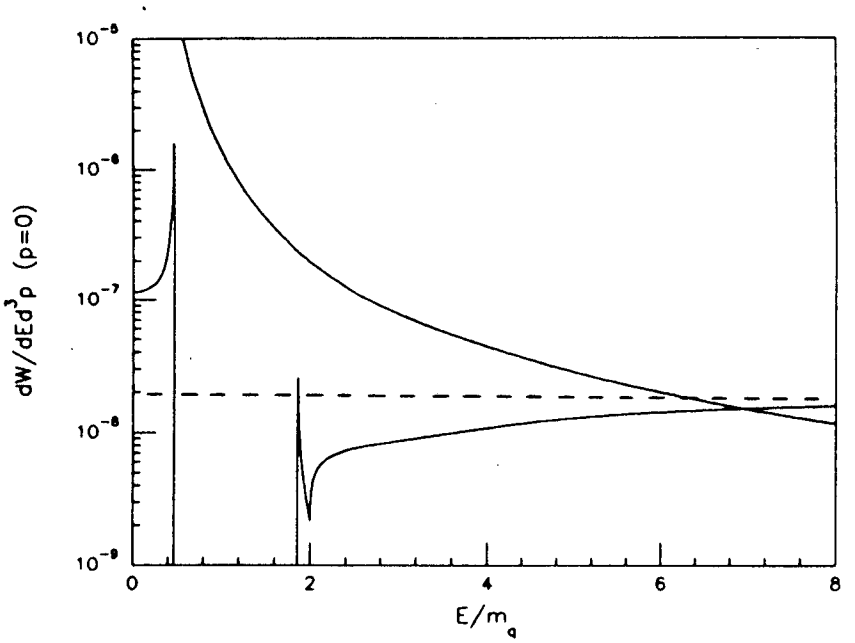

Figure 2. Contributions to the production rate for soft dileptons dW/dEd^3p with total momentum $\vec{p} = 0$ as a function of E/m_q.

Mean Field Pion Interactions in a Hydrodynamic Model

Ramona Vogt
Lawrence Livermore National Laboratory
P. O. Box 808, Livermore, California 94550

A relativistic, three–dimensional, one–fluid hydrodynamic model to simulate heavy–ion collisions has been developed at Livermore. Pions are dynamically coupled to the nuclear fluid, interacting through a mean field. Here we describe our approach. In our hydrodynamic model, we begin with momentum–energy conservation $\partial_\mu T^{\mu\nu} = 0$, where $T^{\mu\nu} = u^\mu u^\nu(\rho + \rho\epsilon + P) + g^{\mu\nu}P$, and baryon–number conservation $\partial_\mu(\rho u^\mu) = 0$. All scalar quantities are defined in the local rest frame of the fluid. We then make the following definitions for the variables tracked by the model: the coordinate baryon density is $D = \gamma\rho$, the coordinate energy density is $E = \gamma\epsilon\rho$, and the coordinate momentum density is $S^\mu = (\rho + \rho\epsilon + P)\gamma u^\mu = (D + E + P\gamma)u^\mu$. Using these definitions and $g = \det g^{ij}$, the continuity equation and the energy and momentum conservation equations are written as [1]

$$\partial_t D + \frac{1}{\sqrt{g}}\partial_i(v^i D\sqrt{g}) = 0 \ , \tag{1}$$

$$\partial_t E + \frac{1}{\sqrt{g}}\partial_i(v^i E\sqrt{g}) + P\partial_t\gamma + \frac{P}{\sqrt{g}}\partial_i(u^i\sqrt{g}) = 0 \ , \tag{2}$$

$$\partial_t S_j + \frac{1}{\sqrt{g}}\partial_i(v^i S_j\sqrt{g}) + \partial_j P = 0 \ . \tag{3}$$

The equations of motion are solved numerically on a fixed spatial grid with the matter flowing through the grid. Mass and momentum conservation are strictly enforced, but the solution scheme used does not explicitly conserve energy. Through rigorous testing, energy is found to be conserved to within a few percent with sufficiently fine gridding. Using this scheme, we can find solutions to the equations of motion with a variety of different geometries: one–dimensional cartesian, two–dimensional cylindrical, and three–dimensional cartesian [2].

In one dimension, the model has been extensively checked for accuracy against analytical solutions of the equations of motion for the shock tube and relativistic wall shock problems [3]. In the shock tube, a highly compressed, hot fluid ajoins an undisturbed fluid. At $t = 0$, the compressed fluid is allowed to expand into the undisturbed state, creating a discontinuity, or shock front. Behind this shock, the compressed region rarifies as it expands. The description of the shock tube depends on the equation of state of the fluid. The solution is analytic for an ideal gas equation of state, expressed in our variables as $P = (\Gamma - 1)E/\gamma$, where Γ is the adiabatic index of the medium. In a nonrelativistic shock tube, the maximum compression of the medium at the shock front is

$$\frac{\rho}{\rho_0} = \frac{\Gamma + 1}{\Gamma - 1} \ . \tag{4}$$

For a gas with $\Gamma = 4/3$, $\rho/\rho_0 = 7$, when $\Gamma = 5/3$, $\rho/\rho_0 = 4$. The relativistic wall shock is the strong shock limit of the relativisitic shock tube. In this limit, the maximum compression depends on γ,

$$\frac{\rho}{\rho_0} = \frac{\Gamma + 1}{\Gamma - 1} + \frac{\Gamma}{\Gamma - 1}(\gamma - 1) \ . \tag{5}$$

This implies that $\rho/\rho_0 = 43$ for a $\Gamma = 4/3$ gas at CERN SPS energies where $\gamma \sim 10$ in the nucleon–nucleon equal speed frame. There is currently no indication of such densities being reached in the

present experiments. However, one–fluid hydrodynamics is exactly solvable without recourse to assumptions about the initial conditions of the system, making it an ideal benchmark against which to compare experimental measurements, as well as other models.

Hydrodynamics alone is not sufficient to describe the global properties of heavy–ion collisions. The hydrodynamic equations of motion do not allow particle production, yet many particles are produced in these collisions. The majority of these particles are pions in the final state. A Monte Carlo scheme to approximate pion production and propagation has been developed which directly couples the pions to the baryonic fluid through momentum and energy exchange. This method guarantees detailed balance of pion production and absorption but does not require or assume that the pions are in thermal equilibrium. The model follows the temporal and spatial evolution of each pion throughout the collision until freezeout. Using different models of the nuclear equation of state, one may be able to determine if the pions at freezeout carry any information about the initial dense system which produced them [4].

Previously, the pions scattered elastically with the nucleons as though the pions and nucleons were free particles [4]. Recently the pion model has been modified to include the effects of the nuclear medium, thought to influence the pion energy spectrum [5]. In medium, the pion exists partly as itself and partly as a nucleon–hole or delta particle–nucleon hole excitation. There are various models of the pion interactions with the medium, which we are investigating. Here we present, as an example, the model of ref. [6]. The energy of the pion in medium, $\omega(k)$, is found from the poles of the pion propagator,

$$\mathcal{D}^{-1}(k,\omega) \equiv \omega(k)^2 - m_\pi^2 - k^2 - \Pi(k,\omega) = 0 \ . \tag{6}$$

The proper polarization, $\Pi(k,\omega)$, includes the effects of the nucleon and delta states on the pion. We use the expression for the dominant contribution to the polarization, the delta–hole resonance polarization, in symmetric nuclear matter since the polarization is the same for π^0 and $\pi^\pm$ and our model does not distinguish between the isospin states of the pion:

$$\Pi_{\rm res} = \frac{8}{9}\left(\frac{g_\Delta k}{m_\pi}\right)^2 \rho \frac{\omega_\Delta(k)}{\omega^2 - \omega_\Delta^2(k)} \ , \tag{7}$$

where $g_\Delta \approx 1.7$ is the coupling of pions and nucleons to deltas and $\omega_\Delta(k) = \sqrt{m_\Delta^2 + k^2} - m_N$ is the energy of the ΔN^{-1} resonance. Summation of multiple scatterings among ΔN^{-1} states gives the proper polarization

$$\Pi(k,\omega) = \frac{\Lambda^2(k)\,\Pi_{\rm res}(k,\omega)}{1 - g'(m_\pi/g_\Delta k)^2\Lambda^2(k)\Pi_{\rm res}(k,\omega)} \ . \tag{8}$$

Here $g' \approx 0.7(g_\Delta/m_\pi)^2$ is a parameter representing the quasi–nucleon interaction [5] and $\Lambda^2(k) = \exp\left(-2k^2/(7m_\pi)^2\right)$ is a vertex cutoff.

With the definitions

$$B(k,\eta) = \frac{8}{9}\left(\frac{g_\Delta}{m_\pi}\right)^2 \omega_\Delta(k)\Lambda^2(k)\rho_0\eta \ , \tag{9}$$

$$\gamma = g'\left(\frac{m_\pi}{g_\Delta}\right)^2 \ , \tag{10}$$

where $\gamma \sim 0.7$ and $\eta = \rho/\rho_0$ is the compression ratio, the inverse propagator in medium is written as

$$\mathcal{D}^{-1}(k,\omega) = \frac{(\omega^2 - \omega_\pi^2)[(\omega^2 - \omega_\Delta^2) - \gamma B] - k^2 B}{(\omega^2 - \omega_\Delta^2) - \gamma B} \ , \tag{11}$$

where $\omega_\pi = \sqrt{m_\pi^2 + k^2}$. When $\eta \to 0$ or $k \to \infty$, $B \to 0$ and the only solution is that of the free pion. There are two positive solutions for finite k and η:

$$\omega_\pm^2 = \frac{1}{2}[\omega_\Delta^2 + \gamma B + \omega_\pi^2 \pm \sqrt{(\omega_\Delta^2 + \gamma B - \omega_\pi^2)^2 + 4k^2 B}] \ , \tag{12}$$

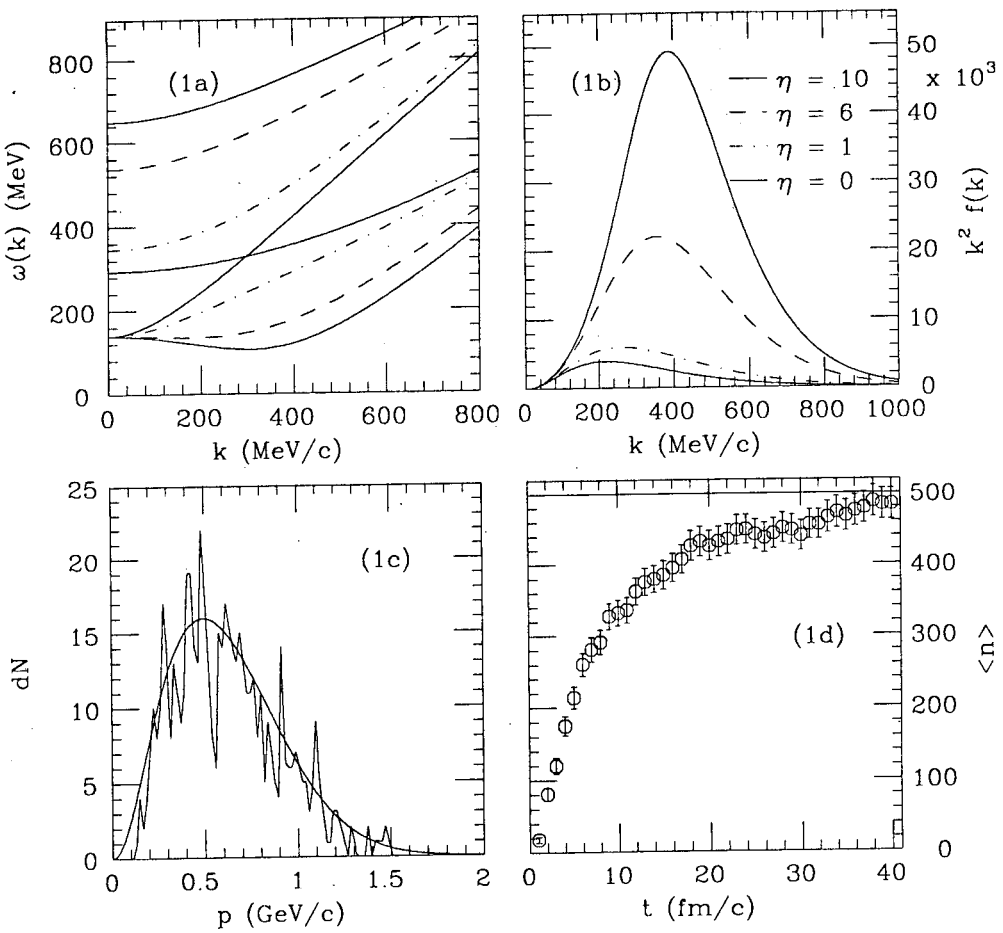

Figure 1:

both of which need to be taken into account. In the limit of vanishing k, $\omega_- \to m_\pi$ and $\omega_+ \to \sqrt{(m_\Delta - m_N)^2 + \gamma B}$, while for large k, $\omega_- \to \omega_\Delta(k)$ and $\omega_+ \to \omega_\pi(k)$. Thus, we see that ω_- behaves like a free pion at small k but like a delta at large k while ω_+ exhibits the opposite behavior.

As $\eta \to 0$, neither ω_+ nor ω_- describe the free pion dispersion at all k, but instead show a switch in their behavior at k_0, the momentum at which $\omega_\Delta = \omega_\pi$, *i.e.* when $k < k_0$, $\omega_-(k) = \omega_\pi(k)$ and when $k > k_0$, $\omega_-(k) = \omega_\Delta(k)$. In fig. 1a, we plot $\omega_-(k)$ and $\omega_+(k)$ for $\eta = 10$, 6, and 1. The $\omega_-(k)$ solution lies below the curves outlined by $\omega_\pi(k)$ and $\omega_\Delta(k)$ while the $\omega_+(k)$ solution lies above. The solid crossed lines represent $\omega_\pi(k)$ and $\omega_\Delta(k)$. The spectral weights, $A_i(k,\eta)$, of the pion component interchange the dominant branch near k_0. They are proportional to the residues of the propagator such that the Bose–Einstein distribution of the free pion is obtained in the limit $\eta \to 0$. Thus

$$A_i(k,\eta) = \left(\frac{2\omega}{\partial \mathcal{D}^{-1}(k,\omega)/\partial\omega} \right)_{\omega=\omega_i}, \tag{13}$$

where $i = +, -$ and the weights obey the sum rule $A_- + A_+ = 1$. In principle it is not enough to consider that only the ω_- branch can excite large k. Even though this branch is lower in energy and has a larger thermal weight, its spectral weight vanishes as k increases. The distribution function obtained using the weighting scheme,

$$k^2 f(k) \propto \frac{k^2 A_-}{\exp(\omega_-/T) - 1} + \frac{k^2 A_+}{\exp(\omega_+/T) - 1} \tag{14}$$

is shown in fig. 1b for $T = 100$ MeV and $\eta = 10$, 6, 1, and 0. Note that increasing the compression ratio η produces an effect on the distribution function much like increasing temperature, causing more pions to be produced in dense systems. So far, we have used the vacuum values of m_Δ and m_N. A more complete treatment would use the effective masses, $m^\star_\Delta(\eta)$ and $m^\star_N(\eta)$.

We are still examining how both branches may be treated in a dynamical model such as ours, *i.e.* specifically how to approach $\omega_\pi(k)$ as $\eta \to 0$. Alternatively, one may construct a parametrization of $\omega(k, \eta)$ that approaches $\omega_\pi(k)$ smoothly with vanishing η, as done in ref. [7].

Our model solves the relativistic Boltzmann equation with pion production, absorption, and transport terms fully included. Now, instead of producing pions with the energy of the free pion, we include medium effects. This treatment of the pion spectrum makes the Bose–Einstein distribution appear to be at a higher temperature, increasing pion production at high compressions. The mean field now exerts a force on the pions as they move through the nuclear fluid, causing them to be accelerated. Scattering of pions off nucleons occurs through this acceleration, rather than through a collision integral. We are now in the process of testing our new pion model to better determine its accuracy and sensitivity to inputs. One straightforward test we have completed using an approximation to the pion spectrum shows that the pions produce a static Bose–Einstein distribution at the appropriate temperature and compression. In fig. 1c we show the Bose–Einstein distribution for $\eta = 1$ and $T = 150$ MeV along with the model distribution at $t = 40$ fm. The approach to equilibrium with time is shown in fig. 1d. The equilibration time of the system is directly dependent on the absorption cross section, thus this test is useful for determining the equilibration time of any given cross section. A comparison can then be made to the time available in a heavy–ion collision to find out if equilibration is possible. We are currently testing the pion acceleration. Once the model has passed our tests, we will apply it to Bevalac, AGS and CERN collisions.

This work has been carried out in collaboration with J. R. Wilson, T. L. McAbee and C. T. Alonso. We are grateful to J. Kapusta, N. K. Glendenning, and M. Prakash for stimulating discussions at the workshop. This research was performed at Lawrence Livermore National Laboratory under the auspices of the United States Department of Energy, Contract No. W-7405-Eng-48.

References

[1] T. L. McAbee, J. R. Wilson, J. A. Zingman and C. T. Alonso, Mod. Phys. Lett. **A4** (1989) 983.

[2] J. A. Zingman, T. L. McAbee, J. R. Wilson and C. T. Alonso, LLNL Report UCID-21126 (1987).

[3] K. W. Thompson, J. Fluid Mech. **171** (1986) 365.

[4] J. A. Zingman, T. L. McAbee, J. R. Wilson and C. T. Alonso, Phys. Rev. **C38** (1988) 760.

[5] B. Friedman, V. R. Pandharipande and Q. N. Usmani, Nucl. Phys. **A372** (1981) 483.

[6] N. K. Glendenning, Nucl. Phys. **A**, in press.

[7] C. Gale and J. Kapusta, Phys. Rev. **C35** (1987) 2107.

Fragmentation Phenomena

A. Z. Mekjian

Rutgers University, Department of Physics, Piscataway, NJ 08855

Many phenomena in nature show a power law behavior in the distribution function of some quantity. A few examples in physics are the size distribution of meteorites, the distribution of cluster sizes at the percolation threshold, droplet sizes at a critical point, and sandpile slides at a self–organized critical point. Power laws in energy and in frequency are also observed such as in $1/f$ noise. In other areas of endeavor similar behavior has been noted such as in the frequency distribution of words in a book when each word is ordered such that $N = 1$ is the most frequent word, $N = 2$ the next most frequent word, *etc.* The frequency distribution then falls as $1/N$.

In many cases the power law is a tabulated or empirically observed property of the system whose origin is not well understood. The purpose here is to present a fragmentation model in which an exact power law is obtained at a critical point in the value of some tuning parameter. Moreover, the model is exactly soluable for all values of the tuning parameter. As the parameter is varied from small to large values of it, a simple expression shows a system passing from evaporation modes to scale invariant behavior to total multifragmentation.

The results of this fragmentation model can be summarized as follows. Starting with a system of A objects, all possible partitions into groups or clusters are considered. The various partitions are specified by the numbers $(n_1, n_2, \ldots, n_A)$ where n_j is the number of clusters or groups of size j. The constraint $A = \sum_j j n_j$ must be satisfied for every partition. The total mass in clusters of size j is $j n_j$. The multiplicity m of a given partition is $m = \sum_j n_j$ which is the total number of clusters or groups.

Using a weight function $W_A(\{n_j\}, x)$ given by

$$\begin{aligned} W_A(\{n_j\}, x) &= \frac{M_2(\{n_j\}) x^m}{x(x+1)\cdots(x+A-1)}, \\ M_2(\{n_j\}) &= \frac{A!}{n_1! 1^{n_1} n_2! 2^{n_2} \cdots n_A! A^{n_A}}, \end{aligned} \tag{1}$$

the mean number of clusters or groups of size k is obtained by ensemble averaging n_k over all possible partitions of A, called Π_A. The above weight function leads to a single, simple

and exact expression for cluster sizes given by

$$Y_A(k,x) = \sum_{\Pi_A} n_k W_A(\{n_j\},x) = \begin{pmatrix} A \\ k \end{pmatrix} xB(x+A-k,\ k). \tag{2}$$

Here $\begin{pmatrix} A \\ k \end{pmatrix} = A!/[(A-k)!k!]$ and $B(x+A-k,\ k) = \Gamma(x+A-k)\Gamma(k)/\Gamma(x+A)$ is a Beta function. The $\Gamma(z) = (z-1)!$ are Gamma functions. The variable x gives a weight for the multiplicity of the decomposition and the range of x is $0 \leq x \leq \infty$. As x is varied from 0 to ∞, the cluster size distribution function varies from the fused mode $k = A$, $n_A = 1$, $Y_A(A, x=0) = 1$ to the totally fragmented mode $k = 1$, $n_1 = A$, $Y_A(1, x=\infty) = A$. At $x = 1$, the $Y_A(k,x)$ is of a power law form

$$Y_A(k, x=1) = 1/k \tag{3}$$

for all $k = 1$ to A, and for any A. Eq.(3) is a hyperbolic behavior for $Y_A(k,\ x=1)$. As x increases from $x = 0$, the fused cluster fragments and $Y_A(k,x)$ is no longer zero for $k \neq A$. For $k = 1$, the $Y_A(1,x)$ is

$$Y_A(1,x) \sim x\frac{A}{A+x} \sim x, \tag{4}$$

for $x \ll A$. For $x \ll 1$, $Y_A(A, x \ll 1) = 1 - (\gamma + \log A)x \sim 1$, where $\gamma = 0.57721$ is the Euler's number and $Y_A(k, x \ll 1) = Ax/[k(A-k)]$. This $Y_A(k, x \ll 1)$ is a U shaped curve in $k = 1, 2, \ldots, A$, and the rise at $k \sim A$ comes from the evaporation residues of the yield curve in a nuclear collision. The evaporation residues disappear at $x \sim 1$. At the other extreme, $x \gg A$, the fragmentation mode is mostly into individual pieces with some remaining clusters:

$$Y_A(j, x \gg A) \equiv N_j \sim \frac{A}{j}\left(\frac{A}{x}\right)^{j-1}, \qquad Y_A(1, x \gg A) \sim A. \tag{5}$$

Comparing Eq.(4) with Eq.(5), it will be noted that x has moved from the numerator in Eq.(4) to the denominator in Eq.(5) and has been raised to the power $(j-1)$. Any barrier behavior in x against evaporation evolves into a Boltzmann binding energy enhancement factor for cluster formation in a multifragmentation limit. Volume factors will also be reversed. The x, in a Fermi gas model, is

$$x \sim \frac{V}{v_0}\left\{exp\left[-\frac{a_B}{k_B T} - \frac{k_B T}{\varepsilon_0}\left(\frac{T_0}{T+T_0}\right)\right]\right\} g(T). \tag{6}$$

where a_B is a coefficient in a binding energy expression $E_B(k) = a_B(k-1)$, with $E_B(k)$ the binding energy of a cluster of size k. The ε_0 is the nuclear level density parameter and T_0 is a cut–off parameter suggested by Randrup and Koonin for internal partition functions. The $g(T)$ is an unknown function expressing our lack of understanding of internal partitioon functions.

As x varies from $x \ll A$ to $x \gg A$, the barrier suppression factor $exp(-a_B/k_BT)$ for evaporation evolves into a Maxwell–Boltzmann enhancement factor $exp(E_B(j)/k_BT)$ for cluster formation. Evaporation and multifragmentation have an underlying reciprocal behavior in both volume and Boltzmann factors:

$$\frac{V_C}{v_0} \rightarrow \frac{1}{(V_f/v_0)^{j-1}}, \qquad e^{-a_B/k_BT} \rightarrow \frac{1}{(e^{-a_B/k_BT})^{j-1}} = e^{E_B(j)/k_BT}. \tag{7}$$

Moreover, with this choice of x, Eq.(4) is a result found in Fermi's monograph "Thermodynamics" for the evaporation of particles into a cavity of volume V. Also Eq.(5) with this same x becomes the law of mass action. Thus limiting forms of Eq.(2) reduce to: 1) an expression for evaporation of a particle into a confining volume V, and 2) laws of chemical equilibrium from chemistry (law of mass–action) or equivalently, the Saha equation of astrophysics. The cavity volume of the Fermi expression is to be taken as the nuclear volume V_N. For the nuclear volume $V_N = SD/6$ where S is the surface area and D the length scale of the volume ($S = 4\pi R^2$, $D = 2R$ for a sphere; $S = 6L^2$, $D = L$ for a cube). A characteristic speed is introduced which is $v_s = \sqrt{\alpha k_BT/m}$, where α is a numerical factor. When v_s is taken to be the *rms* speed of a Maxwell–Boltzmann distribution, the $\alpha = 3$. Introducing a characteristic time $t = D/v_s$ which is the transit time across the distance D, then

$$\frac{Y_A(1,x)}{t} = \frac{\sqrt{2\pi\alpha}}{6} S \left[\frac{2\pi M(k_BT)^2}{h^3} e^{-a_B/k_BT} \right]. \tag{8}$$

The quantity in square bracket is Richardson's formulae (excluding a spin $g_s = 2$ factor) for the evaporation rate per unit area for a Fermi gas. The numerical coefficient $\sqrt{2\pi\alpha}/6$ is of the order of unity.

Since $\sum_k kY_A(k,x) = A$ for all x, a quantity

$$P_A(k,x) = kY_A(k,x)/A \tag{9}$$

has the property $\sum_k P_A(k,x) = 1$ and $P_A(k,x) \geq 0$ which are properties of a probability function. The $kY_A(k,x)/A$ is the fraction of mass in clusters of size k.

The $P_A(k,x)$ distribution has the following moments $\langle k \rangle \equiv \sum_{k=1}^{A} kP_A(k,x) = (A + x)/(x+1)$ and $\langle k^2 \rangle \equiv \sum_{k=1}^{A} k^2 P_A(k,x) = (A+x)(2A+x)/[(x+1)(x+2)]$. At $x = 1$, $\langle k \rangle = (A+1)/2$ is a statement that the sum of the first A integers is $A(A+1)/2$, while $\langle k^2 \rangle = (A+1)(2A+1)/6$ is the result that the sum of the squares of the first A integers is $A(A+1)(2A+1)/6$.

An integral representation of $B(x+A-k,\ k) = \int_0^1 p^{k-1}(1-p)^{x+A-k-1}dp$ can be used to rewrite the main result of Eq.(9) as

$$P_A(k,x) = \int_0^1 \frac{(A-1)!}{(A-k)!(k-1)!} p^{k-1}(1-p)^{A-k} u(x,p)dp, \tag{10}$$

where $u(x,p) = x(1-p)^{x-1}$. Eq.(10) shows the connection of the fractional mass in clusters of size k to probability theory and specifically to a distribution generated by Bernoulli trials on a mixed population pf skewed coins given by $u(x,p)$.

The Bernoulli trial form of Eq.(10) has the Beta density form of probability theory. Specifically, $P_A(k,x) = \int_0^1 \beta_{\mu,\nu}(p)[u(x,p)/A]dp$, where $\nu = k$, $\mu = A - k + 1$ and $\beta_{\mu,\nu}(p) = [\Gamma(\mu+\nu)/\Gamma(\mu)\Gamma(\nu)]p^{\nu-1}(1-p)^{\mu-1}$. Moreover, a simple transformation to a new variable t, with $p = 1/(1+t)$ transforms the Beta density $\beta_{\mu,\nu}(p)$ into the Pareto density $\beta_{\mu,\nu}(t) = [\Gamma(\mu+\nu)/\Gamma(\mu)\Gamma(\nu)]t^{\mu-1}/(1+t)^{\mu+\nu}$ which, for large t, varies with t as $\sim 1/t^{\nu+1} = 1/t^{k+1}$. The Pareto density was used by Pareto to study economic phenomena.

The Jaynes dice model chooses a probability for each side of a die subject to known constraints, and nothing else. A constraint could be the specification of $\langle k \rangle$ and the $P_A(k)$, $k = 1$ to 6, is to be obtained by maximizing $S = -\sum P_A(k) \ln P_A(k)$ subject to this constraint. The partition function for the problem is $Z(\lambda) = \sum e^{-k\lambda}$, where λ is a Lagrange multiplier determined by $\partial \log Z(\lambda)/\partial\lambda = \langle k \rangle$. The $\tilde{n}_k$ which maximize Eq.(1) are $\tilde{n}_k = (x/k)e^{-\lambda k}$ when A is large and Stirling's approximation can be used for $(n_k!)$.

Dynamical Effects in Nuclear Multifragmentation

Jørgen Randrup
Nuclear Science Division, Lawrence Berkeley Laboratory
University of California, Berkeley, California 94720

Several statistical models have been developed in recent years, based on excitable fragments within a specified freeze-out volume.[1-4] Although capable of reproducing a variety of features of the data, such approaches are not entirely satisfactory: the freeze-out volume is not calculable, the potential barriers are not given appropriate consideration, and the dynamics of the disassembling system is not considered in sufficient detail. This situation has motivated us to develop a refined treatment of statistical multifragmentation. By a suitable generalization of the transition-state approximation for ordinary binary fission [5], we first characterize the "transition state", at which the system makes an irreversible transformation into interacting prefragments, and then follow the subsequent dynamical evolution.

Thus, we consider an idealized very excited nuclear system consisting of A nucleons, having a total energy E, and a total angular momentum $\mathbf{J}$. This source is assumed to achieve a transient equilibrium so that statistical considerations can be employed. Assuming that the transition configuration bears some resemblance to a collection of the specified prefragments, we describe the disassembling system as a collection of a (variable) number of interacting (pre)fragments. In this manner, the degrees of freedom associated with a given final channel are included explicitly already at the transition stage, even though the fragments may not yet have been fully developed as separate entities. Any particular fragmentation of the system is then described as a number of distinct but interacting prefragments and is characterized by the quantities $\{A_n, \mathbf{r}_n, \mathbf{p}_n, \mathbf{S}_n, \epsilon_n\}$, where A_n, $\mathbf{r}_n$, $\mathbf{p}_n$, $\mathbf{S}_n$, and ϵ_n denote the mass number, position, momentum, spin, and internal excitation energy of fragment n, respectively. The partial width for the idealized source to break up into a specified mass partition $A_1, ..., A_N$ is denoted by $\Gamma_{A_1\cdots A_N}(E)$ and the total width follows by summation.

In order to make the system amenable to a transition-state treatment, we define, for a given fragmentation F, the *disassembly coordinate* q and the *radial momentum* p as follows, $q_F^2 = 1/m_0 \sum_n m_n r_n^2$ and $p_F = 1/q_F \sum_n \mathbf{p}_n \cdot \mathbf{r}_n$, where m_n is the fragment mass and $m_0 = \sum_n m_n$. The quantity q is simply related to the *rms* radius of the mass distribution of the system and provides a convenient measure of the overall size of the multifragment system. Its conjugate momentum p is a simple measure of the outwards directed motion of the fragments; the associated radial energy is $E_{\text{blast}} = \frac{1}{2}p\dot{q} = p^2/2m_0$.

By counting the number of elementary multifragment states that pass by a given value of q per unit time, it is possible to derive an expression for the outwards probability current $\nu_{A_1\cdots A_N}(E, \mathbf{J})$. Invoking the statistical assumption, the breakup rate of the system is given by the magnitude of the transition current, $\nu_{A_1\cdots A_N}(E)$, divided by the total number of elementary states in the source. The partial transtion width can then be expressed as[6]

$$\Gamma_{A_1\cdots A_N}(E, \mathbf{J}) \approx \frac{1}{\rho_A(\epsilon_0')} \frac{\sqrt{4\pi}}{\Gamma(\frac{3}{2}N - \frac{3}{2})} \left\langle \left(\frac{\mathcal{I}_A \tau_0}{\mathcal{I}_{1\cdots N}\bar{\tau}}\right)^{\frac{3}{2}} \left(\frac{m_0 q_{1\cdots N}^2 \bar{\tau}}{2\hbar^2}\right)^{\frac{3}{2}N-2} \rho_{1\cdots N}(\epsilon_{1\cdots N}') \, \bar{\tau} \right\rangle' , \qquad (1)$$

where ρ_A is the density of states of the decaying compound system, $\mathcal{I}_A$ is its moment of inertia, and τ_0 its temperature; its statistical excitation energy is $\epsilon_0' = \epsilon_0 - J^2/2\mathcal{I}_A$. Similarly, the statistical excitation of the transition configuration is $\epsilon_{1\cdots N}' = \epsilon_{1\cdots N} - J^2/2\mathcal{I}_{1\cdots N}$, and $\rho_{1\cdots N}$ is the corresponding level density. The result has been expressed as an average over transition configurations. For each one, the quantity $q_{1\cdots N}$ denotes that value of q for which the outwards current attains its minimum value. The prime indicates that the average is over fragment positions $\{\mathbf{r}_n\}$ that have been constrained to have their center-of-mass position at the origin, $\mathbf{R}_F = 0$, and have the specified *rms* extension, $q = q_{1\cdots N}$.

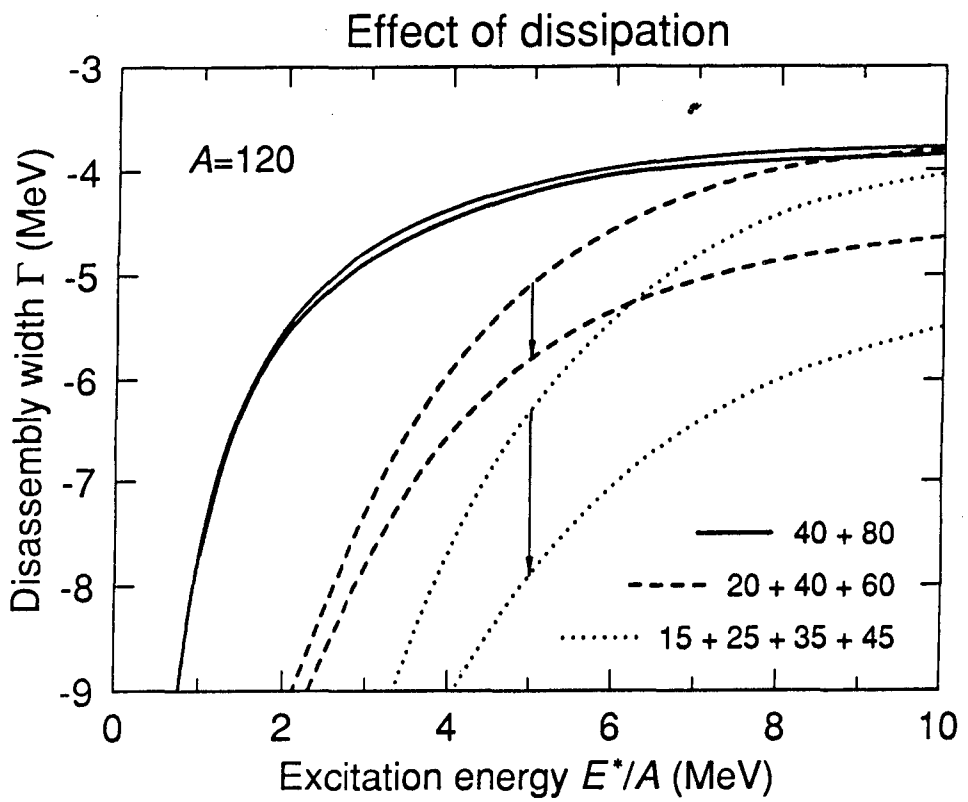

It is necessary to augment the transition-state formulation with a treatment of the post-transition dynamics.[7] For this purpose, the disassembling system is regarded as a generalized damped reaction and the dynamical state of the multifragment system is then described by the variables $\{\mathbf{r}_n, \mathbf{p}_n, \mathbf{S}_n, \epsilon_n\}$. The time development of the system can then be described by a Lagrange-Rayleigh equation, $d(\partial\mathcal{L}/\partial\dot{\mathcal{Q}})/dt + \partial\mathcal{F}/\partial\dot{\mathcal{Q}} = \partial\mathcal{L}/\partial\mathcal{Q}$, where the conservative part of the evolution of the N-fragment system is described by the Lagrangian

$$\mathcal{L}(\mathcal{Q}, \dot{\mathcal{Q}}) = \sum_{n=1}^{N} \frac{\mathbf{p}_n^2}{2m_n} + \sum_{n=1}^{N} \frac{\mathbf{S}_n^2}{2\mathcal{I}_n} - E^0_{1\ldots N} + E_0 - \sum_{n<n'}^{N} V_{nn'}(r_{nn'}) \ . \tag{2}$$

An approximate treatment of the nuclear dissipation can be made on the basis of the nucleon-exchange transport model in which the dissipation is generated by the stochastic exchange of nucleons between the interacting nucleides.[8] Thus, the friction forces are derived from the Rayleigh function

$$\mathcal{F}(\mathcal{Q}, \dot{\mathcal{Q}}) = \frac{1}{2} \sum_{n<n'}^{N} \dot{Q}_{nn'} = n_0 \sum_{n<n'}^{N} \sigma_{nn'}(r_{nn'})[2(u^{\rm rad}_{nn'})^2 + (u^{\rm tan}_{nn'})^2] \ , \tag{3}$$

where $\dot{Q}_{nn'}$ is the dissipation arising from the exchange of nucleons between the fragments n and n'. The dissipation rate thus depends on the radial and tangential components of the local velocity mismatch between the surfaces of the two neighboring fragments. In the friction form factor, the quantity $n_0 = \frac{1}{4}\rho\bar{v} \approx 0.263/\mathrm{fm}^2/10^{-22}$ s is the one-sided nucleon flux in standard nuclear matter and $\sigma_{nn'}$ is the effective window area through which the nucleons are exchanged between the two nuclei. In the present treatment, we adopt the following simple form, $\sigma_{nn'} = 2\pi\bar{R}b\Psi(s/b)$ suggested by the proximity approximation.[9] Here $b \approx 1$ fm is the nuclear surface diffuseness, and the reduced radius is $\bar{R} = R_n R_{n'}/(R_n + R_{n'})$. The smallest separation between the two nuclear surfaces is then given by $s = r_{nn'} - R_n - R_{n'}$ and $\Psi(\zeta)$ is the dimensionless form factor.[8]

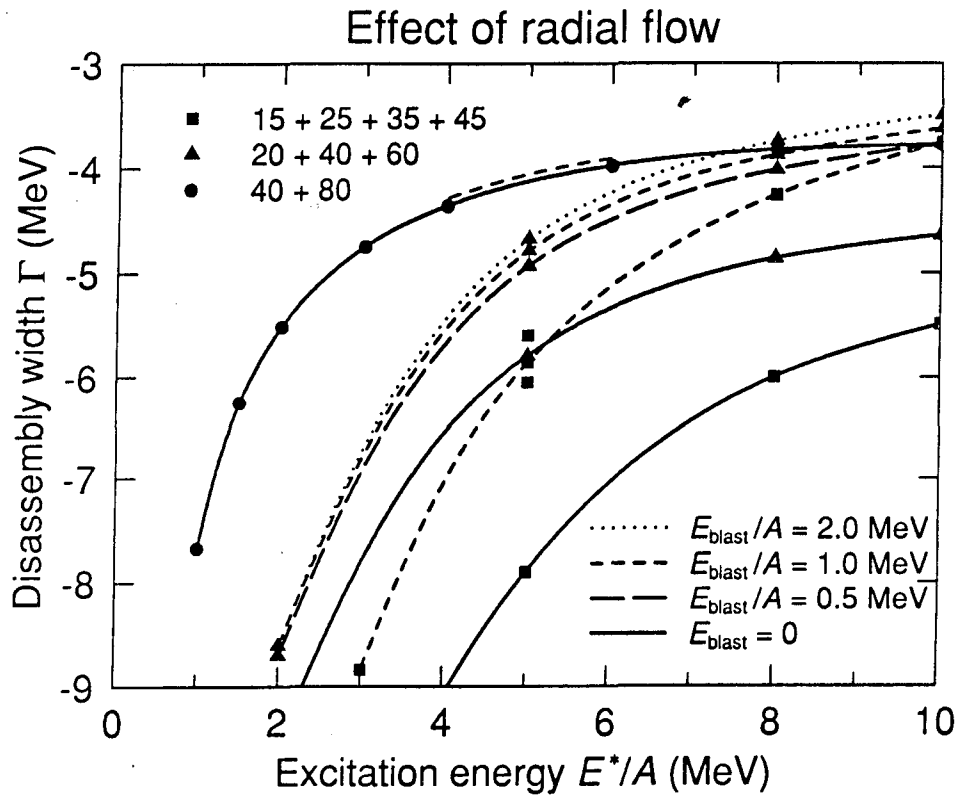

The resulting closed set of equations can be readily solved to yield the dynamical evolution of the system, starting from any specified multifragment transition state, F. For specified prefragment mass numbers, $A_1, ..., A_N$, a sample of transition-state configurations is chosen randomly in accordance with the expression (1). This amounts to first selecting the N prefragment positions $\mathbf{r}_n$ randomly, subject to the constraints that the overall center of mass $\mathbf{R}_F$ be at the origin and the overall *rms* size q_F be equal to an arbitrary but fixed value q_0, and then performing a scale transformation $\mathbf{r}_n \rightarrow (q_{1\cdots N}/q_0)\mathbf{r}_n$ to bring the configuration to the transition surface (where the current $\nu_{1\cdots N}$ has its minimum). [Any multifragment configuration can be decomposed into isolated clusters consisting of fragments that are all in communication with each other; we reject candidate transition configurations that consist of two or more isolated clusters, since no equilibrium can be maintained between the disconnected clusters.] Having thus found an acceptable transition configuration, the initial dynamical state is prepared by endowing the prefragments with linear and angular momenta as well as internal spins. These are selected randomly from the appropriate microcanonical distribution.[10] The internal excitation energy ϵ is distributed on the N fragments in proportion to their heat capacity, $\epsilon_n \sim a_n$, so that they all have the same temperature τ_n at the outset.

The most important effect of the dynamics is that some of the prefragments may fuse. Those processes for which such recombination occurs lead to final states having a correspondingly lower fragment multiplicity and thus, in principle, they contribute to the disassembly widths for those channels. So far such indirect terms have been ignored, although contributions from such side feeding are not necessarily negligible. Figure 1 shows the disassembly widths calculated for selected mass partitions of multiplicity two, three, and four. For a given multiplicity, Γ is not very sensitive to the particular mass partition, which simplifies the analysis. The ternary widths rise more steeply than the binary widths, and the quaternary widths are still steeper, as is generally expected because of the macroscopic factor $\sim q^{3N-4}$ in the transition current. The dissipation acts to facilitate prefragment fusion. For ternary channels the associated reduction is about one order of magnitude, while it is about one and a half order of magnitude for quaternary channels. The effect grows progressively larger for higher multiplicities and the post-transition dynamics plays an indispensable role in the disassembly process.

The exploration of the nuclear equation of state constitutes a focal point in the study of intermediate-energy nuclear collisions; particular efforts have been directed towards extracting the compressibility of nuclear matter. It is generally expected that the early stage of energetic nuclear collision leads to significant enhancements of the density, relative to the standard saturation value of ≈ 0.17 fm^{-3}. Such a compression may in turn produce an overall radial flow in the system at the subsequent disassembly stage. Our multifragmentation treatment can readily be employed to study the effect of such a feature, if it were indeed present. For this purpose, it is convenient to characterize the degree of overall outwards motion by the "blast" energy E_{blast}. The ordinary transition-state treatment described above corresponds to $E_{\text{blast}} = 0$. For a specified finite value of E_{blast}, the method developed in ref. [10] readily allows the preparation of the appropriately modified microcanonical initial multifragment states.

With a radial blast incorporated as described above, we now reconsider the disassembly of the $A = 120$ source. Because of the ordered outwards motion, the prefragments are less likely to recombine during the dynamical evolution. Figure 2 shows the partial widths $\Gamma_{A_1 \cdots A_N}$ obtained for various blast scenarios. It is seen that the presence of an overall radial flow at the transition point significantly increases the survival probability of a particular configuration and, consequently, it will act to increase the corresponding partial width. It should also be noted that such a blast-induced increase in the multifragmentation width is accompanied by a decrease of sequential decays because of the associated reduction of the internal excitation energy. It is apparent from fig. 2 that a relatively small amount of radial flow, a fraction of an MeV per nucleon, sufficies to cause a significant increase in Γ. Moreover, the effect rapidly saturates as a function of E_{blast}. Interestingly, the values thus achieved are relatively similar to those first calculated without considering dissipation, see fig. 1. Thus dissipation and radial flow approximately counterbalance each other, with regard to the partial disassembly width $\Gamma_{A_1 \cdots A_N}$.

A major motivation for undertaking the present work has been the need for a model in which the evolution of the disassembly process from low to high excitation can be addressed. Having attractive limits, the developed model provides such a framework, and a variety of instructive applications of the model are foreseen, at this point primarily for the purpose of gaining theoretical insight. A statistical model provides a relatively well-defined reference that can be useful even if its idealized conditions are not realized in the actual processes accessible for study. Before the theory can provide quantitatively useful results, there are a number of aspects that need further consideration, including the incorporation of light fragments (especially individual nucleons). As the detector technology advances and powerful multifragment detector systems emerge, there are growing demands on theory to provide the tools necessary for making informative analysis of the data. The present theory, though yet incomplete, may prove useful for attempts to investigate the extent to which interesting properties of a produced source, such as a collective flow, are manifested in quantities amenable to experimental measurement.

Most of this work was carried out in collaboration with Jorge López. This work was supported by the Director, Office of Energy Research, Division of Nuclear Physics of the Office of High-Energy and Nuclear Physics of the U.S. Department of Energy under Contract DE-AC03-76SF00098.

1. S.E. Koonin and J. Randrup, Nucl. Phys. A356 (1981) 223
2. S.E. Koonin and J. Randrup, Nucl. Phys. A474 (1987) 173; A471 (1987) 355c
3. D.H.E. Gross, Phys. Lett. 161B (1985) 47; D.H.E. Gross, Zhang Xiao-ze, and Xu Shu-yan, Phys. Rev. Lett. 56 (1986) 1544
4. J.P. Bondorf, R. Donangelo, I.N. Mishustin, C.J. Pethick, and H. Schulz, Nucl. Phys. A443 (1985) 321; J.P. Bondorf, R. Donangelo, I.N. Mishustin, and H. Schulz, *ibid.* A444 (1985) 460
5. N. Bohr and J.A. Wheeler, Phys. Rev. 56 (1939) 426
6. J.A. López and J. Randrup, Nucl. Phys. A503 (1989) 183
7. J.A. López and J. Randrup, LBL-26810 (1989), Nucl. Phys. A (in press)
8. J. Randrup, Nucl. Phys. A327 (1979) 490
9. J. Randrup, Ann. Phys. 112 (1978) 356
10. J. Randrup, LBL-28390 (1990), Comp. Phys. Comm. (in press)

THE SEARCH FOR MULTIFRAGMENTATION*

A. C. Mignerey, W. L. Kehoe, A. Marchetti, S. Bradley
Department of Chemistry and Biochemistry
University of Maryland
College Park, Maryland 20172

D. R. Bowman, R. J. Charity, H. Han, K. Jing, R. J. McDonald, M. A. McMahan, L. G. Moretto, L. Vinet, and G. J. Wozniak
Nuclear Science Division
Lawrence BerkeleyLaboratory
Berkeley, California 94720

I. Iori and A. Moroni
I.N.F.N.
Milano, Italy

Recent improvements in the availability of heavy beams with energies between 25 and 100 MeV/u has allowed experimental investigation of this energy and mass regime and fostered a great deal of theoretical interest. One of the first experimental features to be identified was the increase in the production of products with charge and mass much less than that of the projectile or target but greater than the usually observed light particle emission. These products have been called intermediate mass fragments or complex fragments. The exact definition depends somewhat on the experiment but they are always greater in charge and mass than an alpha particle. They have been attributed to a variety of sources, including the breakup of excited light projectiles, sequential evaporation from excited heavy nuclei and a new mechanism predicted to be characteristic of intermediate energy reactions termed multifragmentation. In this contribution multifragmentation will be used to refer to the simultaneous disassembly of an excited system of nucleons as opposed to a multifragment final state resulting from successive binary decays.

The production of intermediate mass fragments (IMF's) is a key component in the quest for an experimental signature for multifragmentation. Model calculations (as examples see references 1-3 and contributions in this proceeding) of multifragmentation predict large multiplicities for IMF production and a rapid increase in IMF multiplicity at a given excitation energy might be such a signature (see contribution by Y. Blumenfeld in this proceedings). The experimental problem is that other decay mechanisms also produce products in this mass region making IMF production a necessary but not sufficient condition for multifragmentation. This contribution focusses on charge distributions obtained in La-induced reactions at 47 MeV/u and compares the experimental results with those of the sequential decay code Gemini[4].

The detection system used in these experiments consisted of 10 telescopes each composed of a 300-μ Si, a 5-mm SiLi and a 7.6-cm plastic detector. The Si and SiLi detectors were each position sensitive in one direction. By orienting them 90° relative to each other position sensitivity in the x and y directions of ~2mm was obtained, which translates to ~0.4° in θ and ϕ for this

experiment. The ΔE-E obtained by these telescopes allowed discrete charge resolution all the way up to that of the projectile charge of 57. The detected charge was converted to a mass using the mass parameterization from reference 5 and combined with the angular information to produce velocity distributions parallel and perpendicular to the beam direction. Source velocities for events with two or more coincident fragments with Z>3 were generated. The inclusive distributions (for all Z's) for two-, three- and four-fold events are shown in Fig. 1 for 47-MeV/u La on targets of Al, Cu and La. The centriods of the distributions as a function of detected fragment charge for two- and three-fold events are shown in Fig 2. The data for the Al target shows little dependence on charge, with an average value corresponding to 48% linear momentum transfer. The derived source velocities for the two heavier targets are very similar and increase with Z. Linear momentum transfers of only 31% and 16% are obtained for the Cu and La targets, respectively, when source velocities averaged over all Z are used. However, as seen in Fig. 2, higher transfers would be obtained for lower charges, implying more central collisions giving rise to these fragments. Applying simple conservation of momentum arguments, mean excitation energies for the emitting systems of 520 MeV (3.5 MeV/u), 770 (4.9 MeV/u), and 880 (5.4 MeV/u) are obtained for the Al, Cu and La targets, respectively.

Angular distributions in the source frame have been generated for each Z and integrated to obtain the inclusive charge distributions shown in Fig. 3. No cross sections are given for the higher charge products due to the poor angular coverage for these events. There is a marked change in the shape of the distribution in going from the Al to the Cu target. The yield difference between the Cu and La targets scales with approximately A_{target} to the 2/3 power. Comparisons with a statistical model calculation of sequential two-body decay and light particle evaporation using the code Gemini[4] are shown in Figure 4. The cross sections for the medium mass fragments from the Al target are well reproduced by a maximum angular momentum of 74 $h/2\pi$, but the yields of lower Z products are way under predicted. The discrepancy is even greater for the heavier targets. The maximum angular momentum of 82 $h/2\pi$ used for these calculations corresponds to the critical angular momentum for formation of a compound nucleus (where the symmetric fission barrier goes to zero). Even if the effective angular momentum is increased to provide for a better overall normalization between the experiment and calculation, the Z dependence of the calculated cross sections is very different from that of the experimental data.

While such a disagreement between the sequential prediction and experimental data is not sufficient to claim multifragmentation, the increased production of IMF's for the Cu and La targets correspond to estimated excitation energies of ~5 MeV/u, a value predicted by some models to be a threshold for such a process. Confirmation awaits more exclusive experiments capable of measuring the fragment-fragment correlations in a given event, but the results presented indicate that this is a most promising energy and mass regime to pursue.

*Work supported by the U.S. Department of Energy, Grant #DEFG05-87ER40321 and Contract #DEAC03-76SF00098.

References

1) J.B. Bondorf et al., Nucl. Phys. **A443**, 321 (1985) and J.B. Bondorf et al., Nucl. Phys. **A444**, 460 (1985).

2) D.H.E. Gross, Phys. Letts., **203B**, 26 (1988).

3) C. Ngo, Nucl. Phys. **A488**, 233c (1988).

4) R.J. Charity et al., Nucl. Phys. **A483**, 371 (1988).

5) D.R. Bowman et al., Phys. Lett. **189B**, 282 (1987).

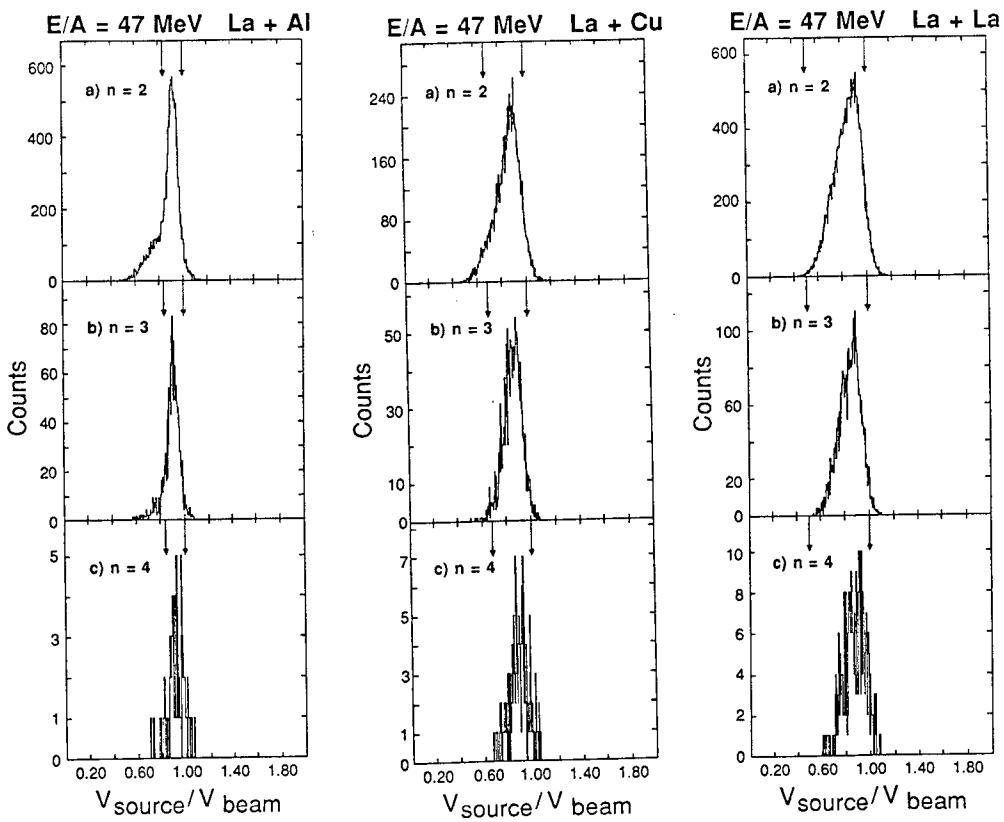

Figure 1

Inclusive source velocity (expressed as the ratio V_{source}/v_{beam}) distributions for the 47-MeV/u La reactions with Al, Cu and La targets, for fragment multiplicities (a) n = 1, (b) n = 2, and (c) n = 4. The velocity corresponding to complete fusion of the projectile-target system is shown by the solid arrow and the beam velocity is shown by the dashed arrow.

Figure 2
Comparison of the source velocities as a function of detected charge for the La + Al, Cu, and La reactions at 47 MeV/u, with fragment multiplicities (a) n =2 and (b) n = 3.

---------->

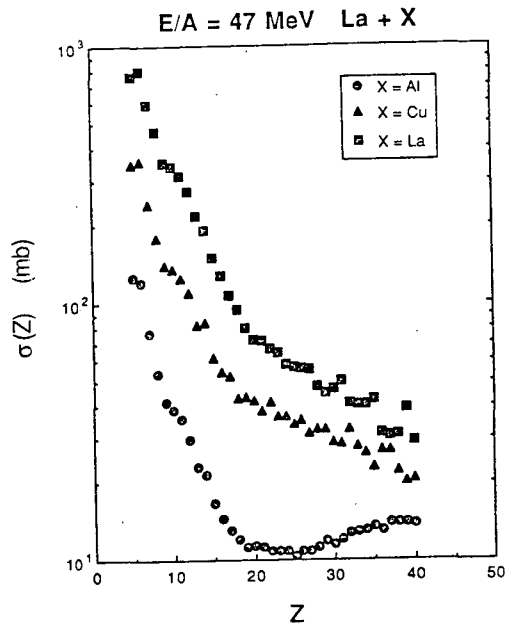

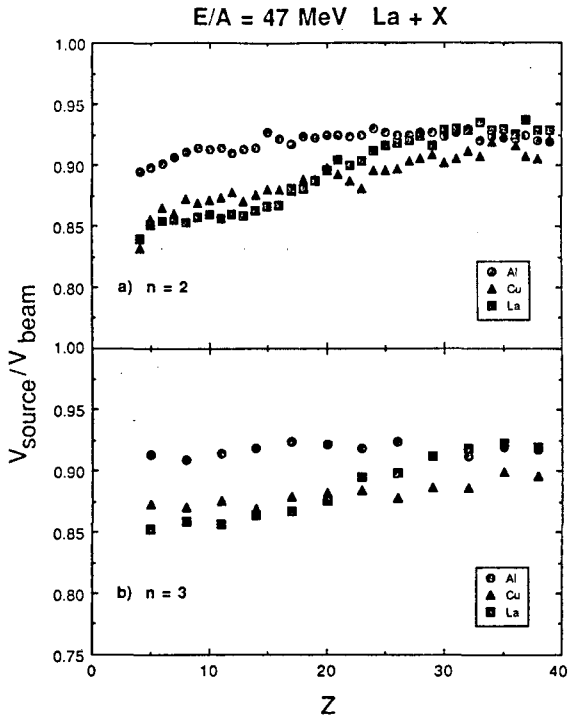

Figure 3
Angle integrated cross sections as a function of detected charge for the La + Al, Cu and La reactions at 47 MeV/u.

<--------

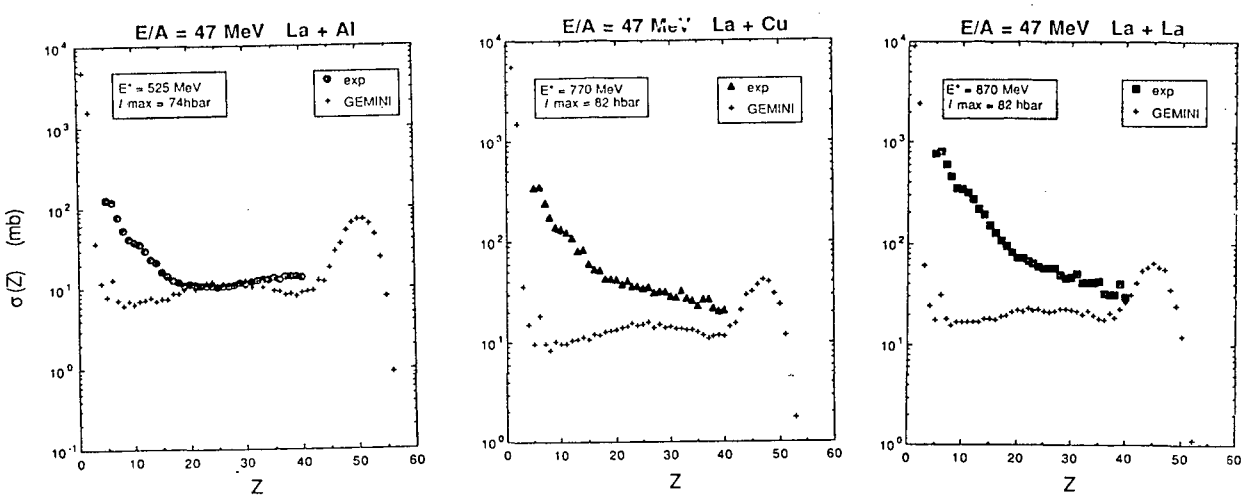

Figure 4
Comparison between the experimental and calculated cross sections of intermediate mass fragments emitted in the reactions of 47-MeV/u La with targets of Al, Cu and La. The crosses are the results of the calculation and the solid symbols are the data.

EXCITATION FUNCTIONS FOR COMPLEX FRAGMENTS EMITTED IN ^{14}N-INDUCED REACTIONS FROM E/A = 20-100 MeV*

D.E. Fields, J.L. Wile, K. Kwiatkowski, S.J. Yennello, E. Renshaw, K.B. Morley and V.E. Viola; Indiana University; Bloomington, IN 47405, and

N. Carlin, R.T. DeSouza, C.K. Gelbke, W.G. Lynch, M.B. Tsang, H.M. Xu and W.G. Gong; Michigan State University; East Lansing, MI 48824

In order to investigate the mechanisms responsible for production of complex fragments in intermediate-energy collisions, a set of systematic inclusive data have been measured for the ^{14}N + ^{nat}Ag and ^{nat}Au systems, using beams from the K500 and K1200 cyclotrons at NSCL. Beams of E/A = 20, 30, 40, 50, 60, 80 and 100 MeV ^{14}N ions bombarded high purity targets of silver and gold. An array of detector telescopes consisting of gas-ion-chamber ΔE, silicon surface barrier or passivated SiO_2 E/ΔE, and Li-drifted Si or scintillator E elements were used to measure full energy spectra, angular distributions from 20° to 165° and absolute cross sections. During these experiments, performed in two sets (E/A = 20-50 MeV at K500 and E/A = 60-100 MeV at K1200), an effort was made to keep all experimental parameters as constant as possible in order to emphasize the systematic nature of the data.

Depending on the reaction dynamics and subsequent evolution of the hot residual system, several different mechanisms have been proposed to account for the emission of complex fragments, or IMFs (IMF: $3 < Z \lesssim 15$). These fall into two general categories: "binary" processes and multifragmentation. The "binary" mechanisms describe events in which only two complex ($A > 4$) fragments are observed in the final state. Included in this category are (1) true two-body decay mechanisms which originate from the statistical decay of a fully equilibrated compound nucleus[1,2]; (2) precompound IMFs,[1,3] which resemble precompound nucleon emission, and (3) in the case of heavy-ion-induced reactions, projectile remnants,[4] e.g., transfer reactions, projectile fragmentation and damped (deep inelastic) collisions. Accordingly, the present data have been analyzed in terms of a three-source fitting routine, as described in Ref. 5. The equilibrium component was parameterized according to the prescription of Moretto,[6] the precompound component with a Maxwellian function, and the projectile remnant component according to Kiss et al.[7]

Multifragmentation, believed to occur at nuclear temperatures above 4-5 MeV, may also be expected to become important at these energies.[4] The onset of this process, which may be either sequential or instantaneous, might be expected to be reflected in these data as a possible anomaly in the excitation function or a change in the character of the energy spectra and/or angular distributions.

The characteristics of the energy spectra and angular distributions are illustrated by the data for Be fragments in Fig. 1. At backward angles (θ_{IMF} = 165°) the spectra are consistent with temperatures corresponding to a composite source with most of the available excitation energy. In addition, the angular distributions are nearly isotropic for $\theta_{IMF} > 90°$, indicating a relatively long-lived source. Coincidence studies[1] demonstrate that backward-emitted IMFs originate in reactions for which nearly full momentum transfer is achieved. Thus, the backward-angle component of the IMF yields is consistent with emission from a fully equilibrated compound nucleus.

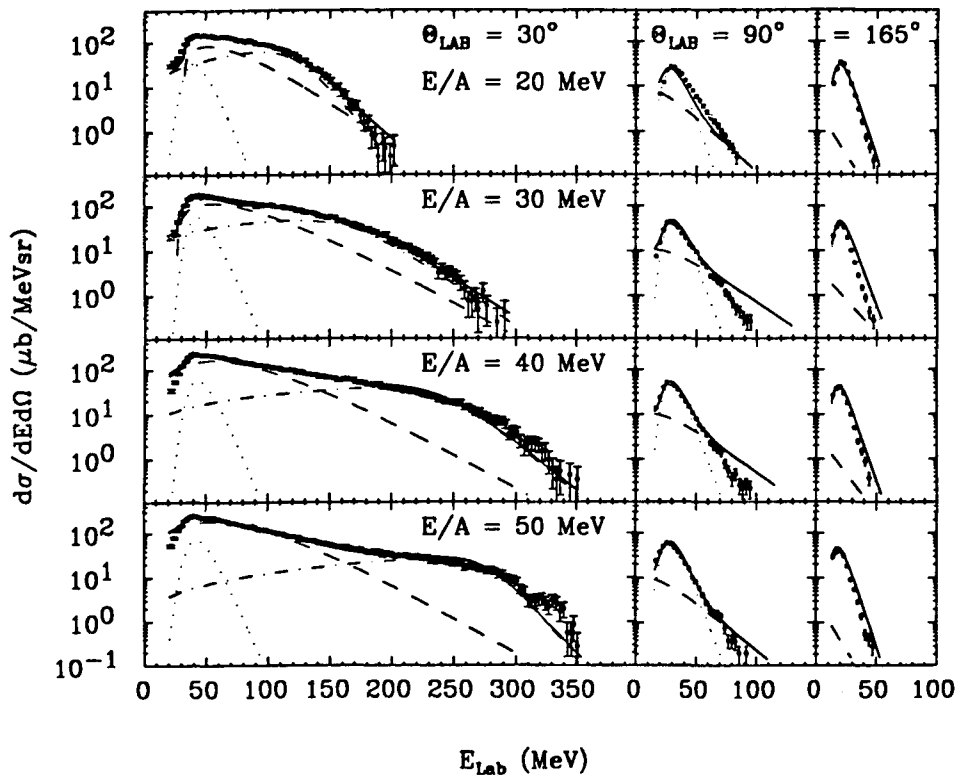

Fig. 1. Energy spectra of Z = 4 fragments from the $^{14}N + {}^{nat}Ag$ reaction. Fit components are equilibrium (dotted lines), precompound (dashed line), projectile remnant (dot-dashed line) and total (solid line). For backward-angle data, the total fit and equilibrium component are identical.

Forward of $\theta_{IMF} = 90°$ the spectral slopes become systematically harder and the angular distributions become strongly forward-peaked, indicating important contributions from non-equilibrium mechanisms to the IMF yields. For example, in Fig. 1 the backward-angle yields have been transformed into the corresponding forward-angle yields (dotted lines) assuming two-body decay kinematics. It is apparent that the non-equilibrium component dominates the yields at forward angles. Examination of such spectra for a full range of IMF Z values indicates that two separate sources contribute to the non-equilibrium yield. For IMFs with $Z > Z_{projectile}$ a Maxwellian distribution is observed with slope temperatures of the order of three times that of the equilibrated composite nucleus. For IMFs with $Z \leq Z_{projectile}$ (e.g. Fig. 1) a broad distribution of events with fragment energies near the E/A of the beam is also observed. The importance of this third source is strongly coupled to the grazing angle, decreasing in importance as the observation angle increases (Fig. 2). Coincidence studies[1] have demonstrated that the Maxwellian distribution is associated with collisions which involve large transfers of linear momentum to the target nucleus (~ 70%), supporting an emission source originating in the composite system and occurring on a fast time scale.

In contrast, the beam velocity IMFs have been shown to be associated with very small linear momentum transfers.[4] These events represent the shortest interaction times and include processes such as inelastic scattering, transfer reactions, damped collisions, etc. Although sometimes lumped together with precompound IMFs,[8] the average properties of the projectile remnants are distinctively different. For example, the energy spectra are peaked near the beam E/A, mass yields are concentrated near the projectile mass, the momentum transfer to the target residue is small,[4] and the average N/Z ratio of the fragments is close to that of the beam. In contrast, the precompound events exhibit Maxwellian spectra with Coulomb peaks, mass yields which decrease according to a power law $Z^{-\tau}$, are associated with large momentum transfers, and have average N/Z ratios greater than that of the projectile; all of these

properties are nearly identical to the IMFs formed in light-ion induced reactions, where projectile contributions are not present. Obviously, all of these classifications are schematic since there must be a continuous evolution from peripheral to precompound to fully equilibrated mechanisms, depending on impact parameter.

To demonstrate the differences between the peripheral and precompound components, it is instructive to examine the yield ratios of beryllium isotopes observed at forward angles (20°, 30° and 40°) in Fig. 2. A clear preference for neutron-excess products is apparent for the Maxwellian component relative to the beam-velocity component in Fig. 2, suggesting that the composition of the precompound equilibrium ejectiles is closely related to the N/Z of the composite target-projectile system. It is also apparent that observation of fragments with a given atomic number represents an average over several spectra which may have quite different characteristics. Hence, spectral temperatures inferred from such data must be interpreted as gross averages. Whereas neutron-excess isotopes are favored in the Maxwellian IMF component, the peripheral component is displaced toward neutron-deficient species and there is only a weak dependence on target N/Z. These data for beryllium, which are representative of all IMFs up to nitrogen, illustrate the evolution of the isotope yields as a function of increasing fragment energy for these primarily non-equilibrium products. Near the Coulomb energy, neutron rich isotopes dominate. With increasing IMF energy this trend systematically reverses, resulting in N = Z or neutron-deficient isotopes for those fragments near the beam E/A value. Thus, the isotope ratios appear to provide a means of tracing the evolution between the peripheral and precompound components of the IMF spectra.

Values of the equilibrium and non-equilibrium cross sections, σ_{EQ} and σ_{PRE} respectively, were determined by integrating the corresponding fitting functions over all energies and angles. Total IMF cross sections from the composite system, σ_{IMF}, were then determined for the sum of σ_{EQ} and σ_{PRE}. This definition has the practical effect of defining equilibrium emission in terms of processes

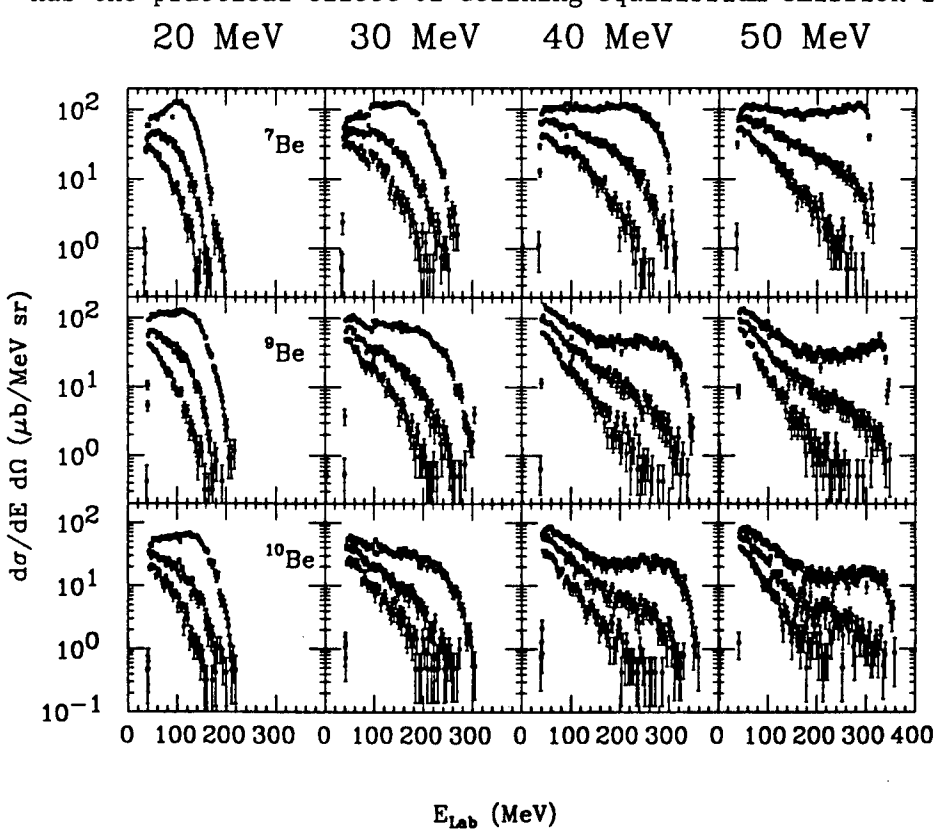

Fig. 2. Isotopic spectra of Z = 4 fragments from ^{14}N + ^{nat}Ag reaction. In each frame top spectrum is for 20°, middle for 30° and bottom for 40°.

for which the interaction time is greater than approximately one rotation period. Our operational definition of the equilibrium component is based on the back-angle data and corresponds to only an upper limit for σ_{EQ}.

Fig. 3 presents the excitation functions for equilibrium and precompound IMFs with even-Z; data above E/A = 50 Mev are preliminary. The excitation functions are slightly different for the two target-projectile combinations, with cross sections for gold exhibiting slightly more pronounced energy dependencies and slightly larger values at higher energies. At each energy the charge distributions for Z = 3-12 decreases monotonically following an approximately power-law behavior. The IMF cross sections increase slowly above energies E/A ≃ 30 MeV and have not reached a limiting value at E/A = 100 MeV. For the Ag target the increase at higher energies is somewhat slower than for the Au target; this is true for both σ_{IMF} and σ_{EQ}. The present data indicate a monotonic increase in the cross section from E/A = 20 to 100 MeV; i.e. no evidence for an anomalous increase in the cross section--which might signal a discrete threshold for multifragmentation--is observed across this energy range. However, coincidence measurements indicate that for specific collisions the fragment multiplicities frequently exceed unity, as could be expected for a multiple sequential emission of heavy fragments and/or multifragmentation processes.[9,10]

---

* Work supported by the US Department of Energy and the National Science Foundation.

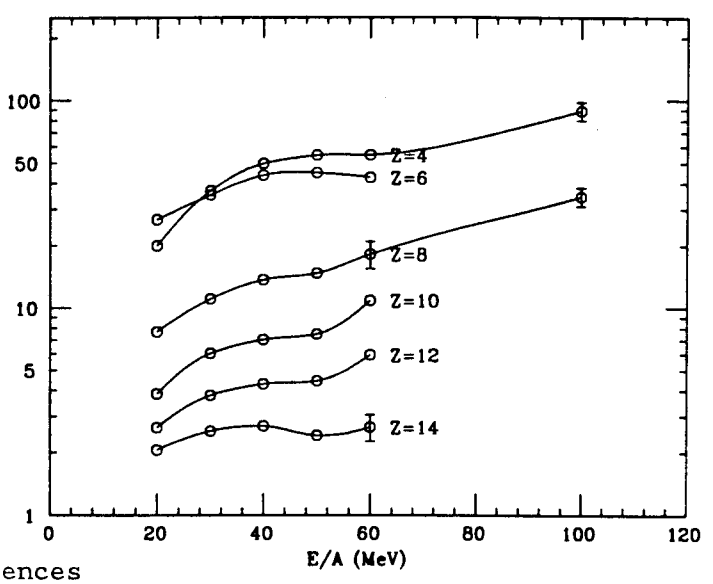

Fig. 3. Excitation functions (in mb) for even-Z fragments from the ^{14}N + ^{nat}Ag reaction. Cross sections include the sum of both equilibrium and precompound fits, i.e., $\sigma = \sigma_{eq} + \sigma_{pre}$.

References

1. M. Fatyga, et al., Phys. Rev. Lett. 58, 2527 (1987).
2. L.G. Sobotka, et al., Phys. Rev. Lett. 51, 2187 (1983).
3. K. Kwiatkowski, et al., Phys. Lett B 171, 41 (1986).
4. B.B. Back, et al., Phys. Rev. C 22, 1927 (1980).
5. D.E. Fields, et al., Phys. Lett. B 220, 356 (1989).
6. L.G. Moretto, et al., Nucl. Phys. A 247, 211 (1975).
7. A. Kiss, et al., Nucl. Phys. A 499, 131 (1989).
8. R. Borderie, et al., Phys. Lett. B 205 21 (1988).
9. R. Trockl, et al., Phys. Rev. C 39, 729 (1989).
10. Y.D. Kim, et al., Phys. Rev. Lett. 63, 494 (1989).

EOS from H.I. Collisions and Many-Body Theory

H. S. Köhler
Physics Department,
University of Arizona, Tucson, AZ 85721

1 Introductory Remarks

In Fig.1 the full curve shows the result of a theoretical saturation curve. The spheres serve to indicate that the momentum distributions in this calculation are taken to be zero-temperature fermi-distributions. Assume we like to test this theory by doing H.I. collisions. We quickly realize that we cannot put two nuclei (two fermi-spheres) together to form one zero-temperature sphere. Instead we get a system deformed in momentum-space. The exclusion-principle will force a larger density to require a higher beam-energy but this will also lead to a larger deformation in momentum-space. This deformation can to a first approximation be represented by two fermi spheres . At low energy these will overlap. We are therefore lead to consider a calculation of the energy of this system of two fermi-spheres. For a qualitative study let us consider doing this calculation with two different assumptions about the effective interaction V_{eff}.
A. $V_{eff} = V_{eff}(\rho)$.
This is a form of interaction used in many microscopic H.I. calculations.
B. $V_{eff} = V_{eff}(\rho, \mathbf{p})$.
Most Nuclear H.F. calculations use a form of this type e.g. Skyrme,Gogny etc.

Both of these effective forces contain parameters which are fitted to exactly reproduce the (full line) saturation curve. The result of the calculations for the two sphere cases are shown in broken curves marked A. and B. The A.-curve lies above the full curve because the deformation increases the kinetic energy, while the potential energy is the same as for the full curve simply because the interaction, depending on density only is independent of the deformation under constant density.

The B.-curve lies above the A.-curve because of the momentum-dependence of the force B.

The implication of this result is that assuming a two fermi-sphere (deformed fermi-sphere) curve can be deduced from the experiments the saturation curve like the full curve in fig.1 can be calculated only with the knowledge of the deformation energy in momentum-space. Furthermore this deformation energy calculation depends on the assumption about the effective force, especially its momentum-dependence.

2 Energy of Deformation in Momentum-Space

The example above serves to illustrate that we need a realistic calculation of the energy of deformation in momentum-space (EOD). One may consider doing such a calculation with one of the available effective interactions remembering that we

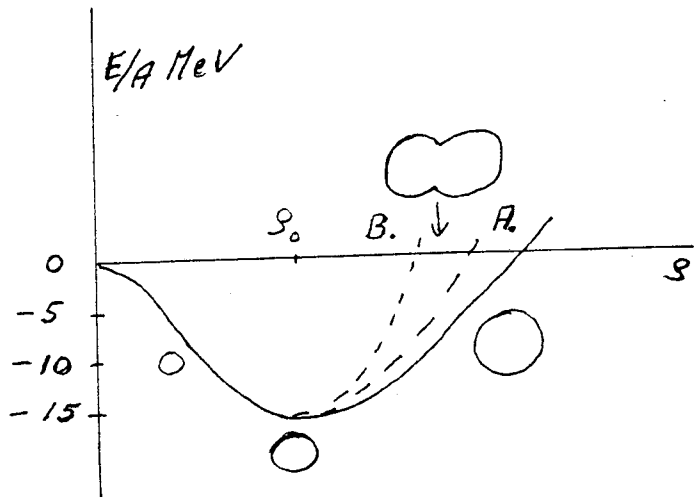

Figure 1: Curves discussed in Section 1.

already have illustrated that the momentum- dependence should be important. We must also realize that we are dealing with an excited system so that we may be outside the range of applicability of our force of choice which usually is fitted to some ground-state properties.

Faessler et al [1] (see also Beck et al [2]) have made extensive Brueckner theory calculations for the two-sphere problem with the purpose of obtaining a H.I. optical potential. Dabrowski and Köhler [3] have shown that for small deformations EOD(**P**) can be easily calculated from a few parameters of the nuclear saturation curve. Here **P** is the relative momentum between the two fermi-spheres. The parameters of the saturation curve are: Volume energy, saturation density, compressibility and effective mass. This result was á priori expected to be valid only for small **P** but was found to be quite good even for $\mathbf{P} \approx 3fm^{-1}$. The formula has also been found to be exact for forces of Skyrme-type (if its parameters are fitted to the saturation curve) which helps to explain the exended range of applicability.

3 Brueckner Calculation

It is desirable to have a microscopic input on the EOS in general , the EOD(**P**), the momentum-dependence of the mean field, possible temperature-dependence of the effective interaction as well as input about the dynamics, i.e. the collisional part of a transport theory.

A relatively simple method of obtaining such information is now shown. The method is a simplified version of Brueckner- theory bystepping the need for a N-N potential model. Instead the phaseshifts are used directly. Much of this goes back to an earlier publication [4].

The reaction matrix in Brueckner theory is for our purpose identical with an

effective interaction V_{eff}. It is defined by

$$K = v + v\frac{Q}{e + i\eta}K. \tag{1}$$

Here Q is the Pauli-operator and the energy-denominator contains propagation through the mean field. The η is included to allow energy-conserving interactions.

The energy of interaction between two nucleons isolated in a large enclosure is proportional to δ/k (δ is phase-shift) [5]. The low-density limit of The K-matrix equation should therefore give $K_0 = \delta/k$. This observation leads to the useful relation for the interaction between two nucleons in the presence of other nucleons in a large enclosure:

$$K = K_0 + K_0\left(\frac{Q}{e + i\eta} - \frac{P}{e_0}\right)K. \tag{2}$$

The nice thing with this equation is that it relates the effective interaction K directly to the phase-shifts through K_0. However this relation is only for the diagonal matrix-elements of K_0 and it is in principle not any easier to solve than the original Eq. (1). It would however still be nice if one could use Eq. (2). It does for example have the exact low-density limit and does not explicitly contain a N-N potential model but rather the phase-shifts. We shall solve Eq. (2) assuming K_0 to be a separable (in momentum-space) matrix. This is done in two steps. First define

$$K_p = v + v\frac{QP}{e}K_p \tag{3}$$

related to K by

$$K = K_p(1 - i\pi K_p Q\delta(e))^{-1} \tag{4}$$

and to K_0 by

$$K_p = K_0 + K_0\left(\frac{QP}{e} - \frac{P}{e_0}\right)K_p. \tag{5}$$

The last equation is readily solvable in momentum space for the diagonal elements K_p if we assume the K_0-matrix to be separable. In fact we find $K_p = D(k)K_0$ where D is a function of relative momentum k only and is related to the integral

$$I(k) = \int_0^\infty |K_0|\left(\frac{QP}{e} - \frac{P}{e_0}\right)d\mathbf{k}'. \tag{6}$$

by $D(k) = 1/(1 - I(k))$. The Reaction-matrix K is then obtained from Eq. (4). It is noted that the solution for the effective interaction essentially reduces to a simple integration over the experimental phaseshifts. It is in general complex . A non-zero imaginary part is obtained whenever we have a pole, that results in energy-conserving transitions. This corresponds to the collision-term and the absorptive part of the optical potential. This imaginary part is

$$K_{Im} \approx m^* \sigma_{eff} Q \tag{7}$$

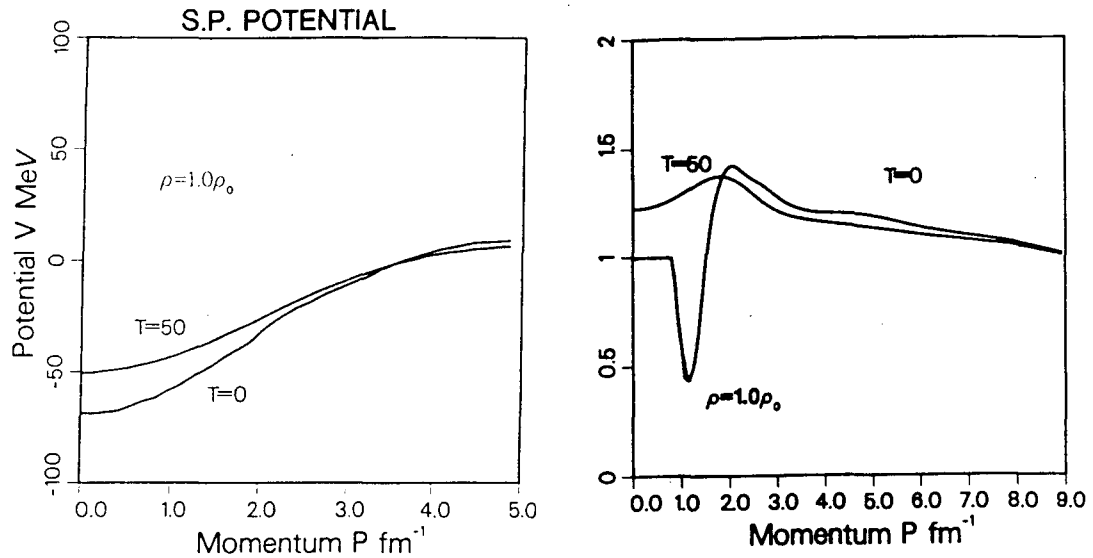

Figure 2: Left curves:Mean field as a function of momentum.Right curves: Ratio of effective to free cross-sections.

For free scattering

$$K_{Im} \approx m^* \sigma_{free} Q \tag{8}$$

We obtain a binding and saturation very similar to many-body calculations using Reid and other potentials. Fig.2 shows the momentum-dependence of the mean field at normal density and temperatures of 0 and 50 MeV respectively.

This work has evolved from discussions with Janusz Dabrowski in Tucson and in Warsaw and with Rudi Malfliet. I wish to thank both of them. This work was supported in part by the National Science Foundation, under grant PHY86-04602.

References

[1] T. Izumoto,S. Krewald and A. Faessler,Nucl. Phys. **A357** (1981) 471;

[2] F. Beck,K.-H. Mueller and H.S. Köhler, Phys. Rev. Lett. **40** (1978) 837;

[3] J. Dabrowski and H.S. Köhler,Nucl. Phys. **A489** (1989) 303.

[4] H.S. Köhler, Nucl. Phys. **A415** (1984) 37.

[5] B.S. DeWitt, Phys. Rev. **103** (1956) 1565.

Relaxation times and particle production in medium energy heavy ion collisions

A.Bonasera[1)], G.F.Burgio[1,2)] and M.Di Toro[1,2)]

1) INFN, Sezione di Catania, Italy
2) Dipartimento di Fisica, Universitá di Catania, Italy

ABSTRACT

We propose a semiclassical model in order to study intermediate energy heavy ion collisions in the framework of kinetic approaches based on the Boltzmann-Nordheim-Vlasov (BNV) equation. This model reproduces very well an exact solution of the collision integral for small deformations in momentum space, corresponding to an isoscalar giant mode. We also analyze proton emission, subthreshold pion production and Δ-resonance.

1. Introduction

In recent years medium energy heavy ion collisions have been studied extensively in the framework of microscopic kinetic equations, i.e. with Boltzmann equations including a Nordheim collision term /1-5/. Since direct solutions of this highly non-linear equation are not available, different numerical simulations of the same equations have been developed, which have appeared in the literature under different names (BUU /2/, VUU /3/, LV /1/,BNV /5/) which differ sometime in the treatment of the collision term. When studying various observables in heavy ion collisions conflicting results have sometimes been reported with the different methods, calling for a need to a better understanding of the simulation of the collision term. It thus appears to be useful to have a simpler model to study these questions, which, however, still retains the essential ingredients of the full equation. We therefore propose a phase space model, which in turn simulates the numerical solutions of the kinetic equations. Its essential feature is, that it treats the development in coordinate space macroscopically while it follows the momentum distribution microscopically. Thus we can in particular study different implementations of the collision integral. In this contribution we will first show that the model reproduces an exact numerical solution of the equations with good accuracy. We will then apply it particularly to the study of proton emission, subthreshold pion production and Δ-resonance in heavy ion collisions.

2. Specification of the model

In coordinate space we divide the nucleons macroscopically in two categories on a geometrical basis: participant nucleons in the overlapping region, which can suffer two-body collisions, and spectator nucleons, which do not. These two categories are treated separately in momentum space, where we use the microscopic test particle method /1/, in

which each nucleon is represented by N_p point test particles. The initial distribution in momentum space of two separated Fermi spheres is kept constant for the spectators but changed for the participants due to particle-particle collisions. Mean field effects are neglected /10/. The macroscopic relative velocity of the participants is calculated from their momentum distribution, thereby providing a coupling of coordinate and momentum space. The evolution is stopped, when the participant momentum distribution is spherical, after which a decay phase of the fireball may be considered.

Collisions between test-particles are treated as in ref.1 and are subjected to the condition that the nucleon mean free path corresponds to its value in nuclear matter $\lambda = \frac{1}{\sigma_{NN}\rho_o}$, where σ_{NN} is an average NN cross section ($\simeq$40 mb) and ρ_o the saturation density. Pauli blocking is treated by checking the occupation in momentum space of the final state /5/. Since the method is microscopic only in momentum space, it is numerically much faster than full BNV /5/ simulations and therefore convergence can be safely achieved using values of $N_p = 50 - 200$. To check the quality of our approach we studied the relaxation time of an isoscalar quadrupole giant resonance, which is well described by deformations of momentum distribution. We start with an ellipsoidal momentum distribution of the test particles as given in /4,5/ and make them collide until the distribution becomes spherical. We use a frozen Fermi sphere Pauli blocking as in ref.4. In fig.1 we compare the results of ref.4 (solid line) with our approach (dashed), which reproduces very well the results of ref.4, where the collision integral was evaluated exactly for small deformations in $\vec{P}$ space. We are thus lead to apply it to energetic particle and pion production.

3. Particle production

The first application of our model is the calculation of the nucleon energy spectra from the final spherical momentum distribution. In fig.2 we show proton spectra for the reaction $^{16}O +^{27} Al$ at $E_{beam} = 94\ MeV/n$ /6/. We note the very nice agreement between the experimental data and the theoretical calculations. The exponential behaviour of the spectra seems to indicate that protons are really coming from an equilibrated source.

We will now proceed to calculate pion spectra in this approach. We calculate in each nucleon-nucleon collision the perturbative probability of producing a pion of energy E_π, and generate the spectra by summing over the collisions. The elementary production cross section is parametrized from experimental data /7/. However pions strongly interact with nuclear matter and there is some absorption. We treat it in a macroscopic way by defining an absorption probability:

$$P_{abs} = 1 - exp(-\frac{d}{\lambda})$$

where d is the absorption length, which we choose equal to the nucleus size, and λ is the pion mean free path, taken to be energy indipendent. In fig.3 we compare pion spectra in the reaction $^{139}La +^{139} La$ at $E_{beam} = 246\ Mev/n$. We note the good agreement between the experimental data (o symbols) and the theoretical calculations (dashed line). We choose a mean free path $\lambda = 5\ fm$. We note that this perturbative approach is not able to reproduce the ratio R between π^- and π^+ production rates /8/.

Another application of our model is the calculation of the hard photon production rate in heavy ion collisions. We assume that photons are produced in the incoherent limit through

p-n bremsstrahlung. Details are given in ref.9. We evaluate in the model the contribution to γ emission due to the Δ-resonance decay, which is experimentally visible as a bump in the γ spectra. Since the photon elementary production cross section is unknown in the Δ-resonance region, we proceed as follows: we assume an equilibrated fireball and calculate the γ production rate by applying the Weisskopf theory and using the γ absorption cross section. Then we evaluate the γ yield for the same fireball in the incoherent limit by using an elementary production cross section which allows us to get the Weisskopf result /11/. This cross section is the input for our model. The results are shown in fig.4. We note a visible bump only for very heavy systems and high beam energy, otherwise it would be destroyed by the large fluctuations.

Conclusions

We have presented a phase space model to treat heavy ion collisions in the framework of kinetic equations, which retains the essential ingredients of full microscopic models. The model was shown to reproduce the results of full calculations and of exact limits, with special reference to the evaluation of relaxation times for giant resonances. In applying the model to heavy ion reactions, we were able to reproduce proton and pion spectra, indicating problems still open like pion reabsorption and its energy dependence, problems which require further investigation. Finally, we discussed the Δ-resonance decay through γ emission and predict a visible bump in the γ spectra only for very energetic heavy ion collisions. This is possible at the Berkeley energies through anticoincidence experiments which eliminate contributions coming from the π^o decay.

References

1. C.Gregoire, B.Remaud, F.Sebille, L.Vinet, J.Raffray, Nucl.Phys. A465(1987)317
2. G.F.Bertsch and S.Das Gupta, Phys.Rep. 160(1988)189
3. J.Molitoris and H.Stoecker, Phys.Rev. C32(1985)346
4. G.F.Bertsch, Zeit.f.Phys. A289(1978)103
5. A.Bonasera, G.F.Burgio and M.Di Toro, Phys.Lett.B221(1989)233
   G.F.Burgio, Ph.D. thesis, Catania University,1990
   A.Bonasera, G.F.Burgio, M.Di Toro and H.H.Wolter, Phys.Rev.C39(1989)2385
6. A.Palmeri, G.Pappalardo, R.Barbera, private communication
7. B.Ver West and R.Arndt, Phys.Rev. C25(1982)1979
   A.Bonasera and G.Russo, submitted for publication
8. A.Bonasera and G.F.Bertsch, Phys.Lett. B195(1987)521
9. A.Bonasera, G.F.Burgio, M.Di Toro, F.Gulminelli and H.Wolter, Nuovo Cimento, January 1990
10. A.Bonasera and C.Gregoire, Nuovo Cimento 102A(1989)1301
11. A.Bonasera and F.Gulminelli, Phys.Rev.C39(1989)1179

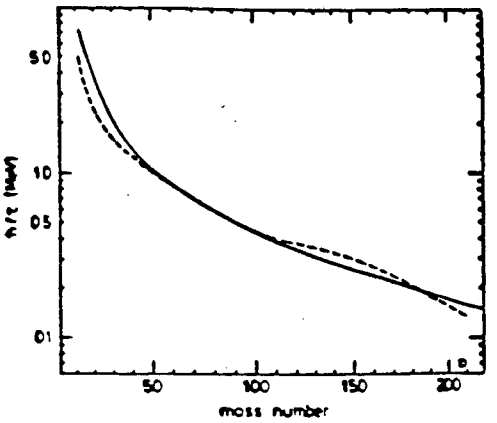

Fig. 1

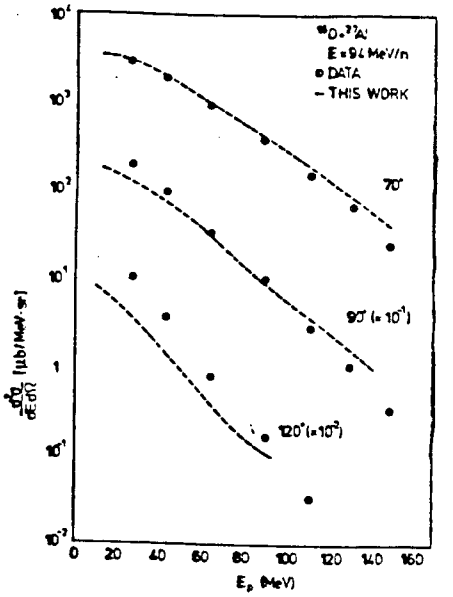

Fig. 2

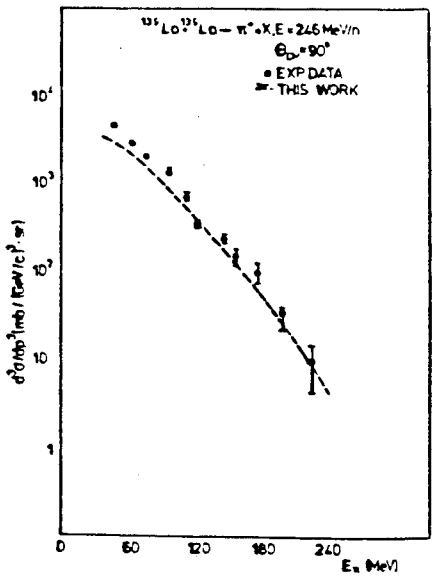

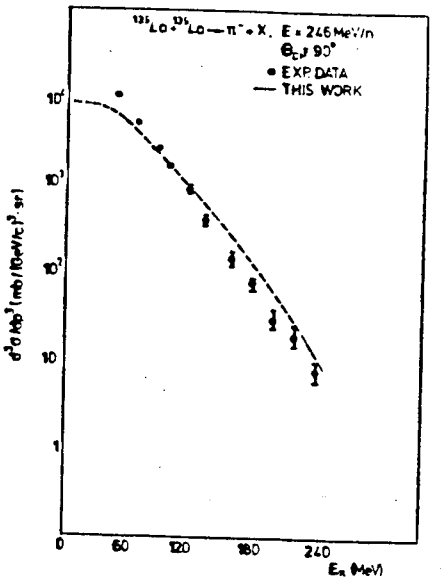

Fig. 3

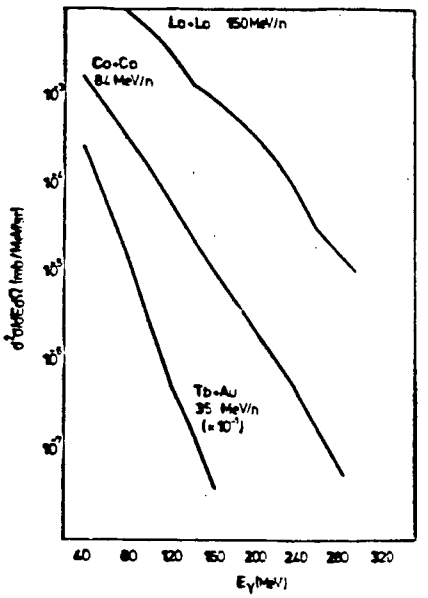

Fig. 4

OFF SHELL EFFECTS IN MULTIPARTICLE SCATTERING

E. A. Remler
Department of Physics
The College of William and Mary
Williamsburg Virginia 23185

This paper emerges from a recent study [1] of the connection between the multiple scattering series of a multi-particle theory and its dynamics as described by a space-time simulation. Assuming the particles' four-point functions and (Feynman) propagators as given, the goal is to derive the simulation's rules. The first step is to take the covariant Wigner transform of the time ordered amplitude approximated by the multiple scattering series.

$$(x_a\ x_b\ x_c\ \ldots|\Psi\rangle = \langle vac|\mathcal{T}\ [\ \Phi(x_a)\ \Phi(x_b)\ \Phi(x_c)\ \ldots]|\Psi\rangle \quad (1)$$

This provides an expression for the amplitude in terms of 8 dimensional phase space variables which can be simplified by using statistical approximations. Statistical approximations cannot be made outside of a density matrix formalism and conversely, using the density matrix without making a statistical approximation is pointless. Thus the assumption is always made that we deal with many particles and that all measurements consist of sums over very many states (inclusivity). This is always true in reality.

The Wigner Transform of Eq. 1 is th quantum analog of the classical Covariant Distribution Function (CDF)

$$(x,p|\rho) \equiv \sum_c \rho_c \prod_a \int_0^\infty d\tau\ \ \delta(x_a - x_{ca}(\tau))\ \delta(p_a - p_{ca}(\tau)) \qquad (2)$$

where $x_{ca}(\tau))$ $p_{ca}(\tau)$ are classical 8 dimensional phase space trajectories for particle 'a'; trajectory 'c' has probability ρ_c. The classical CDF describes particles moving along smooth paths lying on an

shell(Hamiltonian = constant). Thus the classical CDF does not fill 8N dimensions. In contrast, the quantum CDF does fill 8N dimensions. The picture generated by the multiple scattering series is of system trajectories consisting of straight line segments connecting collisions. Collisions produce off-mass shell particles and they are propagated away from the collision point by an off-mass-shell propagator.

From just these facts, one can conclude that:

1) Almost all system paths end up with at least one particle off shell; these paths do not contribute to final state measurements.

2) Such paths provide the overwhelming contribution to intermediate state properties of systems.

3) A theory neglecting such paths is topologically incorrect.

The description of particle propagation between collisions is provided by the Wigner Propagator - the Wigner Transform of the Feynman Propagator. Applying a statistical approximation, for timelike particles it takes the form

$$G(x'-x,p) \approx \int_0^{+\infty} d\tau \; (2\pi) \; \gamma(p,\tau) \; \delta(x'-x-v\tau) \tag{3}$$

$$\gamma = (2\pi|p|)^{-1} \sin((|p|-M)2\tau)/(|p|-M) \tag{4}$$

The factor γ encapsulates the essential difference between classical and QC scattering. It is normalized such that

$$\int_0^{\infty} dp^2 \; \gamma(p,\tau) \approx 1 \tag{5}$$

$$\lim_{\tau \Rightarrow \infty} \gamma = \delta(p^2-M^2) \tag{6}$$

If γ is replaced by $\delta(p^2-M^2)$, G becomes exactly the classical propagator for on mass shell particles. To both understand its behavior and use it in a simulation it is necessary to bin it with respect to $W = |p|-M$ = distance off mass-shell. The statistical weight

$$\Delta\gamma(p,\tau) \equiv \int_{\Delta W} dp^2 \; \gamma(p,\tau) = \int_{\Delta W} dW \; \sin(2W\tau)/(\pi W) \tag{7}$$

is shown plotted in the first figure versus proper time up to 30 Gev^{-1}. The bin widths are .1Gev . The curve marked 0 shows the total weight of

all particles scattered in the .1 GeV wide bin centered on the mass shell. Asymptotically it approaches 1. The curve marked .1 GeV. corresponds to particles scattered with .05 GeV < W < .15GeV. Asymptotically it approaches 0 in accordance with the fact that only on mass-shell particles are measured in counters. The weight effects the contribution of a particle to the unitarity integral. In addition, if a particle is rescattered, the weight multiplies the path's contribtuion to whatever is measured. These properties can be classed as 'formation time' effects.

When a particle is produced on shell and is detected, it has a statistical weight of 1; the figure shows however that most particle have statistical weights < 1 most of the time. When an off-shell particle is 'detected' asyptotically far away, it has a statistical weight of 0. Thus only histories in which all particles emerge on shell contributed to a cross-section. But if a theoretical 'measurement' is made of , say, energy density during the intermediate state, other system histories contribute. Their contribution is generally overlooked even thoug the constitute the overwhelming majority of paths!

The time dependent normalization of scattered particles implies that unscattered particles' normalizations are also time dependent as indicated in the Figure marked Q. The normalization of the incoming beam is indicated by the constant width line. It impinges on a scattering region which will be considered to be very small on the scale of the figure. After scattering, the total weight of scattered particles increases smoothly from zero; it can still change well beyond the interaction region as is shown by the previous figure! Since total normalization must be constant, unscattered particles' weight must change in compensation.

The figure marked C show the classical situation. The emerging scattered beams and unscattered beam add up to the same total width; but each is constant.Classically, there are no time dependent normalization changes. The physics is as follows: classically a particle is either scattered or unscattered by the time it emerges from the force field and so contributes a fixed amount whichever beam it ends up in. Quantally there are waves and there is a near wave zone which can extend far beyond the interaction region. While in it, a particle can transfer gradually to the scattered beam.

In a classical approximation (e.g. a simulation) a particle is deleted from the incoming beam as soon as it is scattered. The unscattered beam looks like that in C. But if account is taken of the 'formation time' effect just discussed, the scattered beam looks like the one in Q. Thus there is a violation of unitarity. To correct this, unscattered particles in classical approximations should have enhanced normalizations! This increases the scattering probability near the surface of systems relative to what would be calculated classically.

[1] E.A.Remler,"Simulation of Multiparticle Scattering", William and Mary Preprint, Nov. 1989. Submitted to Annals of Physics.

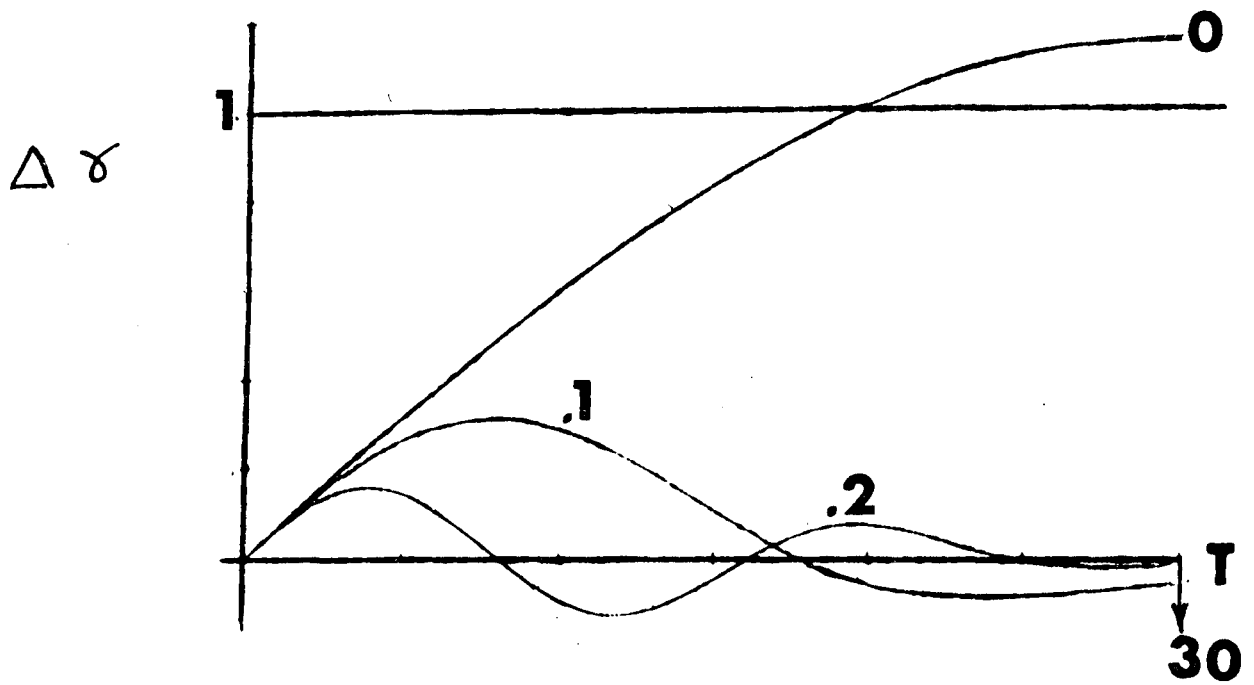

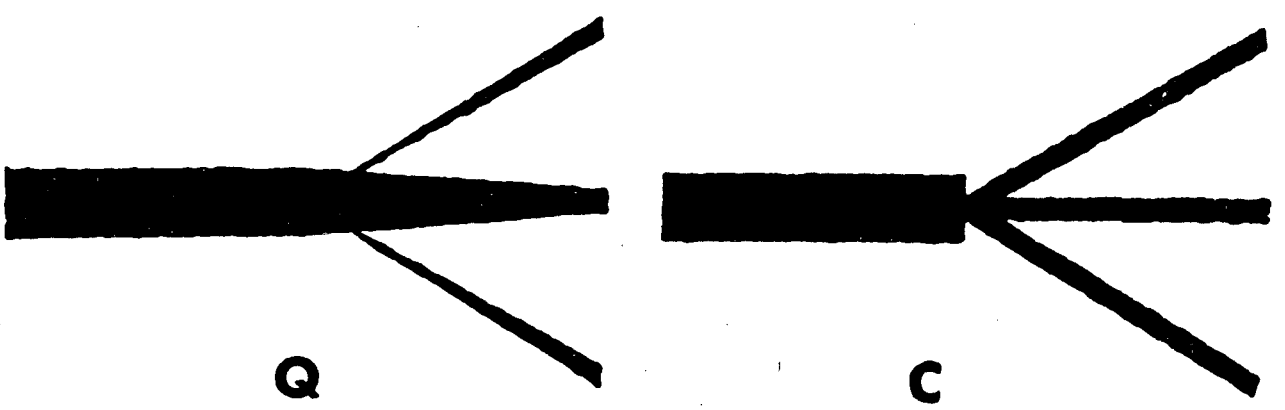

MULTIPARTICLE INTERACTIONS IN HIGH-ENERGY COLLISIONS WITH NUCLEI

P. Danielewicz* and Boyong Chen
National Superconducting Cyclotron Laboratory and Department of Physics and Astronomy, Michigan State University, East Lansing, MI 48824, USA

It is common to treat the high-energy collisions with nuclei as a superposition of elementary binary collisions of particles. Within such tratment it is not possible to account for the phenomenon of backward particle production [1], and findings from electron scattering [2]. It is also difficult to explain the subthreshold particle production [1]. We attempt to describe the experimental results in terms of multiparticle interactions [3].

Figure 1 shows the spectrum of the backward emitted protons in

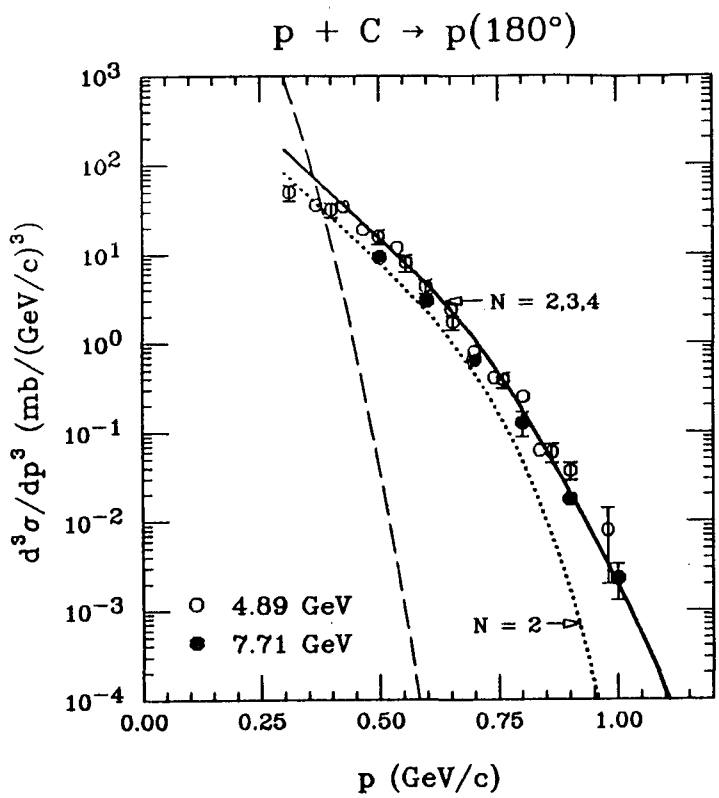

Fig. 1. Cross section for backward proton emission in proton-nucleus interactions. The data are from Refs. [4] (open circles) and [5] (filled circles). Solid line indicates the cross section for emission from the collisions with two, three, and four target nucleons. The dotted line indicates the contribution from collisions with two target nucleons (6). The long-dashed line represents a rough estimate for maximum contribution to the cross section from the fragmentation process, given by $Z\sigma_R f(p)$ with the reaction cross-section σ_R = 255 mb.

high-energy proton-carbon collisions [4,5]. The Fermi momentum limits the low-momentum region where protons originate from the decay of residual nucleus. Further, the Fermi momentum represents the edge of the phase space for the direct emission in an interaction with a single target nucleon. The tails saturating with the bombarding energy and extending into extreme momenta are also observed in the backward direction in the spectra of mesons, as well as when heavier nuclei, mesons, and leptons are used as projectiles.

The threshold energy for antiproton production in pp collisions is equal to 5.6 GeV. The production of antiprotons has been first observed in p-copper collisions at energies 5 and 6.1 GeV [6]. Later the observations have been extended down to 2.9 GeV [7]. The Fermi motion can be used to explain the production cross-sections, assuming an interaction of projectile proton with single target nucleon, but only for energies close to the threshold, Fig. 2.

The dynamics can be studied by examining the products of a reaction or the fate of a projectile. The weakness of electromagnetic interaction ensures

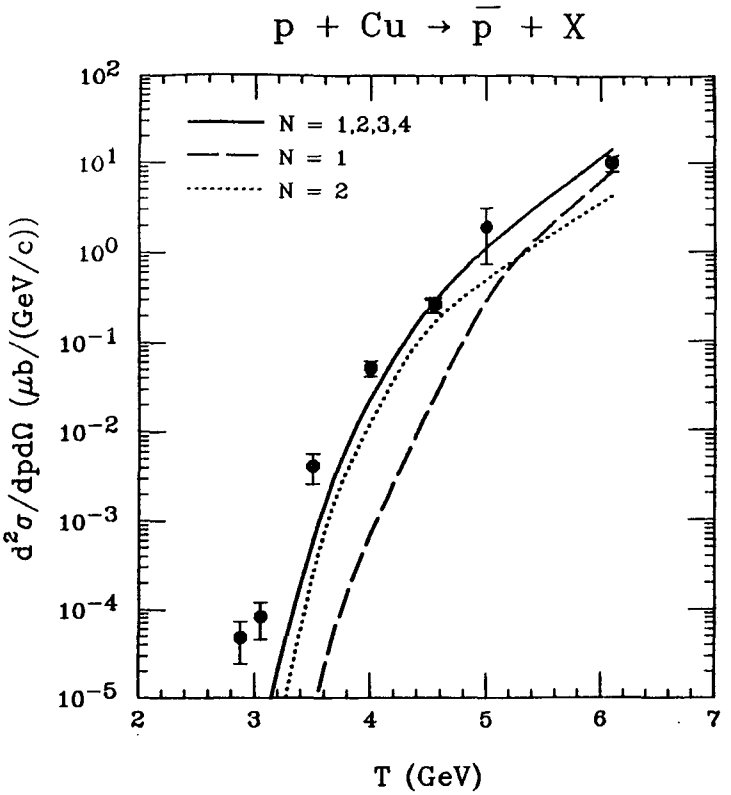

Fig. 2. Cross section for antiproton production as a function of bombarding energy for protons incident on copper. The normalized data are from Refs. [6] and [7]. Solid line indicates the calculated cross section for production in collisions with one, two, three, and four target nucleons. The long-dashed and dotted lines indicate, respectively, the contributions from collisions with one and two nucleons.

that an electron scattered quasielastically from a nucleus interacts only once. The cross section can be factorized for high energies into a factor associated with electromagnetic interaction, and a function F(y) related to the distribution of nucleons in energy and momentum S(p,E) with

$$F(y) = 2\pi \int^{\bar{E}} dE \int_{|y+E-\bar{E}|}^{\infty} dp\ pS(p,E). \tag{1}$$

Here $y = -q + \sqrt{(\bar{E} + \omega)^2 - m^2}$, and q and ω are the momentum and energy, respectively, transferred to the nucleus, $\bar{E} = m - \Delta$, and Δ is the separation energy. In Fig. 3 the scaling function F(y) extracted from the data [2] is compared with the function evaluated assuming an independent-particle motion in the mean potential field,

$$S(p,E) \simeq f(p)\delta(E - (m - B)), \tag{2}$$

with f - the nucleon momentum distribution taken from the oscillator model, and B - the binding energy per nucleon. The experimental function F(y) exhibits a tail extending to large negative values of y, that cannot be explained by considering only an independent motion of nucleons.

Within the real-time many-body theory we examined the possibility of going beyond the superposition of binary collisions in describing a high-energy reaction process. The evolution of the distribution of particles g(p,x) is governed by the equation of Boltzmann form, written here for fermions,

$$\frac{\partial g}{\partial t} + \mathbf{v}\cdot\frac{\partial g}{\partial \mathbf{r}} + \mathbf{K}\cdot\frac{\partial g}{\partial \mathbf{p}} = \Sigma^{<}(1 - g) - \Sigma^{>} g\ . \tag{3}$$

The vector **K** is the average force and $\Sigma^{<}$ and $\Sigma^{>}$ are the production and absorption rates, respectively. We found [8] that the rates can be expanded in the number of interacting particles,

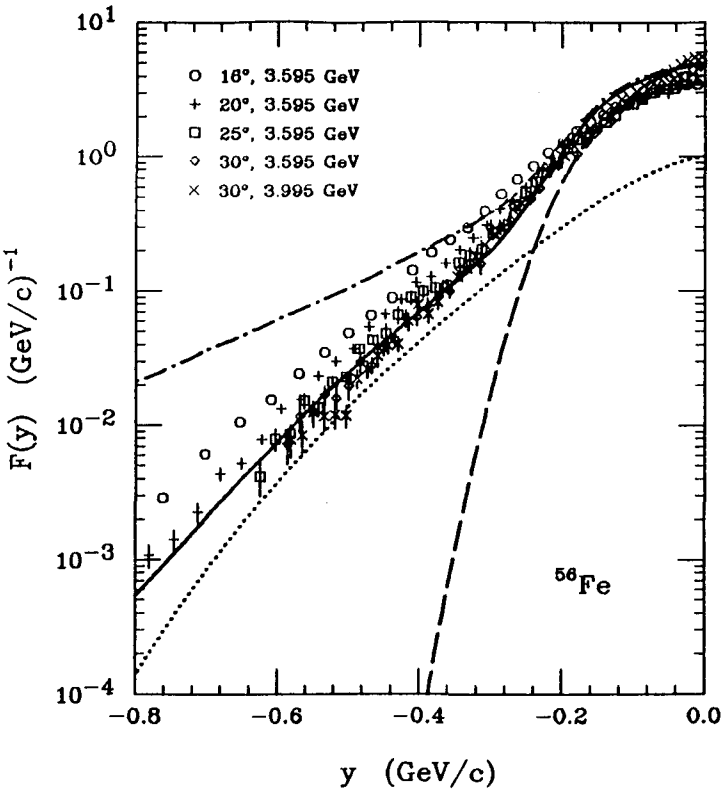

Fig. 3. Scaling function for ^{56}Fe. The experimental data is from Ref. [2]. Solid line indicates the result obtained from the relation of the scaling function to the spectral function. Dashed and dotted lines indicate, respectively, contributions from one and two interacting nucleons in the spectral function. Dash-dotted line indicates the result that follows when one simplifies the energy dependence of the spectral function making the scaling function a functional of momentum distribution only.

$$\Sigma^{<} = \Sigma_2^{<} + \Sigma_3^{<} + \dots , \tag{4}$$

where $\Sigma_k^{<}$ is a rate for production in the processes involving k particles in the initial state. These rates assume a simple form

$$\begin{aligned}\Sigma_k^{<}(p,E) = \sum_n \int & dp_1' \dots dp_k' dp_1 \dots dp_{n-1} \delta(p_1' + \dots + p_k' - p - p_1 - \dots - p_{n-1}) \\ & \times \delta(E_1' + \dots + E_k' - E - E_1 - \dots - E_{n-1}) g(p_1') \dots g(p_k')(1 - g(p_1)) \\ & \times \dots (1 - g(p_{n-1}))|T^{k\to n}|^2 ,\end{aligned} \tag{5}$$

where $T^{k\to n}$ is an amplitude for a process with k particles in the initial state and n in the final. The many-body amplitudes can be expanded in terms of the amplitudes with two bodies in an initial state, that are treated as elementary, and the propagators.

Numerically we have found that the process indicated in Fig. 4 with two target nucleons, gives a large contribution to the backward proton production. On using $g(p,x) = f(p)\rho(x)$, where ρ is spatial density, and integrating the production rate over the projectle trajectory, we get for the production cross section in the limit $p^i \to \infty$:

$$\begin{aligned}\frac{d^3\sigma}{dp^3} = \frac{1}{(2\pi)^3 E} Z\sigma_{NN} \bar{\rho} \int & dp_1' dp_2' f(p_1') f(p_2') \ \frac{1}{2}|T|^2 \left(\frac{2m}{(p_1' + p_2' - p)^2 - m^2}\right)^2 (2(m - B) \\ & - p_1'^z - p_2'^z - E + p^z)\Theta(2(m - B) - p_1'^z - p_2'^z - E + p^z) .\end{aligned} \tag{6}$$

The probability of two nucleons encountering each other is proportional to the average density in a nucleus $\bar{\rho} = \frac{1}{A}\int d^3x\ \rho^2(x)$. In addition to the production in interactions of projectile with two target nucleons, one expects the production

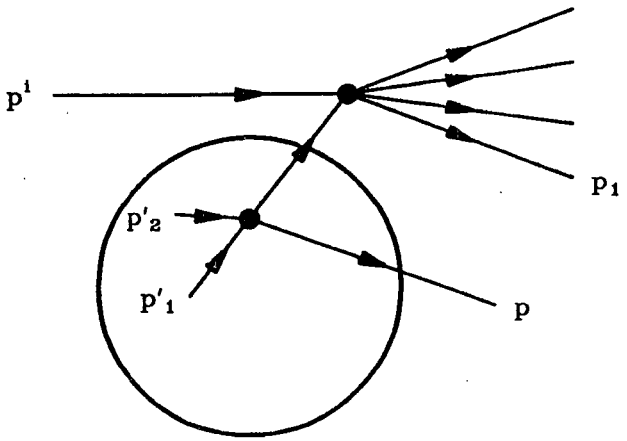

Fig. 4 Three-body collision process.

in interactions with three and more target nucleons. The respective partial cross sections are proportional to the higher powers of density. The net estimated cross section from the tree processes such as in Fig. 4, representing an expansion of the target wavefunction, is shown in Fig. 1. The dependence on density results in the nontrivial dependence of the cross section for backward emission on target mass [3], going beyond the proportionality to proton number, in fair agreement with data.

When the same processes as in the backward proton emission are included in the antiproton production, in addition to the process with a single target nucleon, and with the production taking place in the interaction vertex involving a projectile, a much improved agreement with the subthreshold data is obtained, Fig. 2. The cross section is normalized by assuming that an antiproton can be produced only in the first collision of the projectile.

Finally, we take into account the multiparticle processes in the electron scattering by calculating the scaling function F from Eq. (1), on approximating S(p,E) in a consistent manner by

$$f(p)\delta(E - (m - B)) + \left(\frac{2m}{E^2 - p^2 - m^2}\right)^2 \left[\bar{\rho}\int dp_1' dp_2' f(p_1') f(p_2') \frac{m}{(2\pi)^3 E_{p_1'+p_2'-p}}\right.$$

$$\left. \times \frac{1}{2}|T|^2 \delta(E + E_{p_1'+p_2'-p} - 2(m - B)) + \ldots \right], \qquad (7)$$

see Fig. 3. The dots in (7) indicate the terms involving 3 and 4 target nucleons.

Current efforts concentrate on the use of the NN scattering matrix extracted from microscopic calculations, rather than parametrized, and on the description of backward pion production.

This work was supported in part by the National Science Foundation under Grant No. PHY-8905933.

*On leave of absence from Institute of Theoretical Physics, Warsaw University, Warsaw, Poland.

[1] S. Frederiksson et al., Phys. Rep. **144**, 187 (1987).
[2] D. B. Day et al., Phys. Rev. Lett. **59**, 427 (1987); R. D. McKeown, AIP Conference Proc. **176**, 490 (1988).
[3] P. Danielewicz, report MSUCL-709, 1989.
[4] J. V. Geaga et al., Phys. Rev. Lett. **45**, 1993 (1980).
[5] A. M. Baldin et al., report JINR P1-11302, 1978.
[6] O. Chamberlain et al., Phys. Rev. **100**, 947 (1955).
[7] D. E. Dorfan et al., Phys. Rev. Lett. **14**, 995 (1965); A. Shor et al., report LBL-17067, 1984.
[8] P. Danielewicz, Ann. Phys. (N.Y.) **197**, 154 (1990).

Meson-Quark Coupling in the Chromo-Dielectric Model

M. R. FRANK, G. FAI, and P. C. TANDY
Department of Physics, Kent State University, Kent, OH 44242

Due to the difficulties associated with calculating nuclear properties accurately in QCD, *models* attempting to capture major features of the low-energy behavior are frequently employed. We are interested in nontopological solitons, patented after the Friedberg-Lee model,[1] and capable of generating the coupling to effective meson fields associated with $\bar{q}q$ vacuum fluctuations.

Here we consider a model,[2] which incorporates the confinement mechanism at the outset through a color dielectric function. This chromo-dielectric model (CDM) is described (in Euclidean metric) by

$$\mathcal{L} = \overline{q}(\gamma \cdot \mathcal{D} + m_q)q + \mathcal{L}(\phi) + \frac{1}{4}\kappa(\phi)F^a_{\mu\nu}F^a_{\mu\nu}\,, \tag{1}$$

where F is the usual gluon field strength tensor in terms of the gluon field A^a_μ, the gauge covariant derivative is $\mathcal{D} = \partial - igA^a\frac{\lambda^a}{2}$, and ϕ is a scalar field with $\mathcal{L}(\phi) = \frac{1}{2}(\partial_\mu\phi)^2 + U(\phi)$. The color dielectric function, $\kappa(\phi)$ is chosen so that $\kappa \approx 1$ inside the soliton volume and $\kappa \to 0$ sharply at the edge of the soliton, where $U(\phi)$ approaches the absolute minimum. Thus the inverse gluon propagator is suppressed at large distances, forcing confinement of gluons and thus of the quarks, through an increasingly large self-energy. The CDM has explicit chiral symmetry broken only by the small current quark mass m_q. However, the gluon dressing of the quarks also generates an effective nonlinear coupling of the quarks to ϕ, and the underlying chiral symmetry dictates a Goldstone pion, which can only arise from a $\bar{q}q$ correlation.

It is therefore of interest to apply recent developments[3,4] in the techniques of bosonization of quark fields to the CDM to analyze the effective $\bar{q}q$ fluctuations with particular emphasis on the pion mode. The results can be compared with recent work[5] which deduced the pionic coupling in this model from a Ward-Takahashi identity. Since $\kappa(\phi)$ is supposed to approximately account for much of the nonperturbative gluon self interaction, we consider only a two-point gluon propagator connecting quark currents, so that a generating functional can be written as

$$Z = \int D\overline{q}DqD\phi \exp\left[-\frac{1}{2}TrLn\widetilde{D}^{-1} - S[\phi] - \int d^4x d^4y\left\{\overline{q}G_0^{-1}q + \frac{1}{2}j_\alpha\widetilde{D}_{\alpha\beta}j_\beta\right\}\right]. \tag{2}$$

Here $G_0^{-1}(x-y) = (\gamma\cdot\partial + m_q)\delta(x-y)$, the quark current is given by $j_\alpha(x) = g\overline{q}(x)\frac{\lambda^a}{2}\gamma_\mu q(x)$ with $\alpha = (a,\mu)$, and $\widetilde{D}_{\alpha\beta}(x,y)$ is an effective two-point gluon prop-

agator, whose dependence on the scalar field ϕ through κ is not shown explicitly. Apart from the field ϕ, the model at this level is a nonlocal form of the Nambu-Jona-Lasinio model.[6] Due to the dependence of $\widetilde{D}$ upon ϕ, the $TrLn\widetilde{D}^{-1}$ term cannot be absorbed into the normalization at this stage. For the sake of further discussion, we take a simple form, $\widetilde{D}_{\alpha\beta}(x,y) \approx D_{\alpha\beta}(x-y)/\kappa(\phi(\frac{x+y}{2}))$, where $g^2 D_{\alpha\beta}(x) = \delta_{\alpha\beta}\int d^4q\alpha_s(q^2)q^{-2}\exp(iqx)$, and $\alpha_s(q^2)$ is a running coupling constant to account for short distance non-Abelian effects. In the absence of ϕ and κ, such a phenomenological $D_{\alpha\beta}(x-y)$ was previously shown to give reasonable correspondence with physical meson properties.[7] The above dependence of $\widetilde{D}$ upon $\kappa(\phi)$ is an ansatz proposed[5] for treating κ as locally constant.

Fierz reordering gives $-\frac{1}{2}g^2\int d^4xd^4y f_\theta(y,x)\widetilde{D}(x,y)f_\theta(x,y)$ for the last term of Eq. (2), where $f_\theta(x,y) = \overline{q}(y)\Gamma_\theta q(x)$. (The subscript θ labels the transformation character of the terms $\Gamma_\theta \otimes \Gamma_\theta$ from the Fierz reordering of $\frac{\lambda^a}{2}\gamma_\mu \otimes \frac{\lambda^a}{2}\gamma_\mu$ in color, flavor, and Lorentz space. We keep only color singlets. The color octet sector requires a different procedure.[4]) This bilocal structure can be converted into an integral over bilocal Bose fields $B^\theta(x,y)$, such that only a quadratic dependence on the quark fields remains. The integrand of Eq. (2) is to be multiplied by unity in the form

$$1 = \exp\left\{\frac{TrLn(g^2\widetilde{D})^{-1}}{2}\right\}\int DB^\theta \exp\left\{-\frac{1}{2}\int d^4xd^4y\frac{B^\theta(x,y)B^\theta(y,x)}{g^2\widetilde{D}(x,y)}\right\}. \qquad (3)$$

After a shift $B^\theta(x,y) \to B^\theta(x,y) + g^2\widetilde{D}(x,y)f_\theta(x,y)$, the fourth-order term in the quark fields is eliminated, and the $TrLn$ terms combine into a constant. The integration over the quadratic quark term may now be carried out to give

$$Z = \int D\phi DB \exp\left\{-S[\phi] + TrLnG^{-1} - \int d^4xd^4y\frac{B^\theta(x,y)B^\theta(y,x)}{2g^2\widetilde{D}(x,y)}\right\}, \qquad (4)$$

where $G^{-1}(x,y) = (\gamma\cdot\partial + m_q)\delta(x-y) + \Gamma_\theta B^\theta(x,y)$. Further details of this bosonization may be found in the literature,[3,4,7] for the situation where ϕ is absent. We wish to treat ϕ at the classical level only, and examine 'mesonic' $\bar{q}q$ fluctuations of B above its classical value. The classical configurations are obtained from $\delta\hat{S}/\delta\phi = 0$, $\delta\hat{S}/\delta B^\theta = 0$, where $\hat{S}[\phi, B]$ is the action in Eq. (4). (The classical $\overline{\phi}$ is coupled to a quark source as well as to the source from $U'(\overline{\phi})$, but the details need not concern us here.)

The classical $\overline{B}$ yields a Schwinger-Dyson equation for the quark self energy:

$$\Sigma(x,y) = \Gamma_\theta\overline{B}^\theta(x,y) + m_q\delta(x-y) = g^2\widetilde{D}(x,y)\frac{\lambda^a}{2}\gamma_\mu\bar{G}(x,y)\frac{\lambda^a}{2}\gamma_\mu + m_q\delta(x-y), \qquad (5)$$

where $\widetilde{D}$ depends on $\overline{\phi}$ through $\kappa(\overline{\phi})$, and $\overline{G}$ is the selfconsistent quark propagator containing Σ. In momentum space conjugate to $x-y$, for a fixed value of κ, Σ has the

general form $\Sigma(p) = i(A(p^2)-1)\ \not{p} + B(p^2) + m_q$, where coupled nonlinear equations for $A(p^2)$ and $B(p^2)$ can be obtained from Eq. (5). The dynamical quark mass is $M(p^2) = (B(p^2)+m_q)/A(p^2)$, and approximate solutions for A and B have been considered by a number of authors.[7,8] We first make contact with the limit of a fixed massive quark used recently to estimate Σ.[2] With $\overline{G}(p) \approx \overline{G}(p=0) = 1/B(0)$, A can be set to unity, and one obtains from Eq. (5) the estimate

$$B(0) \approx \frac{1}{\sqrt{\kappa}} \left[\frac{16}{3} g^2 \int \frac{d^4q}{(2\pi)^4} D(q^2) \right]^{1/2} . \tag{6}$$

The coordinate space static version of this integral with an appropriate gauge choice was used earlier[2] with a convergence factor. Since κ varies slowly with $\overline{\phi}(\frac{x+y}{2})$, and sharply falls to zero as $\overline{\phi}$ approaches the vacuum value, the effective quark mass rapidly becomes infinite at the boundary of the soliton, enforcing confinement.

Consider the more general form $B(p^2) \sim c\kappa^{-1/2} \exp(-a^2p^2)$, which has some of the features of solutions to Eq. (5) (for $\kappa = 1$) discussed in recent works.[7] For $\kappa \approx 1$, and for a small a, there is a solution to the condition $p^2 + (B(p^2)+m_q)^2 = 0$ for the existence of a pole in the vacuum quark propagator in the physical ($p^2 < 0$) region. As κ decreases towards zero, the pole is removed as is characteristic of confining solutions. We note that without κ and ϕ (take $\kappa = 1$ over all space), Eq. (5) is capable of generating confining solutions in the sense that $A^2(p^2)p^2 + (B(p^2)+m_q)^2 \neq 0$ for any p^2, if there is enough strength in the poorly understood infrared region of the gluon propagator.[8]

We now consider the fluctuations of the original Bose field $B^\theta(x,y)$, above the classical value.[7] For fixed κ, the replacement $B(x-y) \to B(x-y)(\hat{\sigma} + i\gamma_5\tau\cdot\pi + \ldots)$ is also a solution of Eq. (5), provided $\hat{\sigma}$, π, ... are constants such that the additional factor is unitary, i.e. $\hat{\sigma}^2 + \pi^2 + \ldots = 1$. We keep only the isoscalar-scalar $\hat{\sigma}$ and the isovector-pseudoscalar π here. It is reasonable to expect that mesonic fluctuations should appear in the form $\Gamma_\theta B^\theta(x,y) = B(x-y)\left[\hat{\sigma}(\frac{x+y}{2}) + i\gamma_5\tau\cdot\pi(\frac{x+y}{2}) + \ldots\right]$, where the classical configurations are $\hat{\sigma} \to 1$ and $\pi \to 0$. This corresponds to allowing fluctuations in just those Bose fields characterized by the Fierz reordered vertex factors $\Gamma_\theta = (1, i\gamma_5\tau)$. Here, $\sigma = \hat{\sigma}(\frac{x+y}{2}) - 1$, and $\pi(\frac{x+y}{2})$ are quantum fields describing the center-of-mass motion of composite mesons with a $\bar{q}q$ content. It is not immediately obvious that the $\hat{\sigma}$ and π vertex form factors should be exactly the scalar part $B(x-y)$ of the self-energy Σ. However, this result follows from a more general analysis,[4] and is a consequence of the underlying chiral symmetry and the close connection between Eq. (5) and the ladder Bethe-Salpeter equation for $\bar{q}q$ composites.

The extra complication present in the CDM is that there is a dependence of $B(x-y)$ on $\kappa(\overline{\phi}(\frac{x+y}{2}))$, of the form $\kappa^{-1/2}$, which has been taken to be much slower than the

dependence of the fluctuation fields on $\frac{x+y}{2}$ for the sake of discussion. Any dependence of $\Gamma_\theta B^\theta(x,y)$ upon $\frac{x+y}{2}$ allows the quarks to transfer momentum to other objects (e.g. to σ and π linearly, or to the background $\overline{\phi}$ field in a nonlinear way). For the CDM we have with $B \approx B'/\sqrt{\kappa}$,

$$\overline{q}(x)\Gamma_\theta B^\theta(x,y)q(y) = \overline{q}(x)\frac{B'(x-y)}{\sqrt{\kappa(\overline{\phi}(\frac{x+y}{2}))}}\left[1+\frac{1}{f_\sigma}\sigma(\frac{x+y}{2})+\frac{i\gamma_5}{f_\pi}\tau\pi(\frac{x+y}{2})\right]q(y) \quad (7)$$

as the quark-meson coupling, where the decay constants f_σ and f_π are given by a single quark loop, self-regulated by a pair of vertex form factors $B'(x-y)/\sqrt{\kappa}$. For quark propagators dominated by zero-momentum values, thus scaling as $\sqrt{\kappa}$, the decay constants and masses are independent of κ. The quark-pion vertex function is $B'(x-y)i\gamma_5\tau/(f_\pi\sqrt{\kappa})$, in agreement with what was deduced from PCAC arguments.[5] The chiral partner σ appears naturally in this development.

In summary, bilocal field methods can provide a useful perspective upon the generation of a pionic $\bar{q}q$ field necessary to implement the underlying chiral symmetry in the CDM. However, the spatial dependence of the phenomenological background field ϕ and the assumed dielectric function κ make it difficult to develop an appropriate approximation strategy. Without ϕ and κ, the prospect of confinement being embodied in the strictly translation invariant functions $A(p^2)$ and $B(p^2)$ seems particularly attractive and efficient.

This work was supported in part by grants NSF PHY88-05633 and DOE DE-FG02-86ER40251.

---

[1]R. Friedberg and T.D. Lee, Phys. Rev. D**15**(1977)1694, Phys. Rev. D**16**(1977)1096.

[2]G. Fai, R.J. Perry, and L. Wilets, Phys. Lett. B**208**(1988)1.

[3]J. Praschifka, C.D. Roberts, and R.T. Cahill, Phys. Rev. D**36**(1987)209.

[4]C.D. Roberts, R.T. Cahill, and J. Praschifka, Ann. Phys. (N.Y.)**188**(1988)20, R.T. Cahill, J. Praschifka, and C.J. Burden, Aust. J. Phys. **42**(1989)161.

[5]G. Krein, P. Tang, L. Wilets, and A.G. Williams, Phys. Lett. B**212**(1988)362.

[6]Y. Nambu and G. Jona-Lasinio, Phys. Rev. **122**(1961)345.

[7]R.T. Cahill and C.D. Roberts, Phys. Rev. D**32**(1985)2419.

[8]G. Krein, P. Tang, and A.G. Williams, Phys. Lett. B**215**(1988)145, C.D. Roberts and B.H. J. McKellar, Phys. Rev. D**41**(1990)672.

On Relativistic Hydrodynamics

C. Alonso, J. Wilson, T. McAbee, and R. Vogt
Lawrence Livermore National Laboratory
Livermore, CA, 94550

This addendum to the Proceedings was created post-conference to describe the philosophy and goals of the more detailed papers presented at this Winter Workshop by J. Wilson [1] and R. Vogt [2]. We hope it addresses some of the questions raised by participants during the workshop.

This project was initiated some years ago when it came to the attention of J. Wilson and C. Alonso that the nuclear community was applying hydrodynamics to relativistic nuclear collisions. Since we had extensive experience in numerical hydrodynamics, including relativistic applications in astrophysics, we were interested in determining if our methods had application in relativistic heavy ion collisions.

We soon learned that the word "hydrodynamics" conveys several meanings in the heavy ion field. Many people, especially experimentalists, seem to use the word synonomously with the "Landau hydro" method, which treats only the expansion phase of a nuclear collision by applying relatively simple one-dimensional hydrodynamic equations; the initial conditions must be specified. The problem with this approach, of course, is that the results are highly dependent upon the initial conditions. In the case of relativistic nuclear collisions the initial conditions are likely to be extremely complex, possibly including high-density shock waves and pion and other particle production, including resonances.

Recognizing this, we set out to use our expertise to perform more complete hydrodynamic calculations which would have the following attributes:

- Initial conditions would be exact within a one-fluid model; namely, the two nuclei would initially be separated spatially, travelling toward each other at relativistic speeds in the calculational mesh

- The subsequent collision would be followed with full time-dependence, the time resolution being of the order of 0.01 fm/c

- The calculation would have full 3D spatial resolution, typically of the order of 0.25 fm in the rest frame

- The calculation would include shock structures in full spatial and temporal resolution

- Pion generation, scattering, and absorption would be included with full temporal and spatial resolution

- The pions would fully interact, in detailed energy balance, with the baryonic fluid.

We also wished to correct some inaccurate numerical hydrodynamics results which we observed in the literature.

These goals have been met [3,4,5]. At present we have applied our model to Bevalac [3] and CERN [5] energies.

It is worthwhile also to mention the philosophy with which we undertook these calculations:

• The calculation would be ab-initio pure hydrodynamics; that is, we would include no free parameters except those necessary to specify the equation of state and the pion cross sections.

• To ensure accuracy, our numerical method would be exercised carefully against a battery of analytical tests which we have developed over the years for the purpose of testing such codes.

• Our primary goal was to determine what observables an accurate hydrodynamics calculation actually predicts for relativistic nuclear collisions, without resorting to a set of fitted parameters or initial conditions.

• By so doing, we could learn whether a hydrodynamics approach is in fact useful for deconvolving and removing the dynamics which obscures the underlying physics (the true objective of the experiments).

• We could also examine whether the more popular approximate hydrodynamical methods, which make extensive use of fitted parameters, represent meaningful methods for fitting experimental data, or whether they in fact may be obscuring real physics issues and should therefore be avoided.

• It was only a secondary goal to fit the experimental data. By adding fitted parameters we could probably fit the data reasonably well, but this has not been our primary objective.

• By treating the pions with full spatial and temporal detail, we hoped to determine whether they represent an experimental signature of the complex conditions central in the baryonic fluid (particularly high-density shock regions) or whether they are emitted from the relatively uninteresting surface of the expanding post-shock fluid.

These objectives have also been met, at least in part. Following the above philosophy, the presentation by J. Wilson emphasized areas where accurate relativistic hydrodynamics, as defined above, does *not* do a good job of fitting the experimental data [1]. In brief, detailed hydrodynamics is generally able to predict the calorimetry of the baryonic fluid; but it fails, by about a factor of two, to predict the pion multiplicity (it predicts too few) and energy (it predicts too energetic pions). Our calculations also showed conclusively that the pion component interacts heavily with the baryonic fluid and both components are necessary for a meaningful hydrodynamics calculation.

This already tells us something about the underlying physics: the method with which pions are generated in the nuclear medium, and exchange energy with it, heavily influences some of the observables. To investigate this further, we wished to examine the effects of a mean field upon the detailed tracking of pions in the baryonic fluid. A mean field model was accordingly developed and put into the code by J. Wilson; R. Vogt in this workshop reports some initial testing of this mean field model against known analytical results [2].

A simplified description of our relativistic hydrodynamics code follows:

The dynamics of the nuclear fluid are calculated on a three dimensional grid of rectangular volume elements. The hydrodynamic equations of motion, given in [2], are solved on this fixed spatial grid using the Eulerian method, in which a fluid flows through a fixed mesh. Mass and momentum are rigorously conserved; energy is also forced to be conserved to a few percent. The evolution of the fluid is calculated through discrete small time steps using operator splitting techniques to solve the equations of motion. Our time evolution is explicit; that is, values at one time step are calculated from those at the previous time step.

By operator splitting we mean that we calculate the individual terms of the differential equations separately for each cell on the grid: for example the acceleration, the Van Leer advection, the compression and the pressure heating. In our actual mesh, vectors and scalars are staggered in time as well as in space. Our method of solution is second-order accurate in time and space, and it is stabilized in the shocks by an artifical viscosity pressure correction.

Treating shock phenomena adequately is particularly important. Two analytic shock tests are applied to the code: the relativistic shock tube and the relativistic wall shock in the strong shock limit. These are described briefly in [2].

Nuclear fluid properties are incorporated through the choice of equation of state (EOS). Our code is set up to offer a choice of several frequently used EOS's, such as the Skyrme. For the studies reported at this workshop a simple ideal gas EOS was employed.

In our code, pions are calculated by solving a Boltzmann equation which couples to the hydrodynamic fluid through a direct exchange of momentum and energy. Although our solution scheme employs monte carlo techniques, our pions are not particles per se, but rather represent a numerical discretization of a continuous pion distribution. They need not be in equilibrium; R. Vogt's talk, for example, shows how the pions in our mean field code achieve equilibrium in the course of time [2]. One of the tests we apply is to make sure that the pions do equilibrate to the analytical Bose distribution.

Pions are produced in a cell in the grid, using a probability method, when the energy density is high enough; subsequently their trajectories are tracked as they scatter and absorb in the nuclear medium. Pions that escape become the experimental observables. We are currently using measured pion-nucleon scattering cross sections, but we recognize that pions in the nuclear fluid may in fact be "dressed". The mean field code under development [2] addresses this.

Our code, advances its calculations through small time steps, producing at each step a detailed three dimensional snapshot (see Figure 1) of the nuclear fluid, including its Monte Carlo pion overlay. The evolution proceeds from the initial impact and collision through the early shocked nuclear matter to the expansion phase. During all of these phases the code calculates the detailed thermodynamic and kinematic properties of the baryon fluid and the pions, in full 3D spatial and temporal resolution. Post-processing allows us to predict deducible observables.

To calculate observables that depend on impact parameter is possible but involves many computer simulations. Up until now we have concentrated instead on central collisions because most of the important underlying physics is present and even enhanced in central collisions.

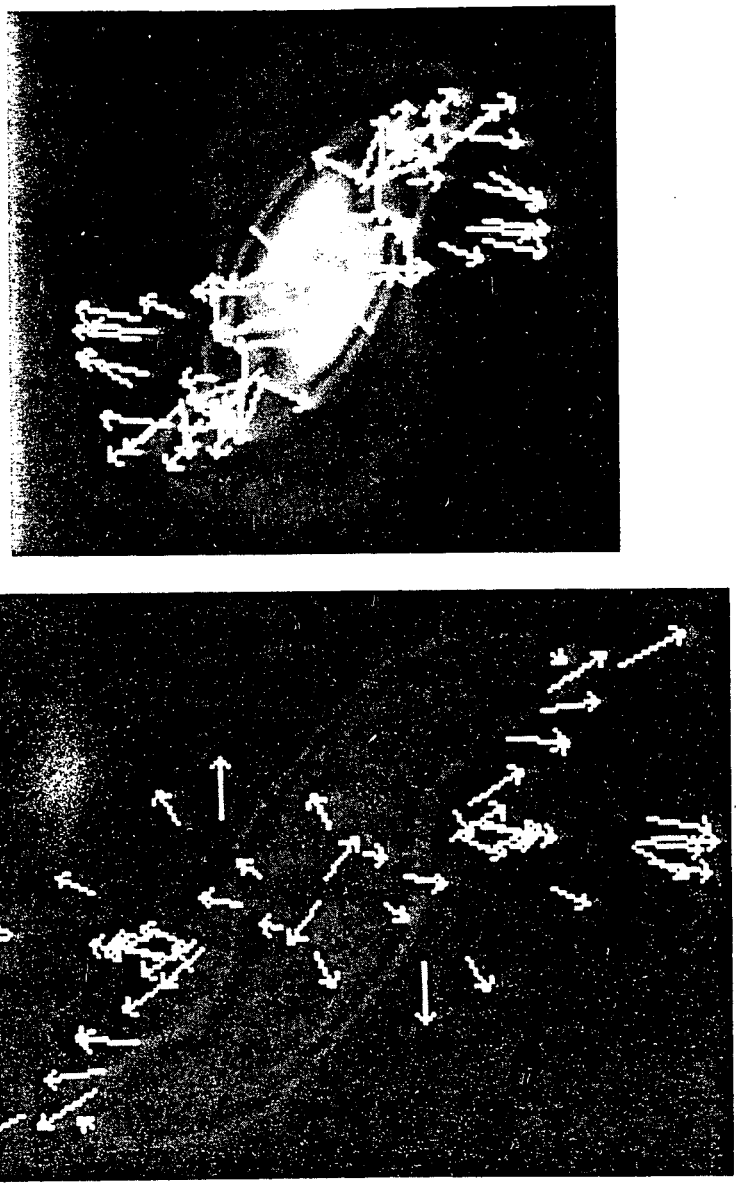

Figure 1. Density plots in the reaction plane for $^{139}La + ^{139}La$ collisions at 1350 MeV/nuc with an impact parameter of 3 fm. The top plot is at time 10 fm/c near maximum compression; the lower is at 15 fm/c when the fragments have started to separate.

This research was performed at Lawrence Livermore National Laboratory under the auspices of the United States Department of Energy, contract No. W-7405-Eng-48. One of us (J.R.W.) is supported by NSF grant PHY 89-20710.

References:

[1] J.R.Wilson, C.T. Alonso, T.L. McAbee, and R. Vogt, "Hydrodynamic Modeling of Heavy Ion Collisions" (this conference).
[2] R. Vogt, "Mean Field Pion Interactions in a Hydrodynamical Model" (this conference).
[3] J. A. Zingman, T.L. McAbee, J.R. Wilson and C.T. Alonso, Phys. Rev. C38 (1988) 760.
[4] T.L. McAbee, J.R. Wilson, J.A. Zingman and C.T. Alonso, Mod. Phys. Lett. A4 (1989) 983.
[5] J.R. Wilson, T.L. McAbee and C.T. Alonso, Int. J. Mod. Phys. A5 (1990) 543.

LAWRENCE BERKELEY LABORATORY
UNIVERSITY OF CALIFORNIA
INFORMATION RESOURCES DEPARTMENT
1 CYCLOTRON ROAD
BERKELEY, CALIFORNIA 94720